UNI
BASEL

Towards NMR analysis of the HIV-1 coreceptor CCR5 and its interaction with RANTES

Inauguraldissertation

zur

Erlangung der Würde eines Doktors der Philosophie

vorgelegt der

Philosophisch-Naturwissenschaftlichen Fakultät

der Universität Basel

von

Maciej Wiktor

aus Polen

Basel, 2013

Genehmigt von der Philosophisch-Naturwissenschaftlichen Fakultät

auf Antrag von

Prof. Dr. Stephan Grzesiek

Prof. Dr. Oliver Zerbe

Basel, den 16.10.2012

Prof. Dr. Jörg Schibler, Dekan

Summary

CCR5 is a chemokine receptor together with CD4 used by HIV-1 as a primary gate of cell infection. For this reason CCR5 is of great interest for medicine as a target for the anti-HIV-1 therapies. Since the binding site of its endogenous ligand RANTES overlaps with the binding site of viral envelope glycoprotein gp120, a noninflamatory RANTES derivative 5P12-RANTES has been developed as an anti-HIV-1 infection microbicide. The primary aim of this thesis was to establish an NMR-amenable system to study CCR5 and to understand better the interaction with RANTES.

For this purpose CCR5 expressed in insect cells was characterized in detail with regards to its secondary structure, oligomeric state, particle size, stability, posttranslational modifications and functionality. In contrast to the previous results, carefully performed detergent screening revealed that FosCholine-12, a detergent which allows high yield purification, does not support CCR5 recognition by 2D7 and cannot be used for studying CCR5 interactions with ligands. Therefore for the functional studies the receptor was solubilized with a milder detergent mixture DDM/CHAPS/CHS, which was shown to support native CCR5 tertiary structure.

Using this setup it could be shown by SPR that 5P12-RANTES binds with higher affinity than another potent RANTES variant PSC-RANTES (Morin et al., manuscript in preparation). This explains why 5P12-RANTES, which unlike PSC-RANTES does not cause CCR5 internalization, is an equally effective anti-HIV-1 microbicide. On the other hand, the wild-type RANTES was shown to aggregate on the receptor micelle using a mechanism compatible with the linear oligomerization, a process that is proposed to serve local chemokine preconcentration.

To obtain an access to a cost-efficient source of isotope-labeled samples, an E. coli expression system was established for CCR5 (Wiktor et al., 2012, J Biomol NMR, in revision). The expression was facilitated by fusing the N-terminus of CCR5 to well expressing protein domains e.g. thioredoxin. The C-terminal CCR5 truncation and the mutation of cysteines increased the protein yield up to 10 mg/L and improved the sample stability. Due to the engineered thrombin proteolytic site the N-terminal fusion partner i.e. thioredoxin could be quantitatively cleaved and removed by size exclusion chromatography. The FC-12-purified receptor was abundant in α-helical secondary

structure but could bind RANTES, MIP-1β and conformation-dependent antibody 2D7 only when solubilized by a DDM/CHAPS/CHS mixture. Using $^{15}N,^{13}C,^{2}H$-labeled CCR5 2D and 3D NMR experiments were recorded but only about 80 backbone resonances could be resolved. The spectral quality was jeopardized by large overlap and line-broadening and needs further improvements to allow the assignment and the structural investigation.

To study 5P12-RANTES by NMR the backbone assignment was completed. The HSQC spectrum revealed that, unlike wild-type RANTES and other chemokines, 5P12-RANTES does not form dimers. The secondary chemical shift analysis suggest that the overall structure of 5P12-RANTES is similar to the wild-type RANTES, with the exception of the mutated N-terminus, which does not participate in the intermolecular β-sheet and was shown to be highly flexible. Another important observation was that RANTES secondary structure is perturbed by Fos-Choline detergents, whereas maltosides shift the RANTES monomer:dimmer equilibrium towards its monomeric form.

The last part of the thesis present an independent study, where using ubiquitin as an example the mechanism of protein unfolding is studied (Vajpai et al., 2012, Proc Natl Acad Sci USA, in revision) manuscript submitted for publication). The secondary chemical shift analysis showed that the alcohol-denatured ubiquitin structure closely resembles the cold- and pressure denatured structure. This suggests that alcohol, low temperature and pressure unfold proteins by reducing the hydrophobic effect, the cost of exposing hydrophobic residues.

The data of this thesis will be presented in the following publications:

1. Wiktor, M., Morin, S., Sass, H-J., Kebbel, F., Grzesiek, S. (2012) Biophysical and structural investigation of bacterially expressed and engineered CCR5, a G protein-coupled receptor. J Biomol NMR (2012, in revision).

2. Vajpai, N., Nisius, L., Wiktor, M., Grzesiek, S. (2012) High pressure NMR reveals close similarity between cold and alcohol protein denaturation due to a reduction of the hydrophobic effect. Proc Natl Acad Sci USA (in revision).

3. Morin, S., Wiktor, M., Sass, H-J., Hartley, O., Grzesiek, S. (2012) Modulation of RANTES binding to CCR5 by modifications in the N-terminus and C-terminus (in preparation).

Table of contents

Acknowledgments

I would like to thank Professor Stephan Grzesiek for the opportunity to perform my PhD project in his laboratory, for his supervision, for the knowledge and expertise that he kindly shared, for his help in research and writing, as well as for his guidance, mentorship, patience and persistence in supporting me during over four years of our cooperation.

I would like to thank Professors Tilman Schirmer and Urs Jenal, the members of my PhD Committee for their support and contribution in providing directions, in which the research should go as well as for the annual evaluation of the progress of my work and to Professor Oliver Zerbe from the University of Zurich for co-referring this thesis.

I would like to thank Dr. Hans-Jürgen Sass and to Dr. Łukasz Skóra for sharing their expertise and for their help in conducting NMR experiments and processing the data.

I would like to thank the co-authors of the manuscript "Biophysical and structural investigation of bacterially expressed and engineered CCR5, a G protein-coupled receptor": Dr. Sébastien Morin for performing SPR experiments, Dr. Hans-Jürgen Sass for modeling CCR5 structure and Fabian Kebbel for obtaining electron microscopy pictures.

I would like to thank the co-authors of the manuscripts "Modulation of RANTES binding to CCR5 by modifications in the N-terminus and C-terminus" and "High pressure NMR reveals close similarity between cold and alcohol protein denaturation due to a reduction of the hydrophobic effect", especially the first authors Dr. Sébastien Morin and Dr. Navratna Vajpai for our fruitful cooperation.

I would like to thank all the past and the present members of Prof. Grzesiek's and Prof. Hiller's group, especially Dr. Hans-Jürgen Sass, Dr. Sébastien Morin, Dr. Łukasz Skóra, Prof. Sebastian Hiller and Dr. Marcel Blommers from Novartis for fruitful

Abbreviations and symbols

2HESO-8	n-octyl-2-hydroxyethylsulfoxide
AIDS	acquired immunodeficiency syndrome
Anameg-7	methyl-6-O-(N-heptylcarbamoyl)-α-D-glucopyranoside
ANZ-8	Anzergent 3-8, n-octyl-N,N-dimethyl-3-ammonio-1-propanesulfonate
Apo-10	dimethyldecylphosphine oxide
ATP	adenosine-5'-triphosphate
BME	β-mercaptoethanol
Brij-58	polyoxyethylene (20) cetyl ether
BSA	bovine serum albumine
C-HEGA	cyclohexylpentanoyl-N-hydroxyethylglucamide
$C_{12}E_9$	polyoxyethylene-9-dodecyl ether
CCD	charge-coupled device
CCL5	chemokine (C-C motif) ligand 5
CCR5	C-C chemokine receptor type 5
CD	circular dichroism
CD4	cluster of differentiation 4
CHAPS	3-[(3-cholamidopropyl)-dimethylammonio]-1-propanesulfonate
CHAPSO	3-[(3-cholamidopropyl)-dimethylammonio]-2-hydroxy-1-propanesulfonate
CHS	cholesteryl hemisuccinate
CMC	critical micelle concentration
CV	column volume
CXCR4	C-X-C chemokine receptor type 4
CYGLU-3	3-cyclohexyl-1-propyl-β-D-glucoside
CYPFOS-3	3-cyclopentyl-1-propylphosphocholin
ddH_2O	double deionized H_2O
DDM	n-dodecyl-β-D-matopyranoside (also MP-12)
DHPC	1,2-diheptanoyl-sn-glycero-3-phosphocholine
DIFOS-12	dodecyl-1,2-diphosphocholine
DLS	dynamic light scattering

DMAO-10	n-decyl-N,N-dimethylamine-N-oxide
DMG-14	n-tetradecyl-N,N-dimethylglycine
DMMAPS	3-(N,N-dimethylmyristylammonio)propanesulfonate
DOPC	dioleoylphosphatidylcholine
ECL	extracellular loop
EDTA	ethylenediaminetetraacetic acid
Fab	fragment antigen-binding
Fc	fragment crystallizable
FC-12	Fos-Choline-12, n-dodecylphosphocholine
GalP-8	n-octyl-β-D-galactopyranoside
GDP	guanosine-5'-diphosphate
GP-6	n-hexyl-β-D-glucopyranoside
gp120	HIV envelope glycoprotein 120 kDa
GPCR	G protein-coupled receptor
GRK	G protein-coupled receptor kinase
GTP	guanosine-5'-triphosphate
HEGA-11	Undecanoyl-N-Hydroxyethylglucamide
HEPES	4-(2-hydroxyethyl)-1-piperazineethanesulfonic acid
HIV	human immunodeficiency virus
HRP	horseradish peroxidase
Hsc70	heat-shock cognate 70 kDa
HSQC	heteronuclear single quantum coherence
ICL	intracellular loop
IEC	ion exchange chromatography
IMAC	immobilized metal ion chromatography
IP	immunoprecipitation
IPTG	isopropyl β-D-1-thiogalactopyranoside
ITC	isothermal titration calorimetry
K_D	dissociation constant
LB	lysogeny broth (also Luria-Bertani broth)
LDAO	N,N-dimethyl-1-dodecanamine-N-oxide
MALDI	matrix-assisted laser desorption/ionization
MD	molecular dynamics
Mega-9	nonanoyl-N-methylglucamide

MIP	macrophage inflammatory protein
MOI	multiplicity of infection
MP-12	n-dodecyl-β-D-matopyranoside (also DDM)
MS	mass spectrometry
MWCO	molecular weight cutoff
NaC	sodium cholate
Ni-NTA	nickel-nitriloacetic acid
NK	natural killer
NP-40	Nonidet P-40 substitute, octylphenoxypolyethoxyethanol
OD	optical density
OmpF	outer membrane protein F
PAGE	polyacrylamide gel electrophoresis
PDZ	postsynaptic density 95-kDa protein (PSD-95), Drosophila discs large protein (DLG), zonula occludens-1 protein (ZO-1)
PKC	protein kinase C
PMSF	phenylmethanesulfonyl fluoride
POPC	1-palmitoyl-2-oleoyl-sn-glycero-3-phosphocholine
PTK	protein tyrosine kinase
PTMs	posttranslational modifications
PVDF	polyvinylidene fluoride
RANTES	regulated on activation, normal T cell expressed and secreted
RT	room temperature
RU	relative unit
SDDSAR	sodium dodecanoyl sarcosine
SD	standard deviation
SDS	sodium dodecyl sulfate
SEC	size exclusion chromatography
SPR	surface plasmon resonance
TB	terrific broth
TCA	trichloracetic acid
TEM	transmission electron microscopy
TM	transmembrane
TMP-12	n-dodecyl-β-D-thiomatopyranoside
Tris	2-amino-2-hydroxymethyl-propane-1,3-diol

Tween-20   polyoxyethylene (20) sorbitan monolaurate

TX-100   Triton X-100, 4-(1,1,3,3-tetramethylbutyl)phenyl-polyethylene glycol

Θ ellipticity

Θ_{MRM} mean residue molar ellipticity

Organization of the thesis

The thesis starts with a general introduction (Chapter 1). Chapter 2 defines the goals. Chapter 3 contains the unpublished data obtained for the insect-expressed CCR5. Chapter 4: Biophysical and structural investigation of bacterially expressed and engineered CCR5, a G protein-coupled receptor is a complete manuscript submitted for publication (Wiktor et al., 2012, J Biomol NMR, in revision). Chapter 5 describes the unpublished results obtained for RANTES. Chapter 6: Modulation of RANTES binding to CCR5 by modifications in the N-terminus and C-terminus (Morin et al., manuscript in preparation) and Chapter 7: High pressure NMR reveals close similarity between cold and alcohol protein denaturation due to a reduction of the hydrophobic effect (Vajpai et al., 2012, Proc Natl Acad Sci USA, in revision) are complete manuscripts submitted for publication. Every manuscript has independent topic-specific introduction, materials and methods, references, figure/table numbering and formatting. Each chapter with results finishes with a separate discussion. The thesis ends with a brief common section Conclusions and perspectives (Chapter 8).

1 Introduction

1.1   Diversity of the GPCR superfamily

G protein-coupled receptors constitute a large protein superfamily found only in eukaryotes. About 4% of the protein-coding human genome codes for ~800 GPCRs (1). Based on phylogenetic analysis human GPCRs cluster into 5 main families: rhodopsin, adhesion, frizzled/taste2, glutamate and secretin which comprise 701, 24, 24, 15 and 15 members, respectively (2). The diversity of the GPCR superfamily members is reflected in the variety of their ligand types. Photons, ions, odorants, nucleotides, fatty acids, amino acids, peptides and proteins are only some of the messages that GPCRs can transduce (3). As GPCRs regulate so many physiological processes such as vision, smell, behavior, mood, immune system, blood pressure, heart rate, digestion or homeostasis, they are the most commonly drugged protein family (4). About 40% of prescribed pharmaceuticals target GPCRs (5).

1.2   GPCR function and turnover

The function of GPCRs is to transduce signals through the plasma membrane from the outside to the inside of a cell and trigger cellular response. On the intracellular side GPCRs are coupled to G-proteins, heterotrimeric molecular switches. Upon agonist binding, a cascade of conformation changes is induced in a GPCR and passed on to a G_α subunit of a G-protein resulting in the dissociation of GDP from G_α. As the cytoplasmic GTP/GDP ratio is about 9 (6), the empty nucleotide binding site is quickly re-occupied by GTP. This, however, renders G_α unable to interact with neither the GPCR nor the $G_{\beta/\gamma}$ subunit and the entire complex falls apart (7). Free G_α and $G_{\beta/\gamma}$ interact with various effector proteins like adenylate cyclase, phospholipase C or ion channels (8). The receptor is downregulated by phosphorylation and subsequent interaction with β-arrestin. This is usually followed by clathrin- and dynamin-dependent endocytosis (9, 10). Subsequently, it can be either recognized by an adaptor protein (e.g. through its PDZ ligand or a dileucine-based motif) and recycled back to the plasma membrane or ubiquitinated and targeted for degradation (11). An alternative

pathway of clatrin-independent receptor internalization has also been reported (12). In the case of rhodopsin, however, the β-arrestin-mediated process of desensitization does not involve endocytosis.
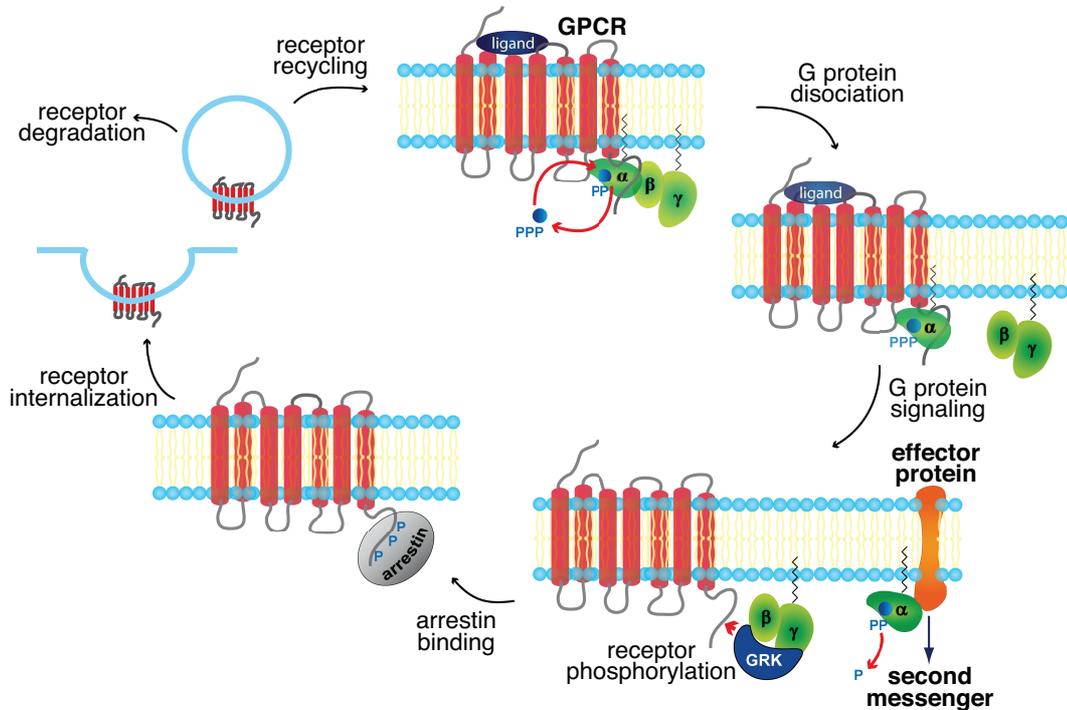
Figure 1.1 GPCR cycle: activation, signaling and downregulation adapted from Nisius (13).

1.3 Known structures of GPCRs

The structure determination of membrane proteins and of GPCRs in particular is notoriously difficult due to the many obstacles impeding membrane protein sample preparation and subsequent structure determination. When this publication was written about 82000 entries appeared in the Protein Data Bank (14) but only as few as 335 unique membrane protein 3D structures were known (15). GPCR structures are even sparser. The first, bovine rhodopsin, was solved in 2000 by Palczewski et al. (16), and until now 12 more unique GPCR structures were solved by X-ray crystallography: β_2-adrenergic (17, 18), β_1-adrenergic (19), adenosine A_{2A} (20, 21), dopamine D3 (22), CXCR4 (23), histamine H_1 (24), M2 muscarinic acetylcholine (25), M3 muscarinic acetylcholine (26), $S1P_1$ lipid (27), μ-opioid (28), κ-opioid (29) and δ-opioid (30) receptors. To obtain high-resolution structural data the replacement of the intracellular (IC) loop 3 with T4 lysozyme (17, 20, 22-30), thermostabilization (19, 21-23) or

stabilization with anti- or nanobodies (17) proved to be successful strategies. Additionally, the majority of the crystallized GPCRs were bound to an agonist (21), an inverse agonist (17, 18, 26) or most often to an antagonist (19, 20, 22-25, 27-30). Although, not GPCRs, prokaryotic sensory rhodopsin II (31) and proteorhodopsin (32) are examples of a 7-TM domain proteins solved by NMR spectroscopy.
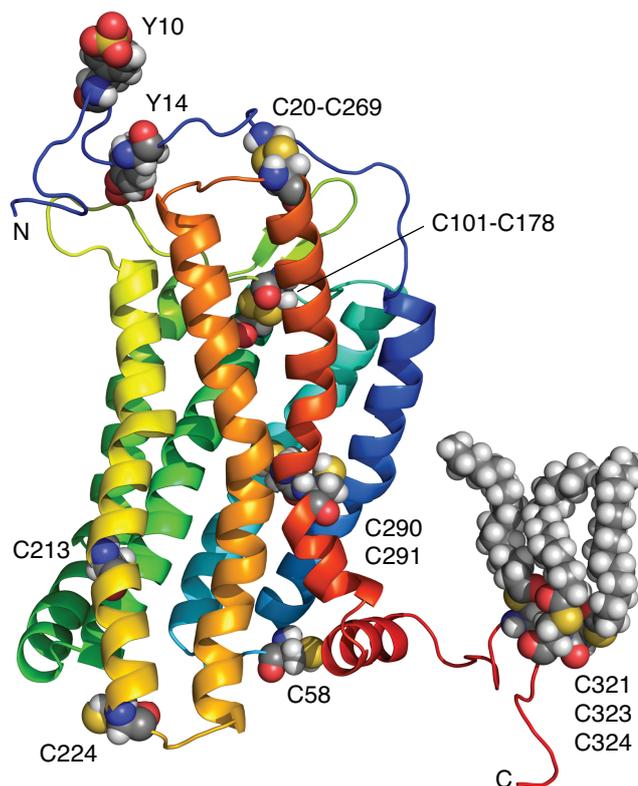
Figure 1.2 Example of GPCR structure: homology model of CCR5 based on CXCR4 structure (23) (see Chapter 4).

1.4 Biology of CCR5 and its involvement in disease

The C-C chemokine receptor 5 (CCR5) belongs to the γ-group of the rhodopsin family of GPCRs. It is found in the plasma membrane of Th1 lymphocytes, macrophages, NK cells and immature dentritic cells and is involved in various infectious and inflammatory diseases as well as cancer (33). Since humans carrying the Δ32 allele of the CCR5 gene, a 32-base pair deletion resulting in a premature stop codon in the extracellular (EC) loop 2 and a nonfunctional receptor, are healthy, the exact role of CCR5 is not completely understood.

The main interest in CCR5 is, however, a consequence of its involvement in AIDS. R5-tropic HIV-1 infection necessitates the sequential interaction of viral envelope glycoprotein gp120 with CD4 and CCR5 (34). Two copies of the CCR5-Δ32 allele confer nearly complete resistance to HIV-1 infection (35, 36). Δ32 occurs at 5-14% frequency in European Caucasians but not in African, Native American, and East Asian populations (37), which is a result of a selective pressure of the epidemics of plague, a viral haemorrhagic fever, that took place in Europe in medieval ages (38). Successful strategies to block HIV entry have been developed based on small-molecule inhibitors of CCR5 (39) as well as derivatives of its natural chemokine ligand RANTES (40-43).
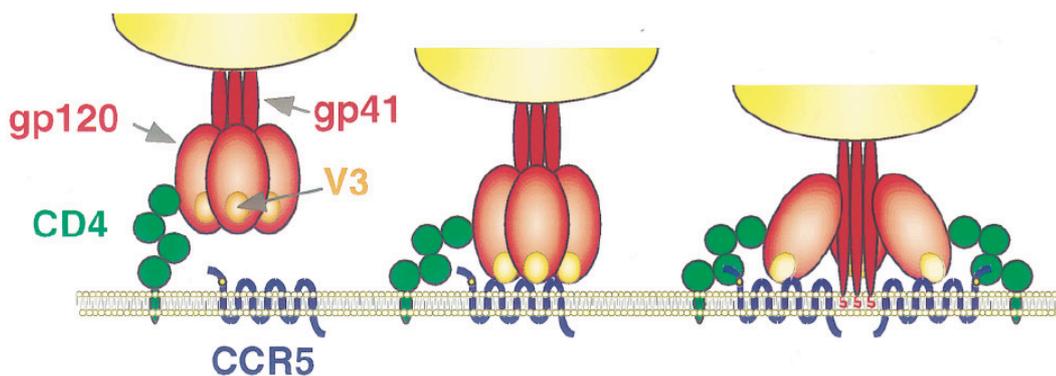
Figure 1.3 Mechanism of the HIV infection adapted from Doms et al. (44). HIV (yellow) using its envelope glycoprotein gp120 (light red) binds to CD4 (green) and to a chemokine coreceptor e.g. CCR5 (blue). This interaction triggers a conformational changes, upon which fusion peptide of gp41 (dark red) is exposed and penetrates the plasma membrane to initiate membrane fusion.

1.5 CCR5 structural features

The sequence of CCR5 is composed of 352 amino acids (40.6 kDa) folding into seven hydrophobic α-helical membrane-spanning segments (domains) with an extracellular N- and a cytoplasmic C-terminus. As a result of CCR5 membrane topology, three extracellular and four intracellular loops are formed with the last loop being closed up by the hydrocarbon chain of S-palmitoyl-L-cysteines 321, 323 and 324 deeping into the membrane.

A characteristic feature of CCR5 shared with other chemokine receptors is the presence of four extracellular cysteines, one per each extracellular segment (N-terminus and three extracellular loops). The first pair Cys101 and Cys178 forms a disulphide bridge between 1st and 2nd ECLs, a structural hallmark of the entire GPCR superfamily

contributing to the GPCR stability. The second disulphide bridge between Cys20 and Cys269 connects the N-terminus with 3rd ECL and is conserved only among the chemokine receptor family (45). The second bridge is thought to impose an additional structural constraint and to stabilize the receptor in the conformation capable to bind ligands.

With CHO-K1 cells stably expressing CCR5 it was shown that alanine mutation of any of the extracellular cysteines completely abolishes MIP-1β binding (46). The situation was somewhat different for the conformation-sensitive antibodies. The interaction with CTC5, CTC8, 2D7, and mAbs 531, 501 and 549 was much more sensitive to the mutation of Cys101 and/or Cys178 than to the mutation of Cys20 and/or Cys269 as shown in CCR5-transfected 293T cells (46). Similarly, the HIV coreceptor CCR5 function was more impaired by Cys101 and/or Cys178 mutation (14-20% of the wild type CCR5 activity) than by Cys20 and/or Cys269 mutation (40-62% of the wild type CCR5 activity) as studied in human CD4-expressing U87 cells (46).

Another conserved features of CCR5 shared with other chemokine receptors are the DRYLAVHA motif in the 2nd ECL playing an important role in the coupling to the G-proteins and the unusually short positively charged 3rd ICL. CCR5 is also subject to many PTMs (posttranslational modifications). The previously mentioned palmitoylation of C-terminal cysteines 321, 323 and 324 facilitates CCR5 transport to the plasma membrane, ligand-stimulated endocytosis, coupling to the signaling pathways as well as GRK or PKC (protein kinase C)-mediated CCR5 phosphorylation (47-49). It was shown that N-terminal tyrosine residues are sulfated in Cf2Th canine thymocytes (50). This plays an important role in the interaction with chemokines and the HIV glycoprotein gp120, which are both known to bind heparin sulfate proteoglycans (51-55). It was also shown that CCR5 N-terminal peptides with minimum two sulfated tyrosines in positions 10 and 14 can efficiently block gp120/CD4 complex binding to CCR5 and therefore Tyr3 and Tyr15 sulfation is thought to be less important (56, 57).

CCR5 is also O-glycosylated, preferentially at Ser6, which also contributes to high affinity chemokine binding (50, 58). The 3rd ECL of CCR5 possesses a potential N-glycosylation site but as neither N-glycosidase endo F nor tunicamycin treatment changes CCR5 electrophoretic mobility (50) and as the elimation of this site by mutagenesis does not impair CCR5 cofactor functions (59), the N-link glycosylation

site is most likely not used. Serines 336, 337, 342 and 349 in the C-terminus of CCR5 are subject to nonhierarchical phosphorylation (60).
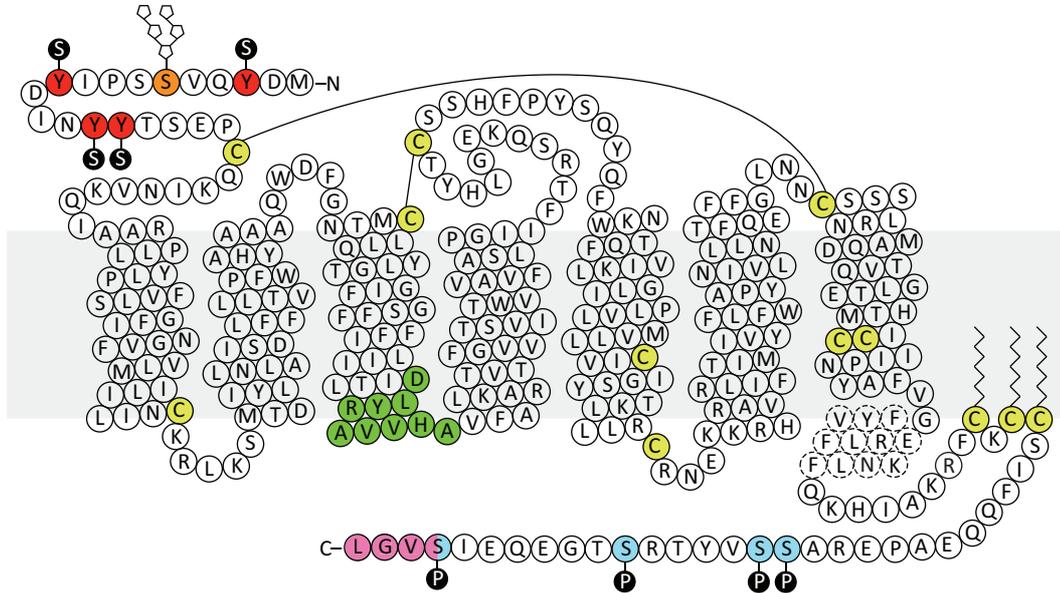
Figure 1.4 Two-dimensional topology of CCR5 derived from CCR5 homology model (see Chapter 4). The position of the important structural features and PTMs were color-coded: N-terminal tyrosine sulfation (red), O-glycosylation (orange), DRYLAVVHA motif (green), C-terminal phosphorylation (cyan), PDZ substrate (pink), the cysteines including those forming disulphide bridges and those modified by palmitic acid (yellow). The position is plasma membrane is approximated with a grey box.

1.6 Biology of RANTES as a chemokine

Chemokines (chemotactic cytokines) are small (8-10 kDa) soluble secreted proteins regulating the immune response. The chemokines act by attracting various cell types to sites of inflammation. Immune cells can localize inflammation site by a chemokine gradient established by signaling leukocytes. Based on the arrangement of two conserved N-terminal cysteines chemokines can be divided into four subclasses: C, CC, CXC, CX$_3$C (61, 62). Two major chemokine subfamilies CC and CXC chemokines are primarily responsible for activation of monocytes, lymphocytes and basophils (CC chemokines) and neutrophiles (CXC chemokines). Chemokines signal via chemokine receptors, which belong to G protein–coupled receptors and which were named after the main chemokine they interact with e.g. CCR5, CXCR4, etc.

RANTES (regulated upon activation, normal T-cell expressed and secreted) known also as CCL5 quickly became interesting for both academia and pharmaceutical

industry, when in 1995 Cocchi et al. discovered that CC chemokines RANTES, MIP-1α, MIP-1β can suppress HIV-1 infection with RANTES being the most potent natural chemokine (63). This discovery was followed by identification of the RANTES receptor, CCR5 (64). Interestingly, it was also shown that at high concentration, instead inhibiting, RANTES can also stimulate viral infection (65, 66). RANTES is known to signal via two distinct pathways (67). The first utilizes low RANTES concentrations (≤50 nM) and via $G_{\alpha i}$-type GPCR pathway regulates chemotaxis and transient calcium mobilization. The second low affinity pathway requires higher RANTES concentrations (≥1 µM), and via PTKs (protein tyrosine kinases) causes general T cell activation, i.e., proliferation, interleukin-2 expression, etc. (67-69).

RANTES and other chemokines can form dimers, higher order oligomers as well as large molecular weight aggregates. Wild type RANTES is particularly aggregation-prone (70). Such properties affect the function of chemokines and may be important for the establishment of chemokine gradients (66, 71). To study the role of RANTES oligomerization and dissect the function of monomeric and aggregated RANTES, the key residues involved in RANTES oligomerization have been identified and the effect of their mutation studied (66, 71). It was shown that E26A and E66S mutations reduce RANTES aggregation tendency rendering predominantly tetrameric and dimeric RANTES, respectively. Although, disaggregated RANTES retained CCR5 binding and $G_{\alpha i}$-dependent signaling properties, it failed to activate the PTK pathway and did not activate T lymphocytes, neutrophils and monocytes (71).

1.7 RANTES structural features

Structures of numerous chemokines including SDF-1α, vMIP-II, MIP-1β and RANTES have been solved by X-ray crystallography and NMR (72-77). Few structural features, that is a flexible N-terminus, three antiparallel β-strands and C-terminal α-helix are highly conserved and constitute structural hallmarks of all chemokines (78). Chemokines share also the position of four cysteines residues: two at the N-terminus near each other, one in the center of the sequence and one in the C-terminal part (79).

At low pH and low protein concentration (conditions preventing precipitation) RANTES was studied in detail by NMR (80). RANTES monomer and dimer are in slow exchange regime and can be observed as separate sets of HSQC resonances. The dissociation constant of RANTES monomer-dimer equilibrium is 17.6 µM at pH 3.8

and only 2.9 µM at pH 6.0, which indicates that at higher pH the dimeric RANTES form is even more stabilized. Subsequently, using chemical shift difference between RANTES monomer and dimer, dimerization interfaced was mapped to residues: 10-16, 19, 21, 31-35, 41, 42, 46-50, 54 and Q48 sidechain. These residues form a continuous patch at one side of RANTES molecule, which overlaps with the RANTES dimerization interface observed before in the crystal structure (81). According to the PDB entry 1EQT (81), residues 8-10 for an important intermolecular β-sheet stabilizing RANTES dimer. Based on the data obtained using various techniques (NMR, MS, SAXS) a rational for RANTES oligomerization was proposed (70). According to this model RANTES dimers can form a tetramer stabilized by the interactions between the second β-strand (residues 25-30) and C-terminal α-helix (residues 62 and 66) of one monomer and the corresponding residues of a monomer from another dimer. Since this interaction involves only one of the monomers forming each dimer, the other monomer can still interact with a monomer being part of a third dimer. In this way interaction can be propagated into long oligomers composed of even number of RANTES molecules. This model explains very well the reduced aggregation properties of RANTES E26 and E66 mutants (71).
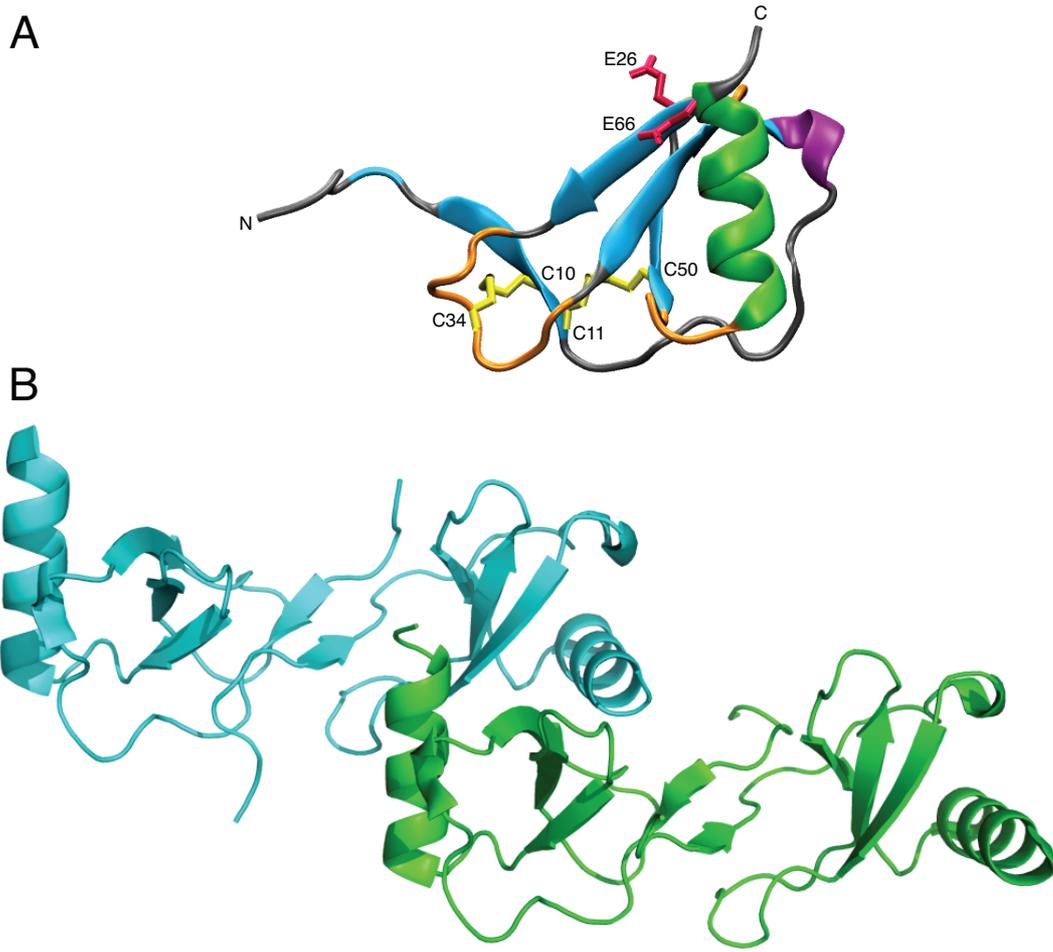
Figure 1.5 Structures of RANTES. (A) Cartoon representation of the three dimensional RANTES crystal structure (one monomer of a dimer) based on the PDB entry 1EQT (81). Secondary structure elements were color-coded: β-strand and β-bridge (cyan), β-turn (orange), α-helix (green), 3_{10}-helix (purple), random coil (grey). Four cysteines forming disulphide bridges were colored yellow. Two glutamic acids important in RANTES aggregation were colored red. (B) Model of RANTES oligomerization based on the PDB entry 2L9H (70). As the interaction interface between two dimers (green and cyan) requires only one of the monomers forming each dimer, the oligomerization can be propagated into elongated polymers composed of even number of RANTES molecules.

2 Aims of the study

The goal of this dissertation thesis was to obtain an NMR-amenable system to study CCR5 and its interactions with ligands in particular with the chemokine RANTES. More specifically the work aimed at: (i) improving the yield and purity of the previously established expression system in insect cells, (ii) further biophysical characterization of the insect-produced material, (iii) optimizing solubilization conditions yielding stable and ligand-binding CCR5 as well as (iv) establishing a bacterial expression system to facilitate uniform isotope labeling, (v) biophysical characterization of the protein produced in *E. coli*, (vi) optimizing sample conditions and studying *E. coli*-expressed CCR5 by NMR and finally (vii) finding suitable conditions and studying CCR5 interaction with RANTES. The work should also help to understand and overcome the general bottlenecks hampering GPCR structure determination by NMR. The last part of the thesis aimed at the investigation of protein cold and alcohol denaturation.

3 Studies of CCR5 expressed in Sf21

3.1 Materials and methods

List of buffers

Buffer 1A   20 mM Na_2HPO_4 pH 7.5, 300 mM NaCl, 10% (v/v) glycerol

Buffer 1B   20 mM Tris-HCl pH 7.5, 100 mM $(NH_4)_2SO_4$, 10% (v/v) glycerol

Buffer 2   20 mM Na_2HPO_4 pH 7.5, 1 M NaCl, 10% (v/v) glycerol,

40 mM imidazole, 0.1% FC-12

Buffer 3   20 mM Na_2HPO_4 pH 7.5, 300 mM NaCl, 10% (v/v) glycerol,

400 mM imidazole, 0.1% FC-12

Buffer 4   10 mM HEPES pH 8.0, 100 mM NaCl, 1 mM EDTA, 0.1% FC-12

Buffer 5   10 mM HEPES pH 8.0, 100 mM NaCl, 1 mM EDTA, 0.1% FC-12,

5 mM D-desthiobiotin

Buffer 6   10 mM HEPES pH 7.4, 150 mM NaCl, 50 μM EDTA, 0.1% FC-12,

0.005% P20 (a surfactant, recommended by the sensor chip and SPR

instrument manufacturer,)

Recombinant CCR5 expression

Recombinant CCR5 was produced using baculovirus-insect cell system essentially as described previously (82). High titer baculovirus stocks were obtained using Sf9 strain. CCR5 was overexpressed on a large scale (5-10 L) in Sf21 in all cases besides a single test expression performed in High Five for a comparison. Cells were grown in WAVE Bioreactor BASE2050EHT (GE Healthcare) in SF-4 Baculo Express Insect Culture Medium (BioConcept, Allschwil, Switzerland) at 27°C until a density of $2.0\text{-}2.4\times10^6$/mL. About 40 h after infection at MOI=1 cells were harvested by centrifugation and stored at -70°C.

Preparation of membrane fraction

A frozen insect cell pellet (typically from 1 L of culture) was suspended in 100 mL of buffer 1A or 1B and supplemented with EDTA-free complete protease inhibitor cocktail (Roche). Cells were broken using a dounce homogenizer (typically 40 strokes). Cell debris was removed by centrifugation at 300 g for 6 min. The supernatant was centrifuged at 100000 g for 30 min and the resulting pellet (from now on called membrane fraction) was washed twice with buffer 1A or 1B. Finally, membrane the fraction was suspended in buffer 1A or 1B and stored at -70°C.

CCR5 purification

A frozen insect cell membrane fraction (typically from 1 L of culture) was thawed and supplemented with EDTA-free complete protease inhibitor cocktail (Roche) and 1.5-2.5% detergent. Protein solubilization was carried out at 4-8°C for 2 h. Unsolubilized material was removed by centrifugation at 100000 g for 30 min. The clarified supernatant was supplemented with 20 mM imidazole and bound to Ni-charged Chelating Sepharose (GE Healthcare) beads for 1.5 h. The resin was washed with 50 CV of buffer 2. The protein was then eluted with buffer 3. Protein-rich fractions were pooled and bound to Strep-Tactin beads (IBA, Göttingen, Germany) for 1.5 h. The resin was washed with 20 CV of buffer 4. The protein was eluted with buffer 5. For the purification in DDM FC-12 was replaced with DDM for buffers 2-5.

Gel electrophoresis and western blotting

Protein samples for SDS-PAGE were mixed with 5x SDS loading buffer (312.5 mM Tris-HCl pH 6.8, 50% (v/v) glycerol, 25% β-mercaptoethanol, 10% SDS, 0.0125% bromophenol blue), incubated at 30°C for 15 min and centrifuged at 17000 g for 5 min prior to loading on a 4-20% gradient precast gel (Pierce). The electrophoresis was performed at 100 V constant voltage. Gels were stained using 0.25% solution of Coomassie Brilliant blue R-250 (AppliChem) in 25% isopropanol and 10% acetic acid and destained in 10% acetic acid.

For western blotting onto PVDF membrane (Bio-Rad), a Criterion Blotter (Bio-Rad) was used. The transfer was performed at 0.5 A constant current for 1 h in the transfer buffer (48 mM Tris-HCl pH 9.2, 39 mM glycine, 0.375% SDS, 20% methanol). The membrane was blocked with 3% BSA in TBST buffer (10 mM Tris-

HCl pH 8, 150 mM NaCl, 0.5% Tween-20). Subsequently the membrane was incubated with mouse monoclonal HIS-1 anti-polyhistidine-peroxidase antibody (Sigma-Aldrich) at 1:6000 dilution for 1 h. After washing 4 x 2 min with TBST buffer, the blot was developed using chemiluminescent HRP substrate (Roche). The signal was recorded using a BioMax XAR Film (Kodak) or using a LAS-4000 luminescent image analyzer (Fujifilm). The signal intensities were quantified using the ImageJ 1.43r (83).

Circular dichroism spectroscopy

CD spectra were recorded on 3-13 μM monomeric CCR5 fractions. Measurements were performed on a Chirascan CD spectrometer (Applied Photophysics) at 20°C in 1 mm quartz Suprasil cuvettes (Hellma). Typically, spectra in a wavelength range of 195-260 nm spectra were recorded in triplicates and averaged. After baseline (buffer) subtraction, the mean residue molar ellipticity Θ_{MRM} was calculated from the following equation $\Theta_{MRM}=\Theta/(C \times n \times l)$, where Θ is the ellipticity (deg), C is the concentration (mol/L), n is the number of residues and l is the optical path length (cm). The α-helical contents α% was calculated as follows $\alpha\%=(-\Theta_{MRM, 222nm}+3000)/39000$ (84), where Θ_{MRM} is given in units of $deg \times cm^2 \times dmol^{-1}$.

Mass spectrometry analysis

MS analysis was performed by the Functional Genomics Center Zurich. Purified ~30 μM CCR5 50 μL solution samples (after Ni-NTA and after both Ni-NTA and Strep-tag purification) were shipped on ice. CCR5 samples (10 μL) were precipitated with 10 μL of 20% TCA and two times washed with cold acetone while centrifuged prior to the analysis. For the PTMs detection samples (also after precipitation as it was expected that samples in a detergent-containing solution cannot be efficiently digested) were subject to a proteolytic digestion with trypsin.

Detergent exchange assay

IMAC and Strep-Tactin-purified CCR5 in buffer 5 (containing FC-12) was concentrated to ~1.3 mg/mL. The protein was first supplemented with 2 M HEPES pH 8 to final concentration of 90 mM and then diluted with ddH_2O to adjust protein concentration to ~0.92 mg/mL. Subsequently, the resulting protein solution was

aliquoted into 24 μL fractions followed by addition of 6 μL 10% detergents (all from Anatrace, DHPC from Avanti Polar Lipids). The resulting mixture (~0.74 mg/mL CCR5 in 51 mM HEPES pH 8, 50 mM NaCl, 0.55 mM EDTA, 2.75 mM D-desthiobiotin and ~1.82x diluted FC-12) was incubated for 6 days at RT. The resulting precipitate was removed by centrifugation at 150000 g for 1h and the supernatant was analyzed for the protein contents on SDS-PAGE.

Detergent solubilization assay

Frozen 20% (w/v) solutions of membrane fraction were thawed, diluted twice and supplemented with detergent to a final concentration of 2%. Solubilization was carried out at RT for 2 h with 1000 rpm shaking. Unsolubilized material was removed by centrifugation at 17000 g for 30 min. The clarified supernatant (2 μL) was loaded onto a Protran BA85 nitrocellulose membrane (Whatman) and dried at RT. Dot blots were blocked, labeled with anti-His-tag antibody, developed and quantified in the same way as western blots described below. Detergents were obtained from Anatrace, DHPC from Avanti Polar Lipids.

Immunoprecipitation

0.5 mL aliquots of insect cell membrane fractions in buffer 1A or 1B were supplemented with detergents to 1% final concentration. Solubilization was carried out for 2 h followed by centrifugation at 17000 g for 15 min. 120 μL of the supernatant was transferred to a clean tube and incubated with 2.5 μL of 2D7 antibody (0.5 mg/mL) for 1 h. Subsequently, after 15 min centrifugation at 17000 g, 100 μL of the supernatant was bound to 25 μL of Protein G Sepharose 4 Fast Flow (GE Healthcare) for 1 h. The resin was washed three times with buffer 1A or 1B supplemented with the tested detergent. To disrupt protein interactions 50 μL 2x SDS loading buffer was added. After 30 min incubation samples were analyzed by SDS-PAGE and western blotting.

Dynamic light scattering

DLS measurements were performed on a Zetasizer Nano ZS instrument (Malvern Instruments) at RT. Samples (typically 80 μL) were placed in UV-transparent cuvettes UVette 220 – 1600 nm (Eppendorf), inserted into the instrument and

equilibrated for 5 min prior the measurement. Spectra were collected at least in triplicates and averaged.

Surface Plasmon resonance

SPR was performed on a BIAlite instrument (Biacore) equipped with an NTA Sensor Chip (Biacore) at 12-20°C and 10-20 μL/min flow rate with buffer 6 as a typical running buffer. For the CCR5 immobilization the chip was functionalized with nickel ions (100 μL injection of 500 μM $NiSO_4$) followed by 3-4 100 μL injections of purified 200-266 nM CCR5. For the binding of RANTES-E66S to CCR5, 0.5 μM solution of RANTES-E66S was injected. To study RANTES-E66S unspecific adsorption to the Ni-charged NTA chip, 10 μM RANTES-E66S solution in a suitable buffer (with adjusted NaCl concentration and pH) was injected. Before proceeding to the next tested condition the chip was stripped with 40 μL injection of 0.1 M HCl, running buffer was changed to another one (with higher NaCl concentration or pH) and the chip was re-functionalized with $NiSO_4$.

3.2 Results

CCR5 purification

3.2.1.1 Introduction

The selection of the purification methods plays a key role in the final outcome and should be made carefully. One has to take into account not only the quality of the final product but also, very importantly, the cost, the time and the workload that need to be applied along the procedure. In the membrane protein field especially, where the system is complicated by the presence of detergents, the application of classical chromatography methods like SEC and IEC is usually more challenging. Therefore, for recombinant proteins, due to its robustness, IMAC, that relies on ~1 μM affinity of polyhistidine to transition metal ions, is often a method of choice for the first purification step. This chapter demonstrates that, despite its limited specificity, upon fine-tuning, IMAC can yield good results.

3.2.1.2 *IMAC chromatography*

The prerequisite of applying IMAC is the presence of a polyhistidine tag, conventionally 6His-tag. Therefore, the wild type CCR5 construct which is used in this study contains one on its C-terminus (followed by Strep-tag). After membrane fraction preparation, which by depleting water-soluble proteins is a purification step by itself, CCR5 is solubilized in a detergent, clarified by centrifugation and bound to an IMAC resin. Subsequently the resin is washed with buffer containing imidazole (typically 20-60 mM), salt (up to 2M) and glycerol (up to 50%) to remove unspecifically bound particles. Protein is usually eluted using high imidazole concentration (typically $\geq$250 mM) or, less frequently, with low pH (4.5-5.3) or EDTA.

In order to ensure the optimal protein purity and yield, the washing concentration of imidazole was systematically optimized (Figure 3.1). The experiment aimed to determine the maximal concentration that does not yet lead to the elution of detectable amount of the protein. IMAC column with bound CCR5 was washed with stepwise increasing concentration of imidazole. The eluting protein was monitored by a UV absorption at 280 nm. First, 20 mM imidazole was applied until UV baseline stabilizes and then the concentration was raised with 20 mM increments until 100 mM, followed by 150, 200, 300 and 400 mM steps, 15 CV each. Eluted peaks were analyzed by anti-His-tag western blotting for the presence of CCR5 (Figure 3.2).
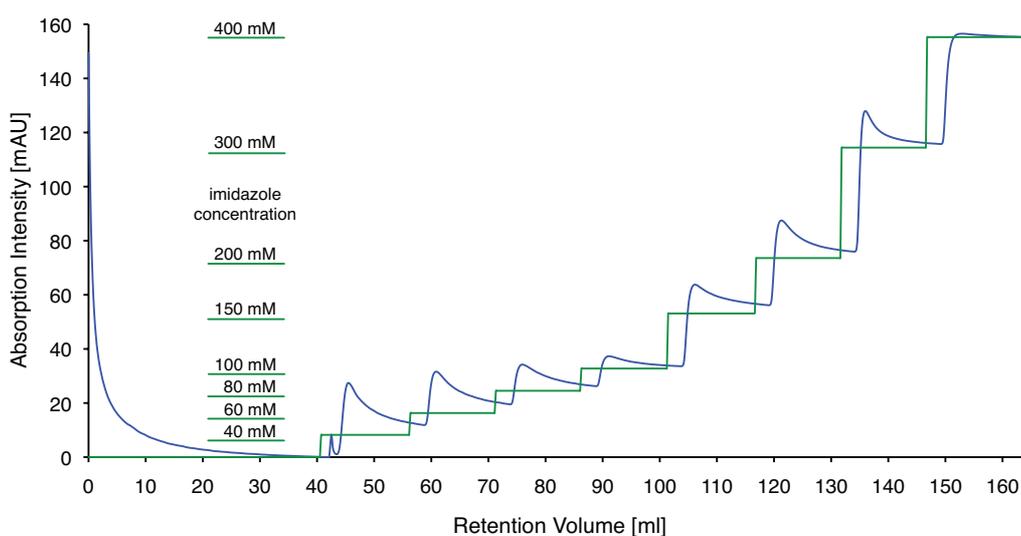
Figure 3.1 Imidazole step gradient elution from IMAC column. UV absorption intensity (blue curve) is a sum of eluting protein (peaks) and increasing imidazole concentration (rectangular baseline shifts).

The experiment showed that the fractions eluted with up to 40 mM imidazole did not contain detectable amount of CCR5 and therefore must have been entirely composed of the contaminants. 60-100 mM imidazole eluted CCR5 monomers, whereas from 150 mM imidazole on, dimers came along. To fully elute all CCR5 oligomeric species minimum 300 mM imidazole was required. Similar experiment was performed earlier, with less resolution, in batch mode. CCR5 monomers eluted at 80 but not at 50 mM imidazole, while 500 mM imidazole eluted all species. Both experiments are consistent with one another and suggest that up to 50 mM imidazole can be applied for washing and at least 300 is required for a complete elution. This experiment also shows that 15 CV is not sufficient for washing and the purity should benefit from larger washing volume.
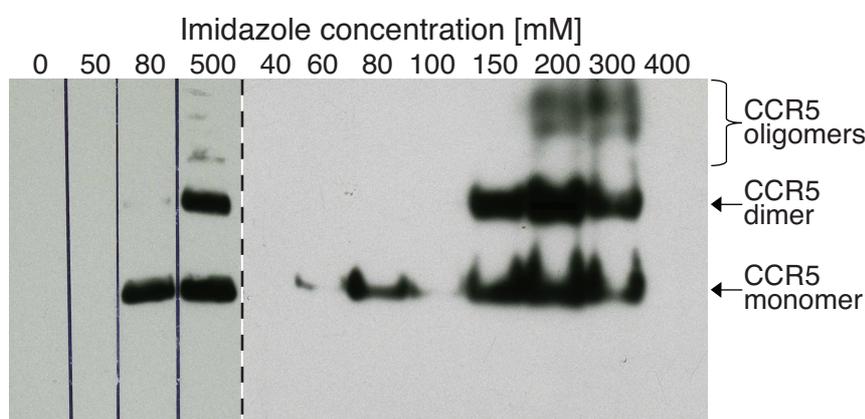
Figure 3.2 Western blotting of IMAC resin-eluted fractions. Two independent experiments (separated by a dashed line) of imidazole step gradient elution, first performed in batch (left) and second on a column with more resolution (right), yield overlapping result.

The concentration of imidazole at which the protein starts to elute depends also on the His-tag length and on a resin type. Intuitively, longer His-tag should need higher imidazole concentration to elute and indeed, a 10His-tagged CCR5 went off the resin at 133 mM imidazole, dimers required 250 mM, whereas a complete elution 500 mM. Similarly, the minimum imidazole concentration required to elute protein from Ni-NTA (IMAC resin from Qiagen), which leaves only two unoccupied nickel coordination sites for polyhistidine binding (resin from GE Healthcare has three), should and is significantly lower. To elute 10His-tagged CCR5 monomers, dimers and all protein 80, 167 and 400 mM imidazole respectively was necessary. A summary of all tested conditions can be found in Table 3.1.

17

Table 3.1 Imidazole concentration required for CCR5 elution from IMAC resin. Values are approximate and represent concentrations at which CCR5 monomer and dimer elution started to be observable on western blot and values necessary to complete the elution of all the oligomeric states.

IMAC Resin	Tag	Monomer	Dimer	All
GE Healthcare	6His-tag	60 mM	100 mM	300 mM
GE Healthcare	10His-tag	133 mM	250 mM	500 mM
Qiagen	10His-tag	80 mM	167 mM	400 mM

3.2.1.3 *Sf21, Sf9 and High Five insect cell lines*

In structural biology there are three most frequently used insect cell lines: Sf21, Sf9 and High Five. Sf21 and Sf9 originate from IPLBSF-21 cell line (85), which was derived from the pupal ovarian tissue of the fall army worm, *Spodoptera frugiperda*, and doubles every 24 and 72 hours, respectively. High Five™ (BTI-TN-5B1-4) (Boyce Thompson Institute for Plant Research, Ithaca, New York, USA) originates from the ovarian cells of the cabbage looper, *Trichoplusia ni*, and doubles every 18 h. Due to smaller size and regular shape Sf9 are exceptional for the formation of monolayers and plaques, while High Five features fastest growth and for selected proteins provide highest secreted expression. However, the fact that most of crystallized GPCRs was expressed in Sf9 suggests that in terms of functional GPCR expression Sf9 proved its high usefulness.

In this section we have compared Sf21 and High Five in terms of the quality of the expressed CCR5. The protein from both cell lines was purified in parallel on Ni-NTA and subsequently on Strep-Tactin resins using FC-12 as a detergent. After each purification step the eluate was analyzed on SDS-PAGE (Figure 3.3). His- and Strep-tagged CCR5 construct (MW=42661.3 Da, for the complete sequence see Figure 3.10 in section PTMs and sequence integrity) migrates on SDS-PAGE like a ~33 kDa protein, whereas CCR5 dimer like a ~55 kDa standard protein. Faster migration is common for membrane proteins and can be caused by the incomplete protein unfolding. The latter seems to be supported by the fact that CCR5 is able to form at least partially SDS-stable oligomers.
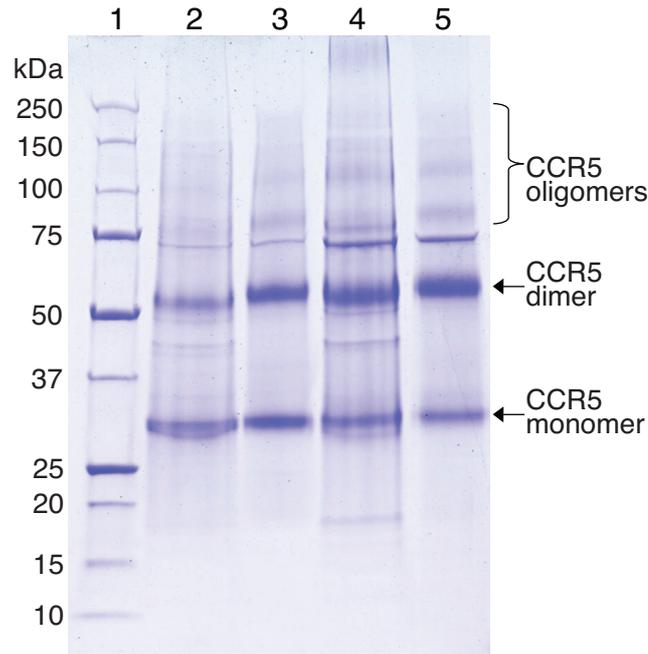
Figure 3.3 Two-step CCR5 purification in FC-12. Lane 1 (protein standards), lane 2 (IMAC-purified CCR5 from High Five), lane 3 (IMAC and Strep-Tactin-purified CCR5 from High Five), lane 4 (IMAC-purified CCR5 from Sf21), lane 5 (IMAC and Strep-Tactin-purified CCR5 from Sf21).

In general, CCR5 expression in Sf21 and in High Five was similar in terms of the yield and the purity. A sharp band of a contaminant migrating at ~75 kDa, later identified as Hsc70 (heat-shock cognate 70 kDa), was somewhat more pronounced in Sf21. The monomer:dimer ratio was a bit higher for High Five but as on SDS-PAGE the oligomeric state of CCR5 might have been altered by the presence of SDS and/or BME, both purified CCR5 samples were additionally analyzed using SEC (Figure 3.4). The chromatogram confirmed that the monomer:dimer ratio of the CCR5 from High Five was indeed somewhat higher but as this difference is rather small and as the physiological oligomeric state of CCR5 is not known definitively, a minor difference in monomer:dimer ratio might not be a good criterion to prefer one cell line over the other.
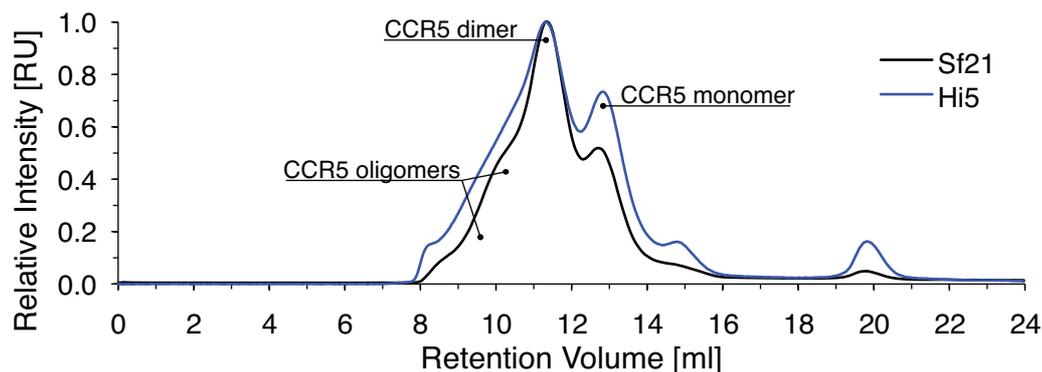
Figure 3.4 Size exclusion chromatography of IMAC and Strep-Tactin-purified CCR5. For convenient monomer:dimer ratio comparison, chromatograms of CCR5 expressed in Sf21 (black curve) and in High Five (blue curve) were scaled in such a way that dimer peak height equals 1.

3.2.1.4   Fos-Choline-12 versus DDM

Based on the research done previously in our group (82) FC-12 was selected as a main working detergent. The criteria that spoke for it at that time were: high CCR5 yield and purity (as judged by SDS-PAGE), homogeneity (as judged by TEM negative stain) and ability to maintain its native conformation (as judged by IP and ITC). While a separate chapter is dedicated to the IP, here the example of the purification in an alternative detergent is presented.

However at the time when this research was performed only a few GPCR structures were solved it was already clear that the number of membrane protein structures (solved by crystallography) in detergents with sugar head groups largely exceeds the number of structures in any other detergent group. DDM is one of the most widely used and it was also tested for CCR5. The parallel purification involved solubilization with 1.5% FC-12 and 2.5% DDM followed by Ni-NTA and Strep-Tactin chromatography. The eluate collected after each purification step was subjected to SDS-PAGE (Figure 3.5). It was possible to purify CCR5 in DDM but despite larger DDM concentration used for solubilization, the purity of CCR5 was clearly lower after each step in comparison to the purification in FC-12 and the final yield was only ~20-40% of the yield achieved for FC-12. Importantly, the presented purification in FC-12 is a representative example, whereas the purification in DDM is the best achieved outcome. Generally, purification in DDM (and other detergents with sugar head groups) resulted in unsatisfactory amounts of still impure protein.
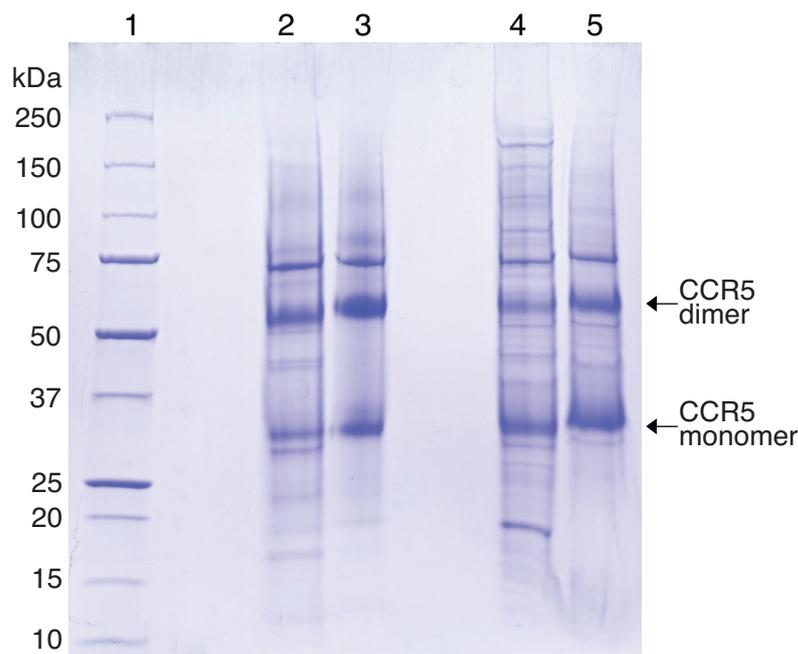
Figure 3.5 CCR5 purification in FC-12 and in DDM. Lane 1 (protein standards), lane 2 (IMAC-purified CCR5 in FC-12), lane 3 (IMAC and Strep-Tactin-purified CCR5 in FC-12), lane 4 (IMAC-purified CCR5 in DDM), lane 5 (IMAC and Strep-Tactin-purified CCR5 in DDM).

3.2.1.5   Removal of the persistent contaminant

Even though the imidazole concentration was carefully optimized and high salt (1M NaCl) and glycerol (10%) included in the washing buffer, there was always one strong contaminant band on SDS-PAGE which seemed completely resistant to the applied washing procedures on both IMAC and Strep-Tactin resins. This made us think (original idea of Sébastien Morin) that this contaminant is likely to interact directly with CCR5 and by this fail to wash out. The band was excised from a gel and send for MS analysis, which revealed that it is Hsc70. As Hsc70 binds substrates in ATP-dependent manner, the presence of ATP could trigger its dissociation from CCR5. Following this hypothesis, IMAC washing buffer was supplemented with 10 mM ATP and 20 mM $MgCl_2$, which resulted in almost complete removal of Hsc70 from CCR5 samples (Figure 3.6).
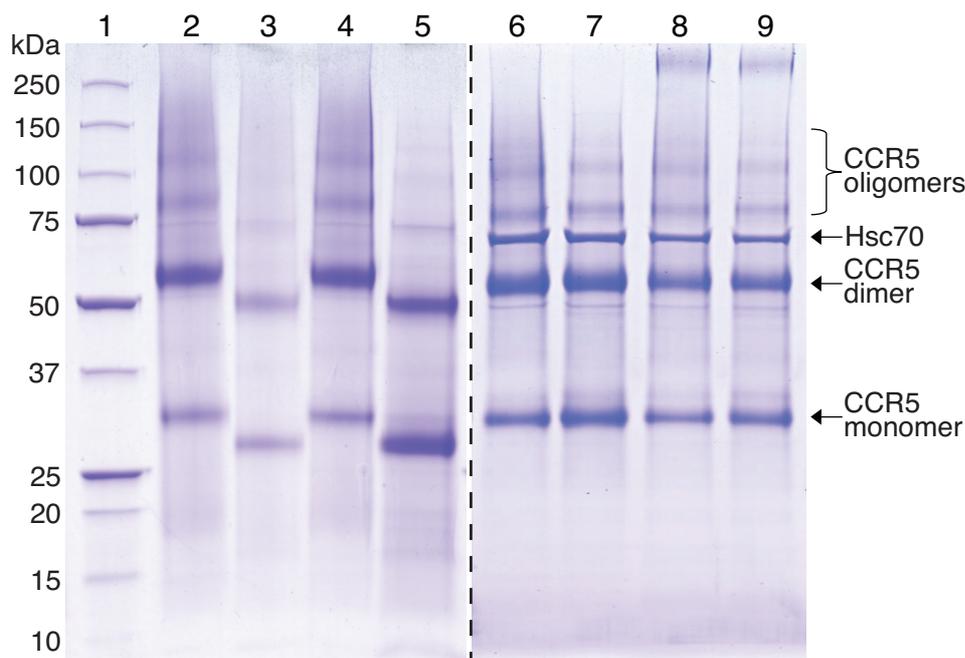
Figure 3.6 Removal of the persistent contaminant. The inclusion of ATP and $MgCl_2$ in the IMAC washing buffer removes Hsc70 from CCR5 samples. Lanes 1 (protein standards), Lanes 2-5 (various CCR5 samples purified with ATP and $MgCl_2$), lanes 6-9 (various CCR5 samples purified without ATP and $MgCl_2$). C-terminally truncated CCR5 constructs (lanes 3 and 5) migrate faster than the full length CCR5 (other lanes).

Characterization of CCR5 secondary structure

Having purified CCR5 we have addressed the question of its quality using CD. As GPCRs are composed of as many as seven α-helical TM domains, it was expected to observe a strong CD signal exhibiting two pronounced minima at around 209 and 222 nm. Approximately 2.5 μM CCR5 purified on IMAC and Strep-tag resins was subjected to the experiment and consistently with the expectation, characteristic double minima shape spectrum was observed (Figure 3.7). From the signal intensity at 222 nm it could be estimated that α-helical contents of CCR5 sample was ~43%. This value is in a good range but may seem a little too low. The reduction in ellipticity may be attributed to the absorption flattening effect, which occurs when chromophores are closely packed and in the case of CCR5 sample may result from the presence of oligomers. It also cannot be excluded that FC-12 micelle does not favor as much α-helical secondary structure as the lipid environment of a membrane.
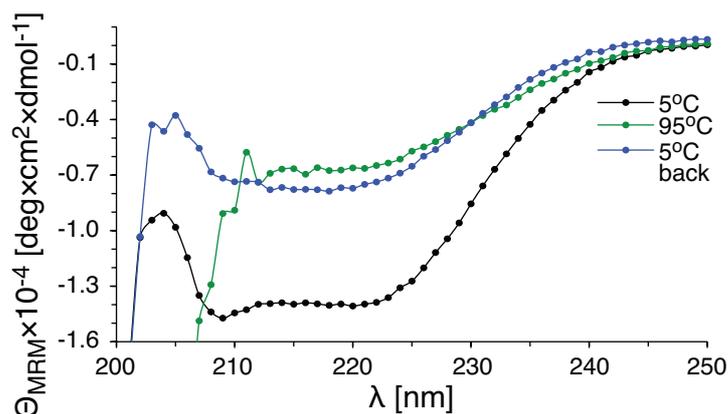
Figure 3.7 Circular dichroism spectrum of CCR5. The spectrum recorded at 5°C exhibits a double minima shape (black curve), which is lost upon heating (green curve). Secondary structure denaturation is irreversible (blue curve).

CD is also a good method to examine thermal stability. The loss of ellipticity can be monitored as a function of temperature. In Figure 3.8 the mean residue molar ellipticity at 222 nm was plotted against increasing temperature from 5 to 95°C. The resulting curve represents a broad thermal transition, which starts already around 10°C. Heating the sample to 95°C causes not only a decrease of signal amplitude but also a loss of the characteristic double minima spectral shape. Cooling the sample down back to 5°C does not restore the initial amplitude of the signal, which suggests that thermal denaturation of CCR5 is irreversible.
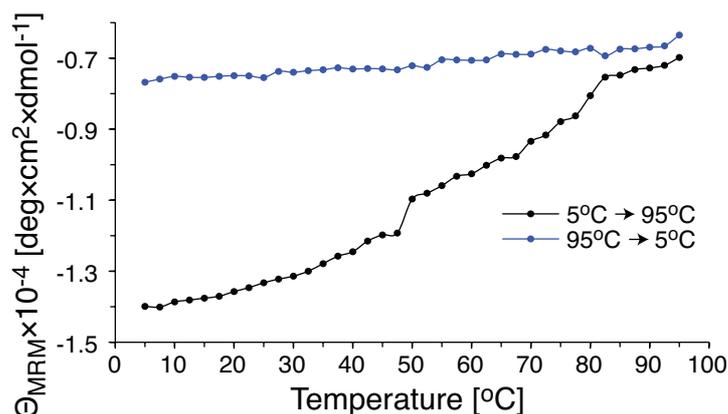
Figure 3.8 Mean residue molar ellipticity of CCR5 at 222 nm upon heating (black points) and cooling (blue points) shows a broad transition and the irreversibility of CCR5 secondary structure denaturation.

PTMs and sequence integrity

The next step in the quality assessment aimed at the confirmation of CCR5 integrity and the presence of the expected PTMs. Two solution CCR5 samples (eluted from IMAC and Strep-Tactin resins) were measured by MALDI-MS (Figure 3.9). Despite both samples were somewhat heterogeneous (contaminated by other proteins), CCR5 could be identified in each case. The pattern of the contamination peaks was similar in both cases, and not surprisingly, in sample 1 (after two purification steps) the CCR5 peak intensity was higher in relation to the intensity of the contamination peaks in comparison to sample 2 (after IMAC only). The measured m/z values 42621.3 and 42633.9 are higher than the monoisotopic mass calculated for the unmodified CCR5 (42359.1 Da), which suggests that the protein is indeed modified.
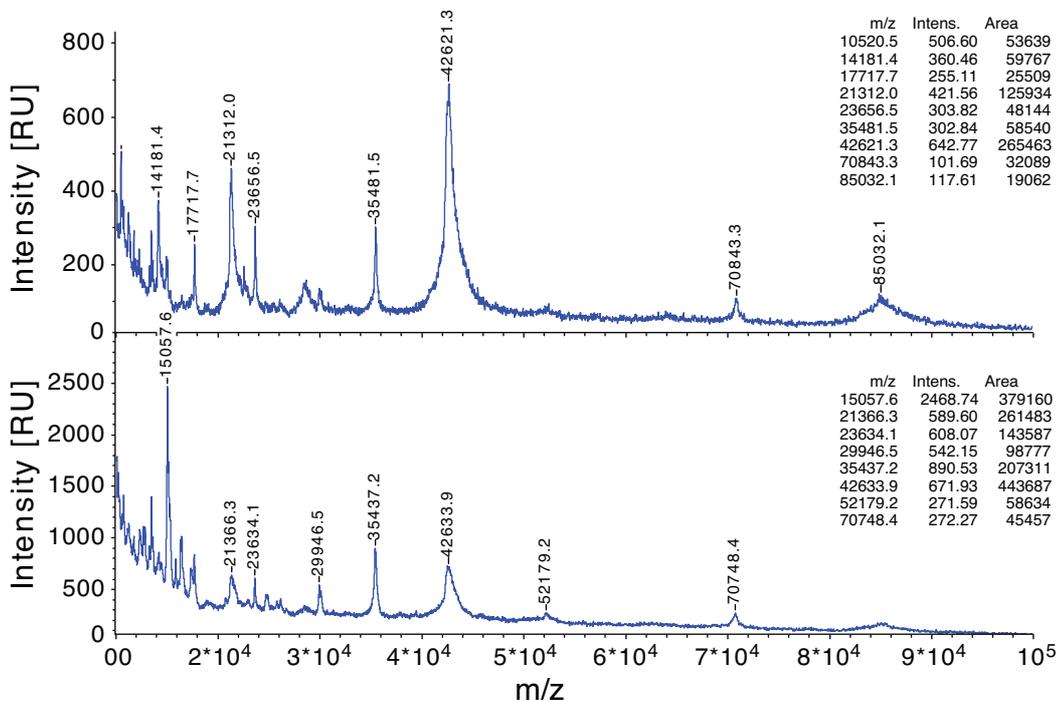
Figure 3.9 Mass spectra of CCR5 samples after IMAC and Strep-Tactin (top panel) and after IMAC (bottom panel). Judging from the elevated m/z values CCR5 seems to be modified.

To enhance the resolution of the analysis, CCR5 sample was precipitated, digested with trypsin and analyzed by MALDI-MS. The following CCR5 peptides could be identified (Figure 3.10):

- the N-terminal fragment MDYQVSSPIYDINYYTSEPCQK (acetylated),
- the 2nd ECL fragment EGLHYTCSSHFPYSQYQFWK,

24

- the 7th TM domain fragment LDQAMQVTETLGMTHCCINPIIYAFVGEK,

- the helix H8 fragment NYLLVFFQK and

- three sequential C-terminal peptides: CCSIFQQEAPER, ASSVYTR and STGEQEISVGLHHHHHHWSHPQFEK.

The identified sequences constitute only ~1/3 of the CCR5 construct sequence and with the exception of 7th domain and potential helix 8 encompass weakly or unstructured regions of the protein (both termini and a long loop). Poor sequence coverage is not surprising as the tightly packed hydrophobic CCR5 core is likely to be resistant to the proteolysis. It was solely proven that N-terminus of CCR5 is acetylated (m/z increased by 42 Da). None of the expected PTMs, that is sulfation and glycosylation of N-terminus and palmitoylation of C-terminus, could be detected despite the respective peptides were identified. After subtraction of acetyl (42 Da) and unmodified CCR5 (42359.1 Da) masses from the bigger of the detected m/z values (42633.9), there is ~233 Da left for other modifications. This is too little for even one palmitoyl moiety (+238) but sulfation (+80) or glycosylation with a single N-acetylglucosamine (+203) could be accommodated.
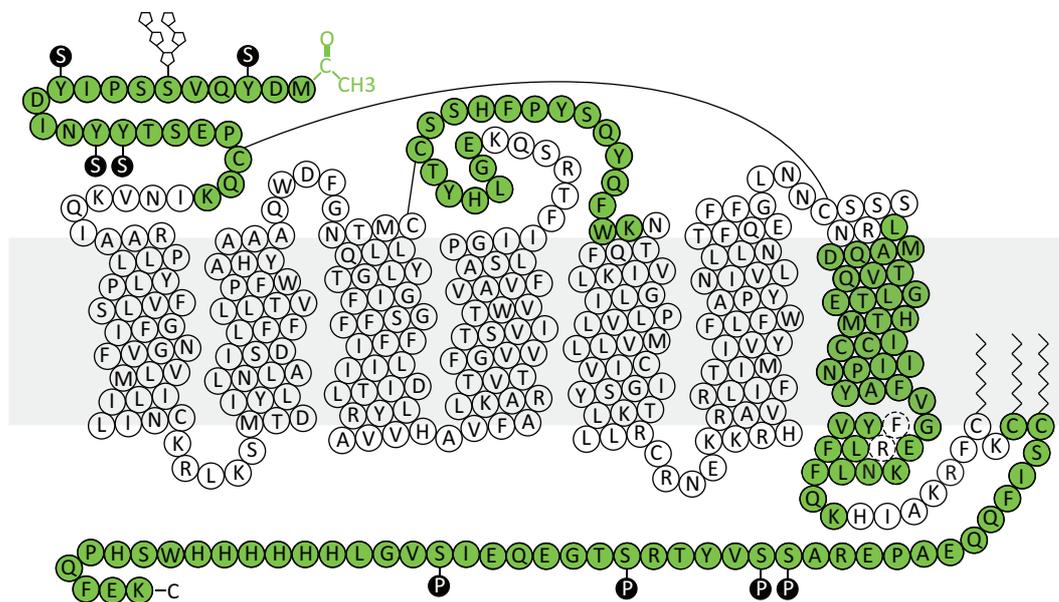
Figure 3.10 Sequence topology of the detected CCR5 peptides after trypsin digestion. Identified fragments (green filled circles) localize in N- and C-termini, 2nd ECL and TM domain 7, leaving TM domains 1-6 unrepresented.

These results taken together show that CCR5 expressed in Sf21 maintains its sequence integrity (both termini are not degraded) but it is not modified in a similar

way as it is in human cells. However, as the presence of PTMs may be dependent on the expression conditions, the latter conclusion holds only for this particular batch of CCR5.

Detergent screening

3.2.1.6   Introduction

Appropriate detergent system is the most important factor conditioning a successful preparation of a membrane protein. Wrong detergent can destabilize the protein, distort native structure, abolish activity or even denature protein completely. It can also lead to the formation of inhomogeneous in size and shape micelles, which will prevent crystal formation and decrease the quality of NMR signal. This chapter addresses the detergent screening issue from two different sides using two separate assays. The obtained readouts classify detergents according to two different parameters.

3.2.1.7   Detergent exchange assay

The first detergent screening assay differentiates detergents according to the ability to keep CCR5 in solution over several days at RT. The advantage of this approach is that it uses purified detergent-solubilized CCR5 as an input and thereby does not require a detergent to be able to solubilize CCR5 from a membrane or any kind of insoluble state. In this way, detergents, which create an environment favoring CCR5 solubility but are too mild to actively solubilize (extract) it into solution, are not excluded from the analysis. On the other hand, as the initial detergent is still present, the requirement for a purified detergent-solubilized protein biases the screen towards potential detergent incompatibilities. In other words, the precipitation of CCR5 resulting from its instability in a new detergent cannot be distinguished from a precipitation of an initial detergent by a new detergent, reasonably assuming that the forming precipitate can pull down CCR5 micelles. A similar complication involves the readout itself, that is SDS-PAGE, where ~2% SDS is present in sample buffer.

As FC-12 efficiently solubilizes CCR5 from insect membrane fraction and gives good yields of purified protein, a detergent exchange assay was performed with the FC-12-solubilized purified protein. CCR5 aliquots were supplemented with the

screened detergents up to 2% final concentration. The precipitate that formed over 6 days was removed by centrifugation. The supernatant was analyzed by SDS-PAGE (Figure 3.11) followed by a densitometric analysis of the monomeric and dimeric CCR5 bands. Subsequently, the obtained intensities were divided by the biggest value and plotted in Figure 3.12.
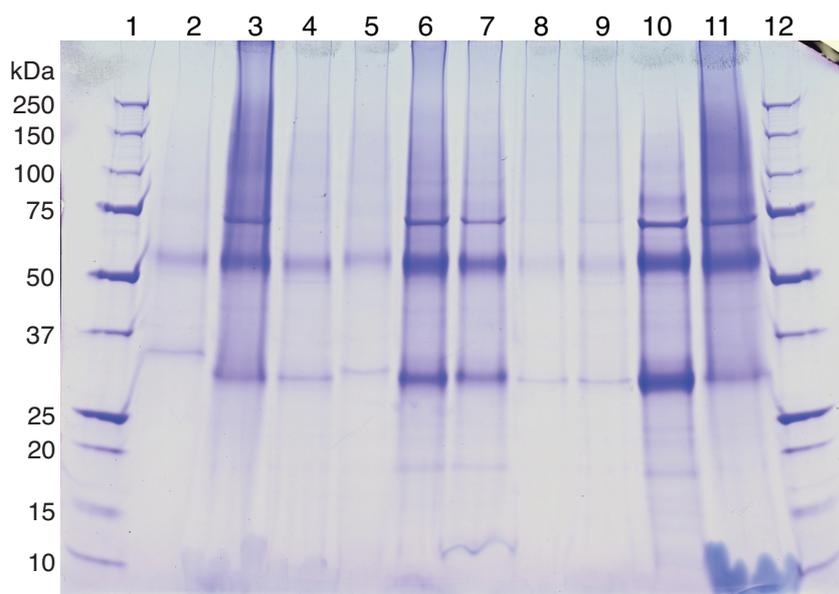
Figure 3.11 Example of detergent exchange screen raw data. Incompatible surfactants precipitate CCR5, which results in decreased CCR5 band intensities. Lanes 1 and 12 (protein standards), lane 2 (MP-8), lane 3 ($C_{12}E_9$), lane 4 (MP-11), lane 5 (Mega-9), lane 6 (DIFOS-12), lane 7 (FC-10), lane 8 ($C_{10}E_6$), lane 9 (DHPC), lane 10 (FC-12), lane 11 (Tween-20).

The amount of CCR5 kept in the solution was very different for various detergents. The results, ranging from no to a complete precipitation demonstrate the applicability of the approach to diversify detergents for their ability to keep CCR5 in solution. In general, alkyl anionic (SDS and SDDSAR) and zwitterionic (Fos-Cholines) but not bile acid based (NaC, CHAPS, CHAPSO) detergents performed better than nonionic detergents. Not surprisingly, the entire group of Fos-Cholines was very good, keeping as much as ~60-90% of CCR5 in a solution. Among nonionic detergents only 9 out of ~60 tested, including Tween-20, Brij-58, $C_{12}E_9$ and several representatives of maltoside family (TMP-12, TMP-10, TMP-8, MP-12, MP-6 and Cymal-7), kept more than half of CCR5 in the solution. Interestingly, detergents with glucose head groups precipitated nearly all CCR5. The only decent result of GP-6 with a CMC of ~6.6%

(similarly as other detergents with very short alkyl chains) is likely due to the insufficient amount of detergent to perturb CCR5 in the remaining FC-12.
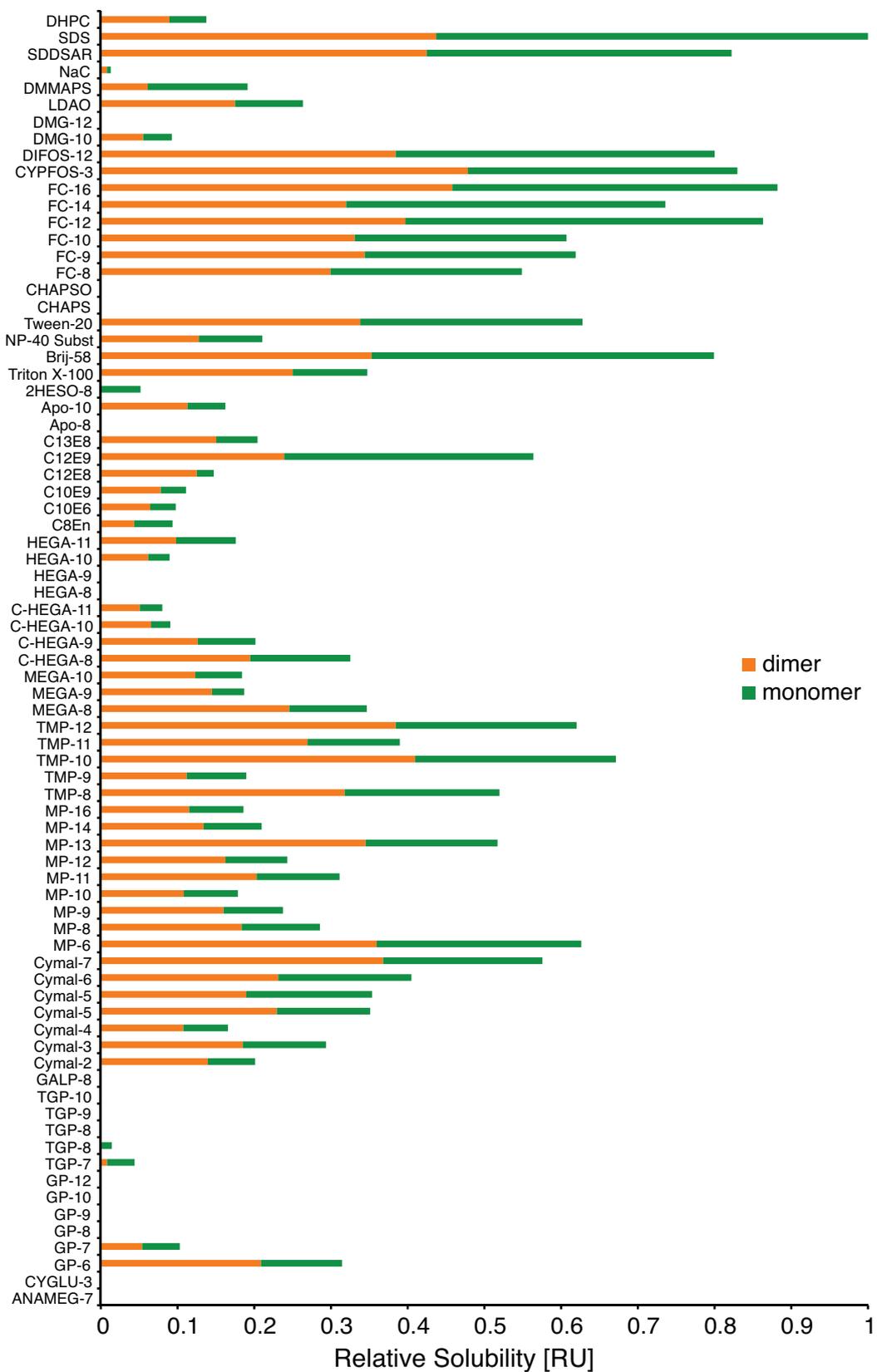
Figure 3.12 Detergent exchange screen with anionic (SDS to NaC), zwitterionic (DMMAPS to CHAPS) and nonionic (Tween-20 to Anameg-7) detergents.

As the solubility of CCR5 and detergent itself may depend on other factors such as pH and ionic strength, screening for optimal surfactants should take them into account. This would, however, add extra dimensions to already extensive analysis and normally requires high-throughput approach. Due to the technical limitation such multidimensional screen could not have been performed but the example of the pH and NaCl concentration effect on SDS-solubilized CCR5 is presented in Figure 3.13. In the case of anionic SDS a decrease of pH reduced CCR5 solubility. A decrease of salt concentration from 560 to 60 mM was however beneficial.
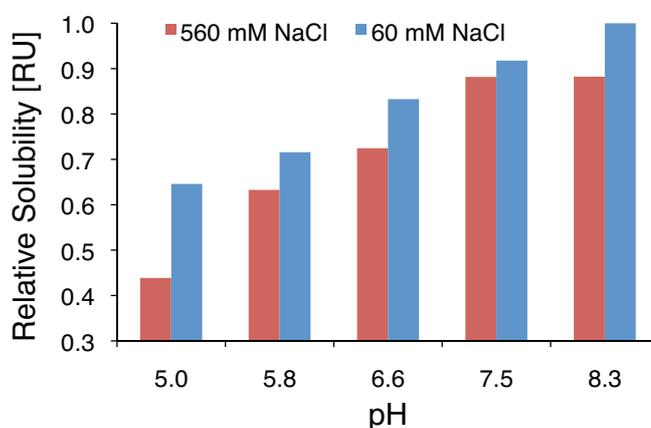
Figure 3.13 Dependence of pH and salt on CCR5 solubility in SDS.

3.2.1.8   Detergent solubilization assay

Another approach to detergent screening relies on the ability of a detergent to solubilize CCR5 from membrane fraction. The advantage of this approach is that it reveals candidates directly applicable for solubilization but in return it does not tell anything about protein stability in a longer timescale. In other words, it does require a detergent to efficiently solubilize CCR5 but does not require to keep it in a solution for more than few hours. Unlike the previous approach, this assay is also less biased because no other but tested detergent is present and the readout is SDS-free (SDS-PAGE is not involved).

Based on the results of the previous screen, the set of tested detergents was modified in a way to contain a broader representation of zwitterionic detergent families (Fos-Cholines, Anzergents, dimethylamine oxides and dimethylglycines) and also a

new family of cationic detergents was included (trimethylammonium chlorides). The nonionic family was represented by maltosides. Each family consisted of detergents with few different lengths of the alkyl chain.
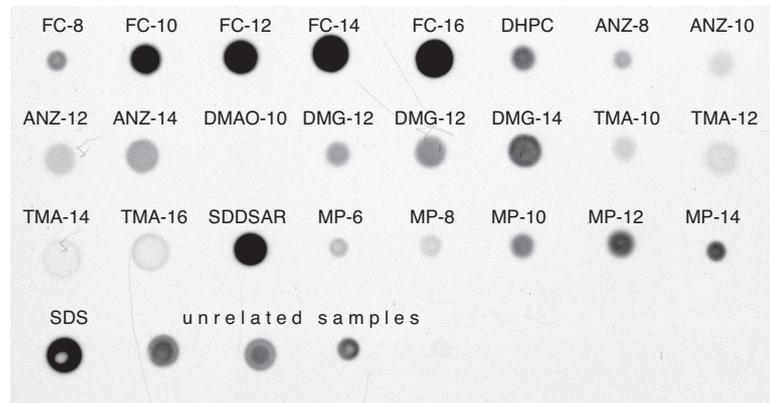
Figure 3.14 Detergent solubilization screen - raw data. Solubilized and clarified insect cell membrane fraction was dried on a nitrocellulose membrane and developed in a form of dot blot.

Due to the presence of other proteins solubilized from the membrane fraction, a CCR5-specific readout was necessary. Hence, the solubilized CCR5 was detected by anti-His-tag western blotting (Figure 3.14). Clear differences between tested detergents were observed, ranging from a complete lack of signal to a saturated spot. After densitometric quantification, analogously as previously, numbers were normalized for the biggest value (Figure 3.15). Similarly as before anionic SDS and SDDSAR and zwitterionic Fos-Cholines performed very well solubilizing ~60-100% of CCR5. Other zwitterionic detergents (with the exception of DMG-14 which solubilized ~40%) solubilized <30% of CCR5, while the best of nonionic maltosides ~30%. A clear trend, the longer the alkyl chain the more solubilized CCR5, can be observed in almost all of the tested detergent families.
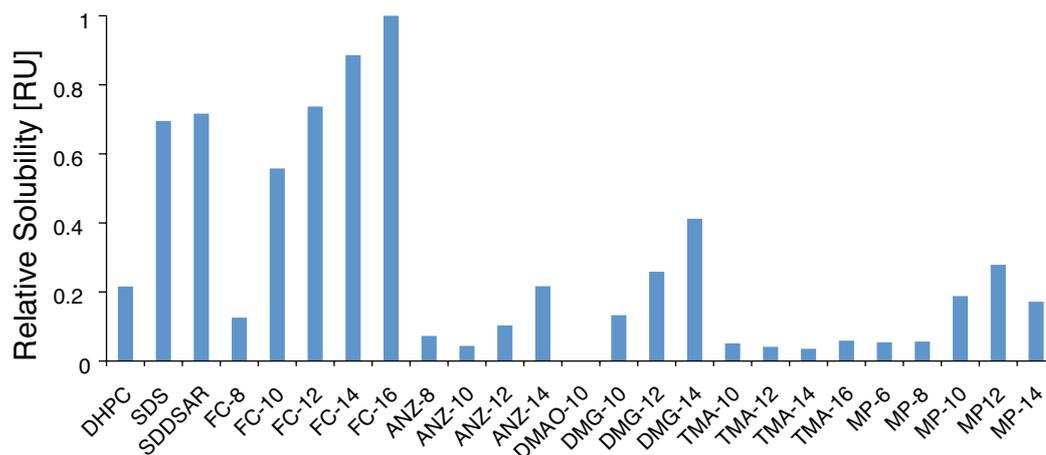
Figure 3.15 Detergent solubilization screen presented as densitometrically-quantified dot blot signal reveals promising candidates for CCR5 solubilization.

Immunoprecipitation with 2D7

3.2.1.9   Introduction

So far the studies focused on the CCR5 yield, purity, integrity and gave some insight into the oligomeric state, secondary structure and its detergent preferences. All these experiments constitute indispensable starting points of structural and functional analysis but do not yet answer the question, whether the isolated CCR5 possesses its native properties. Desirable features would include: the ability to bind ligands, to interact with G proteins and trigger signaling cascade, to interact with drugs or any kind of readout that confirms that CCR5 maintains its native structure.

Some of these properties are very challenging to study because they require many other components (proteins, cellular environment, etc.) to be present and simply cannot be studied in a micellar system. Fortunately, many CCR5-specific antibodies have been already developed and some of them like for example 2D7 (CD195) are conformation-dependent, which means that they recognize a nonlinear structural motif on the 2nd ECL only when CCR5 maintains its native structure. Hence, 2D7 is widely used in the field as a CCR5 native conformation probe.

3.2.1.10 Detergent impact on 2D7 recognition

It has been reported using IP that 2D7 could recognize CCR5 solubilized in Cymal-5 but not in FC-14 or DHPC (86). Another group showed using SPR that CCR5 solubilized in detergents with maltose head group maintain more 2D7 binding ability than CCR5 solubilized in any other detergent family (87). For our purpose, CCR5 native conformation was probed using IP with 2D7 antibody. This assay does not require purified protein and can be performed directly on the clarified detergent-solubilized membrane fractions. In brief, solubilized membrane fraction was centrifuged to remove insoluble material, supernatant was mixed with 2D7 (CCR5 binding to Fab of 2D7) and transferred to a resin with immobilized protein G (binding of 2D7 Fc to protein G). The unbound material was removed by washing. An addition of SDS-PAGE sample buffer (containing SDS and BME) resulted in a dissociation of the proteins, which could be subsequently analyzed by western blotting.

Due to their harshness (SDS is used to disrupt CCR5 interaction with 2D7), SDS and other anionic detergents were not tested in this assay. Instead, the selection of detergents contained a broader representation of maltosides with alkyl or cyclic, shorter or longer chains connected with head groups by glyco- or thioglycosidic bonds. 2D7 immunoprecipitated CCR5 solubilized in any of the tested maltoside detergents, regardless of chain length and type (Figure 3.16). Interestingly, it was not the case for other nonionic ($C_{12}E_9$) and zwitterionic (Fos-Cholines) detergents, which in the previous detergent screens showed to keep CCR5 in the solution ($C_{12}E_9$ and Fos-Cholines) and to efficiently solubilize CCR5 from a membrane fraction (Fos-Cholines). These results clearly overlap with the findings of Mirzabekov (86) and Rich (87).
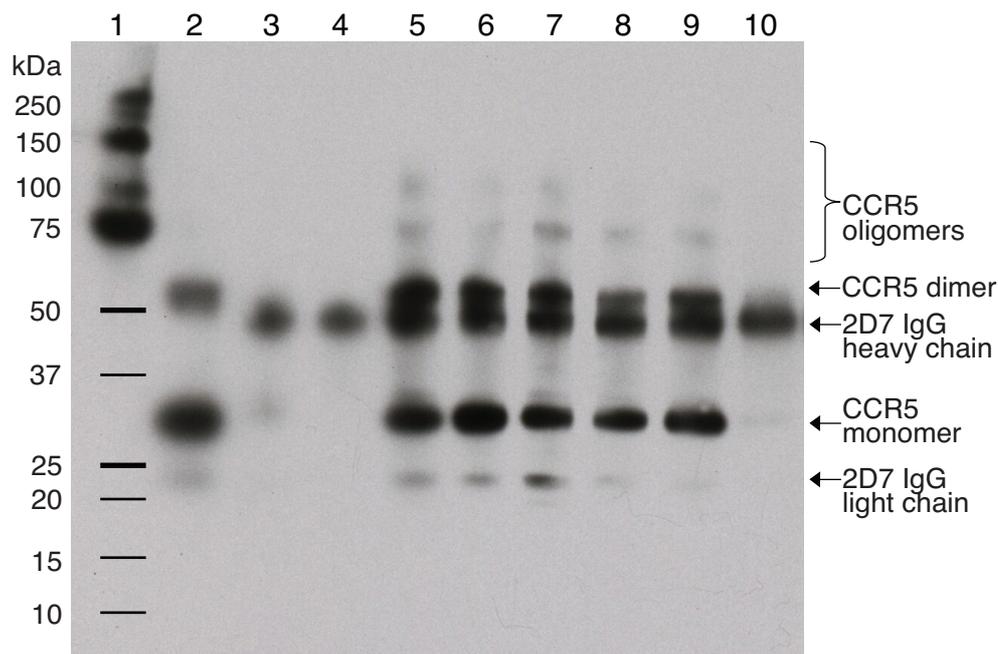
Figure 3.16 2D7 immunoprecipitation of CCR5 solubilized in various detergents. As both, 2D7 and anti-His-tag, antibodies were from mouse and as western blot development involved secondary anti-mouse antibody, both CCR5 and IgG (not always) bands are present. Lane 1 (protein standards), lane 2 (positive control), lane 3 (FC-10), lane 4 (FC-12), lane 5 (DDM), lane 6 (Cymal-5), lane 7 (Cymal-7), lane 8 (TMP-8), lane 9 (TMP-10), lane 10 ($C_{12}E_9$).

3.2.1.11 Effect of buffer conditions

To make sure the outcome of the IP assay is not dependent on other factors such as buffer and salt type as well as salt concentration or the stringency of membrane fraction washing before solubilization, 2D7 recognition was tested for membrane fractions washed either once or three times in two different buffers. Buffer 1A was composed of 20 mM negatively charged phosphate and 300 mM mono-charged NaCl ions. Buffer 1B contained 20 mM positively charged Tris and only 100 mM $(NH_4)_2SO_4$ dissociating into double-charged sulfate (VI) ions. Both buffers contained 10% (v/v) glycerol. Regardless of the conditions, 2D7 always immunoprecipitated CCR5 in Cymal-5 but never in FC-12 (Figure 3.17). This demonstrates that in the tested conditions, buffer conditions and the stringency of membrane fraction washing did not have an effect on 2D7 binding.
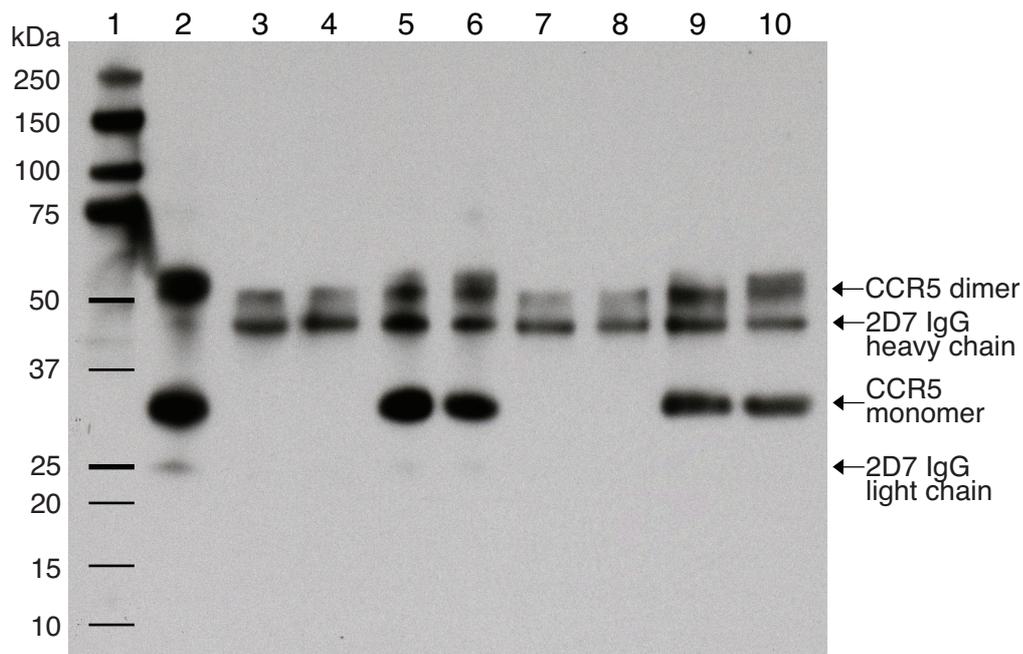
Figure 3.17 CCR5 immunoprecipitation with 2D7 antibody is not affected by buffer conditions and membrane washing. Lane 1 (protein standards), lane 2 (positive control), lane 3 (membranes washed 1x in buffer 1B, solubilized in FC-12), lane 4 (3x, 1B, FC-12), lane 5 (1x, 1B, Cymal-5), lane 6 (3x, 1B, Cymal-5), lane 7 (1x, 1A, FC-12), lane 8 (3x, 1A, FC-12), lane 9 (1x, 1A, Cymal-5), lane 10 (3x, 1A, Cymal-5).

3.2.1.12 Other observations

Following the concept of the IP experiment described above, the impact of several other factors on 2D7 recognition has been checked (Figure 3.18). A sample solubilized 4 days prior to the IP assay could not be immunoprecipitated. This could be a symptom of CCR5 losing its native conformation over time and/or a result of a proteolytic processing of the C-terminus, where His-tag (used for western blot development) is located. To verify the latter hypothesis, samples of solubilized membrane fraction were collected (and frozen) over several days of storage. Even though the samples were not subjected to any further processing (no IP), a decrease of western blot signal could be observed (data not shown).
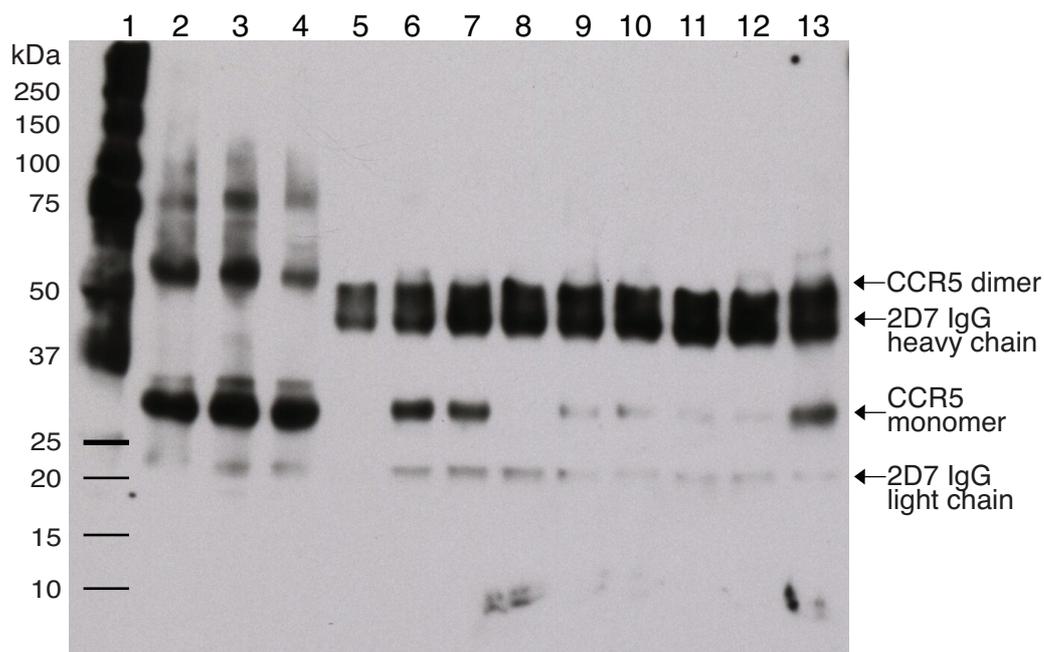
Figure 3.18 Inhibition of 2D7 immunoprecipitation of Cymal-5-solubilized CCR5. After solubilization insect cell membrane fraction was clarified at 17000 g for 15 min (lane 2) or at 100000 g for 20 min (lane 3) and purified on IMAC resin (lane 4). Immunoprecipitation was performed with: membranes solubilized 4 days before (lane 5), solubilized membranes clarified at 17000 g for 15 min (lane 6) and at 100000 g for 20 min (lane 7), protein eluted from IMAC resin (lane 8). A decrease of CCR5 signal was observed when 3.33% Cymal-5 (lane 9), 1.67 M urea (lane 10), 83.3 mM MES pH 5.5 (lane 11) or 1 M imidazole (lane 12) but not when 107 μM RANTES (lane 13) were added.

Secondly, the signal intensities of immunoprecipitated CCR5 after centrifugation at 17000 g for 15 min and at 100000 g for 20 min are very similar, which suggests that clarification using a tabletop centrifuge (17000 g, used for small volumes) and ultracentrifuge (100000 g, used for preparative scale) gives a comparable result. This conclusion holds upon making an assumption that in this assay 2D7 binding sites were in excess.

Thirdly, IMAC-purified CCR5 eluted with imidazole did not immunoprecipitated with 2D7, the same as unpurified CCR5 supplemented with imidazole, suggesting that imidazole inhibits CCR5 and 2D7 interaction. In a similar way CCR5:2D7 interaction was also inhibited by high concentrations of detergent, urea and by a pH decrease. Interestingly, inclusion of RANTES had only a moderate effect.

CCR5 size distribution and stability

Structural biology requires stable and homogenous samples. Although, monodispersity is an important and desirable parameter of a good sample for structural studies, many GPCRs are known to form dimers and higher oligomers. It is a matter of debate if, which and to what extent GPCR oligomers are physiological functional units or a result of biologically irrelevant interactions. The oligomerization behavior of GPCR may depend on the environment such as cell type, expression level, lipid composition, ligands, other proteins, etc. Artificial environment of detergent micelles may strongly affect (inhibit or promote) oligomerization. Sometimes chaotic oligomerization behavior may be a symptom of poor sample stability.

The size and oligomeric state of insect cell-expressed CCR5 was investigated by SEC (Figure 3.4) and DLS (Figure 3.19). Judging from the band pattern on SDS-PAGE (Figure 3.3) or western blot (Figure 3.2), the CCR5 sample was composed of monomers, dimers (dominant) and higher oligomers (trimers and tetramers). SEC column was calibrated using standard globular proteins and from the calculated standard curve it could be estimated than CCR5 monomeric and dimeric micelles are ~120 and 233 kDa, respectively. Values obtained form SLS measurement were somewhat smaller but in the same range, 94 kDa for monomer and 160 kDa for dimer.
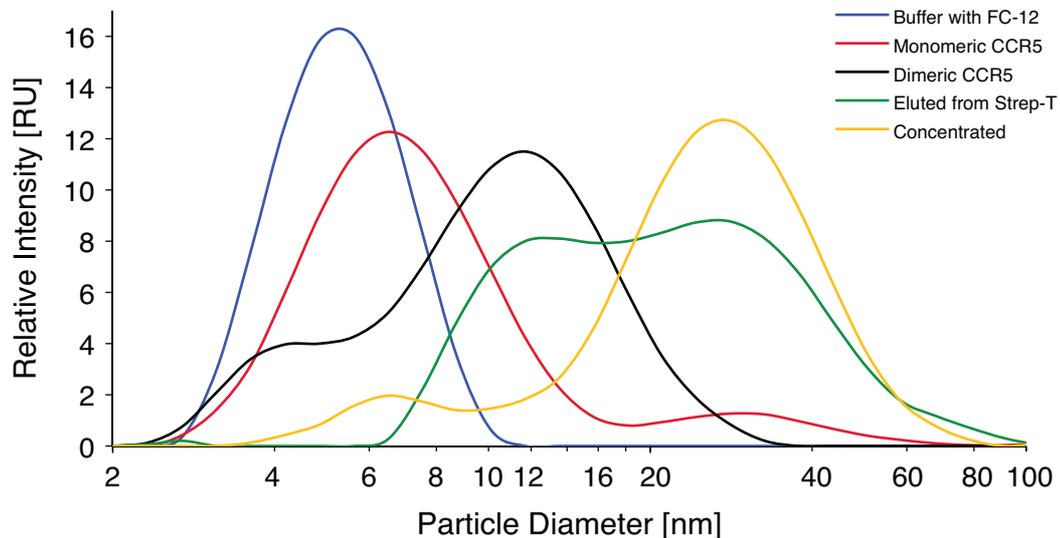
Figure 3.19 Dynamic light scattering with various CCR5 samples.

As for SEC sample usually needs to be concentrated enough to be detectable by UV and is subsequently heavily diluted during the run, conclusions about the initial

oligomeric state have to be drawn with care. In other words, if oligomerization is a concentration derivative of a sample being in an equilibrium, it is difficult to state what protein (and detergent) concentration does a certain elution profile represent. Hence, being more interested in detecting than in the absolute particle sizes, we have turned to DLS, which is a noninvasive technique enabling particle sizing directly in a sample volume. Figure 3.19 shows that it is possible to differentiate between empty micelles, CCR5 monomers, dimers and oligomers and that upon concentration the average particle size increases. It could also be indirectly shown that, at least to some extent, CCR5 oligomerization/aggregation is a result of disulphide bridge formation by reactive cysteines. Average particle size of CCR5 sample increased upon concentration and over time (Figure 3.20A). This effect was much less pronounced when reduced Cys were overreacted with tetramethylrhodamine (Figure 3.20B).
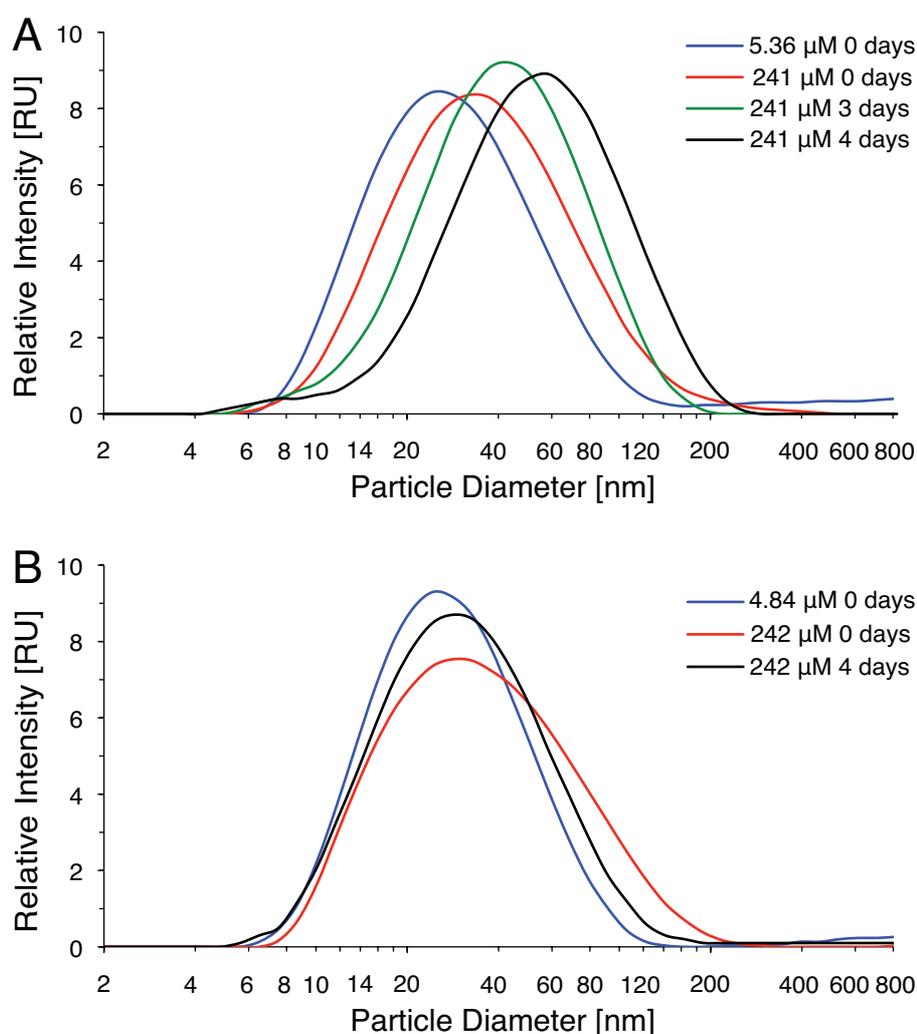
Figure 3.20 Average CCR5 particle size increases upon sample concentration and storage (A) and to much extent after blocking cysteines (B).

Construction of C-terminally truncated CCR5

The observation that CCR5 aggregates in a cysteine-dependent manner led us to the conclusion that CCR5 sample stability may benefit from removing some of the cysteine residues from the CCR5 sequence. After learning from MS analysis that C-terminal cysteines most likely are not palmitoylated, their removal became a logical first step. The C-terminal truncation appeared a better solution than mutagenesis as it also removes a large stretch of the unstructured C-terminus, which would have to be removed anyway, when crystallization trials were considered.

Based on the available CCR5 membrane topology prediction presented by Oppermann (88) two versions of C-terminal CCR5 truncation were designed (Figure 3.21). As according to the proposed topology helix 7 ends at Trp300 and helix 8 is not predicted, in the first version of the C-terminus truncation CCR5 sequence ends at Asn306. In the second version the sequence continues for another 13 amino acids passing hydrophobic stretch YLLVFF and ending on Arg319, which is the last polar residue before a cysteine cluster. In order to improve the purification on Ni-NTA resin (enhance purity by more rigorous washing) the His-tag was extended from 6 to 10 histidines. These two truncation constructs we subsequently expressed in both insect cells, where they were used to study CCR5 oligomerization (Sébastien Morin, unpublished data) and *E. coli* (see Chapter 4). For the expression in insect cells, an eight residue Strep-tag sequence WSHPQFEK was included at the very end to allow for an additional optional Strep-Tactin affinity purification. A list of the new CCR5 constructs for insect cell expression can be found in Table 3.2.

After the CXCR4 structure was published, we have made a CCR5 homology model, from which a topology prediction could be derived (see Chapter 4). Our model predicts also a potential helix 8. This would mean that the position of the Asn306 truncation unfortunately lies in the middle of the α-helical stretch. However, as helix 8 was not always present in the crystallized GPCRs including CXCR4, it is unlikely that such truncation would affect the overall structure of the receptor.
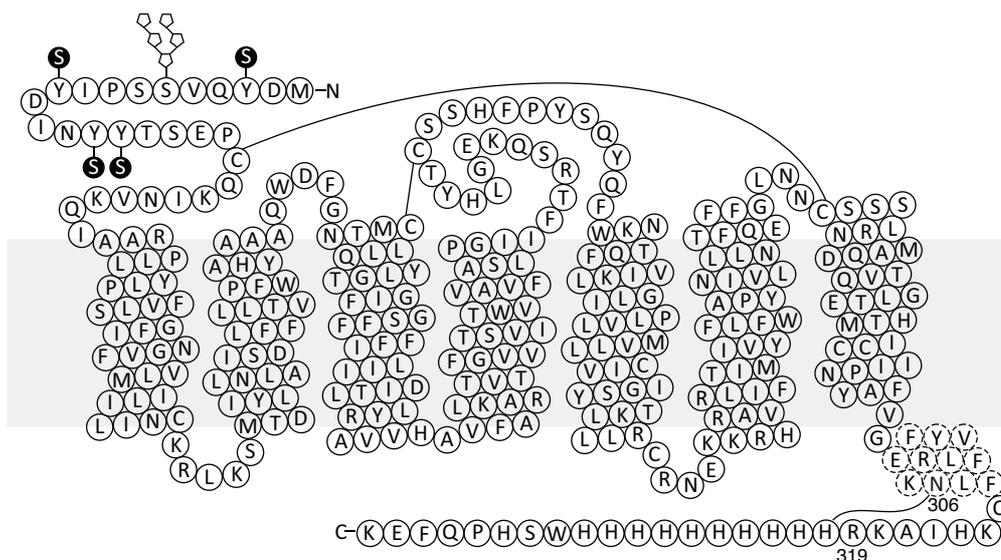
Figure 3.21 Two versions of the C-terminally truncated CCR5 construct designed based on Oppermann's CCR5 topology (88) but depicted on the topology derived from our homology model, which is based on the CXCR4 X-ray structure (23). The potential helix 8 was marked by dashed lines.

Table 3.2 List of CCR5 constructs cloned for insect cell expression. Constructs 2 and 3 are new. The constructs were used to study CCR5 oligomerization (Sébastien Morin, unpublished data).

No.	Name	Length	Mutations	C-terminal Tags
1	CCR5	1-352	wild type	His6-tag, Strep-tag
2	m2CCR5[306]	1-306	C58S, C224S	His10-tag, Strep-tag
3	m2CCR5[319]	1-319	C58S, C224S	His10-tag, Strep-tag

Preliminary SPR studies

SPR is a very robust and sensitive method to study protein interactions. Remarkably low sample requirements (picograms), no necessity of extensive purification or isotope labeling make SPR a widely applicable tool in the GPCR field, where obtaining large amounts of pure labeled material is often challenging. Studying protein-protein or even protein-drug interactions, screening for solubilization and crystallization conditions are only some of the wide variety of SPR applications (89-91).

For our purposes SPR was used to check CCR5 sample quality (interaction with 2D7) and to study its interaction with RANTES. Due to the high aggregation tendency of the wild type RANTES, less aggregating RANTES-E66S was chosen. First, the purified CCR5 was immobilized on Ni-charged NTA chip via its C-terminal His-tag (Figure 3.22). Each CCR5 injection resulted in an increase of SPR signal caused by the

39

presence of the immobilized receptor. The amplitude of each consequent increase was smaller than the previous one, which is a symptom of saturating the binding sites.
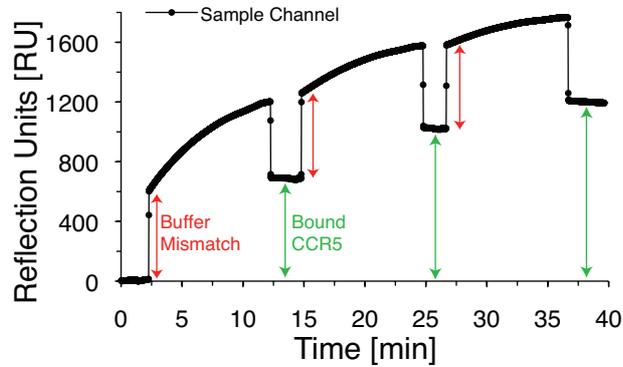
Figure 3.22 Immobilization of the FC-12-solubilized purified CCR5 (266 nM) on Ni-charged NTA chip. Each of the three injections cause a baseline increase, first ~690 RU, second ~340, third ~170 (green lines). The sudden signal jumps in the beginning and in the end of the injections are caused by a buffer mismatch (red lines).

No 2D7 binding could be observed for CCR5 in FC-12, which overlaps with the results of the IP assays. Subsequently, 500 nM RANTES-E66 solution was injected. An increased of SPR signal was observed in both reference (Ni-NTA) and sample (Ni-NTA with immobilizaed CCR5) channels (Figure 3.23A). As the reference and the sample channels are aligned sequentially (sample channel after reference channel), the sample channel experiences a decreased initial RANTES-E66 concentration and initially the net signal (sample channel – reference channel) is negative (Figure 3.23B). When the reference channel saturates, the net signal becomes positive because the RANTES-E66S dissociation rate from the sample channel (with CCR5) is slower than from the reference channel. Unspecific RANTES-E66S adsorption to the reference channel results in the fact that the binding curve is a sum of two separate interaction events (RANTES-E66S to the Ni-charged NTA chip and RANTES-E66S to the Ni-charged NTA chip with immobilized CCR5) and cannot be fitted and interpreted as a single RANTES-CCR5 binding event.
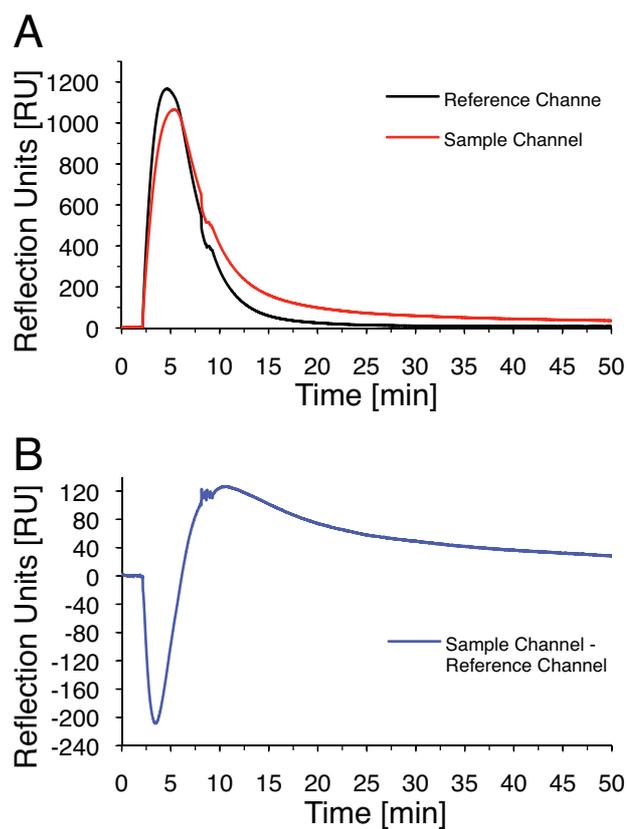
Figure 3.23 Binding of 0.5 µM RANTES-E66S to FC-solubilized purified CCR5 immobilized on Ni-charged NTA chip. (A) Separate signals from the reference (black curve) and the sample (red curve) channels. (B) Net signal (blue curve) signals is a result of subtraction of the reference channel signal from the sample channel signal.

To investigate the unspecific RANTES-E66S binding to the the Ni-charged NTA chip, several difference salt and pH conditions were tested (Figure 3.24). As before, a strong RANTES-E66S adsorption was observed at 150 mM NaCl pH 7.4. An increase of NaCl concentration fro 150 to 300 mM resulted in significant reduction of the unspecific binding. The increase of pH from 7.4 to 8.6 had a similar but much smaller effect. Further increase of NaCl concentration further decreased unspecific interaction up to bearly detectable level at 800 mM pH 7.4 or even at 500 mM pH 8.6.
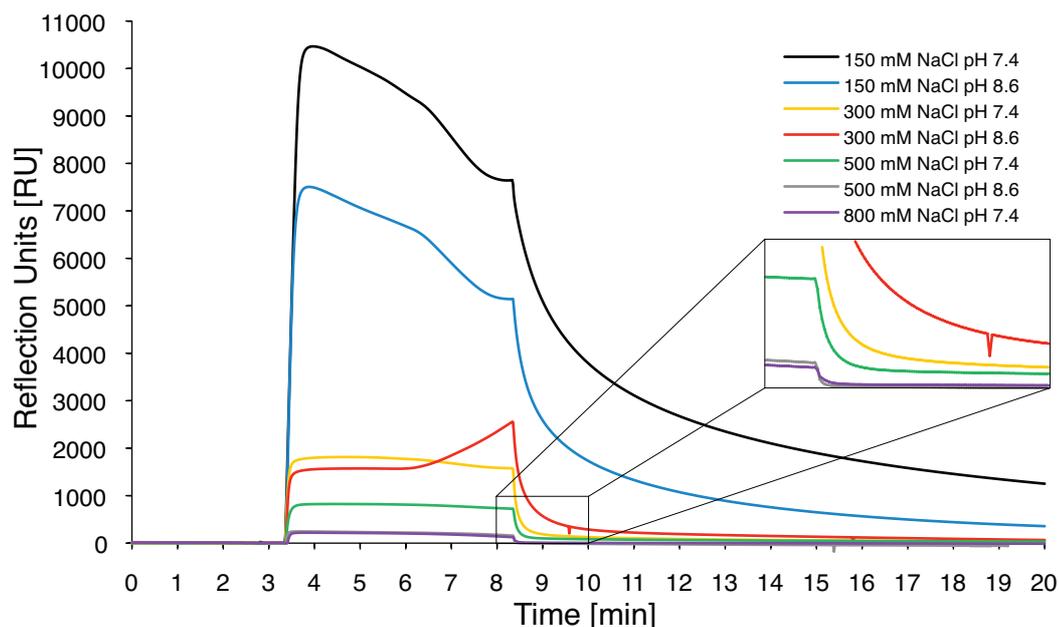
Figure 3.24 Unspecific RANTES-E66S (10 μM) interaction with Ni-charged NTA chip is salt- and pH-dependent.

3.3 Discussion

Due to its direct involvement in HIV infection and other diseases CCR5 is a natural drug target. However, as CCR5 is also involved in immune system regulation, targeting it with drugs requires high precision and selectivity. For this reason a three dimensional CCR5 structure is highly desirable, since it would reveal atomic details of the CCR5 molecular architecture and the mechanism of the interaction with ligands.

To study CCR5, an insect cell-based expression system was previously established in our laboratory (82). It typically provided ~1 mg of CCR5 after two step purification per 1L of insect cell culture. FC-12 was selected for CCR5 solubilization as it gave the most homogenous population of particles as judged by EM negative staining and supported 2D7 recognition as judged by IP assay. In this work we sought to characterize our CCR5 production platform in more detail, polish the protocols towards the higher yield and purity and study CCR5 interactions with ligands.

First, the concentrations of imidazole used for Ni-NTA purification were optimized in a way such that maximum amount of CCR5 and minimum amount of contamination are bound, that no CCR5 is lost during washing and that elution is efficient and complete. For the Ni-charged Chelating Sepharose resin from GE Healthcare and 6His-tag CCR5 these conditions translate to about 20 mM imidazole for

binding, 40 mM for washing and 400 mM for elution. For the Strep-Tactin purification the D-desthiobiotin concentration used for elution was doubled to 5 mM as 2.5 mM was not sufficient to fully and efficiently elute all bound CCR5. It was also noticed that plenty of CCR5 remains unsolubilized and an increase of detergent:protein ratio during solubilization (from 1% to 1.5-2.5%) boosts the yield. All these modifications together doubled or even tripled the final yield of purified CCR5 (maximum 3.2 mg/L) and enabled us to fully take advantage of the established CCR5 insect expression system.

To increase the purity, the biggest CCR5 contamination observed on SDS-PAGE gels was analyzed by mass spectroscopy and identified as Hsc70, which is a ubiquitously expressed heat shock protein, a chaperone that constitutes an important element of protein folding machinery. As Hsc70 binds hydrophobic sequences (e.g. CCR5) in an ATP-modulated manner (binding is reversible in ATP-bound state), it could be successfully depleted by the inclusion of magnesium ions and ATP in the Ni-NTA washing buffer. However, the fact that it interacts with CCR5 may indicate that the receptor is recognized by insect cell as misfolded protein and/or it experiences some folding problems. Perhaps it is also one of the reasons that CCR5 cannot be efficiently and stably solubilized by maltoside detergents (described later).

The expression in an alternative insect cells strain High Five was explored and compared to the expression in Sf21. Both the yield and the purity of the CCR5 purified from each strain were comparable, with a little bit lower Hsc70 contamination of High-Five expressed receptor. The monomer:dimer ratio was a bit higher for High Five but within a batch to batch variability.

Based on the calibration of the size exclusion column with standard proteins it could be calculated that CCR5 dimer and monomer migrate as spherical particles of ~233 and ~120 kDa, respectively. The values obtained by SLS are a bit smaller but within the same range, ~160 for dimer and ~94 kDa for monomer. The sizes obtained previously by Nisius are smaller: 130 and 75 kDa (82), which after careful inspection is likely to be a result of the incorrect SLS device setup (wrongly typed UV extinction coefficient of CCR5, that is 7.110e+2 instead of 1.420e+3 mL/[g×cm]). This seems to be confirmed by the fact that the retention volumes of CCR5 dimer and monomer peaks in Figure 3.25 overlap with the CCR5 chromatogram by Nisius (82), which suggest that the CCR5 particle sizes must have been very similar indeed.
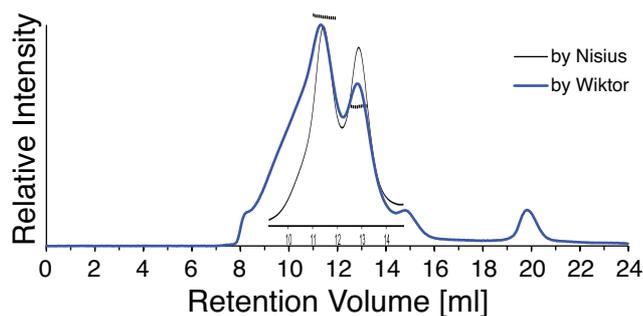
Figure 3.25 Overlay of the CCR5 chromatogram from Figure 3.4 with the chromatogram presented by Nisius (82). The proportions of the chromatogram has been modified to match both scales.

The function of CCR5 in native tissues requires several PTMs. Eukaryotic systems such as insect cells are much closer to human than *E. coli* and are expected to process proteins in a similar way. To investigate the quality of PTMs of the CCR5 expressed in our Sf21 system MS analysis was performed. The measured whole construct mass of 42633.9 kDa is however only slightly (~275 Da) higher than the monoisotopic mass of the CCR5 construct (42359.1 Da), which is by far not sufficient to accommodate the C-terminal palmitoylations. To enhance the resolution of the MS analysis the peptides resulting from CCR5 trypsinolysis were analyzed and also no modifications could be found on the identified N- and C-terminal CCR5 peptides. In addition, it could be solely proven that the N-terminus is acetylated, which was a unexpected modification. However it cannot be completely excluded that some of the more fragile modifications e.g. sulfation may be removed during sample processing and the presence and amount of PTMs is probably to some extent batch to batch dependent, in general, the results were a bit disappointing. This shows that even eukaryotic systems such as insect cells have to be carefully inspected for their ability to perform the expected human-like PTMs.

Based on the CD analysis, the spectrum of FC-12-purified CCR5 exhibited a characteristic double minima shape, which means that the sample is abundant in α-helical secondary structure. Based on the mean residue molar ellipticity at 222 nm it could be estimated that α-helical contents of purified CCR5 is 43%. This value is close to ~50% expected from a typical GPCR (92, 93) and confirms that the FC-12-purified CCR5 is, at least based on CD, reasonably well folded. The subsequent thermal denaturation showed that during heating both features of the CCR5 spectrum: the shape and the amplitude are irreversibly lost. CCR5 undergoes a broad transition, which starts

44

already around 10°C, which suggests that at the tested conditions the receptor is unstable. As melting temperature of CCR5 has not been reported in the literature to compare with, such low thermal stability may be either a natural property of the receptor or a symptom of nonoptimal solubilization conditions.

To search for better surfactants large-scale detergent screening was performed. The selection of a suitable detergent is an important and often a challenging issue in membrane protein research. A suitable detergent:

- should solubilize (destroy) the membrane but should not affect (denature) the protein (its structure and function),
- should keep the protein soluble and prevent aggregation but should not interfere with crystallization,
- should provide enough of hydrophobic environment such that protein function is maintained but should produce small, homogenous, well tumbling micelles for NMR, etc.

In practice, fulfilling all these criteria at the same time is often difficult, especially when it comes to more complex and fragile systems like for example mammalian membrane proteins.

In the case of CCR5 it turns out particularly challenging to find one universal detergent that would fulfill all the expectations. Performed detergent screening revealed several promising candidates able to solubilize CCR5 from the membrane fraction and keep the receptor in solution. As shown by two independent assays anionic (SDS, SDDSAR) and zwitterionic detergents (especially Fos-Cholines) are effective at CCR5 solubilization and keeping in solution to facilitate efficient purification. Unfortunately, as shown by IP, in these detergents CCR5 cannot be recognized by 2D7 antibody. Although it cannot be completely excluded that these detergents perturb the structure of 2D7 itself or that they specifically block the CCR5-2D7 interaction site, it is a certain hint that the native tertiary CCR5 structure may not be maintained in FC-12. This does not contradict the α-helical secondary structure of the FC-12-purified receptor observed by CD, because in the case of the latter the relative orientation of the helices cannot be assessed.

On the other hand, when CCR5 is solubilized in detergents with a maltose head group, CCR5-2D7 interaction takes place. As shown in Figure 3.16 and Figure 3.17 the type (aliphatic or cyclic) and the length of the hydrocarbon chain and the type of buffer

do not affect the outcome in a major way. These results coincide with the work of Mirzabekov, who with IP reported CCR5 recognition by 2D7 in Cymal-5 but not in FC-14 (86) and with the work of Navratilova (91) and Rich (87), who studied CCR5-2D7 interaction using SPR but not with the work of Nisius (82), where using IP 2D7 recognition was reported in FC-12. In the case of the latter, in turned out that detergent was erroneously omitted during washing, which resulted in a false positive. This shows that for IP assays, where precipitation is virtually indistinguishable from pull-down effect, ensuring conditions favoring good protein solubility (also enough detergent in case of membrane proteins) throughout the entire procedure is a key issue.

Having observed that FC-12 may in some way affect CCR5 native conformation we have extensively explored the possibility to solubilize and purify CCR5 in maltoside detergents. The emphasis was put on DDM as it is the most popular and successful detergent in three dimensional structure determination of membrane proteins. Unfortunately, DDM failed to efficiently solubilized CCR5 from the insect membrane fraction, yielding only 20-40% of the amount purified in FC-12. In addition, the receptor stability and purity were not satisfactory for further biophysical experiments. Similar results (low yield and purity, poor stability) were achieved when FC-12 to DDM exchange was performed on the column (Ni-NTA or Strep-Tactin) as well as when other members of maltoside family were used (TMP-8, TMP-9, TMP-10, TMP-12, MP-6, MP-11, MP-13).

Last but not least it could be observed that CCR5 aggregates over time and upon concentration in a cysteine-dependent manner. This means that some of the cysteines are reactive and persuaded us to eliminate the most likely not palmitoylated cysteines 321, 323 and 324 by a C-terminal truncation. For this purpose, based on the CCR5 topology available at that time (88), two C-terminal CCR truncation variants were designed with Asn306 and Arg319 being the last CCR5 residues (Figure 3.21). These constructs were later used both in insect cell and *E. coli* expression systems. However, it could be shown that even the C-terminally truncated CCR5 with additionally mutated C58S and C224 were still prone to aggregation (Sébastien Morin, unpublished data), which may indicate that, at least to some extent, the extracellular cysteines may not be fully oxidized into disulphide bridges. Perhaps this CCR5 population is the same as the one, which co-purifies with the cytoplasmic Hsc70.

To check the quality of CCR5 samples and to study its interaction with ligands we turned to SPR. Using nickel-charged NTA chip CCR5 could be efficiently

immobilized via its C-terminal His-tag. No 2D7 binding could be observed for the FC-12-purified CCR5, which confirms the outcome of the IP assay. Interaction with RANTES-E66S was observed for both: the reference and the sample channel and subsequently using a single channel it was shown that RANTES-E66S exhibits a strong electrostatic affinity to Ni-NTA sensor chip. This observation was a clear indication that functionalized with negatively charged groups NTA chip is not suitable to study interaction with positively charged RANTES and became a starting point for an antibody-based immobilization system, which was established and successfully used by Sébastien Morin to understand the details of CCR5 interaction with various RANTES variants (see Chapter 6).

4   Biophysical and structural investigation of bacterially expressed and engineered CCR5, a G protein-coupled receptor

Original Manuscript

Wiktor, M., Morin, S., Sass, H-J., Kebbel, F., Grzesiek, S.

Biophysical and structural investigation of bacterially expressed and engineered CCR5, a G protein-coupled receptor

Maciej Wiktor[a], Sébastien Morin[a], Hans-Jürgen Sass[a], Fabian Kebbel[b], and Stephan Grzesiek[a,1]

[a]Department of Structural Biology, Biozentrum, University of Basel, Klingelbergstrasse 50/70, 4056 Basel, Switzerland
[b]Center for Cellular Imaging and Nano Analytics (C-CINA), Biozentrum, University of Basel, Mattenstrasse 26, CH-4058 Basel, Switzerland

[1]To whom correspondence should be addressed: Stephan Grzesiek, Department of Structural Biology, Biozentrum, University of Basel, Klingelbergstrasse 50/70, 4056 Basel, Switzerland, Tel.: +41 61 267 21; Fax +41 61 267 21 09; E-mail: stephan.grzesiek@unibas.ch

Abstract The CC chemokine receptor 5 (CCR5) is an integral membrane protein belonging to the class of G protein-coupled receptors (GPCRs). It plays a crucial role in the regulation of leukocyte trafficking and effector function. Furthermore, it is the major HIV-1 coreceptor and therefore a target for virus entry inhibitors. Here, we report *E. coli* expression and a broad range of biophysical studies on *E. coli*-produced CCR5. After systematic screening and optimization, we obtained 10 mg of purified, detergent-solubilized, well folded CCR5 from 1 L culture in a triple isotope-labeled (^{2}H, ^{15}N, ^{13}C) minimal medium. Thus the material is suitable for NMR spectroscopic studies. The expected α-helical secondary structure content is confirmed by CD spectroscopy. The solubilized CCR5 is monodisperse and homogeneous as judged by transmission electron microscopy (TEM). Interactions of CCR5 with its ligands, RANTES and MIP-1β were assessed by surface plasmon resonance (SPR) yielding a K_D in the nanomolar range. Using size exclusion chromatography, stable monomeric CCR5 could be isolated. We showed that cysteine residues affect both the yield and the oligomeric distribution of CCR5. HSQC spectra suggest that the transmembrane (TM) domains of CCR5 are in equilibrium between several conformations. Our robust and efficient *E. coli* expression system overcomes numerous technical bottlenecks and can be used for a wide range of biophysical and structural studies on GPCRs. We also present a model of CCR5 based on the crystal structure of CXCR4 as a useful starting point for CCR5 engineering.

Keywords CCR5; G protein-coupled receptor; Expression in *E. coli*; NMR; homology modeling

Introduction

G protein-coupled receptors constitute a large protein superfamily found only in eukaryotes. About 4% of the protein-coding human genome codes for ~800 GPCRs (1). Based on phylogenetic analysis human GPCRs cluster into 5 main families: rhodopsin, adhesion, frizzled/taste2, glutamate and secretin which comprise 701, 24, 24, 15 and 15 members, respectively (2). The diversity of the GPCR superfamily members is reflected in the variety of their ligand types. Photons, ions, odorants, nucleotides, fatty acids, amino acids, peptides and proteins are only some of the messages that GPCRs can transduce (3). As GPCRs regulate so many physiological processes such as vision, smell, behavior, mood, immune system, blood pressure, heart rate, digestion or homeostasis, they remain the most commonly drugged protein family (4). About 40% of prescribed pharmaceuticals target GPCRs (5).

The structure determination of membrane proteins is notoriously difficult due to the many obstacles impeding membrane protein sample preparation and subsequent structure determination. When this publication was written about 82000 entries appeared in the Protein Data Bank (6) but only as few as 335 unique membrane protein 3D structures were known (7). GPCR structures are even sparser. The first, bovine rhodopsin, was solved in 2000 by Palczewski et al. (8), and until now 12 more unique GPCR structures were solved by X-ray crystallography: β2-adrenergic (9, 10), β1-adrenergic (11), adenosine A2A (12, 13), dopamine D3 (14), CXCR4 (15), histamine H1 (16), M2 muscarinic acetylcholine (17), M3 muscarinic acetylcholine (18), S1P1 lipid (19), μ-opioid (20), κ-opioid (21) and δ-opioid (22) receptors. To obtain high-resolution structural data the replacement of the intracellular (IC) loop 3 with T4 lysozyme (9, 12, 14-22), thermostabilization (11, 13-15) or stabilization with anti- or nanobodies (9) proved to be successful strategies. Additionally, all crystallized GPCRs were bound to an agonist (13), an inverse agonist (9, 10, 18) or most often to an antagonist (11, 12, 14-17, 19-22). Although, not GPCRs, prokaryotic sensory rhodopsin II (23) and proteorhodopsin (24) are examples of a 7-TM domain proteins solved by NMR spectroscopy.

The CC chemokine receptor 5 (CCR5) belongs to the γ-group of the rhodopsin family of GPCRs. It is found in the plasma membrane of Th1 lymphocytes, macrophages, NK cells and immature dentritic cells and is involved in various infectious and inflammatory diseases as well as cancer (25). Since humans carrying the Δ32 allele of the CCR5 gene, a 32-base pair deletion resulting in a premature stop codon in the extracellular (EC) loop 2 and a nonfunctional receptor, are healthy, the exact role of CCR5 is not completely understood.

The main interest in CCR5 is, however, a consequence of its involvement in AIDS. R5-tropic HIV-1 infection necessitates the sequential interaction of viral envelope glycoprotein gp120 with CD4 and CCR5 (26). Two copies of the CCR5-Δ32 allele confer nearly complete resistance to HIV-1 infection (27, 28). Δ32 occurs at 5-14% frequency in European Caucasians but not in African, Native American, and East Asian populations (29), which

is a result of a selective pressure of the epidemics of plague, a viral haemorrhagic fever, that took place in Europe in medieval ages (30). Successful strategies to block HIV entry have been developed based on small-molecule inhibitors of CCR5 (31) as well as derivatives of its natural chemokine ligand RANTES (32-35).

High-resolution structural data would greatly improve the understanding of CCR5 function and the nature of its interaction with the chemokine ligands RANTES, MIP-1α, and MIP-1β, as well as substantially enhance possibilities for anti-HIV drug discovery. So far it has been very challenging to obtain sufficient amounts of this protein suitable for structural studies. Large-scale CCR5 expression at the yield of 1 mg/L was reported in insect cells (36) where screening for mutants is time-consuming and isotope labeling is very costly and has not been achieved for deuterium.

Alternatively, 1-3 mg/L of CCR3 but only 0.1-0.3 mg/L of CCR5 was obtained from *E. coli* after fusing the N-terminus of the chemokine receptor to the C-terminus of thioredoxin (37). However, the described expression system required the usage of rich TB medium, where the yields are usually higher than in minimal media necessary for the isotope labeling. Furthermore, ligand binding of the expressed chemokine receptors was not shown. However, there is a growing number of GPCRs expressed in *E. coli* (38-44), for which ligand binding could be shown as a test for functionality. Petrovskaya et al. recently compared direct expression of 17 diverse GPCRs in *E. coli* to hybrid expression with the N-terminal fusion partners OmpF or Mistic (45). Interestingly, almost all GPCRs expressed in the presence of a fusion partner at >5 mg/L yield, but for most the expression was severely reduced in its absence.

Here we report a CCR5 production platform that yields up to 10 mg of purified protein per 1 L of bacterial culture. CCR5 is solubilized from *E. coli* without the requirement of refolding. As the expression conditions were optimized in minimal medium, triple isotope (^{2}H/^{13}C/^{15}N) labeling does not compromise the yield. In order to boost the expression, we fused the N-terminus of CCR5 to well expressing small proteins or signal sequences. A C-terminal 10His-tag and rigorous washing conditions yield over 90% purity after a single IMAC purification step. The fusion partner can be readily and quantitatively cleaved off by thrombin and separated on a size exclusion column, where CCR5 monomers and dimers migrate as separate symmetric peaks. Both monomers and dimers are monodisperse and homogeneous as judged from electron micrographs. The expected α-helical secondary structure content is confirmed by circular dichroism (CD) spectroscopy. Purified CCR5 interacts with RANTES and MIP-1β with nanomolar affinities. Recorded ^{1}H-^{15}N HSQC spectra suggest that the TM domains of CCR5 are in equilibrium between several conformations. Our system establishes a robust platform for biophysical and structural studies on CCR5. Due to the high yield and the possibility of isotope labeling it is suitable for both X-ray crystallography and NMR. We also show that the number of cysteine residues has a severe impact on both protein yield and oligomeric state. Following Hernanz-Falcón et al. (46) two point mutations I52V and V150A were introduced to reduce the tendency of dimer formation, but no reduction was observed.

Material and methods

Generation of expression constructs

Plasmids pET28F10 and pMT10H10 containing the CCR2b sequence fused to OmpF and Mistic were a generous gift from Prof. A. Arseniev (Russian Academy of Sciences, Moscow, Russia). Plasmid pCA528 was kindly provided by Prof. A. Spang (Biozentrum, Basel, Switzerland). pET vectors were obtained from Novagen. The *E. coli*-optimized CCR5 DNA sequence in the pQE-T7 vector was generated by GeneArt. The CCR5 gene was cloned using standard molecular biology techniques. Plasmid DNA was amplified with the QIAprep Spin Miniprep Kit (Qiagen). Point mutations were carried out using the QuikChange II XL Site-Directed Mutagenesis Kit (Agilent Technologies).

Protein expression

Freshly transformed Rosetta 2(DE3) Competent Cells (Novagen) were transferred to 1-2 L of M9 medium after overnight growth on LB agar plates. The cultures were shaken in 5 L baffled flasks at 100 rpm at 37°C until OD$_{600}$=2.6-2.8. The culture was cooled down on ice with occasional shaking until the temperature dropped to 20-25°C. Bacteria were induced with 1 mM IPTG and were shaken at 100 rpm at 20°C. After harvesting, cells were pelleted and stored at -70°C.

For expression in D$_2$O transformed cells were grown on LB agar plates prepared in 50% D$_2$O. 1-2 L cultures were preceded by 100 mL precultures grown until OD$_{600}$=1. All compounds used in the preparation of M9 medium in D$_2$O (including trace elements, vitamins, antibiotics) were prepared in D$_2$O. Uniform ^{15}N- and ^{13}C-labeling was carried out using ^{15}NH$_4$Cl (1 g/L), and ^{13}C$_6$-glucose (4 g/L) as the sole nitrogen and carbon sources, respectively. Details of the M9 medium composition can be found in Text S1.

Membrane fraction preparation

Frozen *E. coli* cell pellet (1 g) was suspended in 6-8 mL of buffer A (20 mM HEPES pH 7, 150 mM NaCl, 10% (v/v) glycerol) supplemented with 0.5 mM PMSF, 5 mM benzamidine and EDTA-free complete protease inhibitor cocktail (Roche). Cells were broken using a French press at 31600 psi. Cell debris was removed by centrifugation at 6600 g for 15 min. The supernatant was centrifuged at 126000 g for 15 min, and the resulting pellet (from now on called membrane fraction) collected. After suspending in buffer A, a 20% (w/v) solution of the membrane fraction was stored at -70°C.

Detergent screening

Frozen 20% (w/v) solutions of membrane fraction were thawed, diluted twice and supplemented with detergent to the final concentration of 2%. Solubilization was carried out at RT for 2 h with 1000 rpm shaking. Unsolubilized material was removed by centrifugation at 100000 g for 30 min. The clarified supernatant (2 µL) was loaded onto a Protran BA85 nitrocellulose membrane (Whatman) and dried at RT. Dot blots were blocked, labeled with anti-His-tag antibody, developed and quantified in the same way as

western blots described below. Detergents were obtained from Anatrace with the exception of DHPC (1,2-Diheptanoyl-sn-Glycero-3-Phosphocholine, Avanti Polar Lipids).

Protein purification

A frozen 20% (w/v) solution of membrane fraction was thawed and supplemented to a final concentration of 0.5 M NaCl, 20 mM KCl, 10 mM MgCl$_2$ and 2.5% FC-12. Protein solubilization was carried out at 4-8°C for 1-2 h. Unsolubilized material was removed by centrifugation at 126000 g for 30 min. The clarified supernatant was supplemented with 35 mM imidazole and bound to Ni-NTA beads (Qiagen) for 2 h. The resin was washed with 100 column volumes of buffer B (20m M HEPES pH 7, 1 M NaCl, 60 mM imidazole, 10% (v/v) glycerol, 0.1% FC-12). The protein was then eluted with buffer C (20 mM HEPES pH 7, 150 mM NaCl, 0.4 M imidazole, 0.15% FC-12). Protein-rich fractions were pooled and dialyzed against buffer D (20 mM Tris pH 8, 150 mM NaCl, 0.5 mM EDTA, 0.1% FC-12). To cleave the fusion partner, 2 U of thrombin per 1 mg of purified protein was sufficient to complete the cleavage over 16 h at RT. The protein was concentrated using 30 kDa molecular weight cut off (MWCO) concentrator and injected onto Superdex 200 10/300 GL (analytical run) or Superdex 200 26/60 HiLoad (preparative run) columns equilibrated in buffer E (20 Na$_2$HPO$_4$ pH 7.4, 180 mM NaCl, 0.1% FC-12).

Gel electrophoresis and western blotting

Protein samples for SDS-PAGE were mixed with 5x SDS loading buffer (312.5 mM Tris-HCl pH 6.8, 50% (v/v) glycerol, 25% β-mercaptoethanol, 10% SDS, 0.0125% bromophenol blue), incubated at 30°C for 15 min and centrifuged at 17000 g for 5 min prior to loading on a 4-20% gradient precast gel (Pierce). The electrophoresis was performed at 100 V constant voltage. Gels were stained using 0.25% solution of Coomassie Brilliant blue R-250 (AppliChem) in 25% isopropanol and 10% acetic acid and destained in 10% acetic acid.

For western blotting onto PVDF membrane (Bio-Rad), a Criterion Blotter (Bio-Rad) was used. The transfer was performed at 0.5 A constant current for 1 h in the transfer buffer (48 mM Tris-HCl pH 9.2, 39 mM glycine, 0.375% SDS, 20% methanol). The membrane was blocked with 3% BSA in TBST buffer (10 mM Tris-HCl pH 8, 150 mM NaCl, 0.5% Tween-20). Subsequently the membrane was incubated with mouse monoclonal HIS-1 anti-polyhistidine-peroxidase antibody (Sigma-Aldrich) at 1:6000 dilution for 1 h. After washing 4 x 2 min with TBST buffer, the blot was developed using chemiluminescent HRP substrate (Roche). The signal was recorded using a BioMax XAR Film (Kodak) or using a LAS-4000 luminescent image analyzer (Fujifilm). The signal intensities were quantified using the ImageJ 1.43r (62).

Transmission electron microscopy (TEM)

For TEM analysis 5 µL of 10 µg/mL protein solution was adsorbed on carbon-coated copper 200 mesh grids rendered hydrophilic by glow discharge in air during 20 s. The grids were washed in five drops of double distilled water and negatively stained with two drops of 2% uranyl acetate. Electron micrographs were recorded on a Philips CM10 instrument equipped with a LaB6 filament operating at an accelerating voltage of 80 kV. Images were recorded at nominal defocus values of 0.5 µm on a Veleta CCD camera at a nominal magnification of 130000x, corresponding to a pixel size of 3.7 Å at the sample level.

Circular dichroism spectroscopy

CD spectra were recorded on 3-13 µM monomeric CCR5 fractions. Measurements were performed on a Chirascan CD spectrometer (Applied Photophysics) at 20°C in 1 mm quartz Suprasil cuvettes (Hellma). Typically, spectra in a wavelength range of 195-260 nm spectra were recorded in triplicates and averaged. After baseline (buffer) subtraction, the mean residue molar ellipticity Θ_{MRM} was calculated from the following equation $\Theta_{MRM}=\Theta/(C \times n \times l)$, where Θ is the ellipticity (deg), C is the concentration (mol/L), n is the number of residues and l is the optical path length (cm). The α-helical contents α% was calculated as follows α%=$(-\Theta_{MRM, 222nm}+3000)/39000$ (63), where Θ_{MRM} is given in units of deg×cm^2×dmol^{-1}.

Surface Plasmon resonance (SPR)

Interaction assays were performed using a T100 Biacore instrument (GE Healthcare). The setup consisted of a CM5 chip on which an antibody against the His-tag (Qiagen) was immobilized, using amine coupling chemistry. The antibody (4000-10000 RU) could capture ~2000-5000 RU of recombinant His-tagged CCR5, solubilized from membranes using a detergent mixture of 1% DDM, 1% CHAPS, 0.2% CHS, and 1 mM DOPC at pH 7. Thioredoxin removal was performed on the chip using 5 U of thrombin injected in 300 µL over 60 min (5 µl/min) at 20°C. Experiments were performed in the buffer F (20 mM HEPES pH 7.0, 150 mM NaCl, 0.1% DDM, 0.1% CHAPS, 0.02% CHS, 50 nM DOPC, 0.1 mg/mL BSA) with a flow rate of 50 µl/min. Signals were processed with the Biacore T100 Evaluation Software using double referencing with both a reference channel and blank injections.

Nuclear magnetic resonance (NMR)

CCR5 (monomeric fraction) produced in isotope labeled M9 medium was concentrated in 30 kDa MWCO Ultracel-30K Amicon Ultra Centrifugal Filter (Millipore) to ~100 µM concentration. The sample was supplemented with 5% D$_2$O for locking and transferred to a Shigemi tube. HSQC spectra were recorded at 15-35°C on a Bruker DRX800 spectrometer equipped with a triple resonance Z-gradient TCI cryoprobe. For indirect (nitrogen) dimension 63 increments for a total time of 25.2 ms and for direct (proton) dimension 512 points for a total time of 40 ms were collected. Spectra were processed using NMRPipe 3.0 (64).

CCR5 model building

The core of CCR5 (residues 19–298) was built using the SWISS-MODEL server (http://swissmodel.expasy.org/workspace) with the crystal structure of CXCR4 (3ODU(15, 32% sequence identity)

as a template. At the C-terminus of CCR5, helix H8 modeled based on the rhodopsin structure 3C9L (49) was added using VMD 1.9 (65). In addition, the N-terminus of CCR5 (residues 1–18) and another part of the C-terminus including palmitoylated cysteines (residues 312–331) were added as an extended amino acid chain. Residues 332-352 were not included to reduce computational time for energy minimization. Finally, sulfate groups were added to Tyr10 and Tyr14 as well as palmitoyl groups to Cys321, Cys323 and Cys324.

After each manipulation step the structure was energy-minimized and relaxed by a short molecular dynamic simulation (MD) run using NAMD 2.7 (66). For these MD runs the protein was embedded in a lipid bilayer of 137 POPC molecules, hydrated with 10774 TIP3 water molecules and neutralized by adding Na^+ and Cl^- ions. The final structure was embedded in a bilayer of 188 POPC molecules, hydrated with 20781 TIP3 water molecules, neutralized with several short (≤1 ns) equilibration steps and finally equilibrated with a 10 ns MD run.

Results

Protein expression

Even though many approaches are described in the literature, there is no universally applicable strategy to obtain a high yield GPCR expression system. The selection of expression vector, bacterial strain, culturing conditions, etc. remains largely empirical. To increase the chance of achieving high yield, we tested the expression of CCR5 cloned into several different T7-inducible vectors containing various N- and C-terminal fusion partners/tags. The summary of tested constructs can be found in Table 1. As we intended to use our expression system also for isotope labeling, expression was carried out in M9 minimal medium supplemented with Hutner's trace elements (47). To neutralize the codon bias in some of our constructs we used Rosetta 2(DE3) cells carrying the pRARE plasmid encoding for rare tRNAs.

GPCR overexpression was assayed by western blot for each of the cloned constructs. The expression in pET-22b and pQE-T7 vectors, which provide no or only a very small fusion partner, was clearly lower than in others. This suggests that CCR5 expression yield benefits from the N-terminal fusion partner. However, the type of the fusion partner seems of much less importance than expected. For every tested fusion construct, the yield was significantly higher at 20°C than at 37°C (Fig. 1a,b). A further decrease of the temperature to 12°C or a decrease of IPTG concentration from 1 mM to 0.1 mM resulted in a lower yield. The highest yield was achieved at 20°C after 24-48 h after induction (Fig. 1a-d).

For further optimization of the protein construct, it was important to anticipate the sequence-specific position of the secondary elements. Initially constructs were based on the two-dimensional topology predicted by Oppermann et al. (48). However, after the crystal structure of CXCR4 (15) became available, we generated a homology model based on the latter structure and the C-terminal helix H8 of rhodopsin (49) using state-of-the-art molecular dynamics energy minimization in explicit solvent of CCR5 embedded in a lipid bilayer. The result of the simulation is shown as a full structural model in Figs. 2 & S1 and the

subsequently derived secondary structure topology in Fig. 3a.

Anticipating problems with the formation of intermolecular disulphide bridges we have systematically tested the role of all 12 cysteines by the truncation of the cysteine-containing C-terminus (after N306 or R319) and site-directed mutagenesis of the remaining 9 cysteines in other regions. In those regions, solvent-exposed cysteines were mutated to serines, whereas cysteines in the TM domains were replaced by alanines. The locations of the respective residues are highlighted in Figs. 2 and 3A, and the naming convention of the various mutants is listed in Fig. 3b.

The expression of these cloned constructs was again monitored by western blotting against the C-terminal His-tag. The signal from the shorter (1-306) CCR5 constructs was stronger than from the longer (1-319) constructs (Fig. 1a,b). From this observation, we conclude that the shorter constructs were either expressing better or more resistant to C-terminal degradation. Therefore further work was limited to the shorter (1-306) CCR5 constructs (CCR5[306]). Within the latter, a negative correlation exists between the expression yield and the number of cysteine residues (Fig. 1c). Thus the m2CCR5[306] construct containing 7 cysteines (Fig. 3b) expressed worse than m7CCR5[306] (4 Cys) or m6CCR5[306] (3 Cys), and much worse than m9CCR5[306] (0 Cys).

Detergent screening

Detergent selection is a crucial step in the preparation of a membrane protein sample. A suitable detergent should be able to solubilize the protein, keep it stable and functional in solution as well as allow structural studies. Unfortunately, it is often very difficult to find a detergent system that fulfills all these criteria. To address this challenge we performed a systematic screen by solubilizing *E. coli* membrane fractions in various detergents at 2% (w/v) concentration. After removal of the unsolubilized material, the clarified solutions were dried on a nitrocellulose membrane and analyzed by dot blot using an anti-His antibody. The chemiluminescent signal was quantified densitometrically and normalized to the maximum value (Fig. 4).

The results indicate that CCR5 is efficiently solubilized by anionic (sodium dodecanoyl sarcosine and SDS) and zwitterionic detergents (FosCholines and dimethyl glycines) with aliphatic chains. The cationic trimethylammonium chlorides and the zwitterionic Anzergents are intermediate to moderate in their solubilization efficiency. Nonionic detergents (maltosides and Anapoes) turned out to solubilize CCR5 extremely poorly with the single exception of tetradecylmaltoside, which solubilized about a third as much as FosCholines. Due to its relatively mild character and lipid-like headgroup we picked FosCholine-12 (FC-12) as the main working detergent. Even though FosCholines with longer hydrocarbon tails performed better, they are much less suitable for NMR due to their high aggregation number and lower solubility.

Protein purification and identity confirmation

Considering a broad scope of applications we sought to establish a simple, robust and efficient purification

scheme. CCR5 expressed in *E. coli* was only found in the insoluble fraction after cell disruption (Fig. 1d). Subsequently, this insoluble fraction was separated by centrifugation (see Materials and Methods section) into a heavier (cell debris) and a lighter (membrane) fraction with CCR5 being present in both of them. The isolated membrane fraction was readily solubilizable by a number of detergents (see Detergent Screening section). Similarly, the CCR5 could also be solubilized from the heavier fraction. However, for most applications only the preparation from the lighter fraction was used.

The solubilized CCR5 was purified using Ni-NTA chromatography resulting in up to 10 mg of ~90% pure (as estimated from SDS-PAGE) CCR5 (in FC-12) per 1 L of *E. coli* culture (Fig. 1d,e). Interestingly, purification by Ni-NTA triggered CCR5 oligomerization on SDS-PAGE, which was reversible by dialysis (Fig. 1e). The fusion partner was cleavable with thrombin (Fig. 1e). Other proteases were also tested including TEV, PreScission (GE Healthcare) and 3C proteases with no (TEV) or partial success (Fig. S2).

Trials to solubilize CCR5 in dodecylmaltoside and shorter chain maltosides failed. Some protein could be purified in tetradecylmaltoside but precipitated within few hours after elution from the Ni-NTA column. CCR5 solubilized in FC-12 followed by a detergent exchange to dodecylmaltoside on Ni-NTA also resulted in nearly complete protein precipitation.

The purified CCR5 migrated as a mixture of partially stable dimers at apparent MW of ~50 kDa and monomers at ~30 kDa on an SDS-PAGE (Fig. 1e). Both MW values are smaller than expected. This phenomenon is common for membrane proteins and can be caused by incomplete protein unfolding by SDS and/or by binding more SDS molecules than soluble proteins. Besides monomers and dimers also higher order oligomers were often observed (Fig. 1e), especially after protein concentration.

Discrete and sharp bands of CCR5 monomer and oligomers on the SDS-PAGE suggest that the primary structure of the protein is maintained. The identity and integrity of the C-terminus of the expressed constructs were confirmed by anti-His antibody western blotting (Fig. 1a-d). To further confirm the protein identity, trypsinized FC-12-solubilized CCR5 was analyzed by mass spectrometry. We were able to identify large stretches of fusion partners and the N-terminal fragment of CCR5 in both CCR5 monomer and oligomer bands (Fig. S3). Peptides from TM domains of CCR5 were not detectable, which suggests that the CCR5 core was resistant to proteolysis.

Characterization of CCR5 size distribution, stability and homogeneity

It is commonly observed that GPCRs form homo- and heterodimers as well as higher oligomeric structures. For both *E. coli* (Fig. 1) and insect cell expressed CCR5 (36), besides monomers also oligomers are detected on SDS gels. The biological relevance of GPCR oligomerization is not clear. Thus heterogeneity also presents a problem for structural studies. For this reason, the question of oligomerization was further investigated under non-denaturing conditions using size exclusion chromatography (SEC).

After Ni-NTA purification and digestion by thrombin, cleaved TrxA-m11CCR5[306] was concentrated and injected onto a Superdex 200 column. CCR5 migrated as a mixture of monomers, dimers and higher order oligomers (Fig. 5a). This observation is consistent with the results of the SDS-PAGE (Fig. 1e). Good protein separation was achieved on a 60 cm long size exclusion column. According to a column calibration with standard soluble proteins, the monomer and dimer peaks migrated similarly to particles of about 95±3 (SD) kDa and 184±9 kDa MW, respectively (N=7). This suggests that the monomeric (dimeric) CCR5 micelle contains ~165 (~313) FC-12 molecules. The ratio of monomer and dimer micelles depended on the stringency of Ni-NTA washing conditions, since higher imidazole concentrations depleted the monomeric fraction. Apparently, this is due to the weaker binding of monomers to Ni-NTA. Relative to the monomers and dimers, the fraction of higher order oligomers was much smaller.

In order to assay the influence of disulphide formation on the quality of the preparation, the cysteine-containing CCR5 mutants were compared to the cysteine-free mutants under non-reducing conditions by SEC (Fig. 6). The number of cysteines clearly correlates with enhanced oligomerization. The m2CCR5[306] mutant (7 Cys) formed the most oligomers, whereas m6CCR5[306] (3 Cys) and m7CCR5[306] (4 Cys) mutants were less oligomerized. Interestingly, the effect of EC Cys mutations (m6CCR5[306]) seems similar to the effect of TM Cys mutations (m7CCR5[306]), which suggests that both EC and TM Cys may mediate disulphide bond formation. The higher oligomer formation of the cysteine-containing mutants could be suppressed by the addition of a reducing agent (Fig. S4). Mutation of all Cys residues (m9CCR5[306] and m11CCR5[306]) resulted in a significant reduction of oligomerization, essentially rendering most of the protein in monomeric and dimeric form. Hence, it is likely that the remaining dimers and the residual higher oligomers are stabilized by non-disulphide interactions, presumably between the TM domains.

As non-dimerizing CCR5 would be of advantage for structural studies, following the findings by Hernanz-Falcón et al. that point mutations I52V and V150A strongly reduce dimer formation in HEK-293 cells (46), we tested these mutations in the m9CCR5[306] mutant, which does not contain cysteines that could lead to intermolecular disulphide bridges. In contrast to the in vivo findings (46), these mutations did not reduce the CCR5 dimerization propensity (Fig. 6).

To assess the stability of CCR5 monomer and dimer preparations, both fractions were concentrated to ~40 μM and incubated for 5 days at RT. After 2 days of incubation, almost no change in the size distribution was detected, whereas after 5 days only a small fraction of monomers interconverted to dimers and some of dimers fell apart to monomers or formed higher order oligomers (Fig. 5b). We tested a maximum monomer CCR5 concentration of 137 μM, which also did not show any significant oligomerization after 4 days of incubation. Thus on the time scale of several days, both CCR5 monomer and dimer preparations are very stable. The homogeneity of the monomeric and dimeric CCR5 preparations was confirmed by negative stain TEM. Monomeric CCR5 particles were on average ~6.6 nm in diameter (Fig. 5c) and dimeric ~8.3 nm (Fig. 5d).

Characterization of CCR5 secondary structure

The secondary structure content of the CCR5 monomer preparations was assessed by CD. For all studied constructs we observed double minima at about 208 and 222 nm characteristic for α-helical proteins (Fig. 7). The absolute mean residue molar ellipticity Θ_{MRM} for Mistic-m7CCR5[306] (46%) was slightly larger than for OmpF[34]-m7CCR5[306] (43%) and TrxA-m7CCR5[306] (42%). This can be explained by the fact that Mistic is a purely helical bundle and increases the Θ_{MRM} of the whole fusion construct. This is not the case for the other fusion constructs, where the fusion partners contribute much less to Θ_{MRM} due to their mixed α/β (TrxA-m7CCR5[306]) or likely β secondary structure (OmpF[34]-m7CCR5[306]). The 42% α-helical content of TrxA-m7CCR5[306] is similar to the value of ~40% obtained by Ren et al. for the thioredoxin-CCR3 fusion construct (37). For the m7CCR5[306] monomer, that is after removal of the fusion partner from CCR5, the CD signal was the strongest and indicated an α-helical content of 52%. This is in a good agreement with the ~50% helical content of a typical GPCR (39, 50).

To assess the thermal stability of the CCR5 preparation, the CD spectrum of TrxA-m7CCR5[306] was followed over the range from 5 to 95°C in 5°C increments (Fig. S5a). With increasing temperature the spectrum lost amplitude and its characteristic double minima. Decreasing the temperature from 95°C back to 5°C did not restore the initial shape and intensity, which indicates that denaturation was irreversible. The plot of the ellipticity at 222 nm against temperature (Fig. S5b) shows that a very broad thermal transition between 20 and 80°C. Low thermal stability is common within the GPCR family, however in the case of our preparation it may further reduced by a non-optimal detergent system that lacks important lipids of the native membrane, as well as the absence of stabilizing ligands.

Functional studies of CCR5

Due to the numerous differences in the expression machinery and the cellular environment, the production of functional GPCRs in heterologous systems is very challenging. To prove the proper folding and the functionality of our CCR5 preparation, we tested binding of several ligands to CCR5 using SPR. High sensitivity, automatization and high-throughput makes this method widely used in the GPCR field for screening ligands (51), solubilization (52) and crystallization (53) conditions.

For the SPR experiments, CCR5 was solubilized in a mixture of DDM/CHS/CHAPS and DOPC as a similar detergent/lipid composition was demonstrated to give best receptor activity for CCR5 and CXCR4 (52) as opposed to FC-12 where little binding could be detected. The protein was immobilized on the sensor chip via the anti-His-tag antibody. Binding was assayed for the CCR5 natural chemokine ligands RANTES and MIP-1β as well as for the conformation-dependent antibody 2D7 (Fig. 8), which recognizes several residues from the second EC loop (54). Each of the studied analytes showed fast binding and slow dissociation reactions. K_D values obtained from fitted k_{on} and k_{off} rates were all in the nanomolar range. m7CCR5[306] bound RANTES with K_D=1.6 nM. m11CCR5[306] for which cysteines involved in disulphide bridge formation were

mutated showed a decreased binding ability manifested in 2-fold increase of K_D (3 nM) and 3-fold decrease of the response amplitude. 2D7 and MIP-1β bound with 3 nM and 70 nM affinity, respectively.

NMR studies of CCR5

As opposed to crystal structures, which provide frozen snapshots of GPCR structures, NMR in principle can give simultaneous access to protein structure, dynamics and interactions. Thus it emerges as a promising method to rationalize GPCRs' function. However, due to the numerous challenges in the sample preparation, the success of NMR studies on GPCRs has been very limited so far.

To make our system suitable for NMR, the expression optimization was carried out directly in minimal medium. In this way isotope labeling does not compromise the final yield, which for detergent-solubilized, cleaved, monomeric CCR5 was 2 mg per 1L of cell culture in triply isotope-labeled (^{2}H, ^{15}N, ^{13}C) minimal medium. For NMR measurements, samples were prepared from monomeric CCR5 fractions of the m11CCR5[306] mutant. To estimate the quality of the preparation ^{1}H-^{15}N correlation spectra were recorded (Figs. 9 & S6). To optimize spectral quality, a variation of salt (0-180 mM NaCl), pH (4.2-7.4) and temperature (5-35°C) was carried out. Optimal conditions were found at 20°C, 0 mM NaCl and pH 4.2. Under these conditions, the spectra did not change over a period of few months. An increase in temperature to 35°C gave only marginal improvement. However, it had a destabilizing effect on the protein and caused a decrease of the NMR signal over time. The spectrum of m11CCR5[306] under optimal conditions (Fig. 9) has a narrow dispersion, characteristic for an α-helical protein. It contains on the order of 60-80 intense and narrow resonances that presumably correspond to flexible backbone amides in the N- and C-terminal tails and the interhelical loops. Furthermore, a background of many more broad resonances is observed that most likely correspond to protein core residues. The line broadening in this region may be related to intermediate conformational exchange and/or to the large size of the protein micelle.

Discussion

Due to its involvement in HIV infection, CCR5 is a major target for structural biology and the pharmaceutical industry. Despite that expression and purification schemes have been described for numerous GPCRs, there is a lack of an efficient isotope labeling platform for CCR5. 1 mg/L expression of CCR5 was reported in insect cells (36) where screening for mutants is time-consuming and isotope labeling very costly. On the other hand, so far no high-yield expression in isotope-labeled form has been reported for CCR5 in *E.coli* where these limitations are not present (37). Our goal is to develop methods that allow structural and biophysical characterization in particular by NMR for CCR5 and potentially other GPCRs. Here, we have achieved large overexpression of CCR5 by fusing small stable protein domains or signal sequences to its N-terminus.

As the induction of CCR5 expression essentially arrested *E. coli* growth, increasing cell density proved to be a successful strategy to maximize the CCR5 yield. The

highest CCR5 overexpression was observed 24-48 h post induction at OD_{600} ~3. The induction at earlier or later phase of growth resulted in lower yields. Temperature had a dramatic effect on the expression level with the optimum ~20°C. Variation of the CCR5 sequence also influenced the final yield. Thus the expression of the longer CCR5 constructs (1-319) seemed much lower than the expression of the shorter ones (1-306). The number of cysteines in the CCR5 sequence correlated negatively with the expression level. When all 9 Cys residues were mutated (m9CCR5[306] and m11CCR5[306]), the yield was highest. Intermediate expression, ~60% of m11CCR5[306], was observed for m6CCR5[306] (2 IC Cys and 4 EC Cys mutated) and m7CCR5[306] (2 IC Cys and 3 TM Cys mutated), while the yield of m2CCR5[306] (2 IC Cys mutated) was lowest, i.e. ~1/3 of m11CCR5[306].

As a suitable detergent is a crucial element of a successful membrane protein preparation, we have performed a systematic detergent screening. Charged detergents, especially anionic and zwitterionic were very efficient in CCR5 solubilization. Nonionic detergents, with the exception of tetradecylmaltoside, which solubilized about ~1/3 of available CCR5, worked very poorly. Generally, the results are in agreement with previously obtained data (37) strongly proposing FosCholines as promising candidates. Unfortunately, a good surfactant for solubilization is not always also well suited for other purposes. For some applications, like the SPR functional assay, other detergents or detergent/lipid mixtures were reported to provide better receptor activity (51). Therefore, the optimal detergent system as well as efficient detergent exchange protocols are currently being developed in our laboratory.

Protein oligomerization can severely decrease homogeneity of a sample and in this way compromise the quality of a sample for structural studies. In the case of CCR5 expressed in *E. coli*, the Cys residues, besides affecting the yield, also mediate oligomerization. Using SEC we have shown that the number of cysteines in TrxA-CCR5[306] constructs correlates with the amount of oligomerized protein (Fig. 6). The fact that Cys-mediated oligomerization was also observed in the case of m7CCR5[306], for which all but the EC Cys were mutated, may suggest that in our system, at least to some extent, EC disulphide bridges are not properly formed. On the other hand, the oligomerization of m6CCR5[306], for which all but the TM cysteines C213, C290, C291 were mutated, implies that also TM Cys residues are reactive. This observation is consistent with our model, where C213 and C291 are present on the surface of the CCR5 core (Fig. 2) and where they are accessible for intermolecular disulphide formation.

When not jeopardized by intermolecular disulphide bridge formation, CCR5 exists as a mixture of monomers, dimers and higher order oligomers. Due to their high stability, dimers and oligomers can be also visible on SDS-PAGE. Both monomeric and dimeric species can be separated, concentrated and studied separately. The interconversion between monomers and dimers occurs after few days and goes both possible directions. As judged by TEM, both fractions are homogenous and monodispersed with a clear difference in size. Based on the retention volume, the size of monomers and dimers was estimated to be 95±3 (SD) kDa and 184±9kDa, respectively (N=7).

Based on computer modeling followed by the cross-linking of CCR5-transfected cells it was proposed that two point mutations together I52V and V150A yield a nonsignaling, nondimerizing mutant of CCR5 (46). Even though these findings were later contradicted by another group with co-immunoprecipitation and BRET experiments (55), a nondimerizing CCR5 mutant would be so desirable for NMR studies, that we decided to test these findings again in our laboratory. Unfortunately, in our hands none of the I52V + V150A mutants (m7CCR5[306] or m11CCR5[306]) had significantly smaller propensity for dimerization in comparison to the wild type CCR5 with regards to these two residues (Fig. 6), however, due to the low resolution and limitations of our methodology (Ni-NTA chromatography and SEC), a subtle effect cannot be excluded. The hypothesis of the involvement of these two residues in dimerization is further challenged by the recently published CXCR4 structure, a chemokine receptor family member, which crystallized as dimer with the interaction surface created by helices V and VI (CXCR4 bound to IT1t) or by the IC ends of helices III and IV for the CXCR4 bound to CVX15 (16).

Due to its robustness, polyhistidine-tag chromatography is widely used as a first purification step. Using a 10His-tag we achieved strong binding and could apply more rigorous washing conditions without compromising the final yield. This resulted in ~10 mg of purified TrxA-m11CCR5[306] from 1 L of *E. coli* culture. This is a vast improvement over the previously described system, where ~0.3 mg of CCR5 per L was reported (37). Importantly, this yield is not compromised when isotope labeling including D_2O is applied, which makes our system fully suitable for NMR studies. Out of 10 mg of CCR5 oligomeric mixture it is possible to isolate 2 mg of cleaved monomeric CCR5.

The quality of our preparations was assessed by CD, where all CCR5 constructs showed the characteristic features of an α-helical secondary structure. NMR supports this observation as the HSQC spectrum of CCR5 exhibits, typical for α-helical proteins, rather narrow peak dispersion (~2 ppm). Based on the circular dichroism data, we estimate that α-helices constitute ~52% of the sequence of m7CCR5[306] monomer which suggests that CCR5 produced with our method has a correct secondary structure. The CD data indicate that the thermal stability of CCR5 is not very high. Some secondary structure is already lost at 5°C but, as the amplitude of these changes is relatively small, it is difficult to judge their consequence on CCR5 structure and activity. Low thermal stability can be explained by several factors, most importantly suboptimal detergent system, lack of important lipids, absence of a ligand, nano/antibody or a small molecule drugs, that would stabilize CCR5.

Besides the CD-confirmed secondary structure, the quality of the protein preparation was further validated using an interaction assay. Using SPR we observed high-affinity binding of RANTES to m7CCR5[306] (K_D = 1.6 nM) and m11CCR5[306] (3 nM). The observed affinity is close to the 0.38 nM obtained in a cellular binding assay (56). The remaining difference can be understood by the lack of posttranslational modifications (Tyr sulfation), which strongly contribute to the affinity of CCR5 for chemokines (57). The drop in affinity of m11CCR5[306] relative to m7CCR5[306] may be related to the lack of cysteines involved in disulphide bridges important for chemokine

binding (58). High-affinity (3 nM) binding of m11CCR5[306] was also observed for the antibody 2D7 antibody, which is commonly used as a native conformation probe. For MIP-1β a 70 nM affinity was detected, which again is only about one order of magnitude lower than the 7.2 nM measured for CCR5 stably expressed in Cf2Th cells (56). All these observations confirm that the *E.coli*-expressed, detergent-solubilized CCR5 has the ability to bind ligands.

Due to the substantial challenges in the preparation of isotope labeled samples, NMR spectra of GPCRs are very sparse in the literature. Therefore, only few HSQC spectra of ^{15}N labeled GPCRs have been reported, including the vasopressin V2 receptor (59), bovine rhodopsin (60), and the chemokine CXCR1 receptor (61).

Here, we present a spectrum of uniformly ^{15}N-labeled CCR5. Our initial HSQC spectrum of CCR5 had low dispersion and very broad lines besides for a number of apparently mobile terminal or loop residues. Similar observations have been made for other GPCRs (59-61). However, the quality of the CCR5 spectrum could be improved substantially by a decrease of the pH from 7.4 to 4.2 and the removal of salt, which reduced hydrogen exchange and increased the sensitivity of the measurement. Unfortunately, even with these improvements the quality of the spectra is still not sufficient for structural analysis and needs further improvement but presents a starting point in the NMR investigation of CCR5. Obviously, the key bottleneck is the severe line broadening, which may be the result of conformational heterogeneity of the TM domains and/or chemical exchange on an intermediate time scale in the microsecond to millisecond range. Therefore CCR5 stabilization, locking in a single conformation, may be an important step towards the improvement of the NMR spectra.

Due to major difficulties in sample preparation for structural studies, protein engineering is very common in the GPCR field. This process alters the protein sequence and may modify its native properties, but so far has been indispensible for gaining insights into the structure and function of this important class of proteins. As all solved GPCR structures were obtained by crystallography, not surprisingly, alterations comprised stabilization (rigidification, fixation in selected conformations), removal of unstructured regions, introduction a soluble domain into a loop, etc.

NMR spectroscopy on the other hand requires isotope labeling. However, so far efficient isotope labeling has not been possible for insect cells or natural tissues from which all solved GPCRs were derived. Thus simple prokaryotic organisms, like *E. coli* are often the system of choice for an NMR spectroscopist, as they allow cost-effective isotope labeling in addition to fast access to protein engineering. Due the size limitations of NMR, the preparation of stable, monomeric and non-aggregating GPCRs is vital. Taking advantage of *E. coli*, we developed a highly efficient and robust CCR5 expression platform, which may find applications in broad biophysical, functional as well as structural characterization of CCR5. We also believe that many of our observations have more general character and may be useful and applicable for other GPCRs.

References

1. Takeda, S., Kadowaki, S., Haga, T., Takaesu, H. and Mitaku, S. (2002) Identification of G protein-coupled receptor genes from the human genome sequence. *FEBS Lett.* **520**, 97-101.

2. Fredriksson, R., Lagerstrom, M. C., Lundin, L. G. and Schioth, H. B. (2003) The G-protein-coupled receptors in the human genome form five main families. Phylogenetic analysis, paralogon groups, and fingerprints. *Mol. Pharmacol.* **63**, 1256-1272.

3. Overington, J. P., Al-Lazikani, B. and Hopkins, A. L. (2006) How many drug targets are there? *Nat. Rev. Drug. Discov.* **5**, 993-996.

4. Bockaert, J. and Pin, J. P. (1999) Molecular tinkering of G protein-coupled receptors: an evolutionary success. *EMBO J.* **18**, 1723-1729.

5. Filmore, D. (2004) It's a GPCR world. *Modern Drug Discovery* **7**, 24-28.

6. Bernstein, F. C., Koetzle, T. F., Williams, G. J., Meyer, E. F., Jr., Brice, M. D., Rodgers, J. R., Kennard, O., Shimanouchi, T. and Tasumi, M. (1977) The Protein Data Bank: a computer-based archival file for macromolecular structures. *J. Mol. Biol.* **112**, 535-542.

7. White, S. H. (2004) The progress of membrane protein structure determination. *Protein Sci.* **13**, 1948-1949.

8. Palczewski, K., Kumasaka, T., Hori, T., Behnke, C. A., Motoshima, H., Fox, B. A., Le Trong, I., Teller, D. C., Okada, T., Stenkamp, R. E., Yamamoto, M. and Miyano, M. (2000) Crystal structure of rhodopsin: A G protein-coupled receptor. *Science* **289**, 739-745.

9. Rasmussen, S. G., Choi, H. J., Rosenbaum, D. M., Kobilka, T. S., Thian, F. S., Edwards, P. C., Burghammer, M., Ratnala, V. R., Sanishvili, R., Fischetti, R. F., Schertler, G. F., Weis, W. I. and Kobilka, B. K. (2007) Crystal structure of the human beta2 adrenergic G-protein-coupled receptor. *Nature* **450**, 383-387.

10. Cherezov, V., Rosenbaum, D. M., Hanson, M. A., Rasmussen, S. G., Thian, F. S., Kobilka, T. S., Choi, H. J., Kuhn, P., Weis, W. I., Kobilka, B. K. and Stevens, R. C. (2007) High-resolution crystal structure of an engineered human beta2-adrenergic G protein-coupled receptor. *Science* **318**, 1258-1265.

11. Warne, T., Serrano-Vega, M. J., Baker, J. G., Moukhametzianov, R., Edwards, P. C., Henderson, R., Leslie, A. G., Tate, C. G. and Schertler, G. F. (2008) Structure of a beta1-adrenergic G-protein-coupled receptor. *Nature* **454**, 486-491.

12. Jaakola, V. P., Griffith, M. T., Hanson, M. A., Cherezov, V., Chien, E. Y., Lane, J. R., Ijzerman, A. P. and Stevens, R. C. (2008) The 2.6 angstrom crystal

structure of a human A2A adenosine receptor bound to an antagonist. *Science* **322**, 1211-1217.

13. Lebon, G., Warne, T., Edwards, P. C., Bennett, K., Langmead, C. J., Leslie, A. G. and Tate, C. G. (2011) Agonist-bound adenosine A2A receptor structures reveal common features of GPCR activation. *Nature* **474**, 521-525.

14. Chien, E. Y., Liu, W., Zhao, Q., Katritch, V., Han, G. W., Hanson, M. A., Shi, L., Newman, A. H., Javitch, J. A., Cherezov, V. and Stevens, R. C. (2010) Structure of the human dopamine D3 receptor in complex with a D2/D3 selective antagonist. *Science* **330**, 1091-1095.

15. Wu, B., Chien, E. Y., Mol, C. D., Fenalti, G., Liu, W., Katritch, V., Abagyan, R., Brooun, A., Wells, P., Bi, F. C., Hamel, D. J., Kuhn, P., Handel, T. M., Cherezov, V. and Stevens, R. C. (2010) Structures of the CXCR4 chemokine GPCR with small-molecule and cyclic peptide antagonists. *Science* **330**, 1066-1071.

16. Shimamura, T., Shiroishi, M., Weyand, S., Tsujimoto, H., Winter, G., Katritch, V., Abagyan, R., Cherezov, V., Liu, W., Han, G. W., Kobayashi, T., Stevens, R. C. and Iwata, S. (2011) Structure of the human histamine H1 receptor complex with doxepin. *Nature* **475**, 65-70.

17. Haga, K., Kruse, A. C., Asada, H., Yurugi-Kobayashi, T., Shiroishi, M., Zhang, C., Weis, W. I., Okada, T., Kobilka, B. K., Haga, T. and Kobayashi, T. (2012) Structure of the human M2 muscarinic acetylcholine receptor bound to an antagonist. *Nature* **482**, 547-551.

18. Kruse, A. C., Hu, J., Pan, A. C., Arlow, D. H., Rosenbaum, D. M., Rosemond, E., Green, H. F., Liu, T., Chae, P. S., Dror, R. O., Shaw, D. E., Weis, W. I., Wess, J. and Kobilka, B. K. (2012) Structure and dynamics of the M3 muscarinic acetylcholine receptor. *Nature* **482**, 552-556.

19. Hanson, M. A., Roth, C. B., Jo, E., Griffith, M. T., Scott, F. L., Reinhart, G., Desale, H., Clemons, B., Cahalan, S. M., Schuerer, S. C., Sanna, M. G., Han, G. W., Kuhn, P., Rosen, H. and Stevens, R. C. (2012) Crystal structure of a lipid G protein-coupled receptor. *Science* **335**, 851-855.

20. Manglik, A., Kruse, A. C., Kobilka, T. S., Thian, F. S., Mathiesen, J. M., Sunahara, R. K., Pardo, L., Weis, W. I., Kobilka, B. K. and Granier, S. (2012) Crystal structure of the micro-opioid receptor bound to a morphinan antagonist. *Nature* **485**, 321-326.

21. Wu, H., Wacker, D., Mileni, M., Katritch, V., Han, G. W., Vardy, E., Liu, W., Thompson, A. A., Huang, X. P., Carroll, F. I., Mascarella, S. W., Westkaemper, R. B., Mosier, P. D., Roth, B. L., Cherezov, V. and Stevens, R. C. (2012) Structure of the human kappa-opioid receptor in complex with JDTic. *Nature* **408,** 327-332.

22. Granier, S., Manglik, A., Kruse, A. C., Kobilka, T. S., Thian, F. S., Weis, W. I. and Kobilka, B. K. (2012) Structure of the delta-opioid receptor bound to naltrindole. *Nature* **485**, 400-404.

23. Gautier, A., Kirkpatrick, J. P. and Nietlispach, D. (2008) Solution-state NMR spectroscopy of a seven-helix transmembrane protein receptor: backbone assignment, secondary structure, and dynamics. *Angew. Chem. Int. Ed. Engl.* **47**, 7297-7300.

24. Reckel, S., Gottstein, D., Stehle, J., Lohr, F., Verhoefen, M. K., Takeda, M., Silvers, R., Kainosho, M., Glaubitz, C., Wachtveitl, J., Bernhard, F., Schwalbe, H., Guntert, P. and Dotsch, V. (2011) Solution NMR structure of proteorhodopsin. *Angew. Chem. Int. Ed. Engl.* **50**, 11942-11946.

25. Balistreri, C. R., Caruso, C., Grimaldi, M. P., Listi, F., Vasto, S., Orlando, V., Campagna, A. M., Lio, D. and Candore, G. (2007) CCR5 receptor: biologic and genetic implications in age-related diseases. *Ann. N. Y. Acad. Sci.* **1100**, 162-172.

26. Choe, H., Martin, K. A., Farzan, M., Sodroski, J., Gerard, N. P. and Gerard, C. (1998) Structural interactions between chemokine receptors, gp120 Env and CD4. *Semin. Immunol.* **10**, 249-257.

27. Liu, R., Paxton, W. A., Choe, S., Ceradini, D., Martin, S. R., Horuk, R., MacDonald, M. E., Stuhlmann, H., Koup, R. A. and Landau, N. R. (1996) Homozygous defect in HIV-1 coreceptor accounts for resistance of some multiply-exposed individuals to HIV-1 infection. *Cell* **86**, 367-377.

28. Samson, M., Libert, F., Doranz, B. J., Rucker, J., Liesnard, C., Farber, C. M., Saragosti, S., Lapoumeroulie, C., Cognaux, J., Forceille, C., Muyldermans, G., Verhofstede, C., Burtonboy, G., Georges, M., Imai, T., Rana, S., Yi, Y., Smyth, R. J., Collman, R. G., Doms, R. W., Vassart, G. and Parmentier, M. (1996) Resistance to HIV-1 infection in caucasian individuals bearing mutant alleles of the CCR-5 chemokine receptor gene. *Nature* **382**, 722-725.

29. Stephens, J. C., Reich, D. E., Goldstein, D. B., Shin, H. D., Smith, M. W., Carrington, M., Winkler, C., Huttley, G. A., Allikmets, R., Schriml, L., Gerrard, B., Malasky, M., Ramos, M. D., Morlot, S., Tzetis, M., Oddoux, C., di Giovine, F. S., Nasioulas, G., Chandler, D., Aseev, M., Hanson, M., Kalaydjieva, L., Glavac, D., Gasparini, P., Kanavakis, E., Claustres, M., Kambouris, M., Ostrer, H., Duff, G., Baranov, V., Sibul, H., Metspalu, A., Goldman, D., Martin, N., Duffy, D., Schmidtke, J., Estivill, X., O'Brien, S. J. and Dean, M. (1998) Dating the origin of the CCR5-Delta32 AIDS-resistance allele by the coalescence of haplotypes. *Am. J. Hum. Genet.* **62**, 1507-1515.

30. Duncan, S. R., Scott, S. and Duncan, C. J. (2005) Reappraisal of the historical selective pressures for the CCR5-Delta32 mutation. *J. Med. Genet.* **42**, 205-208.

31. Kondru, R., Zhang, J., Ji, C., Mirzadegan, T., Rotstein, D., Sankuratri, S. and Dioszegi, M. (2008) Molecular interactions of CCR5 with major classes of small-molecule anti-HIV CCR5 antagonists. *Mol. Pharmacol.* **73**, 789-800.

32. Gaertner, H., Cerini, F., Escola, J. M., Kuenzi, G., Melotti, A., Offord, R., Rossitto-Borlat, I., Nedellec, R., Salkowitz, J., Gorochov, G., Mosier, D. and Hartley, O. (2008) Highly potent, fully recombinant anti-HIV chemokines: reengineering a low-cost microbicide. *Proc. Natl. Acad. Sci. USA* **105**, 17706-17711.

33. Lederman, M. M., Veazey, R. S., Offord, R., Mosier, D. E., Dufour, J., Mefford, M., Piatak, M., Jr., Lifson, J. D., Salkowitz, J. R., Rodriguez, B., Blauvelt, A. and Hartley, O. (2004) Prevention of vaginal SHIV transmission in rhesus macaques through inhibition of CCR5. *Science* **306**, 485-487.

34. Lusso, P., Vangelista, L., Cimbro, R., Secchi, M., Sironi, F., Longhi, R., Faiella, M., Maglio, O. and Pavone, V. (2011) Molecular engineering of RANTES peptide mimetics with potent anti-HIV-1 activity. *FASEB J.* **25**, 1230-1243.

35. Nardese, V., Longhi, R., Polo, S., Sironi, F., Arcelloni, C., Paroni, R., DeSantis, C., Sarmientos, P., Rizzi, M., Bolognesi, M., Pavone, V. and Lusso, P. (2001) Structural determinants of CCR5 recognition and HIV-1 blockade in RANTES. *Nat. Struct. Biol.* **8**, 611-615.

36. Nisius, L., Rogowski, M., Vangelista, L. and Grzesiek, S. (2008) Large-scale expression and purification of the major HIV-1 coreceptor CCR5 and characterization of its interaction with RANTES. *Protein Expr. Purif.* **61**, 155-162.

37. Ren, H., Yu, D., Ge, B., Cook, B., Xu, Z. and Zhang, S. (2009) High-level production, solubilization and purification of synthetic human GPCR chemokine receptors CCR5, CCR3, CXCR4 and CX3CR1. *PLoS One* **4**, e4509.

38. Attrill, H., Harding, P. J., Smith, E., Ross, S. and Watts, A. (2009) Improved yield of a ligand-binding GPCR expressed in *E. coli* for structural studies. *Protein Expr. Purif.* **64**, 32-38.

39. Baneres, J. L., Martin, A., Hullot, P., Girard, J. P., Rossi, J. C. and Parello, J. (2003) Structure-based analysis of GPCR function: conformational adaptation of both agonist and receptor upon leukotriene B4 binding to recombinant BLT1. *J. Mol. Biol.* **329**, 801-814.

40. Dodevski, I. and Pluckthun, A. (2011) Evolution of three human GPCRs for higher expression and stability. *J. Mol. Biol.* **408**, 599-615.

41. Furukawa, H. and Haga, T. (2000) Expression of functional M2 muscarinic acetylcholine receptor in Escherichia coli. *J. Biochem.* **127**, 151-161.

42. Krepkiy, D., Wong, K., Gawrisch, K. and Yeliseev, A. (2006) Bacterial expression of functional, biotinylated peripheral cannabinoid receptor CB2. *Protein Expr. Purif.* **49**, 60-70.

43. Shibata, Y., White, J. F., Serrano-Vega, M. J., Magnani, F., Aloia, A. L., Grisshammer, R. and Tate, C. G. (2009) Thermostabilization of the neurotensin receptor NTS1. *J. Mol. Biol.* **390**, 262-277.

44. Weiss, H. M. and Grisshammer, R. (2002) Purification and characterization of the human adenosine A(2a) receptor functionally expressed in Escherichia coli. *Eur. J. Biochem.* **269**, 82-92.

45. Petrovskaya, L. E., Shulga, A. A., Bocharova, O. V., Ermolyuk, Y. S., Kryukova, E. A., Chupin, V. V., Blommers, M. J., Arseniev, A. S. and Kirpichnikov, M. P. (2010) Expression of G-protein coupled receptors in Escherichia coli for structural studies. *Biochemistry (Mosc)* **75**, 881-891.

46. Hernanz-Falcon, P., Rodriguez-Frade, J. M., Serrano, A., Juan, D., del Sol, A., Soriano, S. F., Roncal, F., Gomez, L., Valencia, A., Martinez, A. C. and Mellado, M. (2004) Identification of amino acid residues crucial for chemokine receptor dimerization. *Nat. Immunol.* **5**, 216-223.

47. Abramoff, M. D., Magalhaes, P. J. and Ram, S. J. (2004) Image Processing with ImageJ. *Biophotonics International* **11**, 36-42.

48. Morrow, J. A., Segall, M. L., Lund-Katz, S., Phillips, M. C., Knapp, M., Rupp, B. and Weisgraber, K. H. (2000) Differences in stability among the human apolipoprotein E isoforms determined by the amino-terminal domain. *Biochemistry* **39**, 11657-11666.

49. Delaglio, F., Grzesiek, S., Vuister, G. W., Zhu, G., Pfeifer, J. and Bax, A. (1995) NMRPipe: a multidimensional spectral processing system based on UNIX pipes. J Biomol NMR 6, 277-293.

50. Stenkamp, R. E. (2008) Alternative models for two crystal structures of bovine rhodopsin. *Acta Crystallogr. D Biol. Crystallogr.* **D64**, 902-904.

51. Humphrey, W., Dalke, A. and Schulten, K. (1996) VMD: visual molecular dynamics. *J. Mol. Graph.* **14**, 33-38, 27-38.

52. Phillips, J. C., Braun, R., Wang, W., Gumbart, J., Tajkhorshid, E., Villa, E., Chipot, C., Skeel, R. D., Kale, L. and Schulten, K. (2005) Scalable molecular dynamics with NAMD. *J. Comput. Chem.* **26**, 1781-1802.

53. Hutner, S. H., Provasoli, L., Schatz, A. and Haskins, C. P. (1950) Some approaches to the study of the role of metals in the metabolism of microorganisms. *Proc. Am. Philos. Soc.* **94**, 152-170.

54. Oppermann, M. (2004) Chemokine receptor CCR5: insights into structure, function, and regulation. *Cell. Signal.* **16**, 1201-1210.

55. Baneres, J. L., Mesnier, D., Martin, A., Joubert, L., Dumuis, A. and Bockaert, J. (2005) Molecular characterization of a purified 5-HT4 receptor: a structural basis for drug efficacy. *J. Biol. Chem.* **280**, 20253-20260.

56. Navratilova, I., Besnard, J. and Hopkins, A. L. (2011) Screening for GPCR Ligands Using Surface Plasmon Resonance. *ACS Med. Chem. Lett.* **2**, 549-554.

57. Navratilova, I., Sodroski, J. and Myszka, D. G. (2005) Solubilization, stabilization, and purification of chemokine receptors using biosensor technology. *Anal. Biochem.* **339**, 271-281.

58. Navratilova, I., Pancera, M., Wyatt, R. T. and Myszka, D. G. (2006) A biosensor-based approach toward purification and crystallization of G protein-coupled receptors. *Anal. Biochem.* **353**, 278-283.

59. Khurana, S., Kennedy, M., King, L. R. and Golding, H. (2005) Identification of a linear peptide recognized by monoclonal antibody 2D7 capable of generating CCR5-specific antibodies with human immunodeficiency virus-neutralizing activity. *J. Virol.* **79**, 6791-6800.

60. Lemay, J., Marullo, S., Jockers, R., Alizon, M. and Brelot, A. (2005) On the dimerization of CCR5. *Nat. Immunol.* **6**, 535; author reply 535-536.

61. Bannert, N., Craig, S., Farzan, M., Sogah, D., Santo, N. V., Choe, H. and Sodroski, J. (2001) Sialylated O-glycans and sulfated tyrosines in the NH2-terminal domain of CC chemokine receptor 5 contribute to high affinity binding of chemokines. *J. Exp. Med.* **194**, 1661-1673.

62. Springael, J. Y., Le Minh, P. N., Urizar, E., Costagliola, S., Vassart, G. and Parmentier, M. (2006) Allosteric modulation of binding properties between units of chemokine receptor homo- and hetero-oligomers. *Mol. Pharmacol.* **69**, 1652-1661.

63. Blanpain, C., Lee, B., Vakili, J., Doranz, B. J., Govaerts, C., Migeotte, I., Sharron, M., Dupriez, V., Vassart, G., Doms, R. W. and Parmentier, M. (1999) Extracellular cysteines of CCR5 are required for chemokine binding, but dispensable for HIV-1 coreceptor activity. *J. Biol. Chem.* **274**, 18902-18908.

64. Tian, C., Breyer, R. M., Kim, H. J., Karra, M. D., Friedman, D. B., Karpay, A. and Sanders, C. R. (2005) Solution NMR spectroscopy of the human vasopressin

V2 receptor, a G protein-coupled receptor. *J. Am. Chem. Soc.* **127**, 8010-8011.

65. Werner, K., Richter, C., Klein-Seetharaman, J. and Schwalbe, H. (2008) Isotope labeling of mammalian GPCRs in HEK293 cells and characterization of the C-terminus of bovine rhodopsin by high resolution liquid NMR spectroscopy. *J. Biomol. NMR* **40**, 49-53.

66. Park, S. H., Casagrande, F., Das, B. B., Albrecht, L., Chu, M. and Opella, S. J. (2011) Local and global dynamics of the G protein-coupled receptor CXCR1. *Biochemistry* **50**, 2371-2380.

Figure legends

Fig. 1 Summary of the expression and purification of CCR5 in *E. coli* monitored by western blot and SDS-PAGE. (a-b) Comparison of the expression of longer (319) and shorter (306) constructs of OmpF[34]-CCR5 (a) and Mistic-CCR5 (b) at 20°C and 37°C. CCR2b constructs are used as a positive control. (c) Comparison of the expression of various Cys mutants of TrxA-CCR5[306]. (d) Expression, membrane preparation and binding to Ni-NTA of TrxA-m11CCR5[306]. Broken *E. coli* cells expressing CCR5 were centrifuged to remove cell debris. Decanted suspension (tot) was subsequently separated into insoluble membrane (ins) and soluble cytoplasmic (sol) fractions. CCR5 was found in the membrane fraction (ins) but not in the cytoplasmic fraction (sol). Solubilized membranes (inp) were loaded on Ni-NTA. (e) Purification of TrxA-CCR5[306]. After elution from Ni-NTA oligomerized TrxA-CCR5[306] was dialyzed and digested with thrombin

Fig. 2 Modeled 3D structure of CCR5 (residues 1-331) based on the CXCR4 structure (15). Sulfation of Tyr10 and Tyr14 as well as palmitoylated Cys321, Cys323 and Cys324 are depicted as spheres

Fig. 3 CCR5 topology and engineered mutations. (a) Membrane topology prediction of the human CCR5 according to the CXCR4 homology model (Fig. 2). The grey rectangle approximates the position of the membrane. EC (IC) space is at the top (bottom). The potential posttranslational modifications include sulfation of Y3, Y10, Y14 and Y15, phosphorylation of S336, S337, S342 and S349 (both marked as black circles), palmitoylation of C321, C323 and C324 as well as glycosylation of S6. The positions of mutated residues are highlighted (C in blue, other in green). C-terminal truncations are marked with red circles and potential helix H8 with dashed lines. Disulphide bridges form between C20 and C269 and between C101 and C178. (b) Table summarizing the introduced point mutations of the listed CCR5 mutants

Fig. 4 Detergent screening for solubilization of OmpF[34]-m7CCR5[306]. Values were normalized against FC-16. Abbreviations: DHPC, DiMetPhOx-10: n-decyl-N,N-dimethylamine-N-oxide, TriMetAmm-10: N-dodecyltrimethylammonium chloride, Sarcosine-12: sodium dodecanoyl sarcosine, DiMetPhOx-8: dimethyloctylphosphine oxide, HESO-8: N-octyl-2-hydroxyethyl sulfoxide, Maltoside-6: n-hexyl-β-D-maltopyranoside

Fig. 5 Monomers and dimers of CCR5. (a) Size exclusion chromatography of m11CCR5[306] on a Superdex 200 HiLoad 26/60 column. The 60 cm long column enables isolation of monomers and dimers. (b) Stability test of m7CCR5[306] monomers and dimers. To prevent Cys oxidation 1 mM TCEP was included. Purified monomers and dimers were concentrated separately to ~40 µM and re-run on a Superdex 200 10/300 GL column. For easier comparison all 6 chromatograms were scaled to 1. Negative stain pictures of m7CCR5[306] monomers (c) and dimers (d)

Fig. 6 Size exclusion chromatography of various CCR5[306] mutants demonstrates the impact of Cys residues on the oligomeric state of the purified CCR5. No observable difference between m9CCR5[306] and m11CCR5[306] suggests that I52V and V150A mutations are not involved in CCR5 dimerization

Fig. 7 CD spectra of several CCR5[306] constructs show characteristic features of α-helical secondary structure

Fig. 8 SPR functional assay of m7CCR5[306] (cyan) and m11CCR5[306] (other colors). The graph contains 4 overlaid independent runs, normalized for the amount of immobilized receptor and plotted to the same scale. Each run is composed of 3 phases separated by the dashed lines: equilibration, binding and dissociation. Fitted curves are in red

Fig. 9 TROSY spectrum of ~100 µM ^{2}H,-^{15}N-labeled m11CCR5[306] monomers recorded at 20°C

Table 1 Summary of GPCR constructs tested for expression. *(residues 1 to 34 from 362 total)

Vector	N-term. tag	Fusion partner	Cleavage site	GPCR	cDNA	C-term. tag	Expression
pET28F10	-	OmpF (1-34/362)*	-	CCR2b	*H. sapiens*	6His	+++
pMT10H10	-	Mistic (1-110/110)	thrombin	CCR2b	*H. sapiens*	10His	+++
pET-22b	-	pelB (1-22/374)	pelB	CCR5	*H. sapiens*	8His	+
pGEV2	-	GB1 (1-56/56)	thrombin/3C	CCR5	*H. sapiens/E. coli*	6/8His	+++
pQE-T7	6His	-	TAGZyme	CCR5	*E. coli*	-	+
pET28F10	-	OmpF (1-34/362)	-	CCR5	*E. coli*	6/10His	+++
pMT10H10	-	Mistic (1-110/110)	-	CCR5	*E. coli*	10His	+++
pET-41a	-	GST (1-218/218)	-	CCR5	*E. coli*	6/10His	+++
pCA528	6His	SUMO (1-98/101)	Ulp1/3C	CCR5	*E. coli*	0/10His	+++
pET-32b	-	TrxA (1-109/109)	-/3C/TEV/thrombin	CCR5	*E. coli*	6/10His	+++

Fig. 1

Fig. 2

a

b

Mutant	Extracellular Cys	Transmembrane Cys	Intracellular Cys	Other Mutations
m2CCR5[306]	- -	- - - - - - - - - - - - - - - -	C58S C224S	- - - - - - - - - -
m6CCR5[306]	C20S C101S C178S C269S	- - - - - - - - - - - - - - - -	C58S C224S	- - - - - - - - - -
m7CCR5[306]	- -	C213A C290A C291A	C58S C224S	I52V V150A
m9CCR5[306]	C20S C101S C178S C269S	C213A C290A C291A	C58S C224S	- - - - - - - - - -
m11CCR5[306]	C20S C101S C178S C269S	C213A C290A C291A	C58S C224S	I52V V150A

Fig. 3
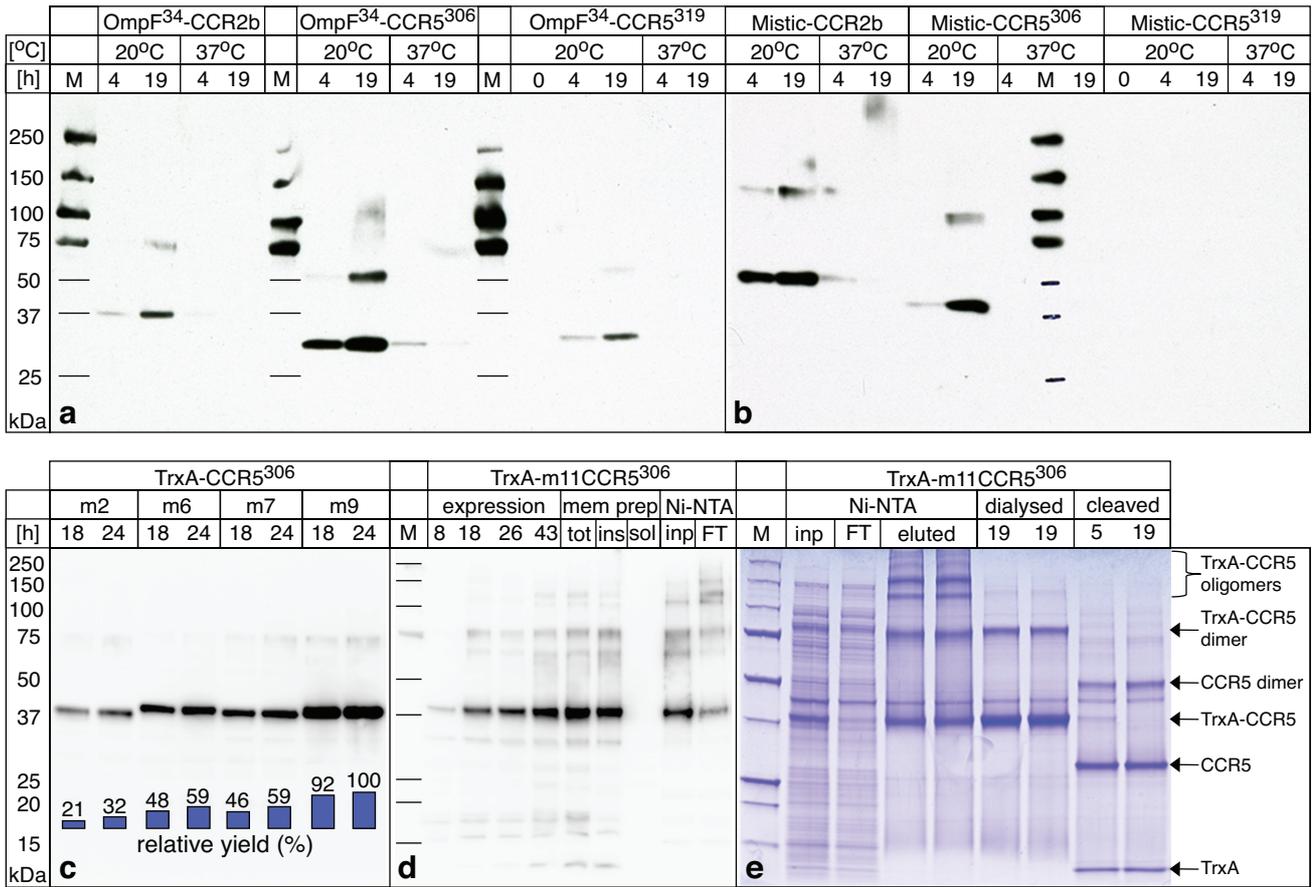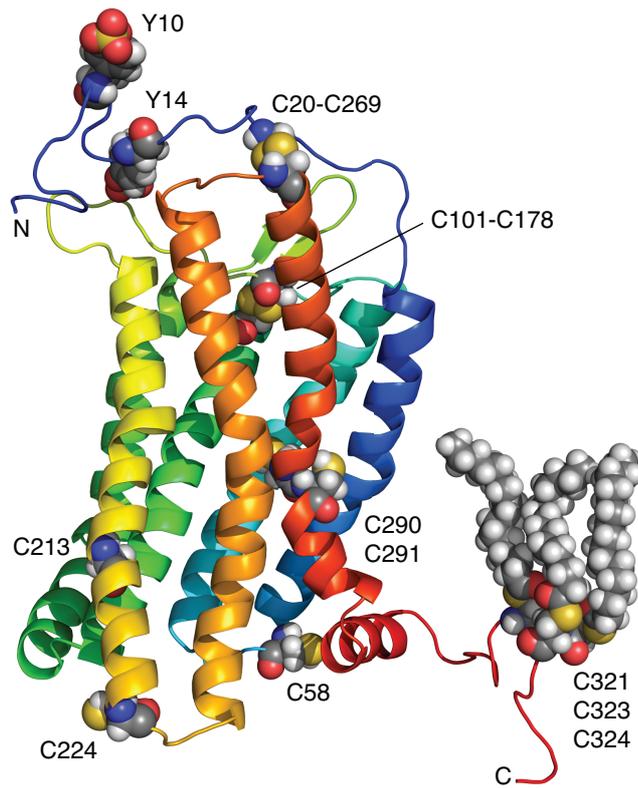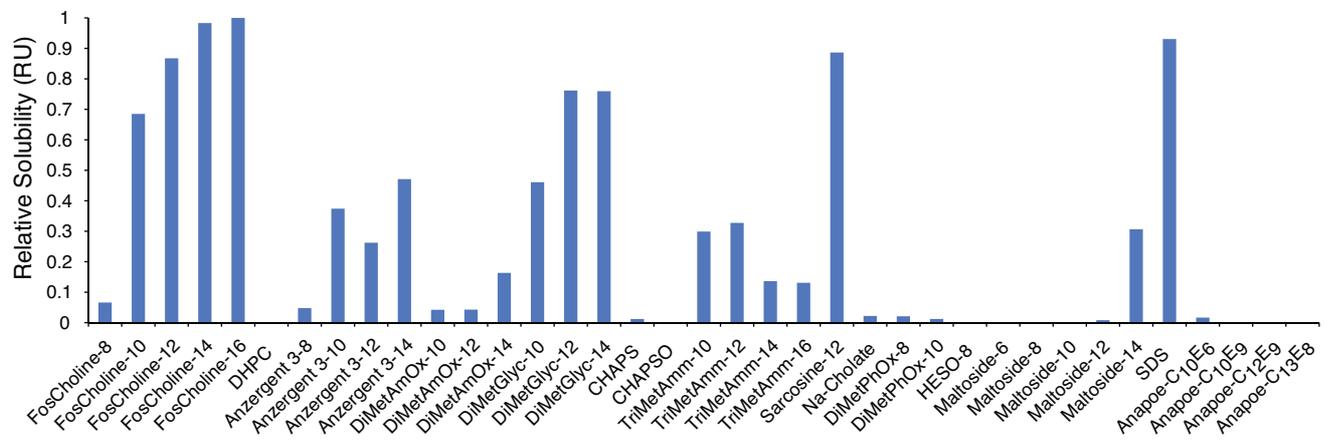
Fig. 4
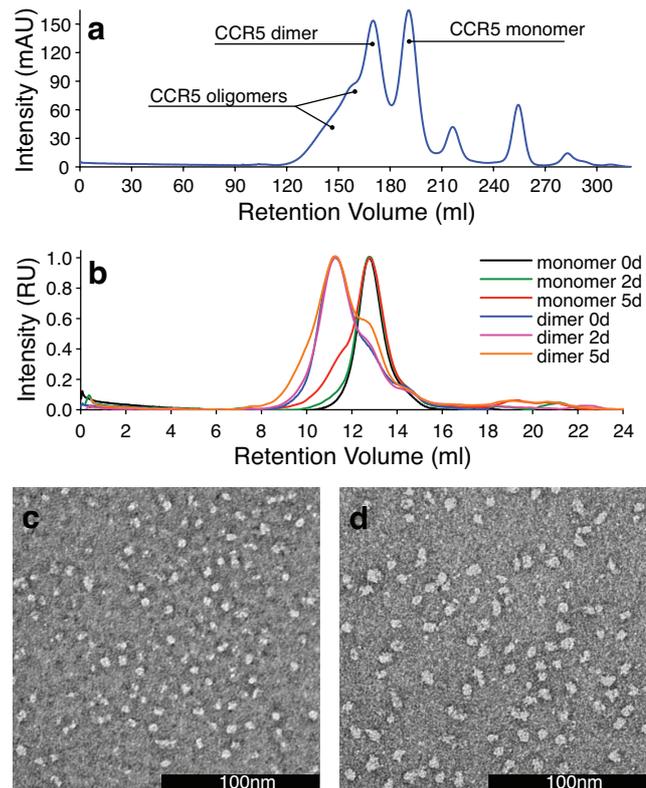
Fig. 5
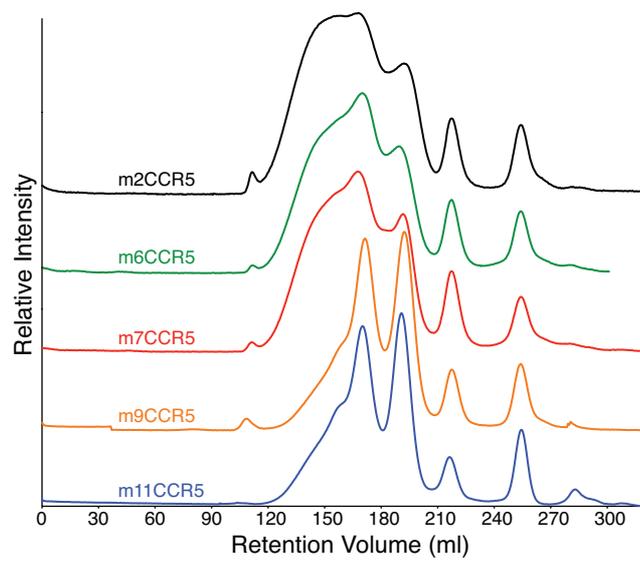
Fig. 6
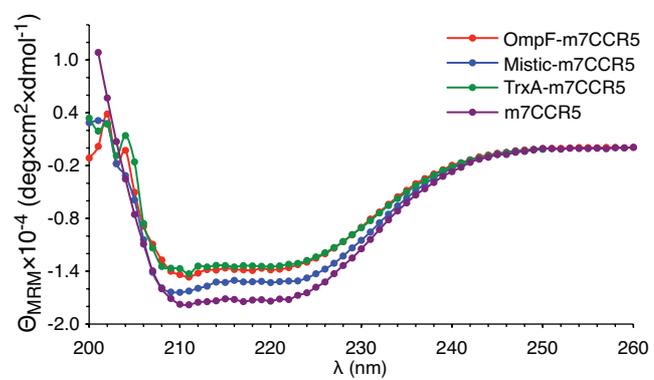
Fig. 7
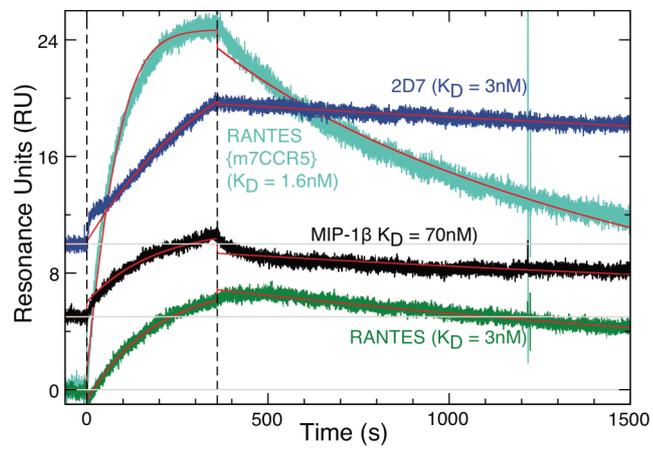
Fig. 8

Fig. 9

Biophysical and structural investigation of bacterially expressed and engineered CCR5, a G protein-coupled receptor

Maciej Wiktor[a], Sébastien Morin[a], Hans-Jürgen Sass[a], Fabian Kebbel[b], and Stephan Grzesiek[a,1]

[a]Department of Structural Biology, Biozentrum, University of Basel, Klingelbergstrasse 50/70, 4056 Basel, Switzerland
[b]Center for Cellular Imaging and Nano Analytics (C-CINA), Biozentrum, University of Basel, Mattenstrasse 26, CH-4058 Basel, Switzerland

[1]To whom correspondence should be addressed: Stephan Grzesiek, Department of Structural Biology, Biozentrum, University of Basel, Klingelbergstrasse 50/70, 4056 Basel, Switzerland, Tel.: +41 61 267 21; Fax +41 61 267 21 09; E-mail: stephan.grzesiek@unibas.ch

Supporting information

Text S1 The exact composition of M9 medium used in this study

To make 1L of M9 medium mix:
- 851 mL autoclaved ddH_2O,
- 0.1 mL 0.22 μm-filtered 1 M $CaCl_2$,
- 2mL 0.22 μm-filtered 1 M $MgSO_4$,
- 10 mL 0.22 μm-filtered Hutner's trace elements,
- 3 mL 0.22 μm-filtered 10 mg/mL thiamine hydrochloride,
- 4 mL 0.22 μm-filtered 0.25 mg/mL biotin,
- 20 mL 0.22 μm-filtered 20% glucose,
- 10 mL 0.22 μm-filtered 10% NH_4Cl pH 7.4,
- 100 mL 0.22 μm-filtered 10 x M9 salts (67.8 g Na_2HPO_4, 30 g KH_2PO_4, 5 g NaCl pH 7.4).

To prepare 200 mL of 100 x Hutner's trace elements use the procedure below:
1. Dissolve 1 g $FeSO_4$ and 10 g EDTA in 80 mL of ddH_2O. Adjust pH. A golden yellow solution results above around pH 5.5 and this is sufficient to proceed.
2. Dissolve the listed salts in 80 mL of ddH_2O:
- 4.4 g $ZnSO_4 \cdot 7H_2O$,
- 2.2 g H_3BO_3,
- 1 g $MnCl_2 \cdot 4H_2O$,
- 0.32 g $CoCl_2 \cdot 6H_2O$,
- 0.235 g $CuCl_2 \cdot 2 H_2O$,
- 0.22 g $(NH_4)_6Mo_7O_{24} \cdot 4H_2O$.
3. Combine solutions 1 and 2 and adjust pH to 6.9 using KOH and bring volume to 200 mL. Solution is bright green.
4. Filter through 0.22 μm and store at 4°C. Solution turns purple.
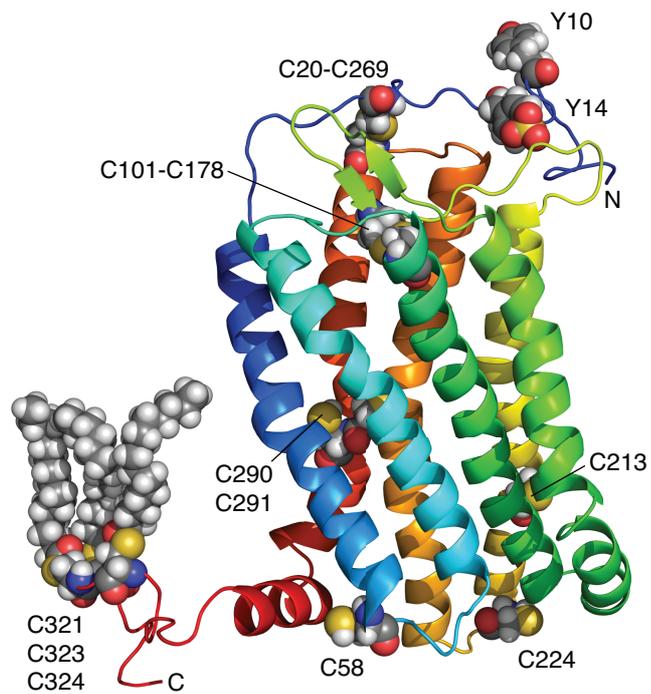
Fig. S1 Modeled 3D structure of CCR5. Model was rotated by 180° in relation to Fig. 2
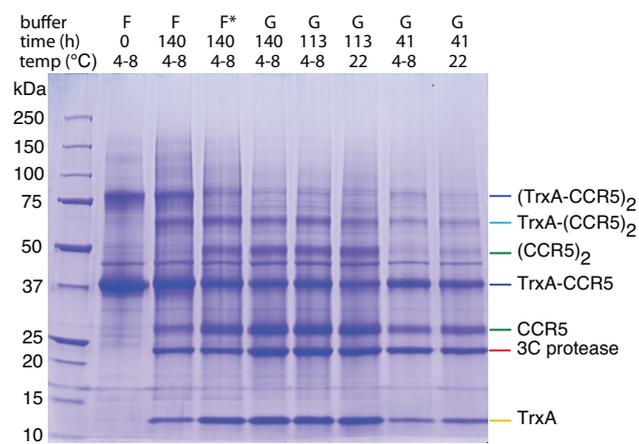
Fig. S2 TrxA-m7CCR5[306] cleavage with 3C protease. Protein eluted from Ni-NTA with buffer F (20 mM HEPES pH 7, 300 mM NaCl, 0.4 M imidazole, 0.1% FC-12, 10 mM β-mercaptoethanol) is cleaved very poorly. Certain improvement is achieved upon adding 1 mM DDT and 1 mM EDTA (*). Cleavage in buffer G (50 mM Tris-HCl pH 8, 150 mM NaCl, 0.1% FC-12, 1 mM DDT and 1 mM EDTA) is more efficient but still not complete after 140 h even when large amounts of 3C protease are used. Increase of temperature from 6°C to 22°C does not make a significant difference

a
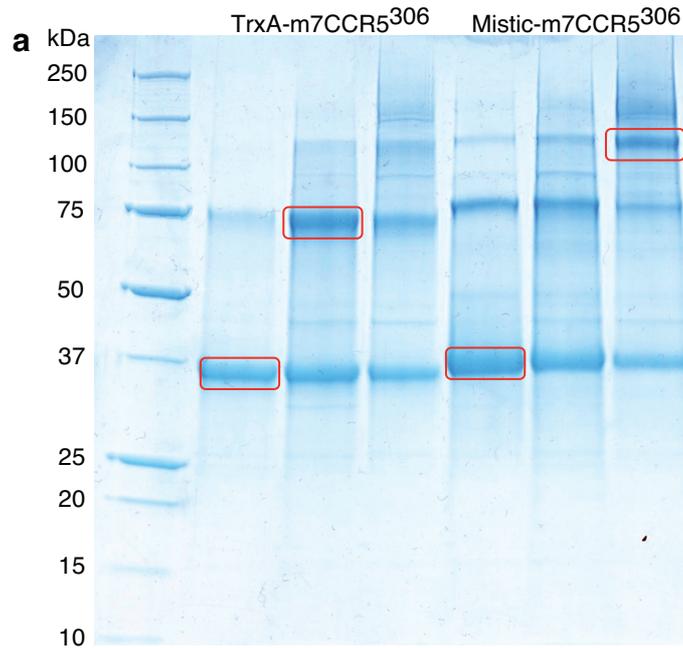
b

TrxA-m7CCR5^306 monomer

MSDK**IIHLTDDSFDTDVLK**ADGAILVDFWAEWCGPCK**MIAPILDEIADEYQGKLTVAKLNIDQNPGTAPK**YGIR**GIPTLLLFKNGEVAA
TKVGALSKGQLK**EFLDANLAGSGSGHMDYQVSSPIYDINYYTSEPCQKINVKQIAARLLPPLYSLVFIFGFVGNMLVVLILINSKRLKSMTDI
YLLNLAISDLFFLLTVPFWAHYAAAQWDFGNTMCQLLTGLYFIGFFSGIFFIILLTIDRYLAVVHAVFALKARTVTFGVVTSAITWVVAVFAS
LPGIIFTRSQKEGLHYTCSSHFPYSQYQFWKNFQTLKIVILGLVLPLLVMVIAYSGILKTLLRSRNEKKRHRAVRLIFTIMIVYFLFWAPYNIVL
LLNTFQEFFGLNNCSSSNRLDQAMQVTETLGMTHAAINPIIYAFVGEKFRNLEHHHHHH

TrxA-m7CCR5^306 dimer

IIHLTDDSFDTDVLKADGAILVDFWAEWCGPCK**MIAPILDEIADEYQGKLTVAKLNIDQNPGTAPKYGIRGIPTLLLFKNGEVA
ATKVGALSKGQLK**EFLDANLAGSGSGHMDYQVSSPIYDINYYTSEPCQKINVKQIAARLLPPLYSLVFIFGFVGNMLVVLILINSKRLKSMT
DIYLLNLAISDLFFLLTVPFWAHYAAAQWDFGNTMCQLLTGLYFIGFFSGIFFIILLTIDRYLAVVHAVFALKARTVTFGVVTSAITWVVAVF
ASLPGIIFTRSQKEGLHYTCSSHFPYSQYQFWKNFQTLKIVILGLVLPLLVMVIAYSGILKTLLRSRNEKKRHRAVRLIFTIMIVYFLFWAPYNI
VLLLNTFQEFFGLNNCSSSNRLDQAMQVTETLGMTHAAINPIIYAFVGEKFRNLEHHHHHH

Mistic-m7CCR5^306 monomer

MGFCTFFEKHHR**KWDILLEKSTGVMEAMKVTSEEKEQLSTAIDR**MNEGLDAFIQLYNESEIDEPLIQLDDDTAELMKQAR**DMYGQEKL
NEKLNTIIKQILSISVSEEGEKE**GSGSGLVPRGSHMDYQVSSPIYDINYYTSEPCQKINVKQIAARLLPPLYSLVFIFGFVGNMLVVLILINS
KRLKSMTDIYLLNLAISDLFFLLTVPFWAHYAAAQWDFGNTMCQLLTGLYFIGFFSGIFFIILLTIDRYLAVVHAVFALKARTVTFGVVTSAIT
WVVAVFASLPGIIFTRSQKEGLHYTCSSHFPYSQYQFWKNFQTLKIVILGLVLPLLVMVIAYSGILKTLLRSRNEKKRHRAVRLIFTIMIVYFL
FWAPYNIVLLLNTFQEFFGLNNCSSSNRLDQAMQVTETLGMTHAAINPIIYAFVGEKFRNLEHHHHHHHHHH

Mistic-m7CCR5^306 trimer

MGFCTFFEKHHR**KWDILLEKSTGVMEAMKVTSEEKEQLSTAIDR**MNEGLDAFIQLYNESEIDEPLIQLDDDTAELMKQAR**DMYGQEKL
NEKLNTIIKQILSISVSEEGEKE**GSGSGLVPRGSHMDYQVSSPIYDINYYTSEPCQKINVKQIAARLLPPLYSLVFIFGFVGNMLVVLILINS
KRLKSMTDIYLLNLAISDLFFLLTVPFWAHYAAAQWDFGNTMCQLLTGLYFIGFFSGIFFIILLTIDRYLAVVHAVFALKARTVTFGVVTSAIT
WVVAVFASLPGIIFTRSQKEGLHYTCSSHFPYSQYQFWKNFQTLKIVILGLVLPLLVMVIAYSGILKTLLRSRNEKKRHRAVRLIFTIMIVYFL
FWAPYNIVLLLNTFQEFFGLNNCSSSNRLDQAMQVTETLGMTHAAINPIIYAFVGEKFRNLEHHHHHHHHHH

Fig. S3 Identity confirmation of TrxA-m7CCR5^306 and Mistic-m7CCR5^306. (a) Monomer and dimer (TrxA-m7CCR5^306) or monomer and trimer (Mistic-m7CCR5^306) CCR5 bands (red rounded rectangles) were excised from SDS-PAGE gel stained with Colloidal Blue Stain Kit (Novex) and digested with trypsin prior to mass spectrometry analysis. (b) Identified peptide fragments of the analysed fusion constructs were marked in bold. Individual components of the fusion constructs (fusion partner, linker, cleavage site, CCR5 sequence, His-tag) were marked with colors
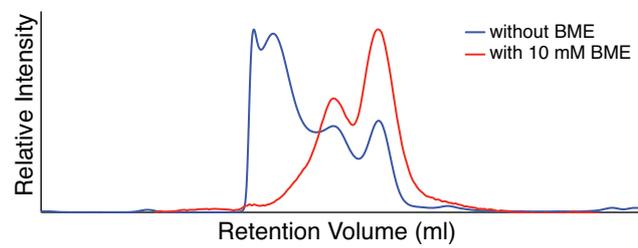
Fig. S4 Effect of β-mercaptoethanol (BME) on the oligomeric state of TrxA-m7CCR5[306]
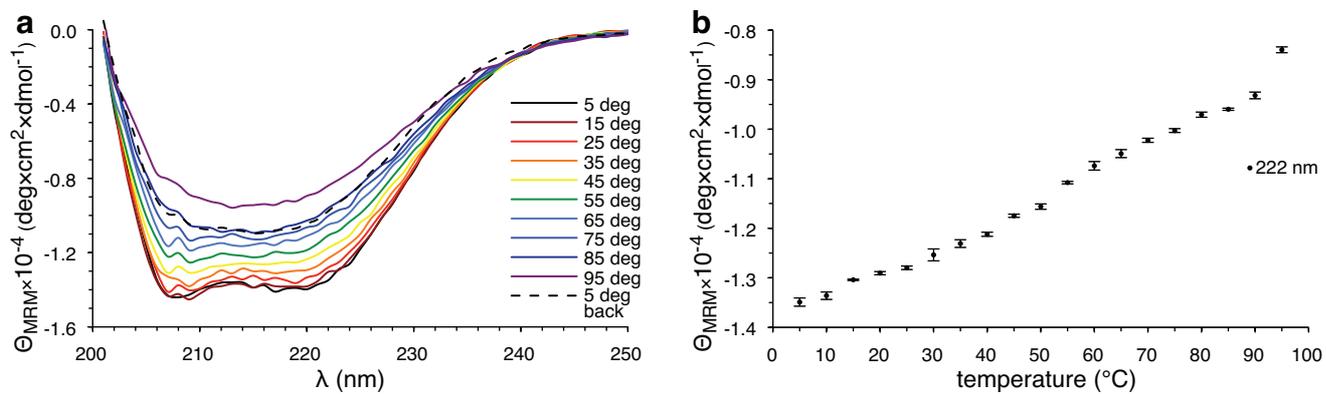
Fig. S5 Heat denaturation of TrxA-m7CCR5[306] measured using CD. (a) 200-250 nm CD spectra of TrxA-m7CCR5[306] at series of temperatures in the range of 5-95°C. Heat irreversibly changes the shape and the amplitude of the spectrum. (b) Plot of mean residue molar ellipticiy at 222 nm versus temperature shows a broad transition
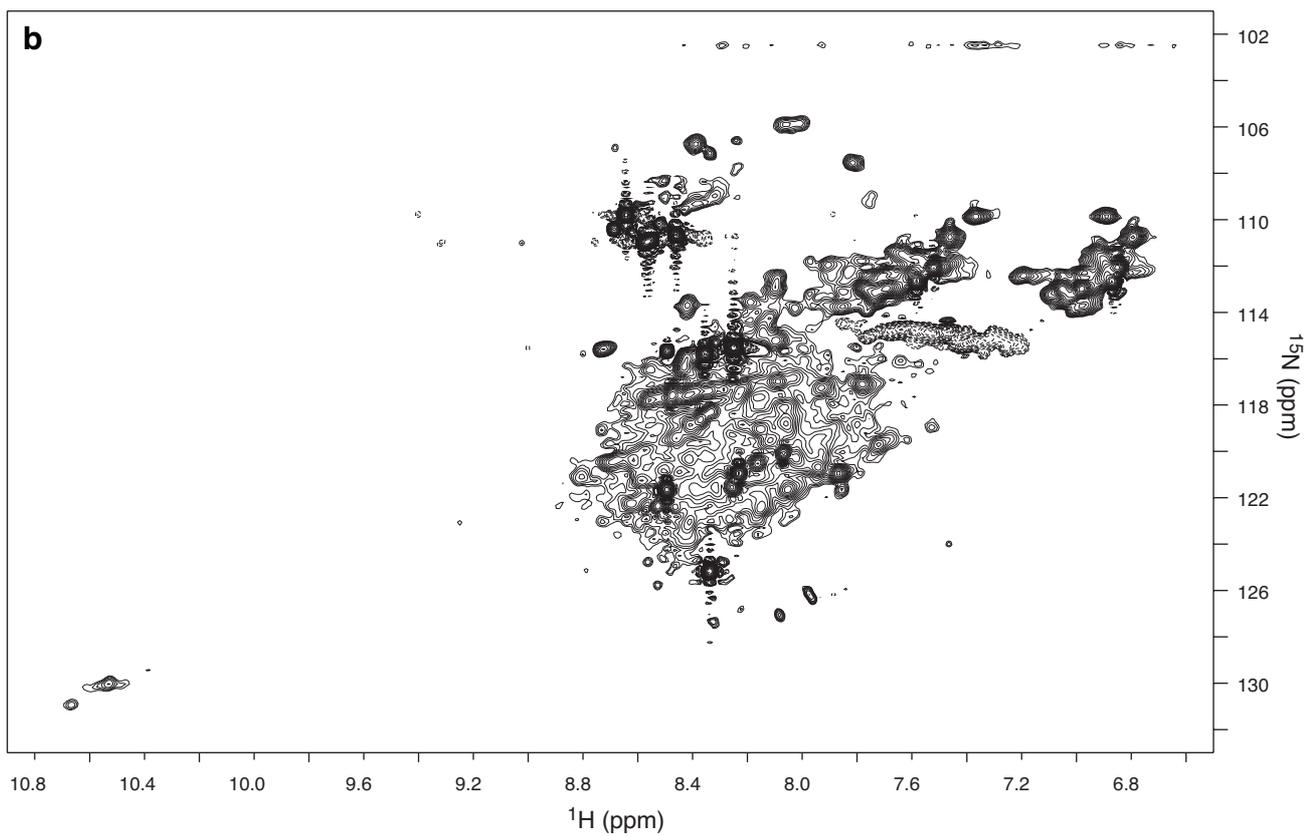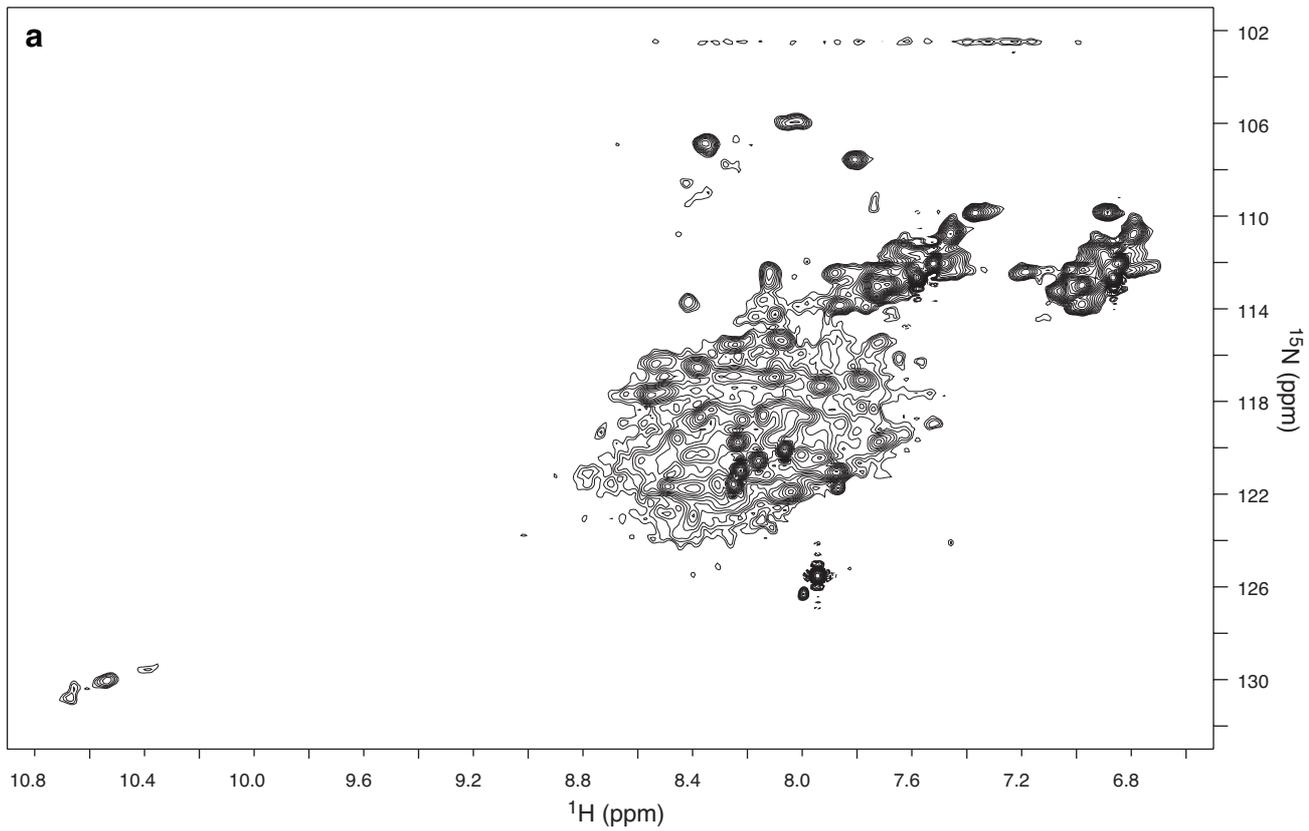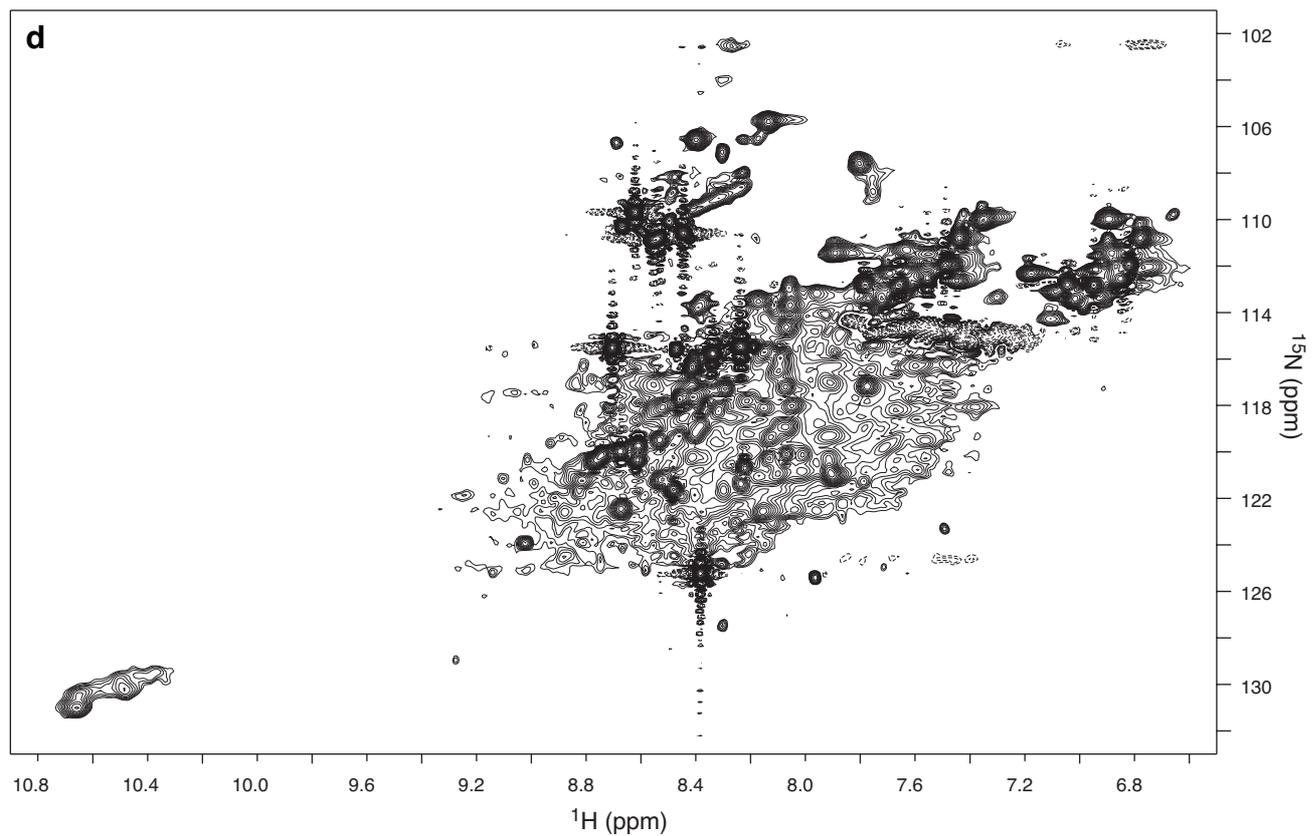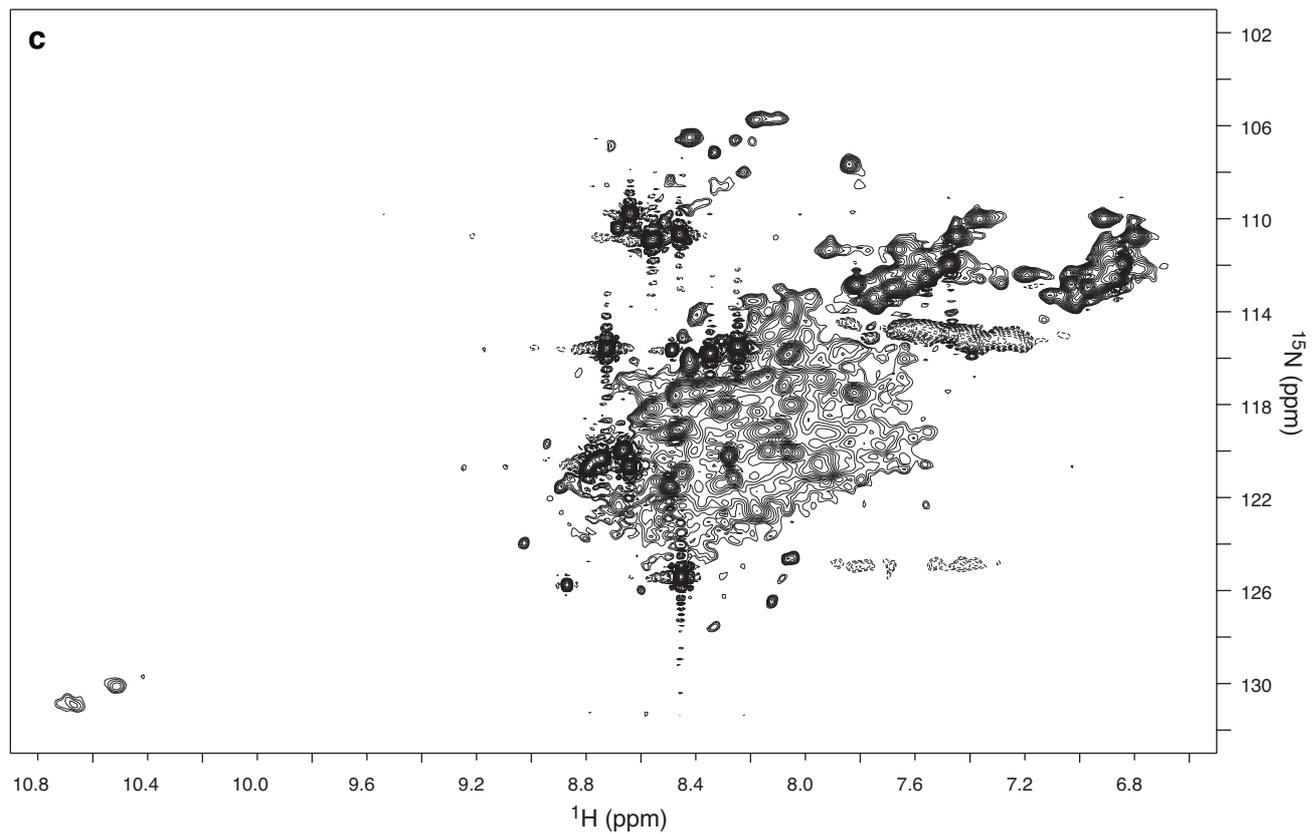
Fig. S6 Normalized HSQC spectra of ~100 μM ^{2}H,-^{15}N-labeled m11CCR5^{306} at various conditions. Upon pH change from 7.4 (a) to 5.8 (b) and 4.2 (c) new resonances become visible. Upon removal of 180 mM NaCl an increase of sensitivity is observed (d)

5 Studies of RANTES

5.1 Materials and methods

Cloning, expression and purification

The DNA sequence of 5P12-RANTES-E66S DNA was obtained by mutating the RANTES-E66S gene inside the pGEV2 plasmid containing the enterokinase-cleavable GB1-RANTES-E66S fusion construct under the T7 promoter (plasmid from our laboratory collection). The cloning strategy omitted gene amplification and ligation using the fact that the mutated nucleotides formed three clusters. The procedure involved three sequential site-directed mutagenesis PCR steps, each mutating 3-7 nucleotides and resulting in a mutation of 2-4 amino acids. After each PCR step plasmid was amplified in self-prepared TOP10 cells and sequenced to screen for the correctly mutated clones. To check the expression, pGEV2-transformed self-prepared BL21 cells were grown in 500 mL M9 medium at 37°C in baffled flasks with 130 rpm shaking. When OD_{600} reached 2, protein expression was induced with 1 mM IPTG. Collected culture samples were analyzed on SDS-PAGE followed by Coomassie staining. Isotope labeled RANTES was expressed and purified essentially as described previously (80).

Nuclear magnetic resonance

Isotope labeled RANTES samples were in 50 mM KH_2PO_4 pH 3.8, 0.02% NaN_3 (RANTES-E66S and 5P12-RANTES-E66S samples in Figures 5.3-5.7 and Table 5.1) or in 50 mM DCOONa pH 3.8 (RANTES-E66S and 5P12-RANTES-E66S samples in Figures 5.8-5.11 and Table 5.2). NMR samples were supplemented with 5% D_2O for locking and transferred to a Shigemi tube (5P12-RANTES-E66S in Figures 5.3-5.7 and Table 5.1, 250 µL) or glass tubes (all other samples, 400 µL). NMR experiments were recorded on a Bruker DRX600 spectrometer (5P12-RANTES-E66S in Figures 5.3-5.7 and Table 5.1) or on a Bruker DRX800 spectrometer equipped with a triple resonance Z-gradient TCI cryoprobe (all other spectra). $^{15}N,^{13}C$-labeled 5P12-

RANTES-E66S and $^{15}N,^{13}C,^{2}H$-labeled RANTES-E66S in FC-12 resonances were assigned using CBCANH (600 MHz, 37°C) and HNCACB (800 Mhz, 25°C) spectra, respectively. NMR spectra were processed using NMRPipe (94) and Sparky (95). C^{β}, C^{α} chemical shifts were obtained from CBCANH (HNCACB) experiment, whereas HN, N and C' from HNCO. Proton dimension was referenced for the water chemical shift according to pressure and temperature, while the heteronuclei according to the IUPAC-IUBMB-IUPAB recommendations (96). Random coil shifts, that were subtracted from the experimental shifts in order to calculate secondary chemical shifts, were obtained from the web server of the University of Kopenhagen (http://www1.bio.ku.dk/english/research/pv/sbin_lab/staff/MAK/randomcoil/script), which uses protein sequence, pH and temperature corrections (97-99). Standard ^{15}N relaxation measurements (T_1/T_2, {^{1}H}-^{15}N NOE) were recorded on uniformly $^{15}N,^{13}C$-labeled 5P12-RANTES-E66S at 600 MHz at 37°C. T_1/T_2 decay curves were fitted by an in-house written routine implemented in MATLAB (MathWorks, Inc.) using a simplex search minimization and Monte Carlo estimation of errors.

Circular dichroism

CD spectra of 50 μM $^{15}N,^{13}C,^{2}H$-labeled RANTES-E66S in 50 mM DCOONa pH 3.8, 5% D_2O were recorded at 20°C in 1 mm quartz Suprasil cuvettes (Hellma) using a Chirascan CD spectrometer (Applied Photophysics). Data points in a wavelength range of 200-260 nm were collected in triplicates and averaged followed by buffer subtraction (buffer + 0.5% FC-12 for RANTES-E66S spectrum in 0.5% FC-12).

5.2 Results

Cloning and expression testing

As a natural consequence of being a potent HIV-entry inhibitor and CCR5 ligand, 5P12-RANTES became an important subject of our studies. Although a very efficient and well characterized 5P12-RANTES expression platform was established in yeast, to obtain isotope labeled samples for NMR studies, we turned to our *E. coli*-based production system, which by that time was well established in our laboratory and

for many years has been successfully used to obtain milligram quantities of isotope labeled wild type RANTES and RANTES-E66S samples.

From the previous research performed in our laboratory and by others (71, 80) it was known that the wild type RANTES is very prone to aggregation and easily precipitates, especially at high concentration and high pH, which makes it quite challenging to study. Mutation E66S turns out to be a remedy as it significantly reduces aggregation tendency leaving molecular structure, dimerization property and other RANTES characteristics intact. For those reasons E66S mutations was included to the 5P12-RANTES sequence.

RANTES-E66S

```
5'-gga tcc gac gac gac gac aag    tcc cca tat tcc tcg gac acc aca ccc tgc tgc ttt gcc tac att gcc-3'
    G   S   D   D   D   D   K      S   P   Y   S   S   D   T   T   P   C   C   F   A   Y   I   A
   -7  -6  -5  -4  -3  -2  -1      0   1   2   3   4   5   6   7   8   9  10  11  12 13  14  15 16
    G   S   D   D   D   D   K   Q   G   P   L   M   A   T   Q   S   C   C   F   A   Y   I   A
5'-gga tcc gac gac gac gac aag cag ggc cca cct tta atg gcc acc caa tcc tgc tgc ttt gcc tac att gcc-3'
```

5P12-RANTES-E66S

0Q-S1G-RANTES-E66S primer pair
5'- ga tcc gac gac gac gac aag cag ggc cca tat tcc tcg gac acc -3'
5'- ggt gtc cga gga ata tgg gcc ctg ctt gtc gtc gtc gtc gga tc -3'

T8Q-P9S-RANTES-E66S primer pair
5'- c cca tat tcc tcg gac acc caa tcc tgc tgc ttt gcc tac att g -3'
5'- c aat gta ggc aaa gca gca gga ttg ggt gtc cga gga ata tgg g -3'

Y3P-S4L-S5M-D6A-RANTES-E66S primer pair
5'- gac gac aag cag ggc cca cct tta atg gcc acc caa tcc tgc tgc -3'
5'- gca gca gga ttg ggt ggc cat taa agg tgg gcc ctg ctt gtc gtc -3'

Figure 5.1 Generation of 5P12-RANTES-E66S DNA. Fragment of pGEV2 plasmid with the N-terminus of RANTES-E66S (top) and three primer pairs designed for site-directed mutagenesis PCR (bottom). Differing nucleotides and amino acids were marked with green (RANTES-E66S) and red (5P12-RANTES-E66S).

pGEV2 plasmid bearing enterokinase-cleavable GB1-RANTES-E66S fusion was used as a starting point for constructing 5P12-RANTES-E66S. The wild type RANTES and 5P12-RANTES differ in their N-termini and to go from one to the other the insertion of the very N-terminal glutamine and the mutation of seven more residues are necessary. This 8 amino acid difference translates to 15 nucleotides and after sequence alignment it becomes visible that differing nucleotides cluster in three groups (Figure 5.1). This feature made it possible to conveniently use site directed mutagenesis and avoid often problem-prone re-ligation of the new insert and empty plasmid. Three sequential site-directed mutagenesis PCR reactions intertwined with plasmid

amplification and sequencing resulted in expression-ready 5P12-RANTES-E66S sequence. Subsequently, the test showed large overexpression of 5P12-RANTES-E66S proving that the construct is ready for the isotope labeling for NMR studies (Figure 5.2).
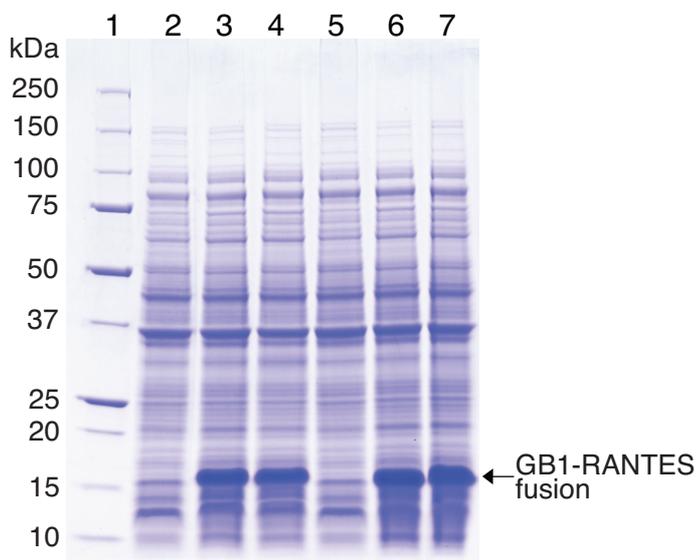
Figure 5.2 Expression test of GB1-5P12-RANTES-E66S fusion (lanes 5-7) with T7E-RANTES-E66S as control (lanes 2-4). Whole *E. coli* cells were analyzed on SDS-PAGE after 0 (lanes 2 and 5), 2 (lanes 3 and 6) and 4 h after induction (lanes 4 and 7).

5P12-RANTES-E66S heteronuclear fingerprint

^{15}N-^{1}H HSQC experiment enables observation of NH groups. Resonances in the spectrum represent a fingerprint of amino acids making up the protein. Most of the resonances come from the backbone amide groups but side chain HN groups of Asn, Gln, His, Trp, and sometimes Lys can also be observed. For these reasons and due to its sensitivity HSQC experiment is widely used as a sample quality check and at the same time constitutes the first chapter of NMR analysis.

HSQC spectrum of ^{15}N,^{13}C-labeled 5P12-RANTES-E66S is composed of 63 well-resolved backbone amide peaks, which correspond to 63 nonproline residues of 5P12-RANTES-E66S (Figure 5.3). This means that 100% of the observable residues is visible in the spectrum. Apart from the backbone amides a number of side chain resonances from Trp, Asn and Gln is also present. The backbone resonances span over 4 ppm in hydrogen dimension. Such wide peak dispersion is a characteristic feature of a well-folded protein, where each amino acid experiences a unique, well-defined,

nonrandom chemical environment. The sample could be stored for years without any measurable signs of deterioration or quality loss.

Assignment and Gln0 cyclization

The next step of the NMR analysis requires the exact knowledge of the identity of the observed resonances. For such small proteins like RANTES it was sufficient to record a single CBCANH experiment, which correlates C^β, C^α, N and HN chemical shifts. As N is coupled not only to its own C^α but also to the C^α of the preceding residue, CBCANH spectrum allows to "walk" along the sequence.
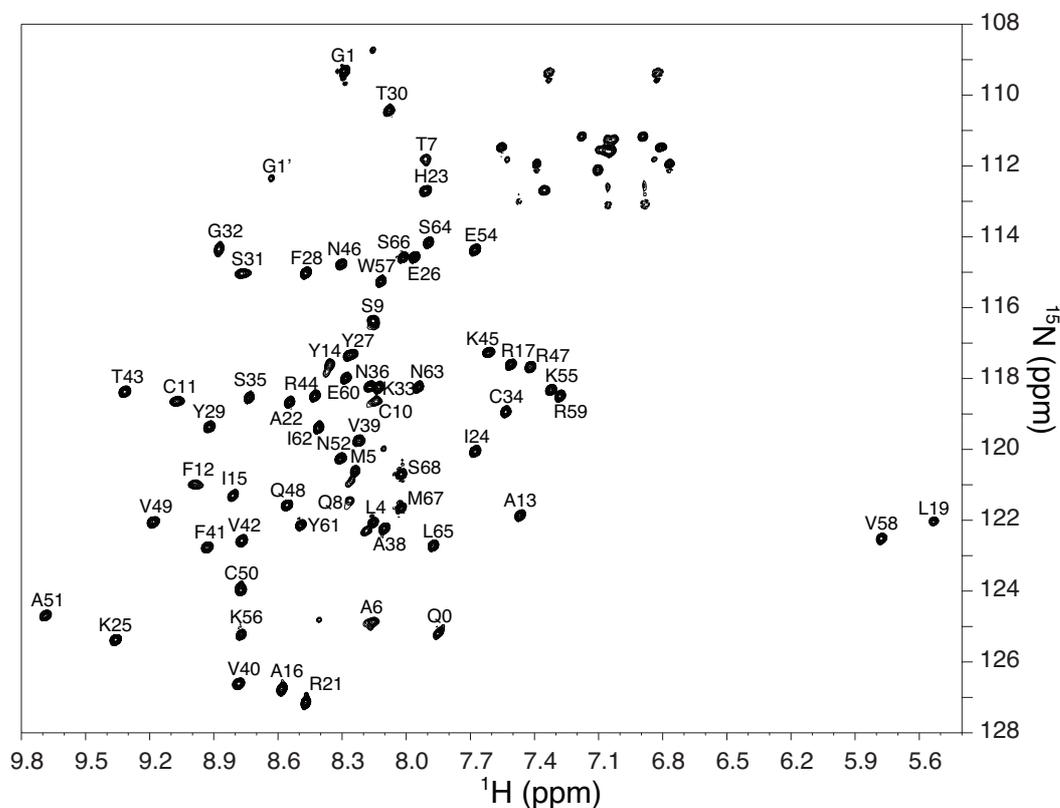
Figure 5.3 ^{15}N-^{1}H HSQC spectrum of ^{15}N,^{13}C-labeled 5P12-RANTES-E66S at pH 3.8 at 37°C with assigned backbone resonances. Due to the incomplete Gln0 cyclization two Gly1 peaks: big G1 and small G1' are observed corresponding to the cyclic (dominant) and the free (residual) forms, respectively.

The quality of 5P12-RANTES-E66S CBCANH spectrum and very limited overlap permitted a complete assignment using only CBCANH information (Figure 5.3). As 5P12-RANTES-E66S has an extra Gln0 at the very N-terminus, it was possible to assign Gly1, which normally would not be visible due to the protonated N-terminus.

Interestingly, the very N-terminal Gln0 peak can also be observed because of a spontaneously occurring irreversible glutamine cyclization (Figure 5.4A). A stable pentacyclic pyroglutamate ring is formed as a result of nucleophilic attack of the backbone nitrogen lone pair on the side chain carbonyl carbon with a release of NH_3. The reaction requires a deprotonated nitrogen and therefore at low pH takes days to complete. When HSQC is recorded soon after sample preparation a second resonance of Gly1 (G1') corresponding to the free N-terminus is also observed (Figure 5.3). The G1'/G1 peak intensity ratio decreases from ~8 right after sample preparation to ~2.5 day after. After four days the reaction is nearly complete The approximate estimation of the reaction half life yields ~2 days (Figure 5.4B).
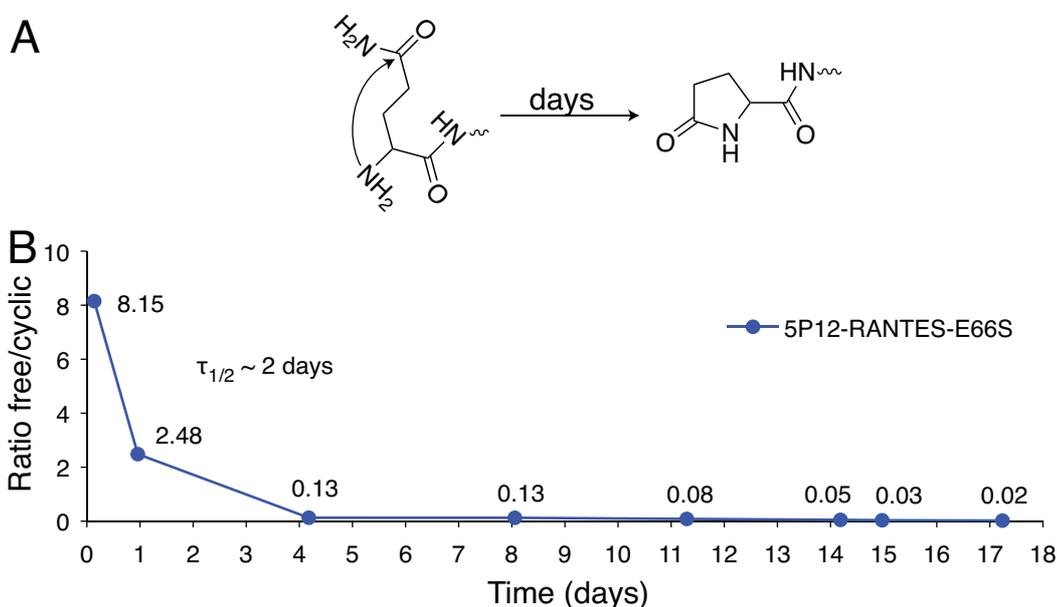
Figure 5.4 N-terminal Gln cyclization. Mechanism of the reaction relies on the nucleophilic attack of the backbone nitrogen on the side chain carbonyl carbon (A). Speed of the reaction was followed as a free/cyclic glutamine peak intensity ratio (B).

Chemical shift table

HNCACB spectrum was also used to construct a table of 5P12-RANTES-E66S chemical shifts (Table 5.1). Such table constitutes a valuable data set since:

- by calculating chemical shift differences for each residue structure of 5P12-RANTES-E66S can be compared to the known structure of RANTES,

- by subtracting random coil chemical shifts from the experimental shifts, the positions of secondary structure elements and unstructured regions can be mapped (see the secondary chemical shift analysis in Figure 5.6),
- using a suitable software e.g. CS-ROSETTA (100, 101) a low resolution 5P12-RANTES-E66S structure could be even calculated.

Table 5.1 Chemical shift (HN, ^{15}N, ^{13}C$^{\alpha}$, ^{13}C$^{\beta}$ and ^{13}C') table of 5P12-RANTES-E66S (cyclized side chain of Gln0). N/AV (not available), N/AP (not applicable).

No.	HN (ppm)	^{15}N (ppm)	^{13}C$^{\alpha}$ (ppm)	^{13}C$^{\beta}$ (ppm)	^{13}C' (ppm)
Q0	7.893	125.229	59.896	28.008	178.165
G1	8.334	109.399	44.372	N/AV	N/AV
P2	N/AP	N/AV	N/AV	N/AV	N/AV
P3	N/AP	N/AV	62.939	31.821	N/AV
L4	8.196	122.127	55.359	42.553	177.569
M5	8.283	120.699	55.477	33.061	175.979
A6	8.201	124.955	52.791	19.369	178.097
T7	7.959	111.865	62.103	69.709	174.815
Q8	8.305	121.549	55.964	29.400	175.669
S9	8.201	116.435	58.690	64.023	173.934
C10	8.185	118.712	52.792	39.408	174.112
C11	9.105	118.744	56.281	44.573	174.479
F12	9.025	121.092	58.117	40.272	173.786
A13	7.523	121.961	51.121	21.355	175.302
Y14	8.400	117.730	55.496	41.503	177.142
I15	8.863	121.347	61.520	38.969	175.934
A16	8.632	126.849	53.810	20.409	177.762
R17	7.562	117.712	52.732	31.143	N/AV
P18	N/AP	N/AV	62.373	31.503	176.707
L19	5.583	122.092	52.683	42.451	N/AV
P20	N/AP	N/AV	63.088	31.359	177.830
R21	8.516	127.209	58.918	29.444	178.766
A22	8.590	118.762	53.760	18.529	178.592
H23	7.963	112.856	54.835	29.393	174.320
I24	7.731	120.183	62.119	38.871	174.699
K25	9.413	125.520	57.029	35.571	175.765
E26	8.017	114.655	55.012	31.663	172.973
Y27	8.309	117.445	56.105	43.076	172.871
F28	8.526	115.136	56.324	40.700	173.219
Y29	8.965	119.491	57.989	39.881	177.748
T30	8.138	110.574	61.945	70.875	174.923
S31	8.806	115.140	58.483	64.127	176.894
G32	8.916	114.359	46.434	N/AP	174.563
K33	8.179	118.407	56.498	32.096	177.665
C34	7.590	119.031	54.244	38.907	175.435
S35	8.778	118.620	61.190	63.216	174.190
N36	8.209	118.310	50.218	39.203	N/AV

P37	N/AP	N/AV	62.970	32.287	176.602
A38	8.158	122.311	52.488	24.539	175.724
V39	8.273	119.852	60.353	34.472	172.460
V40	8.839	126.735	60.251	32.175	176.040
F41	8.987	122.877	56.600	41.138	174.817
V42	8.826	122.692	60.931	33.175	177.725
T43	9.366	118.479	60.893	71.591	177.023
R44	8.480	118.582	59.019	29.624	177.143
K45	7.670	117.356	55.819	31.383	175.225
N46	8.359	114.885	54.723	36.762	174.687
R47	7.468	117.735	55.520	31.166	175.436
Q48	8.599	121.670	55.396	29.931	175.972
V49	9.232	122.077	60.835	35.102	174.640
C50	8.819	124.050	57.562	48.066	173.811
A51	9.736	124.801	50.843	24.114	174.486
N52	8.357	120.396	50.176	38.883	N/AV
P53	N/AP	N/AV	63.824	32.012	175.610
E54	7.739	114.512	56.239	28.882	177.813
K55	7.377	118.426	54.318	32.297	177.626
K56	8.819	125.330	60.543	32.191	179.010
W57	8.157	115.328	59.151	26.686	176.947
V58	5.842	122.601	66.030	30.867	177.578
R59	7.334	118.614	59.408	29.596	179.140
E60	8.332	118.102	59.159	28.532	179.662
Y61	8.545	122.199	60.227	37.423	179.035
I62	8.461	119.465	65.913	37.673	178.509
N63	7.999	118.361	55.959	38.350	177.139
S64	7.952	114.265	60.212	63.821	175.655
L65	7.926	122.808	56.044	43.383	177.715
S66	8.060	114.663	59.004	64.035	174.268
M67	8.075	121.761	55.662	33.328	175.736
S68	8.061	120.917	59.403	64.748	N/AV

Similarity and differences to the wild type RANTES

Last but not least it needs to be noticed that 5P12-RANTES-E66S HSQC spectrum to a large extent overlays well with the spectrum of RANTES-E66S (Figure 5.5). This helped with the assignment of 5P12-RANTES-E66S but obviously not in the case of the N-terminus, which sequence has been modified (Figure 5.5, red resonances). Since RANTES-E66S similarly to the wild type RANTES readily forms dimers, two sets of HSQC peaks are observed even at such low concentrations as 25 μM. This is not the case of 5P12-RANTES-E66S, for which even at 0.6 mM only one set of peaks is observed and proves that at the tested conditions 5P12-RANTES-E66S does not form dimers. This seems logical, as the N-terminus, which vastly contributes to the

dimerization interface has been significantly modified. As a natural consequence of its monomerism, 5P12-RANTES-E66S resonances should also overlap better with the resonances of RANTES-E66S monomer than with the resonances of RANTES-E66S dimer. This is indeed the case, particularly obvious for Ser31 and Gly32, for which the difference between monomer and dimer RANTES-E66S resonances of is the most striking but also for many other residues e.g. Ala13, Leu19, Arg21, Phe28, Ala51, Tyr61, etc. (Figure 5.5).
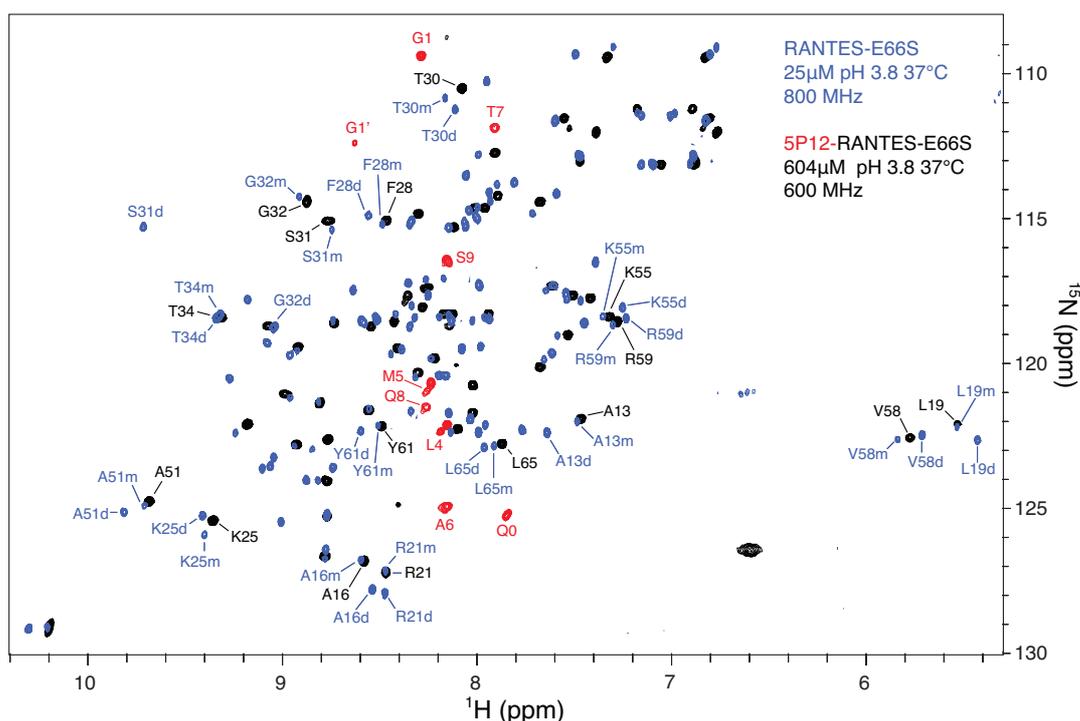
Figure 5.5 Similarity of 5P12-RANTES-E66S to RANTES-E66S. The ^{15}N-^{1}H HSQC spectra of 604 μM 5P12-RANTES-E66S (black and red) and 25 μM RANTES-E66S (blue) were overlaid. As RANTES-E66S readily forms dimers, low concentration was used to increase monomer:dimer ratio. The exemplary nonoverlaping resonances of both RANTES variants were labeled with assignment information. 5P12-RANTES-E66S resonances overlap well with the resonances of monomeric RANTES-E66S (particularly clear for S31 and G32) with the exception of the N-terminus (red), for which the amino acid sequence has been mutated.

Similarity of 5P12-RANTES-E66S to the wild type RANTES is also visible from the secondary chemical shift analysis in Figure 5.6, where $^{13}C^\alpha$, $^{13}C^\beta$, $^{13}C'$, ^{15}N shifts were plotted against 5P12-RANTES-E66S residue number. The secondary structure elements according to the PDB entry 1EQT were drawn on the top. Although, 1EQT structure contains RANTES with a minor modification of the N-terminus (missing Ser1 and Pro2Gly mutation), it should be representative for the secondary

structure elements of the wild type RANTES. This is because the very N-terminus of RANTES is neither a part of any secondary structure element itself nor is involved in RANTES dimerization interface. Therefore is unlikely that such a modification could affect the overall RANTES structure in any major way. On the other hand 1EQT structure offers a high resolution of 1.6 Å, lacks other mutations or chemical modifications and was crystallized alone (without a disaccharide ligand).

The positive $^{13}C^{\alpha}$ and $^{13}C'$ and and negative $^{13}C^{\beta}$ shifts are an indication of helical secondary structure and are clearly observed for 3_{10} (η_1) and α-helix (α_1). Amino acids participating in β-strands, on the other hand, often have negative $^{13}C^{\alpha}$ and $^{13}C'$ and positive $^{13}C^{\beta}$. With the exception of the oxidized Cys50 this is clearly the case for β_1 and β_3 strands. However, in the case of Cys50 the positive value of $^{13}C^{\alpha}$ in the middle of a β-strand and an extraordinary large $^{13}C'$ shifts (Figure 5.6, grey bars) may suggest that the used random coil values for oxidized cysteine (102) may not be adequate. For β_2 strand, $^{13}C^{\alpha}$ and $^{13}C^{\beta}$ shifts predict the presence of a β-strand, whereas the information from $^{13}C'$ is more ambiguous. The chemical shift values of the N-terminus do not deviate significantly towards any type of secondary structure, which is understandable as the intermolecular β_N strand cannot be formed in monomeric 5P12-RANTES-E66S. Therefore it is likely that the N-terminus is flexible and adopts random coil conformation. The outstanding very large $^{13}C^{\alpha}$ shift of the very N-terminal Gln0 can be easily rationalized by the cyclization of the Gln0 side chain. Secondary shift analysis goes along with the similarity of HSQC spectra and suggests that 5P12-RANTES-E66S structure is similar to the structure of the wild type RANTES monomer.
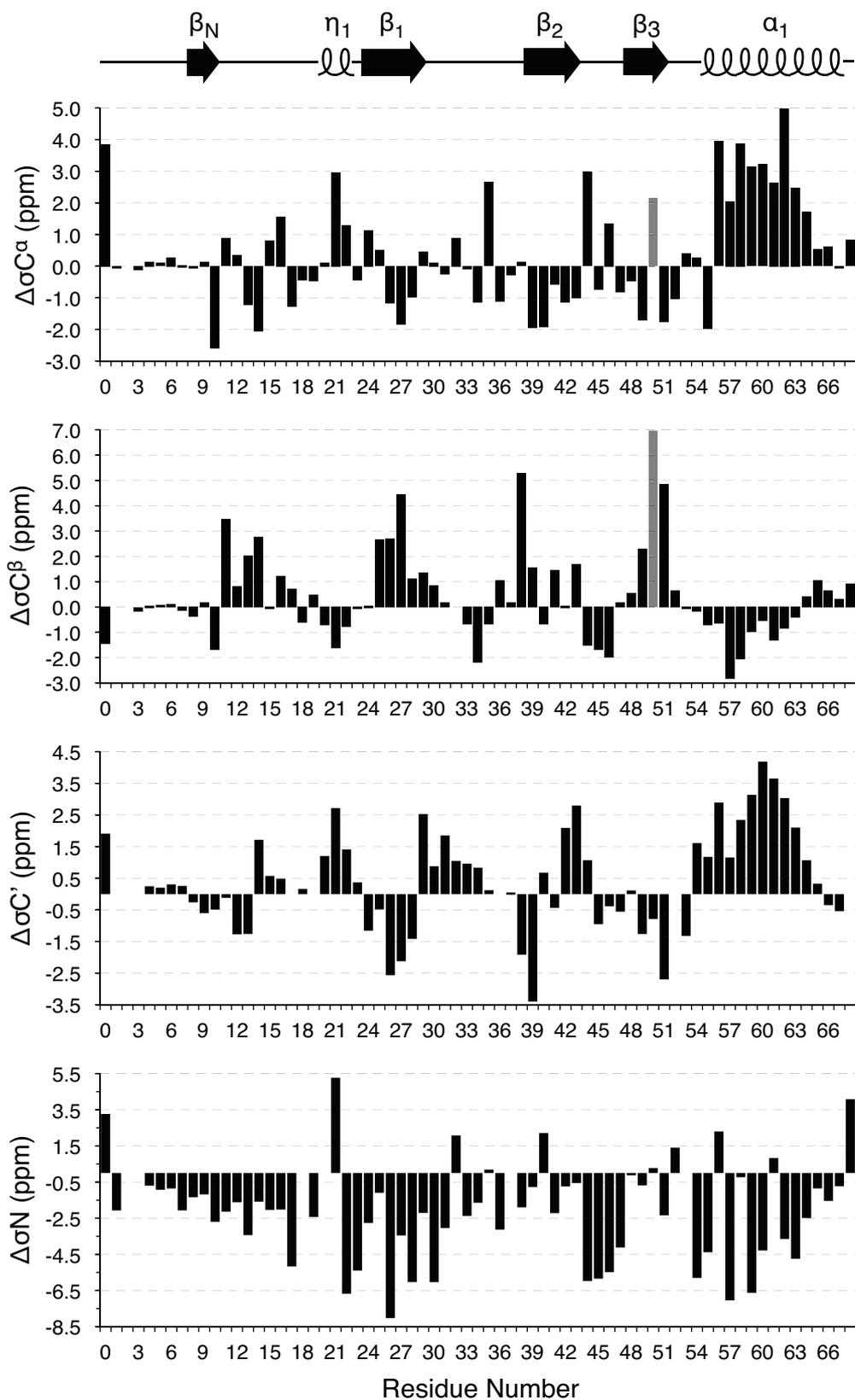
Figure 5.6 Secondary chemical shift analysis ($^{13}C^{\alpha}$, $^{13}C^{\beta}$, $^{13}C'$, ^{15}N) of 5P12-RANTES-E66S. Secondary structure elements according to PDB entry 1EQT (81) are drawn at the top.

Relaxation experiments

A complete protein biophysical characterization on a molecular level requires both solving its three dimensional structure and knowledge about its dynamics, that is about the flexibility/rigidity of its parts on various timescales. Although, due to the similarity of the 5P12-RANTES-E66S and the wild type RANTES HSQC spectra and due to the extensive workload (months), high resolution structure determination was not attempted, 5P12-RANTES-E66S dynamics has been characterized. For this purpose three following relaxation experiments were performed (Figure 5.7):

- T_1 called also spin-lattice or longitudinal relaxation,
- T_2 called also spin-spin or transverse relaxation and
- $\{^1H\}$-^{15}N heteronuclear NOE cross-relaxation.

For the vast majority of 5P12-RANTES-E66S resonances (residues 10-66) $1/T_1$, $1/T_2$ and $\{^1H\}$-^{15}N NOE values remain on steady levels of 2.25 ± 0.14 s^{-1} (SD), 6.36 ± 1.84 s^{-1} and 0.71 ± 0.05, respectively. This means that the tumbling rate is relatively uniform along the protein's amino acid sequence and that the protein behaves like a rigid particle. This situation is different for the C-terminus (residues 67-68) and for the N-terminus especially (residues 0-9), for which all $1/T_1$, $1/T_2$ and $\{^1H\}$-^{15}N NOE values significantly deviate from the protein's average. For the C-terminus the $1/T_1$, $1/T_2$ and $\{^1H\}$-^{15}N NOE values drop to 1.03 s^{-1}, 1.55 s^{-1} and -0.63 (for Ser68), whereas for the N-terminus even more up to 0.55 s^{-1}, 1.06 s^{-1} and -2.59 (for Gln0), respectively. These low values of the N- and C-termini result from the ps-ns motions i.e. the enhanced flexibility of 5P12-RANTES-E66S backbone in these regions. The hump of $1/T_2$ around residues 5-9 comes from the additional motions on the μs-ms timescale. Such an increased N-terminal flexibility goes along with the fact that, unlike for the wild type RANTES, the N-terminus on the 5P12-RANTES-E66S is not involved in a dimerization interface i.e. in the formation of the intermolecular β-sheet.
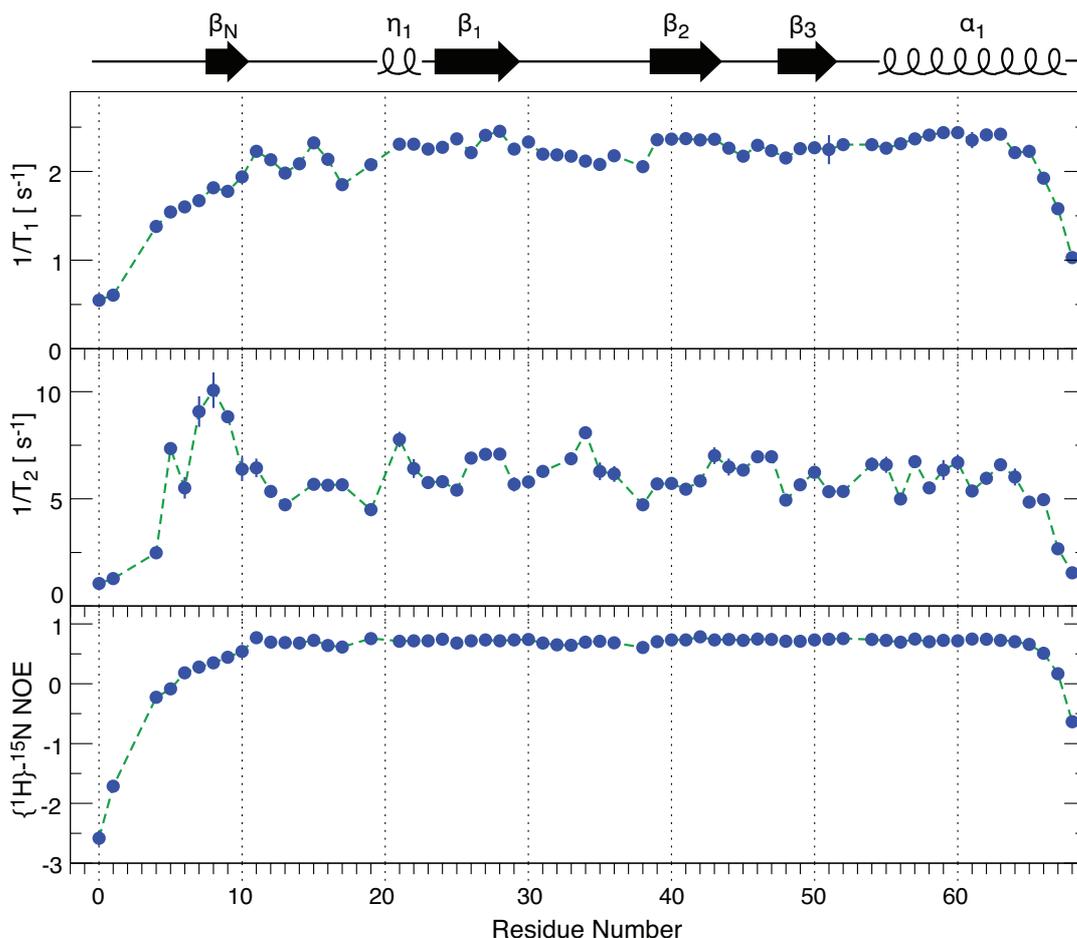
Figure 5.7 Relaxation of 5P12-RANTES-E66S measured on 600 MHz spectrometer at 37°C. The presented data is an average of two ($1/T_1$ and $\{^1H\}$-^{15}N NOE) or three ($1/T_2$) independent experiments. The error bars represent the standard deviation. Secondary structure elements according to PDB entry 1EQT (81) are drawn at the top.

RANTES-CCR5/detergent interaction

5.2.1.1 Introduction

CCR5 interaction with chemokines and with RANTES especially plays a key role in CCR5 biology. Since RANTES can compete HIV infection, revealing details of RANTES-CCR5 interaction became increasingly interesting as a door to understand an exact molecular mechanism of CCR5 involvement in the disease. RANTES-CCR5 interaction was studied using SPR by Navratilova and coworkers (103) and also in our laboratory using ITC and NMR by Lydia Nisius (13, 82) and using SPR by Sébastien Morin (unpublished data). Since SPR setup relies on a selective (usually via an antibody) CCR5 capture on a chip, receptor pre-purification is usually not necessary. The situation changes when it comes to ITC or NMR, which do not provide an intrinsic

purification possibility and both require purified CCR5 and RANTES. Additionally, SPR is far more sensitive than ITC or NMR and therefore requires much smaller protein amounts, which becomes an asset when obtaining large receptor yields is challenging.

The RANTES-CCR5 interaction studies performed previously in our laboratory used insect cell-expressed CCR5 solubilized in FC-12 (13, 82). After comparing several detergents, FC-12 was selected because it solubilized CCR5 with the largest yield, gave the most homogenous electron micrograph of purified CCR5 and preserved CCR5 native conformation as judged by immunoprecipitation with 2D7 (see section Discussion of Chapter 3). With ITC it was observed that RANTES interacts with CCR5 with a K_D of ~ 1 μM. However, when unlabeled CCR5 was titrated into ^{15}N-labeled RANTES-E66S, no chemical shift perturbations could be observed, and what's more, RANTES-E66S resonances weakened with the increasing amounts of the injected receptor and a set of new resonances appeared.

5.2.1.2 NMR analysis

By that time, we have already found that 2D7 does not immunoprecipitate CCR5 in FC-12. This could indicate that the structure of the receptor is affected but another explanations e.g. perturbation of 2D7 structure by FC-12, electrostatic repulsion of 2D7 antigen-binding epitope by positively charged head groups of FC-12/CCR5 micelle or a simple competition could not be completely excluded. However, besides a potential effect of FC-12 on CCR5, there was no other evidence suggesting that in FC-12, CCR5-RANTES interaction could not be studied. In addition, despite extensive detergent screening (see sections Detergent screening of Chapters 3 and 4) no better detergents could be found to replace FC-12 for CCR5 solubilization and purification. Those detergents that were showed to support CCR5 recognition by 2D7 did not permit purification of the stable receptor at high yields.

Therefore, to compare with the previous results of Nisius (13), namely RANTES interaction with the FC-12-solubilized insect cell-expressed wild type CCR5, FC-12-solubilized *E. coli*-expressed m9CCR5[306] monomer was stepwise titrated into a 50 μM ^{15}N,^{13}C,^{2}H-labeled RANTES-E66S solution. The RANTES-E66S resonances weakened with the increasing FC-12-solubilized m9CCR5[306] concentration (Figure 5.8). The effect was much greater than what could result from a moderate (~10%)

sample dilution and was resonance-selective. A set of ~15 pronounced resonances, all around 8.2 ppm (Figure 5.8C), distinguished itself from the previously intensity-homogenous RANTES-E66S dimer spectrum (Figure 5.8A). These observations coincide with the previous findings of Nisius for the wild type CCR5 expressed in insect cells (13).
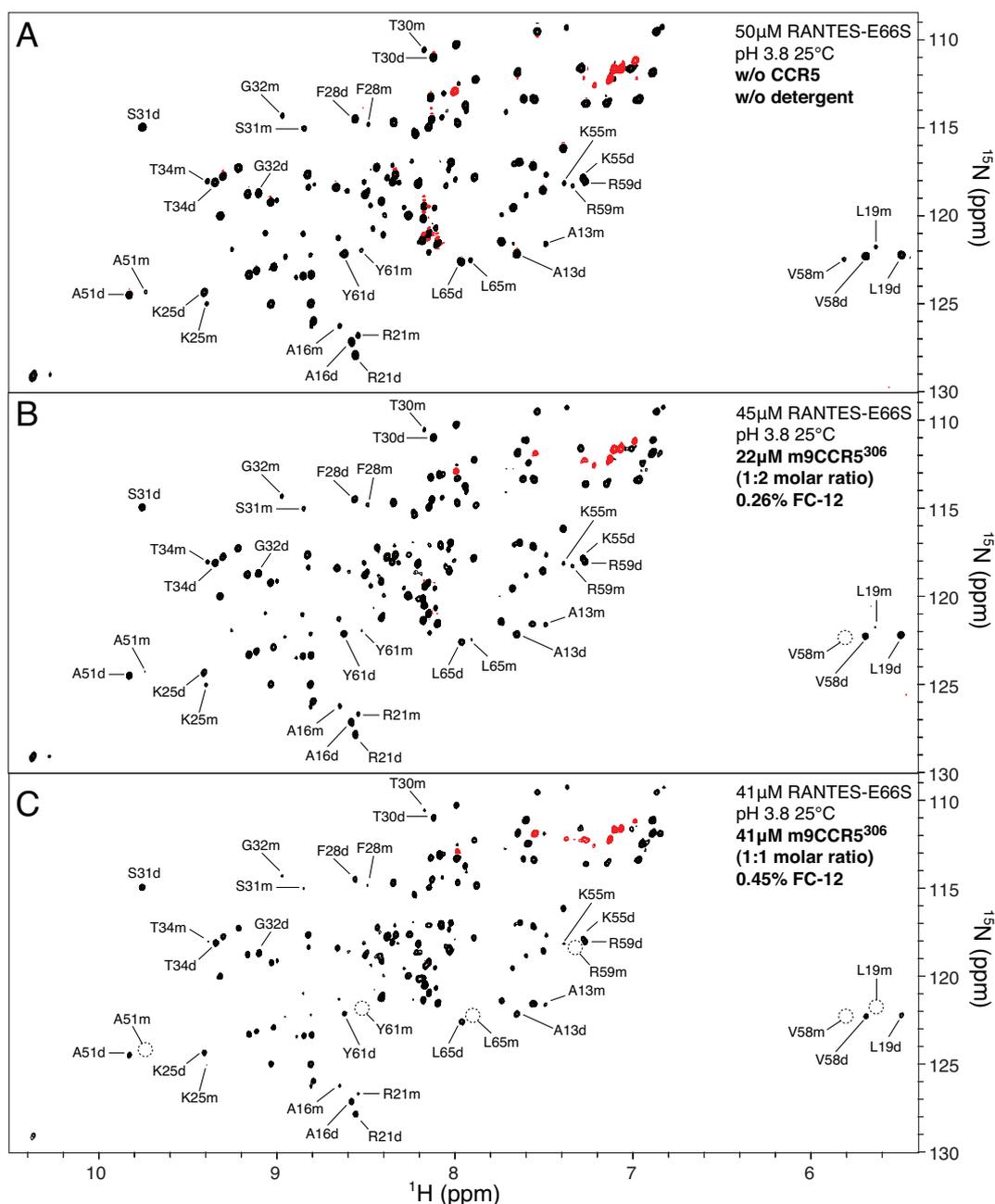
Figure 5.8 HSQC spectra of RANTES-E66S at pH 3.8 at 25°C without detergent (A) and with 1:2 (B) and 1:1 (C) molar ratio of CCR5. Negative peaks resulting from folding are colored red. The exemplary nonoverlaping resonances were labeled with the assignment information. The resonances below the threshold were surrounded by black dashed circles.
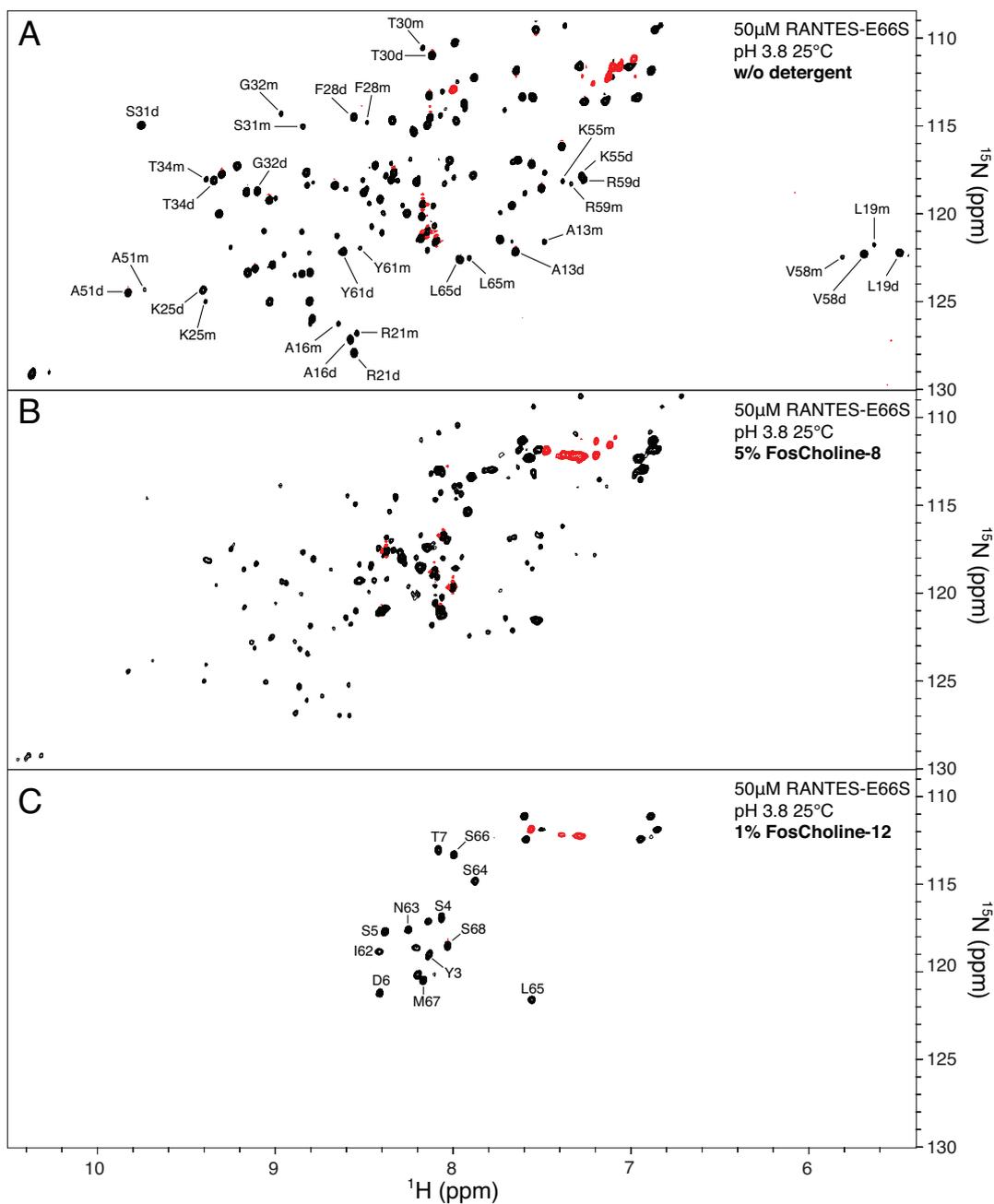
Figure 5.9 HSQC spectra of 50 µM RANTES-E66S at pH 3.8 at 25°C without detergent (A) and with 5% FC-8 (B) and 1% FC-12 (C). Negative peaks resulting from folding are colored red. The exemplary nonoverlaping resonances were labeled with the assignment information.

However, the very similar observation was made when Fos-Choline detergents solutions without CCR5 were injected. The intensity of RANTES-E66S resonances decreased upon addition of a detergent from the Fos-Choline family (Figure 5.9). The resonances of RANTES-E66S weakened up to a complete disappearance. Fos-Cholines with various hydrocarbon chain length from 8 to 16 were tested and with the exception

of FC-8 (CMC in H_2O 3.4%) each of them at 1% concentration bleached the vast majority of the original RANTES-E66S resonances. FC-12 was additionally tested at 0.5% (by diluting the sample at 1%) with the same effect. When FC-8 concentration was raised to 5%, RANTES-E66S resonance were largely but not completely gone (Figure 5.9B).

The remaining set of RANTES-E66S resonances (most of them) could be assigned solely based of the HNCACB data to the N- and C- RANTES-E66S termini. The visible residues until T7 (Y3-T7) and all the residues from I62 onwards could be unambiguously identified (Figure 5.9C). The secondary shift analysis of the assigned resonances suggests that within the very terminal regions the RANTES-E66S secondary structure was not severely perturbed (Figure 5.10). The N-terminus remained largely unstructured, whereas the C-terminus with large positive $^{13}C^{\alpha}$ shifts was still a part of α_1 helix.

At pH 6.3 the effect of 1% FC-12 addition was milder than at pH 3.8 (data not shown). This indicates that the phenomenon of disappearing RANTES-E66S resonances is in some way also pH-modulated.

Unlike Fos-Choline detergents DHPC with a similar head group did not bleach RANTES-E66S resonances even at 5% concentration (Figure 5.11A). Similarly, when 1% Cymal-5 or 2.2% DDM/CHAPS/CHS mixture (1/1/0.2) were injected no resonance bleaching occurred. Interestingly, detergents with a maltose head group shifted RANTES-E66S equilibrium towards its monomeric form (Figure 5.11A,B). Such effect was not observed for any other tested detergent.
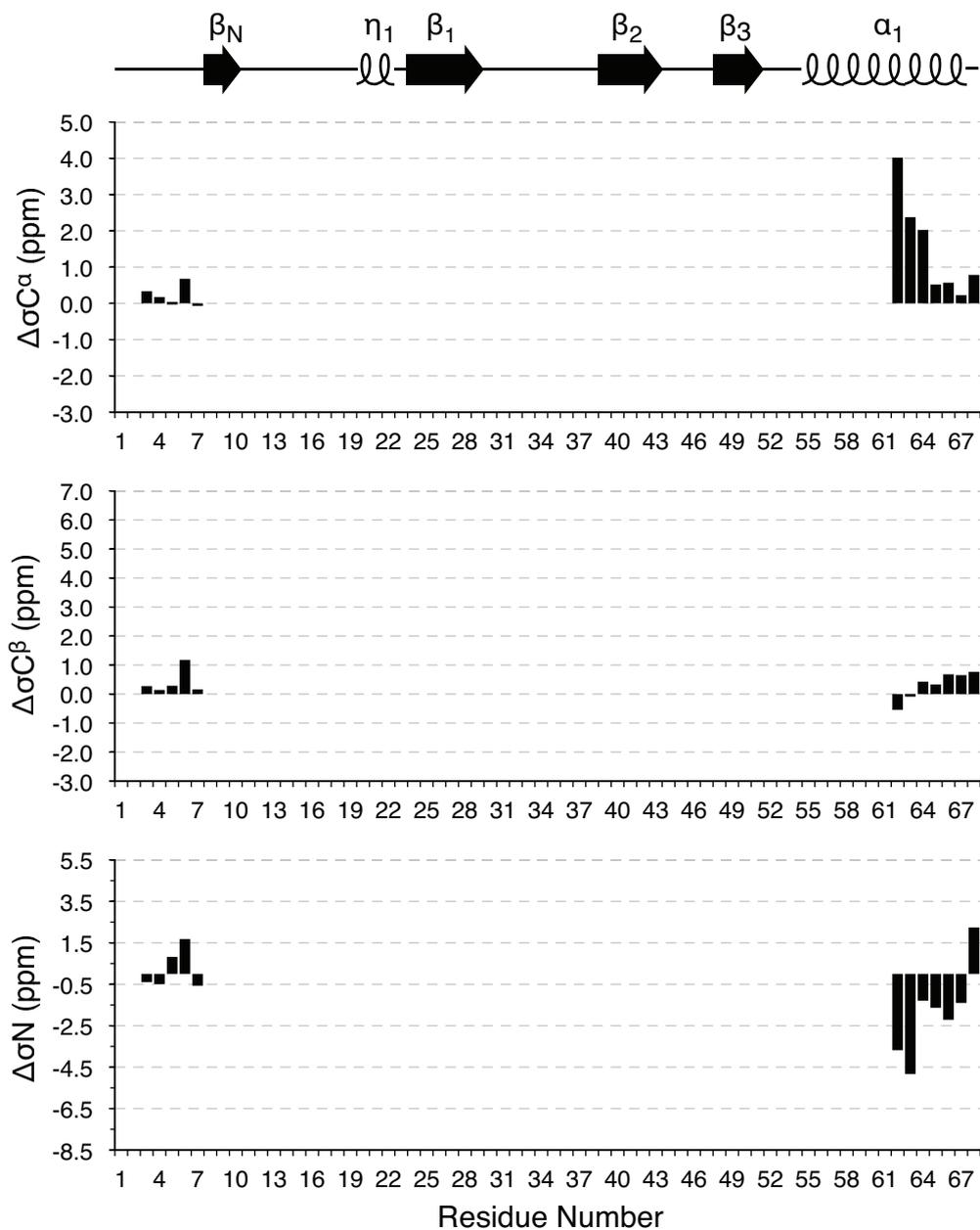
Figure 5.10 Secondary chemical shift analysis ($^{13}C^{\alpha}$, $^{13}C^{\beta}$, ^{15}N) of RANTES-E66S in the presence of 1% FC-12. For a convenient comparison to Figure 5.6 data was plotted to the same scale. Although HNCACB spectrum of RANTES-E66S was recorded at 25°C (5P12-RANTES-E66S at 37°C), the secondary chemical shift pattern closely resembles the patter of 5P12-RANTES-E66S. Secondary structure elements according to PDB entry 1EQT (81) are drawn at the top.
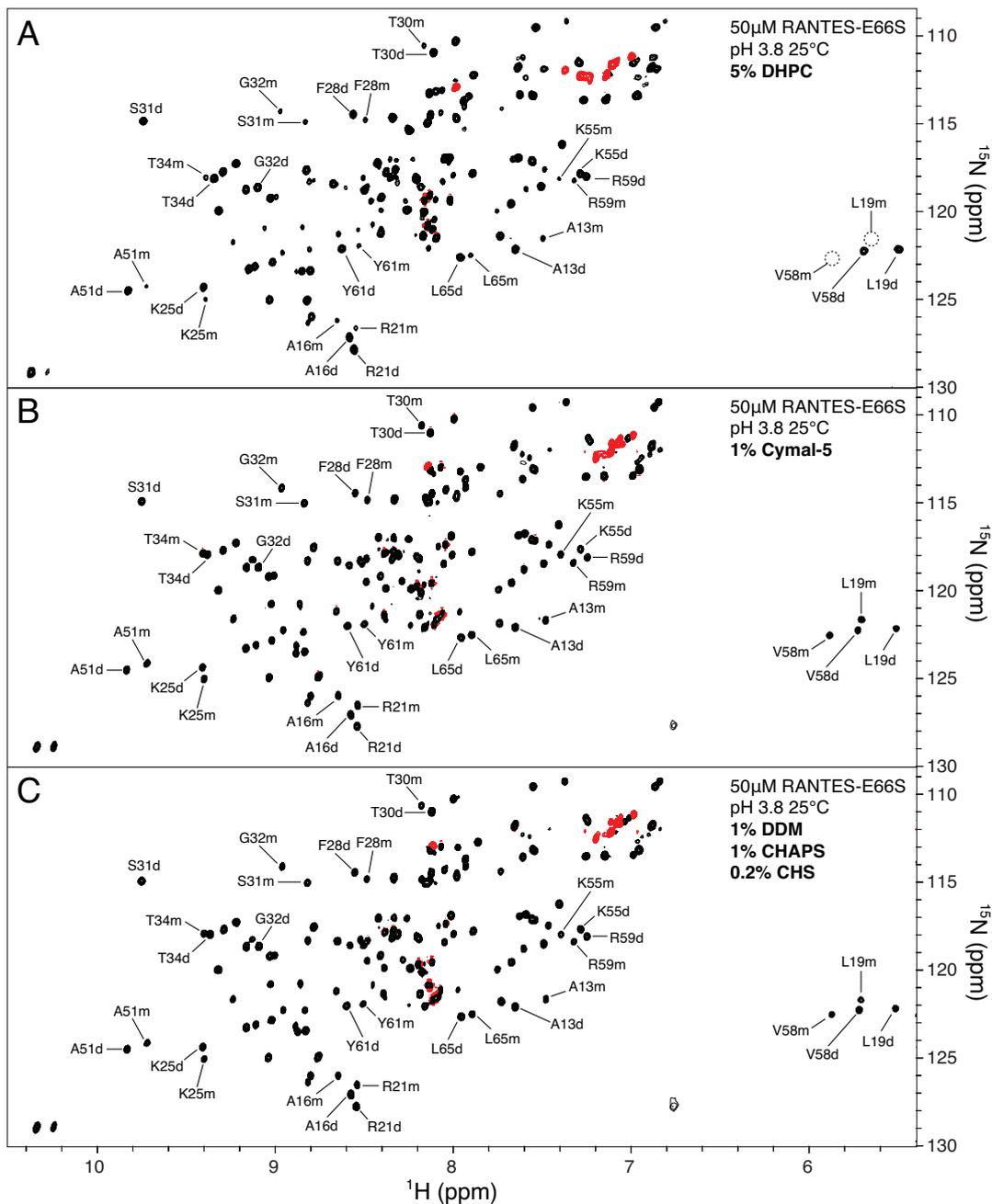
Figure 5.11 HSQC spectra of 50 µM RANTES-E66S at pH 3.8 at 25°C with 5% DHPC (A), with 1% Cymal-5 and with 2.2% DDM/CHAPS/CHS (1/1/0.2) mixture. Negative peaks resulting from folding are colored red. The exemplary nonoverlaping resonances were labeled with the assignment information. The resonances below the threshold were surrounded by black dashed circles.

The impact of detergents on the HSQC spectrum turns out to be the same also for 5P12-RANTES-E66S (data not shown). Similarly to RANTES-E66S, FC-12 cleared all of its original resonances leaving a set of new ones, again corresponding to both termini, whereas DDM/CHAPS/CHS did not have an effect. A summary of tested conditions can be found it Table 5.2.

Table 5.2 The effect of detergents on RANTES resonances – summary of tested conditions.

No.	RANTES	pH	Detergent	CMC in H_2O	HSQC	Intensity ratio (M:D)
1	E66S	3.8	------	------	folded	M<D
2	E66S	3.8	1% FC-8	3.4%	folded	M<D
3	E66S	3.8	5% FC-8	3.4%	mixed	M≈D
4	E66S	3.8	1% FC-10	0.35%	unfolded	------
5	E66S	3.8	0.5% FC-12	0.047%	unfolded	------
6	E66S	3.8	1% FC-12	0.047%	unfolded	------
7	E66S	6.3	1% FC-12	0.047%	mixed	M<D
8	E66S	3.8	1% FC-16	0.00053%	unfolded	------
9	E66S	3.8	1% DHPC	0.06742%	folded	M<D
10	E66S	3.8	5% DHPC	0.06742%	folded	M<D
11	E66S	3.8	1% Cymal-5	0.12%	folded	M≈D
12	E66S	3.8	1% DDM 1% CHAPS 0.2% CHS	0.0087% 0.49% ------	folded	M≈D
13	E66S	3.8	0.26% FC-12 1:2 CCR5 ratio	0.047%	folded	M<D
14	E66S	3.8	0.45% FC-12 1:1 CCR5 ratio	0.047%	mixed	M<D
15	5P12-E66S	3.8	1% FC-12	0.047%	unfolded	------
16	5P12-E66S	3.8	1% DDM 1% CHAPS 0.2% CHS	0.0087% 0.49% ------	folded	M only

5.2.1.3 Circular dichroism

The disappearance of RANTES HSQC resonances in the presence of some detergents implies that some kind of direct RANTES-detergent interaction takes place. The fact that the RANTES resonances become invisible upon contact with detergents but not with the other was not reported previously and has a strong impact on the selection of the detergent for RANTES-CCR5 interaction studies and on the interpretation of the results obtained by Nisius in FC-12 (82).

To investigate this phenomenon further CD of RANTES-E66S was measured without and with the presence of FC-12 (Figure 5.12). First, the spectra of plain buffer and of buffer with 0.5% FC-12 were measured to check for the contribution of detergent to the measured ellipticity. The spectra of both the plain buffer and the buffer with detergent did not show any differential absorbance of left and right circular polarized light (straight lines, data not shown). Subsequently, after collecting the spectrum of RANTES-E66S in the plain buffer, few microliters of concentrated FC-12 stock was mixed into the cuvette to 0.5% final concentration. The overall shape of the RANTES-E66S spectrum changed dramatically after the addition of the detergent. The

positive hump at 230-235 nm disappeared and the negative amplitude of the signal increased. A minimum at ~208 nm became very pronounced. These changes suggest that in the presence of FC-12 RANTES-E66S secondary structure may be severely perturbed.
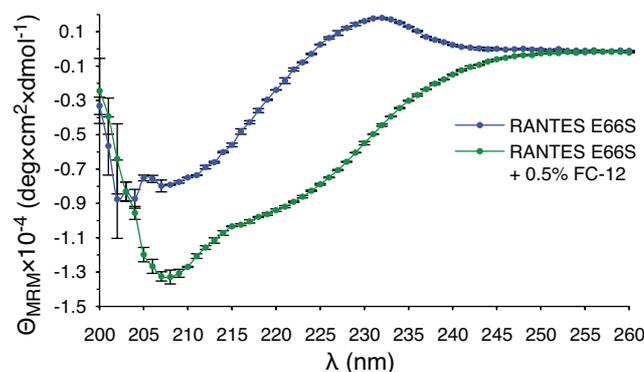
Figure 5.12 CD spectra of 50 µM RANTES-E66S after subtraction of the plain buffer (blue) and of 50 µM RANTES-E66S with 0.5% FC-12 after subtraction of the buffer with 0.5% FC-12 (green).

5.3 Discussion

Gaining insights into CCR5-RANTES interaction is an important step towards understanding RANTES-mediated CCR5 signal transduction as well as the mechanism of HIV-infection inhibition. Although CCR5-RANTES interaction have been studied in vivo and in vitro, no atomic resolution details could be elucidated. To facilitate CCR5-RANTES interaction studies by NMR, in parallel to establishing an NMR-emendable system for CCR5, we have looked into RANTES itself and into a suitable system, in which its interaction with CCR5 could be studied.

For this purpose 5P12-RANTES-E66S, a clinically relevant, noninflammatory and highly-effective against HIV infection RANTES variant was cloned. Using the previously established protocols, 5P12-RANTES-E66S was expressed in $^{15}N,^{13}C$-labeled minimal medium as N-terminal fusion to GB1 domain of protein G and purified with milligram yields. The sample could be concentrated to mM concentration and could be stored for years without any signs of deterioration.

The HSQC spectrum of 5P12-RANTES was composed of 63 sharp backbone resonances (corresponding to 63 nonproline RANTES residues) spanning over 4 ppm of hydrogen dimension. Such large peak dispersion is characteristic for well folded proteins. The fact that no second set of resonances is observed even at 0.6 mM and that

HSQC spectrum overlaps better with RANTES-E66S monomer is an evidence that 5P12-RANTES-E66S is purely monomeric. Differences with regards to the oligomerization behaviour between 5P12-RANTES-E66S and the wild type RANTES are expected as in the 5P12-RANTES-E66S the N-terminus providing a dimerization interface and E66 involved in tetramerization are mutated. The monomerizm of 5P12-RANTES-E66S is a clear benefit for its anti-microbicide properties (aggregation of RANTES causes inflammation and enhances HIV infection) as well as an advantage for NMR studies.

As the N-terminus of 5P12-RANTES-E66S starts with a glutamine, a cyclic pyroglutamate is spontaneously formed. Right after sample preparation the N-terminus is mostly free. After one day at pH 3.8 ~30% is already cyclic and after four days of incubation at mixed temperatures (37°C form NMR measurement and 4°C for storage) the reaction is complete in ~90%. The half life is the reaction is approximately 2 days.

Based on the data obtained from CBCANH ($^{13}C^{\alpha}$, $^{13}C^{\beta}$ shifts) and HNCO ($^{13}C'$, ^{15}N shifts) experiments a chemicals shift table of 5P12-RANTES-E66S was composed. By subtracting random coil values a secondary chemical shifts were calculated. The obtained secondary shift plot predicts the expected helical secondary structure elements present in the wild type RANTES, namely the short 3_{10} helix (η_1, residues 20-22) and the long C-terminal α-helix (α_1, residues 55-67) as well as the three β_1 (residues 24-29), β_2 (residues 39-43), and β_3 (residues 48-51) strands but not the N-terminal β_N (residues 8-10). The absence of the first β-strand is expected as for the wild type RANTES it was a part of the intermolecular β-sheet, which for the monomeric 5P12-RANTES-E66S is not formed. In general, with the exception of the unstructured N-terminus and the inability to dimerize, 5P12-RANTES-E66S secondary structure closely resembles the wild type RANTES. A remarkable overlap of the 5P12-RANTES-E66S HSQC spectrum with the spectrum of the RANTES-E66S monomer supports this conclusion.

Performed T_1, T_2 and $\{^1H\}$-^{15}N NOE relaxation experiments showed that the tumbling rate of 5P12-RANTES-E66S is relatively uniform for residues 10-66 of the 5P12-RANTES-E66S molecule. This means that the main body of 5P12-RANTES-E66S behaves like a rigid particle. The relaxation of the residues 67-68 is slower and is a consequence of the increased flexibility of the C-terminus (C-terminal fraying). As the N-terminus of 5P12-RANTES-E66S in not involved in the intermolecular β-sheet,

large flexibility of the N-terminus is expected. The observed low $1/T_1$, $1/T_2$ $\{^1H\}$-^{15}N NOE values are the consequence of ps-ns motions (residues 0-9), whereas the $1/T_2$ hump (residues 5-9) a result of the additional motions on the μs-ms time scale.

Both RANTES-E66S and 5P12-RANTES-E66S were shown to interact with Fos-Choline detergents. The interaction appeared as an intensity decrease of the majority of the HSQC peaks. Interestingly, it was not the case for a set of ~15 backbone (and few side chain) resonances, which remained visible even after a complete bleaching of all other signals. Most of these peaks (12 out of 15) could be assigned based on HNCACB experiment to the N- (residues 3-7) and C-termini (residues 62-68). From the secondary chemical shifts of the residues 62-68 it could be concluded that in the presence of FC-12 the C-terminal α-helix (or at least its second half) is present.

The RANTES-E66S resonance bleaching was observed for all tested Fos-Cholines with C_8, C_{10}, C_{12} and C_{16} aliphatic chains. The effect was dependent on detergent concentration, the length of its aliphatic chain (directly related to CMC) and pH. Depending on the combination of these factors, unperturbed (e.g. 1% FC-8 pH 3.8), mixed (e.g. 5% FC-8 pH 3.8 or 1% FC-12 pH 6.3) or completely bleached (e.g. 1% FC-12 pH 3.8) RANTES-E66S spectra could be observed.

The very similar resonance bleaching was observed when FC-12-solubilzied unlabeled m9CCR5[306] monomer was titrated into RANTES-E66S. The observation that 0.45% FC-12 introduced with 1:1 molar ratio of m9CCR5[306] did not bleach RANTES-E66S spectrum completely, whereas 0.5% FC-12 with m9CCR5[306] did, can be rationalized by the involvement of a part of FC-12 in the interaction with m9CCR5[306] (solubilization). If to assume that 165 FC-12 molecules (see section Characterization of CCR5 size distribution, stability and homogeneity of Chapter 4) solubilize one m9CCR5[306] monomer, then the presence of 41 μM m9CCR5[306] leaves ~0.24% less FC-12 for the interaction with RANTES-E66S. Therefore, despite total 0.45% FC-12 contents, the effective FC-12 concentration affecting RANTES-E66S resonances is only ~0.2%.

Extending the analysis on other detergents, we have tested the impact of DHPC (similar head group as Fos-Cholines but two short aliphatic chains), Cymal-5 (maltoside head group) and DDM/CHAPS/CHS mixture (frequently used in functional CCR5 studies) on RANTES-E66S HSQC spectrum. DHPC up to 5% concentration did not affect RANTES-E66S in any major way. This suggests that the property of RANTES-E66S (and also 5P12-RANTES-E66S) resonance bleaching cannot be

attributed solely to the choline head group of Fos-Choline detergents but rather results from the interplay between the head group and the aliphatic chain. This is supported by the fact that Cymal-5, having the same aliphatic chain as FC-12 but different head group did not bleach the intensities of RANTES-E66S. On the other hand both Cymal-5 and DDM/CHAPS/CHS mixture shifted the RANTES-E66S equilibrium towards monomer.

The impact of FC-12 on RANTES-E66S was further analyzed by CD. A dramatic change of the shape of the spectrum suggests that in the presence of FC-12 RANTES-E66S secondary structure is affected. The appearance of a pronounced minimum at ~208 nm may suggest that RANTES-E66S adopted more α-helical structure. Although the disappearance of protein resonances is often cause be aggregation (the so-called "dark state"), this mechanism is less likely, as the resonance bleaching is observed also for the nondimerizing 5P12-RANTES-E66S at pH 3.8 (conditions strongly promoting high solubility, where even heavily aggregating wild type RANTES can be studied).

Taken together, these findings show that careful detergent selection for CCR5-RANTES studies is absolutely crucial. The lack of 2D7 recognition may suggest that in the presence of FC-12 the native CCR5 structure is not maintained. The disappearance of the HSQC resonances upon the addition of FC-12 is a clear evidence of the RANTES-FC-12 interaction. The CD spectrum distortion indicates that FC-12 perturbs RANTES secondary structure. These three observations suggest that the FC-12 should be considered unsuitable for CCR5-RANTES interaction studies and that the previous observations by Nisius by NMR (13) and ITC (82) were erroneously interpreted as CCR5-RANTES binding.

6 Modulation of RANTES binding to CCR5 by modifications in the N-terminus and C-terminus

Original Manuscript

Morin, S., Wiktor, M., Sass, H-J., Hartley, O., Grzesiek, S

(in preparation)

Modulation of RANTES binding to CCR5 by modifications in the N-terminus and C-terminus

Sébastien Morin[a][†], Maciej Wiktor[a], Hans Jürgen Sass[a],
Oliver Hartley[b] and Stephan Grzesiek[a]

[a]Division of Structural Biology, Biozentrum,
University of Basel, Basel, Switzerland
[b]Department of Structural Biology and Bioinformatics,
Centre Médical Universitaire, Geneva, Switzerland
[†]Now in: Swiss Institute of Bioinformatics and Biozentrum,
University of Basel, Basel, Switzerland

Abstract

Currently no experimental 3D structure for the GPCR and HIV-1 coreceptor CCR5 are available that would help understanding its diverse roles and allow the development of better drugs, both against HIV-1 infection and inflammation diseases. Here, we present a comprehensive SPR-based study of the interactions of CCR5 with different ligands, including the small-molecule inhibitor Maraviroc, diverse variants of the chemokine RANTES, as well as the conformation-dependent antibody 2D7. Our data suggest that the similar anti-HIV potency for two RANTES variants differing in their N-terminus (5P12-RANTES and PSC-RANTES) is due to two different mechanisms: to the higher affinity of 5P12-RANTES for CCR5, while the lower affinity of PSC-RANTES for CCR5 is compensated by internalization and sequestration of CCR5 in the cell. Hence, 5P12-RANTES efficiently blocks CCR5 which still sits on the membrane, while PSC-RANTES hides CCR5 in the cell, making it inaccessible to gp120 on HIV-1 particles. In addition to these observations, our data show linear oligomerization of WT-RANTES and its modulation by variations in the C-terminus of the chemokine.

Introduction

The G protein-coupled receptor (GPCR) CC chemokine receptor 5 (CCR5) regulates immune-cell trafficking upon activation by its endogenous ligands: macrophage inflammatory protein 1α (MIP-1α, also known as CCL3, chemokine (C-C motif) ligand 3), MIP-1β (also known as CCL4), and RANTES (Regulated on Activation, Normal T-cell Expressed and Secreted, also known as CCL5) (reviewed in [1]). These agonists activate G protein signaling and regulate CCR5 by processes involving phosphorylation by G protein coupled receptor kinases (GRK), desensitization by β-arrestin, internalization in the cell, and either recycling to the cell surface or degradation.

The entry of the human immunodeficiency virus type 1 (HIV-1) into host cells requires the sequential interaction of the viral envelope glycoprotein 120 (gp120) with the host-cell factor CD4 and with either CCR5 or CXCR4 (CXC chemokine receptor 4, reviewed in [1–3]). This process is facilitated by the fact that these three receptors cluster on microvilli of macrophages and T cells [4]. This encounter leads to the fusion of viral and host cell membranes which results in the infection of the cell by HIV-1. In general, CCR5 serves as the coreceptor during both the early stages and the asymptomatic phase of infection. CXCR4 can serve this function in later stages: during progression of the disease to AIDS, possibly as a result from pressure of the immune system against R5-tropic viruses (*i.e.* viruses using CCR5), thus favoring X4-tropic viruses (*i.e.* viruses using CXCR4).

Since both, viral gp120 and the chemokines bind to overlapping extracellular parts of the receptor, the presence of a chemokine prevents the interaction of CCR5 with the viral protein, thereby hindering HIV-1 infection [5, 6]. Indeed, RANTES, MIP-1α, and MIP-1β were identified as HIV-1 suppressive factors in CD8+ T cells [5]. Blocking of CCR5 as a medical approach to prevent HIV-1 infection was further encouraged by the observation that homozygous individuals with the $\Delta32$ mutation (a 32 base-pair deletion in the CCR5 gene which results in a frameshift and the expression of a truncated nonfunctional receptor) are virtually resistant to HIV-1 infection, while not suffering from any major health issues [7, 8]. This effect results from the absence of CCR5 on the surface of cells and thus the impossibility for gp120 to find its coreceptor [9].

As the use of natural chemokines as drugs would induce undesirable effects (*i.e.* inflammation), different approaches have been undertaken in order to develop noninflamatory chemokine variants (especially RANTES variants) with high activity against HIV-1 infection. These include N-terminal truncations [10–16], chemical modifications (among others, PSC-RANTES) [17–20], mutagenesis and elongation (among others, 5P12-RANTES) [21–24], as well as fusion strategies [25, 26]. Other approaches have used peptidic fragments of the chemokine such as the N-terminus [27–29] or the N-loop/β1-strand [30–32].

Some RANTES variants with N-terminal modifications showed promising characteristics as topical microbicides. For example, PSC-RANTES protected from vaginal challenges for HIV-1 infection in macaques [6]. Later, 5P12-RANTES and 6P4-RANTES were developed in order to lower the high production cost for chemical synthesis of PSC-RANTES [24]. These fully-recombinant variants showed similar anti-HIV effects as PSC-RANTES [24, 33], *i.e.* $\sim$20x anti-HIV potency over WT-RANTES [24]. Moreover, their stability indicated that they are suitable for use as topical microbicides [34]. 5P12-RANTES is currently being tested in clinical trials. This variant was chosen over 6P4-RANTES (and PSC-RANTES) because it is not an agonist, but an inverse agonist (also known as antagonist), and thus elicits neither CCR5 signaling nor internalization (and subsequent recycling), but simply blocks the binding site for chemokines and gp120 [24]. This is explained by the different N-terminus on these variants, as shown in Figure 1 and discussed below.

Small-molecule antagonists have been developed by several pharmaceutical companies. These include compounds such as TAK-779 [37], SCH-C [38], Aplaviroc [39], Vicriviroc [40], TAK-220 [41], and Maraviroc [42]. These small molecules are CCR5 antagonists and bind to a common area: a groove on the extracellular side of CCR5 which is formed by the transmembrane helical bundle ([43–47], see below). Whereas small-molecule inhibitors listed above prevent the binding of gp120 by an allosteric mechanism, Kang et al. [48] recently presented a sligthly larger small-molecule inhibitor which, in addition to binding to the allosteric site, can protrude out of the transmembrane groove and sterically block interactions involving the second extracellular loop of CCR5. This kind of dual-mechanism inhibitor should be valuable for anti-HIV drugs. Maraviroc, however, is currently the only drug towards

```
            1......... 11........ 21........

WT-R.       SPYSSDTTPC CFAYIARPLP RAHIKEYFYT

PSC-R.      XXXSSDTTPC CFAYIARPLP RAHIKEYFYT

5P12-R.   Q GPPLMATQSC CFAYIARPLP RAHIKEYFYT

            31........ 41........ 51........ 61....68

WT-R.       SGKCSNPAVV FVTRKNRQVC ANPEKKWVRE YINSLEMS

PSC-R.      SGKCSNPAVV FVTRKNRQVC ANPEKKWVRE YINSLEMS

5P12-R.     SGKCSNPAVV FVTRKNRQVC ANPEKKWVRE YINSLEMS
```
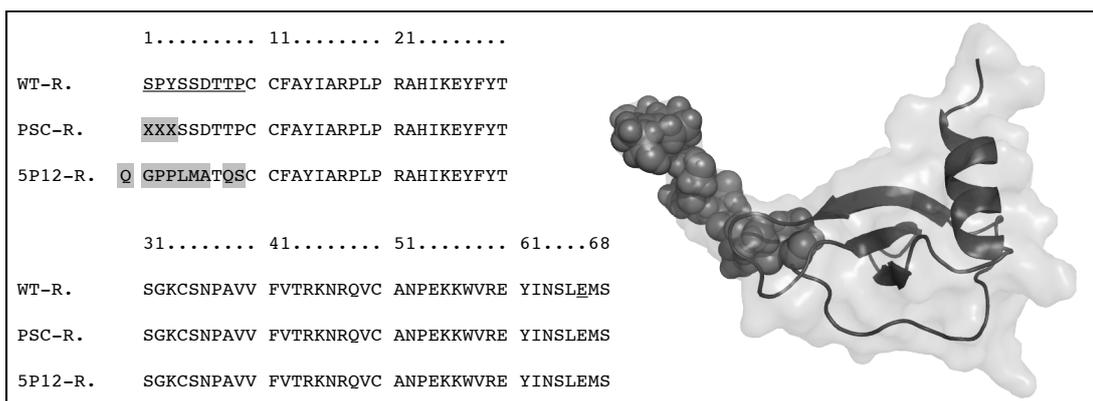
Figure 1: The RANTES variants PSC-RANTES and 5P12-RANTES differ from WT-RANTES by their N-terminus sequence (underlined in the sequence and shown as spheres on the RANTES monomer structure). The differences in PSC-RANTES and 5P12-RANTES compared to WT-RANTES are highlighted in gray on the sequence. XXX stands for the n-nonanoyl-thioprolyl-cyclohexylglycyl moiety, which replaces the first three amino acids in PSC-RANTES. The glutamine residue at the N-terminus of 5P12-RANTES undergoes spontaneous cyclization to pyroglutamate [35]. The figure with PDB 1RTO [36] was prepared using PyMOL (Schrödinger).

CCR5 on the market. It reached the market after accelerated approval by the FDA in 2007. It is now being used for treatment of R5-tropic HIV-1 infections under the commercial names of Selzentry®/Celsentri®. Although Maraviroc has been administered to patients for the medical treatment of HIV-1 for only a few years, cases of resistance to this drug and other entry inhibitor candidates [49–52] indicate that new drugs will be needed, calling to a better understanding of CCR5 and its interactions with different ligands.

Whereas chemokines are expected to interact with the extracellular side of CCR5, the small-molecules, as already discussed, bind to CCR5 in an extracellular groove present in the center of the transmembrane helices [43–47]. This was shown indirectly through mutagenesis and modeling studies using Maraviroc, Vicriviroc, Aplaviroc, TAK-779 and TAK-220 [43–46], and also directly using a cross-linking approach [47]. This is consistent with the fact that both small-molecule inhibitors and antibodies recognizing the N-terminus of CCR5 can bind simultaneously, as indicated by their apparent synergy against HIV-1 infection [53]. The binding mode for chemokines involves the use of different parts of the chemokine for binding to the extracellular loops of CCR5 (core domain of the chemokine) and CCR5's transmembrane domain (N-terminus of the chemokine) [54–56]. These also have a different function. The core domain of the chemokine allows tight binding to the various extracellular parts of CCR5 (including the N-terminus [55]), while the N-terminus of the chemokine protrudes into the groove formed by the transmembrane helices and elicits activation of the receptor [54]. This is the so-called two-site model [57]. The binding site for small-molecule inhibitors is termed the allosteric site, as opposed to the extracellular chemokine binding site which is termed the orthosteric site [46, 58].

For the characterization of CCR5 and its interactions with different ligands, several groups turned to surface plasmon resonance (SPR) and used detergent-solubilized CCR5. Navratilova et al. [59] optimized solubilization conditions for maximal stability of CCR5 and focused on improving the recognition of the extracted receptor by the conformation-dependent antibody 2D7 [60]. It was shown that a detergent mix (DDM/CHAPS/CHS) supplemented with lipids (DOPC and DOPS) could both extract properly folded CCR5 and stabilize it, consistent with the fact that cholesterol (from which CHS is a derivative) is essential for conformational integrity of CCR5 [61]. Later, Navratilova et al. [62] showed that CCR5 in these conditions was able to bind both its natural ligand RANTES and several small-molecule inhibitors, including TAK-779 [37]. Also, binding of nine HIV-1 gp120 variants with CCR5 was shown [63]. As a follow-up on the detergent screen by Navratilova et al. [59], Rich et al. [64] published a method by which high-throughout detergent screening could be performed using SPR. For this study, they used CCR5 as a model and probed the recognition by the conformation-dependent antibody 2D7 [60]. Although details for each detergent were not made available, the authors noted the general trends that maltoside detergents with a C9 to C13 alkyl tail were the ones which, while being able to solubilize CCR5, could

106

also maintain the highest binding ability. Recently, Navratilova et al. [65] proposed an elegant approach to probe binding of ligands to a specific binding site. Their approach consisted in using three different channels for recording the SPR data. The first and second channels were as in a standard setup and consisted of a reference channel without CCR5 and a channel with CCR5. A third channel consisted of CCR5 saturated with the small-molecule inhibitor Maraviroc. That way, ligands could be discriminated as whether their binding was affected by the presence of a small-molecule inhibitor in the allosteric site, an important feature for anti-HIV small-molecule drug screening.

Contrary to the studies cited above which used detergent-solubilized CCR5, Silin et al. [66] directly coupled CCR5-containing membrane vesicles to the SPR chip. Using this setup, they could show the highly functional nature of CCR5 with the interaction of almost stoichiometric amounts of RANTES. Yoshiura et al. [56] used SPR-based recognition of CCR5 by 2D7 to show the long term stability of CCR5 embedded in lipids of nanodiscs. The authors also showed MIP-1α binding to CCR5 using both SPR and NMR (nuclear magnetic resonance) data.

Previously, we have described large-scale expression of CCR5 based on the baculovirus / insect cell system [67]. This system, while still taking advantage of eukaryotic cells, provides an improvement in terms of yield when compared to mammalian cell expression as pioneered by Mirzabekov et al. [68] for CCR5. The yield is also higher than for expression in *E. coli* as demonstrated by Ren et al. [69]. In theory, an advantage of using eukaryotic expression (*e.g.* with the insect cell system) over prokaryotic expression, is the possibility of obtaining proteins including posttranslational modifications [70]. This is important as CCR5 contains several posttranslational modifications (disulfide bridges, sulfated tyrosine residues, O-glycosylation, palmitoylation of selected cysteine residues, and phosphorylation, discussed in [71]).

Here, we present an extensive set of SPR data showing the ligand binding competency of our recombinant, insect cell-overexpressed CCR5 [67]. We show the binding of RANTES variants and the interference by the presence of Maraviroc or the 2D7 antibody. These data give insights on the binding modes of RANTES variants, in particular on the different mechanisms by which both PSC-RANTES and 5P12-RANTES (which differ in their N-terminus) reach similar anti-HIV potencies, despite displaying different phenotypes and affinities for CCR5. Moreover, we observe linear oligomerization of WT-RANTES through a mechanism related to aggregation, a process speculated to serve for pre-concentration of chemokines near their target receptors [72–74].

Materials and Methods

Materials

Detergents were purchased from Anatrace (High Wycombe, UK) and lipids from Avanti Polar Lipids (Alabaster, USA), while other reagents were either from Applichem (Darmstadt, Germany), Roth (Arlesheim, Switzerland), or Sigma-Aldrich (Buchs, Switzerland). The 2D7 and anti-His antibodies were from BD Pharmingen (Allschwil, Switzerland) and Qiagen (Hombrechtikon, Switzerland), respectively.

5P12-RANTES-E66S and RANTES E66S were overexpressed as described previously for RANTES-E66S by Duma et al. [55]. Importantly, we ensured that the N-terminal glutamate residue in 5P12-RANTES-E66S was cyclized to pyroglutamate [35] using both mass spectrometry and nuclear magnetic resonance (NMR, data now shown). WT-RANTES, WT-RANTES-biotin, PSC-RANTES, 5P12-RANTES-biotin, as well as MIP-1β were prepared by total chemical synthesis as described before [20, 75]. The variants used in this study differed in the presence or absence of the mutation E66S, which prevents aggregation of RANTES at pH >4.

CCR5 was overexpressed in the baculovirus / insect cell system as described before [67]. It contained a C-terminal 6-His tag followed by a Strep-tag. Insect cell membranes containing the β1 adrenergic receptor mutant m23 (β1AR-m23) were prepared as in [76] and used as a control.

SPR

SPR experiments were performed with a T100 instrument from GE Healthcare (Zürich, Switzerland) running at 20°C (with samples kept at 8°C) with a flow rate of 50 μL/min. In general, injections were performed for 360 s (6 min) with dissociation recorded for 1200 s (20 min). Between injections, one or more additional 1000 s ($\sim$17 min) waiting periods were generally inserted for proper dissociation of accumulated ligands in order for the captured receptor to return to the apo state. Data were analyzed using the Biacore T100 Evaluation Software (GE Healthcare, Zürich, Switzerland). Curve fitting was performed using a 1:1 interaction model and took into account both refractive index contributions [77] and mass transport effects [78]. In order to allow comparison of signal amplitudes, sensorgrams were also normalized for the amount of CCR5 on the chip. Indeed, capture of CCR5 on the chip varied from 2000 to 6000 RU (resonance units) and was normalized between different experiments to the same amount (*i.e.* 5000 RU). The variation in the noise, especially visible for Maraviroc, is a consequence of the normalization procedure based on the effective level of receptor captured on the chip. For β1AR-m23 (control), only low amounts of the receptor mutant (known to overexpress poorly [76]) were captured on the chip surface.

The SPR setup consisted of a sensor chip CM5 (*i.e.* gold surface modified with carboxymethylated dextran, purchased from Biacore, Zürich, Switzerland) on which an amine-coupled (using EDC, 1-Ethyl-3-[3-dimethylaminopropyl]carbodiimide hydrochloride, and NHS, N-hydroxysuccinimide, purchased from Biacore, Zürich, Switzerland) anti-His antibody (Qiagen, Hombrechtikon, Switzerland) was immobilized and used for the capture of CCR5 through its C-terminal His-tag. The capture was used as an on-chip affinity purification for the isolation of CCR5 from clarified detergent-solubilized crude membrane solutions. This allowed fast immobilization of CCR5 and, consequently, retention of activity, as CCR5, like other GPCRs, is known to lose activity as a function of time when in solution with detergents [56, 59]. After capture of CCR5 on the chip, it was important to wait sufficiently long (from 5 to 10 hours) such that the initial decay from the antibody surface became negligible. This ensured a stable baseline and did not affect the quality of captured CCR5. Indeed, no noticeable loss of activity was observed as a function of time (up to several days) when CCR5 was captured on the SPR chip (data not shown). The reference channel was used to subtract background signal due to, for example, changes in refractive index during injection of analytes. The reference channel also contained the anti-His antibody and served as a control for binding to either the chip dextran matrix surface or the anti-His antibody. Subtraction of blank injections was used in addition to the use of the reference channel (*i.e.* double-referencing, [79]).

For SPR experiments, insect cell membranes containing baculovirus-overexpressed CCR5 were prepared according to Nisius et al. [67], except that the buffer consisted of 10 mM HEPES (4-(2-hydroxyethyl)-1-piperazineethanesulfonic acid) pH 7.5, 150 mM NaCl, 50 μM EDTA (ethylenediaminetetraacetic acid), 10% (v/v) glycerol (buffer A) and contained no protease inhibitors. The membrane preparations were frozen at -70°C in 200 μL aliquots (equivalent to 15 mL of CCR5 culture, *i.e.* $\sim$30 μg of CCR5). CCR5 was solubilized from these aliquots for 2 h at 4-8°C. The aliquots were first thawed and mixed with 133 μL of 6% (w/v) DDM (n-Dodecyl-β-D-maltopyranoside) in buffer A, 200 μL of 4% (w/v) CHAPS (3-[(3-cholamidopropyl)dimethylammonio]-1-propanesulfonate) + 0.8% (w/v) CHS (cholesteryl hemisuccinate) + 0.3144% DOPC (1,2-dioleoyl-sn-glycero-3-phosphocholine) in buffer A: for final detergents and lipids concentrations as follows: 1% (w/v) DDM, 1% (w/v) CHAPS, 0.2% (w/v) CHS, and 0.0786% (w/v) DOPC. For the control with FC-12 (n-dodecylphosphocholine), the final concentration was 1% (w/v). After solubilization, soluble material was separated from insoluble material by centrifugation at 17000 g for 60 min at 4-8°C. The SPR running buffer consisted of 20 mM HEPES pH 7.0, 150 mM NaCl, 0.1 mg/mL BSA (bovine serum albumin), 0.02% (w/v) CHS, 0.1% (w/v) CHAPS, 0.1% (w/v) DDM, and 50 nM DOPC (buffer B). For the control with FC-12, the final concentration was 0.1% (w/v).

Non-E66S RANTES variants (WT-RANTES and PSC-RANTES) displayed high-amplitude non-specific binding to the dextran matrix of the CM5 sensor chip at concentrations equal or above 108 nM (data not shown). Hence, experiments with these variants were performed with concentrations up to 36 nM (where no such unspecific interaction to the chip was observed). The ability of E66S RANTES variants to form higher order oligomers (or to interact with the dextran matrix) was reduced [80–82] and no unspecific binding to the CM5 chip was observed for concentrations up to 1 μM.
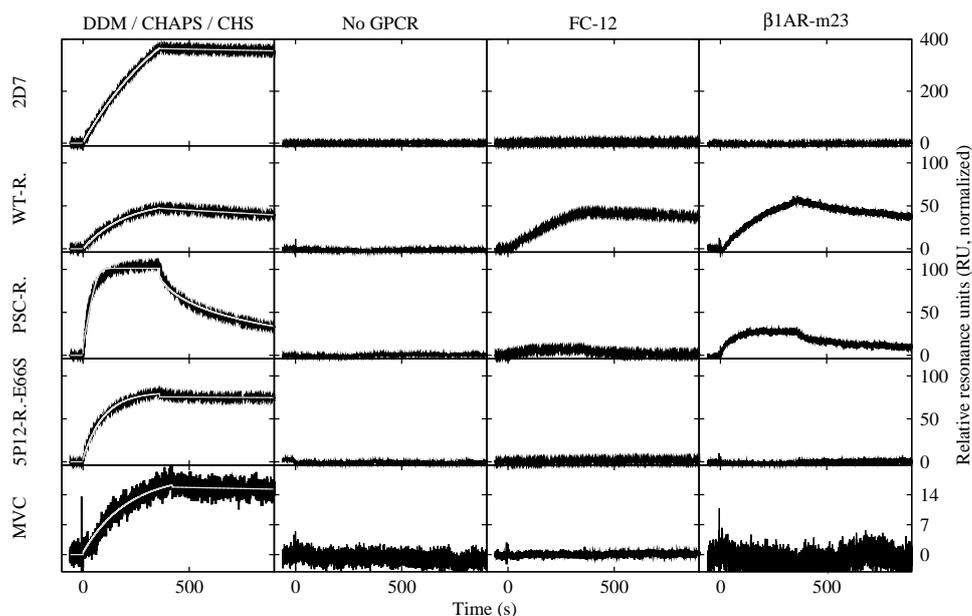
Figure 2: Interaction of different ligands with CCR5. Interactions with a CCR5 surface in DDM/CHAPS/CHS (the detergent mix used for subsequent experiments, left). Controls include surfaces without any receptor, with CCR5 solubilized in FC-12, as well as with a different GPCR (β1AR-m23). Fits for data in DDM/CHAPS/CHS are shown in light gray (with fitted values available in Table 1). RANTES variants were injected at 36 nM, Maraviroc at 108 nM, and 2D7 at 5 nM. For each case, both solubilization and the SPR experiment were performed using the corresponding detergent mix.

Results and Discussion

Interaction of different ligands with CCR5

In order to study interactions of CCR5 with its ligands, we turned to SPR, as it allows direct, real-time, and label-free observation of molecular interactions [83]. SPR was already successfully used to study CCR5 and other GPCRs (reviewed in [84]). Immunoprecipitation and SPR experiments using the conformation-dependent 2D7 antibody (which recognizes the natively folded first half of the second extracellular loop of CCR5, ECL2, [60, 85]) showed that maltoside detergents are best suited for recognition of CCR5 [59, 62, 64, 68]. Using SPR and CCR5 solubilized using a detergent mix including the maltoside detergent DDM (DDM/CHAPS/CHS), we could observe binding of all the ligands tested: the 2D7 antibody, RANTES variants WT-RANTES, PSC-RANTES, and 5P12-RANTES-E66S, as well as Maraviroc (see Figure 2). As all ligands tested (including MIP-1β, see Supplementary Figure S1 and accompanying text) showed interaction with CCR5 solubilized in DDM/CHAPS/CHS, this mix was used for subsequent experiments. A very similar mixture was previously shown to be optimal for the stabilization of GPCRs [86, 87] and was also used for CCR5 in a previous SPR study [62].

Interaction with the conformation-dependent antibody 2D7 [60, 85], was clearly observed in this detergent mix. This interaction, with a K_D on the sub-nM range, confirmed the quality of our protein (see Figure 2 and Table 1). A similar approach was used by Myszka and coworkers to assess the quality and quantity of solubilized CCR5 in their SPR experiments [59, 63, 64].

The observed K_D values for each RANTES variant were in the nM to sub-nM range, with 5P12-RANTES-E66S displaying a higher ($\sim$20-25x) affinity than the other ligands: $\sim$2.6 nM for WT-RANTES, $\sim$2.1 nM for PSC-RANTES, and $\sim$0.1 nM for 5P12-RANTES-E66S (see Figure 2 and Table 1). Previously, the affinity of RANTES for CCR5 was characterized and yielded an IC$_{50}$ of $\sim$7 nM in a competition experiment with MIP-1β [88] and K_D values from 0.2 to 6.2 nM in different setups [22, 45, 89] including SPR [62].

Table 1: Fitted parameters for 1:1 interaction with CCR5.

Variant	MW (kDa)	Detergents	k_{on} ($s^{-1}M^{-1}$)	k_{off} (s^{-1})	K_D (nM)	R_{max} (RU)	χ^2 (RU^2)
2D7	$\sim$150	DDM/CHAPS/CHS	5×10^5	5×10^{-5}	0.1	638	0.156
WT-RANTES	7.851	FC-12	6×10^4	3×10^{-4}	4.7	83	0.0804
WT-RANTES	7.851	DDM/CHAPS/CHS	1×10^5	3×10^{-4}	2.6	60	0.0589
PSC-RANTES	7.894	DDM/CHAPS/CHS	3×10^6	7×10^{-3}	2.1	96	1.38
5P12-RANTES-E66S	7.884	DDM/CHAPS/CHS	3×10^5	2×10^{-5}	0.1	78	0.183
5P12-RANTES-biotin	8.434	DDM/CHAPS/CHS	5×10^5	2×10^{-4}	0.4	70	0.0750
Maraviroc	0.514	DDM/CHAPS/CHS	4×10^4	6×10^{-5}	1.4	19	0.0657

MW: Molecular weight.

R_{max}: Maximal amplitude extracted from fit. Fitted parameters were rounded for presentation purposes.

Although the fitted K_D values were in a similar range for the different RANTES variants, the binding profiles displayed significant differences with regards to both association (k_{on}) and dissociation (k_{off}) rates. Indeed, PSC-RANTES associated with a fast k_{on} of $\sim$3 x 10^6 $s^{-1}M^{-1}$, whereas WT-RANTES and 5P12-RANTES-E66S had very similar k_{on} values of $\sim$1 x 10^5 and 2 x 10^5 $s^{-1}M^{-1}$, respectively. For the k_{off}, all RANTES variants behaved differently with PSC-RANTES dissociating relatively fast (k_{off} = 7 x 10^{-3} M^{-1}), WT-RANTES dissociating on an intermediate timescale (k_{off} = 3 x 10^{-4} M^{-1}) and 5P12-RANTES-E66S dissociating more slowly (k_{off} = 2 x 10^{-5} M^{-1}). The fitted association and dissociation parameters for WT-RANTES are discussed in light of data previously reported by Navratilova et al. [62] in the Supporting Material (see Supplementary Figure S2 and accompanying text).

To probe whether the E66S mutation affected the interaction of 5P12-RANTES-E66S with CCR5, we used 5P12-RANTES without the E66S mutation (5P12-RANTES-biotin, a 5P12-RANTES variant C-terminally coupled to biotin). As shown in Supplementary Figure S3 the binding profiles for both 5P12-RANTES variants were analogous, yielding similar affinities (see Table 1). As the E66S mutation in 5P12-RANTES-E66S allowed working at higher concentration (see further below), we worked with 5P12-RANTES-E66S for most experiments.

Although of very low amplitude due to the low molecular weight (514 Da), the signal for the binding of Maraviroc could be observed with 1.4 nM affinity (see Figure 2 and Table 1). This is in agreement with K_D values of $\sim$0.07-0.86 nM reported by Napier et al. [90].

Several control experiments showed the specificity of observed signals to the captured CCR5 (see Figure 2). In a first control, insect cell membranes in which CCR5 was absent were solubilized in DDM/CHAPS/CHS (see Figure 2). In this case, no binding was observed, confirming the absence of interaction to other proteins from in insect cell membranes that could have been captured on the chip, either by adsorption on the dextran matrix or recognition by the anti-His antibody.

A second control was performed with CCR5 solubilized using the detergent FC-12 (see Figure 2), from the fos-choline series of detergents in which the absence of recognition by 2D7 was previously shown [59, 68]. In agreement with these results, 2D7 did not bind to CCR5 in FC-12, similarly to most ligands tested. However, surprisingly, WT-RANTES could also bind CCR5 in FC-12, where no other ligands (except PSC-RANTES to a very low amplitude) could interact with the receptor. These results could indicate unspecific binding of the wild type chemokine to the protein/detergent mixed micelle. This topic is discussed in more detail below.

In a third control, we immobilized a different GPCR on the chip, namely the m23 mutant of the β1 adrenergic receptor (β1AR-m23) [76]. As shown in Figure 2, no interaction was observed for 2D7, 5P12-RANTES-E66S and Maraviroc on β1AR-m23. For WT-RANTES, a clear binding signal was observed. This could be fitted to a K_D of 2.2 nM, in the same range as for WT-RANTES with CCR5 in DDM/CHAPS/CHS and FC-12 (*i.e.* 2.6 and 4.7 nM, respectively, see Table 1). However, both the association and dissociation phases appeared faster. The normalized amplitude was also very similar with a fitted R_{max} of 65 RU compared to 60 RU for interaction with CCR5 in DDM/CHAPS/CHS. This result indicates that WT-RANTES is likely interacting with the mixed micelle formed by a GPCR and a
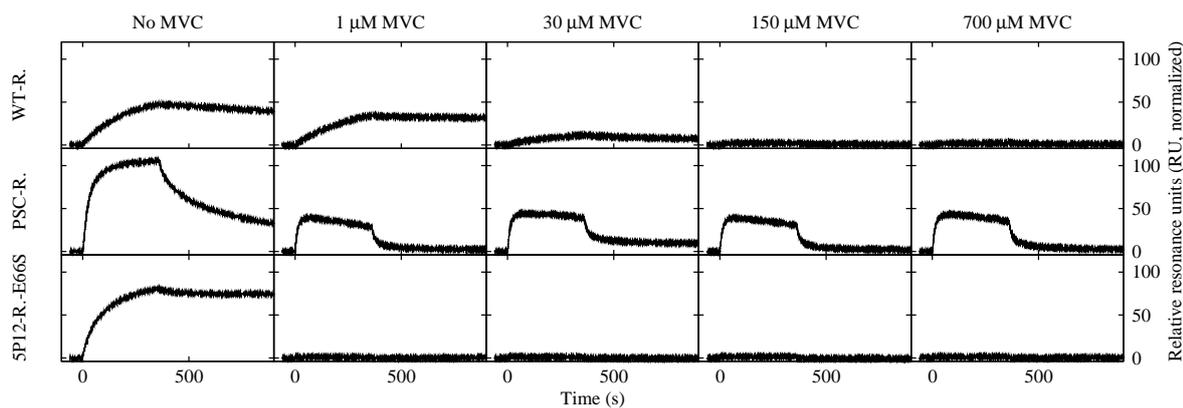
Figure 3: Effect of Maraviroc on binding of RANTES variants in DDM/CHAPS/CHS. RANTES variants were injected at 36 nM. Maraviroc was included in the running buffer, which allowed constant saturation. The binding profiles in absence of both 2D7 and 5P12-RANTES-E66S are shown as references on the left.

detergent. Alternatively, WT-RANTES might simply interact with the many charges on both receptors. However, the details of this interaction are probably slightly different on the two receptors, as based on the faster association and dissociation phases for WT-RANTES with β1AR-m23 compared to interaction with CCR5. For PSC-RANTES, some binding to β1AR-m23 was observed, although to a low amplitude (similarly to the control with CCR5 in FC-12).

Effect of Maraviroc on RANTES binding

In cell assays Maraviroc inhibits binding of RANTES (and other chemokines) to CCR5, with an IC_{50} of $\sim$5 nM [42]. The effect of Maraviroc on the binding of the different RANTES variants was assessed (see Figure 3). At a concentration of 1 μM, which should be sufficient for total saturation of CCR5 based on the IC_{50} and the fitted K_D for Maraviroc binding (1.4 nM, see Table 1), binding of 5P12-RANTES-E66S was completely inhibited, although WT-RANTES bound with the same amplitude and the same interaction profile as in the absence of Maraviroc. Up to a concentration of 30 μM Maraviroc, WT-RANTES bound without changes in the profile (although interaction in the presence of 30 μM Maraviroc was with lower amplitude). However, above 150 μM Maraviroc, the interaction was abrogated. This could indicate a second Maraviroc binding site on CCR5, or the presence of different populations of CCR5 with different affinities for Maraviroc. Alternatively, this observation might simply arise because of unspecific interactions of Maraviroc to any of the components at the very high concentration used (0.15 mM).

The interaction of PSC-RANTES was affected already by 1 μM Maraviroc, but in a different manner compared to 5P12-RANTES-E66S. Indeed, at 1 μM Maraviroc, PSC-RANTES interacted with a fast dissociation rate and with a total amplitude of binding reduced by $\sim$60%. At all higher Maraviroc concentrations tested, this profile was identical to the situation at 1 μM Maraviroc. This contrasts with the case of WT-RANTES where virtually no binding was observed at Maraviroc concentrations equal or higher than 150 μM. PSC-RANTES in the presence of Maraviroc might simply yield unproductive binding to CCR5. This is indicated by a very fast dissociation rate (and thus low affinity), and could result from partial interaction of PSC-RANTES with CCR5 allowing its docking on CCR5, but preventing the interaction to lock in.

Importantly, the inhibition observed for 5P12-RANTES-E66S and PSC-RANTES above 1 μM Maraviroc, and for WT-RANTES above 150 μM Maraviroc, were both reversible after long enough dissociation (consistent with the fitted k_{off}, see Table 1) of Maraviroc from CCR5 (data not shown). Effects of Maraviroc on the binding of RANTES variants were also observed in other detergent systems (data not shown), qualitatively consistent with results from in cell assays showing inhibition of RANTES binding in the presence of Maraviroc [42].

111
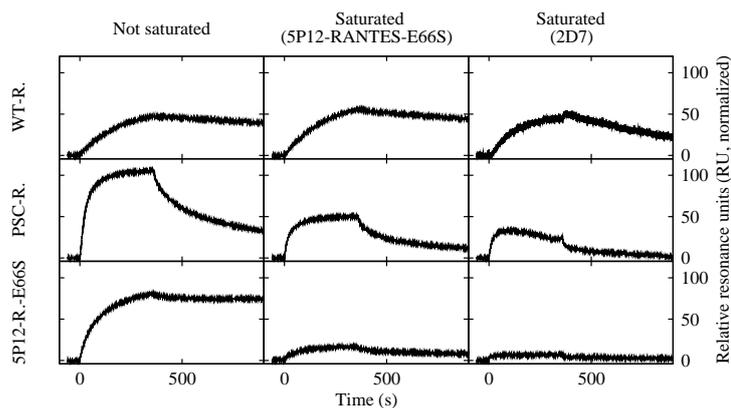
Figure 4: Competition experiments with 5P12-RANTES-E66S or the 2D7 antibody in DDM/CHAPS/CHS. RANTES variants were injected at 36 nM, while the saturating injection of 5P12-RANTES-E66S (before each individual RANTES variant tested) was performed at 1 μM (middle). For 2D7 (right), saturation was achieved by multiple 10 nM injections prior to measurement of the different RANTES variants. The binding profiles in absence of both 2D7 and 5P12-RANTES-E66S are shown as references on the left.

RANTES competition assay

In order to test whether RANTES variants bind to a common location, an experiment was designed in which CCR5 was saturated with a 1 μM injection of the slow-dissociating variant 5P12-RANTES-E66S prior to injection of the different RANTES variants (see Figure 4). After this saturating injection, the binding of 5P12-RANTES-E66S was considerably reduced (positive control). The effect was intermediate for PSC-RANTES, similar to the effect of Maraviroc. There was no effect on binding of WT-RANTES. These data show a clear separation of binding sites for WT-RANTES and 5P12-RANTES-E66S, and are in agreement with data from the Maraviroc competition assay.

An equivalent, but reversed, experiment using WT-RANTES would have been interesting, but proved impossible since, at concentrations equal or above 108 nM, WT-RANTES interacts with the dextran matrix of the CM5 chip used in the SPR setup (data not shown). Moreover, as shown below, binding sites for WT-RANTES are not saturable. However, the same experiment was possible with the 2D7 antibody (see Figure 4). This 2D7 competition experiment gave very similar results to the 5P12-RANTES-E66S competition assay (see Figure 4). WT-RANTES was not competed by 2D7, although the dissociation rate became faster. This could indicate that 2D7 covers a small portion of the binding site for WT-RANTES or that some allosteric effects destabilize the interaction. The 2D7 competition results for 5P12-RANTES-E66S and PSC-RANTES were consistent with previously published data where 2D7 blocked binding of RANTES, MIP-1α, and MIP-1β to CCR5 [85, 91]. Indeed, 2D7 recognizes the second extracellular loop of CCR5 [85] which is also a major determinant of chemokine binding specificity [60, 92].

In summary, these competition experiments indicate that binding sites for PSC-RANTES and 5P12-RANTES-E66S partially overlap together and with the binding site for 2D7, while WT-RANTES appears not to share its binding site with 5P12-RANTES-E66S, but slightly with 2D7.

RANTES saturation assay

A saturation experiment was performed during which WT-RANTES was injected several times (*i.e.* 40-50 times). WT-RANTES accumulated on CCR5 upon the first injection. However, contrary to what would happen for a saturable and stoichiometric interaction, the amplitude of WT-RANTES association to CCR5 did not decrease for subsequent injections. Overall, WT-RANTES accumulated in similar amounts after each injection on the chip surface with captured CCR5/DDM/CHAPS/CHS mixed micelles (see Figure 5). The same phenomenon was observed for CCR5 solubilized in FC-12 (data not shown), where
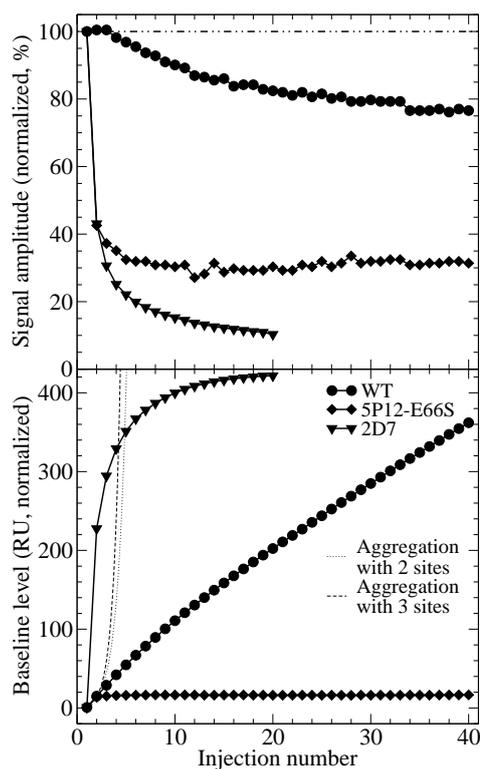
Figure 5: Saturation experiments with WT-RANTES (circles), 5P12-RANTES-E66S (diamonds) or the 2D7 antibody (triangles). Shown is the binding amplitude of each successive injection (normalized to the amplitude of the first injection, top) and the baseline level for subsequent injections (which reports on total accumulation on the chip, bottom). The dashed/dotted line on the top represents 100%, while dashed and dotted lines on the bottom represent theoretical exponential curves for aggregation with two or three binding sites, respectively. The different molecular weights for RANTES variants ($\sim$8 kDa) and 2D7 ($\sim$150 kDa) scale the respective saturation profiles.

WT-RANTES is the only ligand showing clear interaction (see Figure 2), as well as with β1AR-m23. Accumulation of WT-RANTES was constant: each new injection increased the signal with the same amplitude. This indicates that the phenomenon observed is not unspecific aggregation of WT-RANTES to multiple sites (see Figure 5), as the signal buildup would then get higher after each injection. Indeed, this is more consistent with molecules injected in each round having access to a constant number of binding sites (not less, not more). This is reminiscent of the WT-RANTES linear oligomers discussed in the work of Wang et al. [82] (see further below).

On the contrary, binding of 5P12-RANTES-E66S reached saturation after only a few injections (see Figure 5), consistent with 5P12-RANTES-E66S competition assay results (see Figure 4) Similarly, binding of the 2D7 antibody saturated after only a few injections (see Figure 5).

Effect of salt

As shown by the absence of interaction in the presence of 500 mM NaCl in the running buffer (see Figure 6), WT-RANTES binds in a mostly electrostatic manner. Also, high salt concentrations (*i.e.* 500 mM NaCl) completely remove bound protein (data not shown). On the contrary, 5P12-RANTES-E66S, which interacts on the orthosteric site of CCR5 (as shown above, by the Maraviroc competition assay), can still bind to CCR5 (with similar affinity, but lower amplitude) in the presence of 500 mM NaCl (see Figure 6), and is not removed by 500 mM NaCl (data not shown). The relative protection of 5P12-RANTES-E66S binding to CCR5 from the effect of salt is probably related to its uncharged N-terminal pyroglutamate residue [35] and generally hydrophobic N-terminal residues. Similarly, PSC-RANTES, which contains a very hydrophobic N-terminus modification (*N*-nonanoyl, des-Ser[1] [6-thioproline[2], L-cyclohexylglycine[3]]
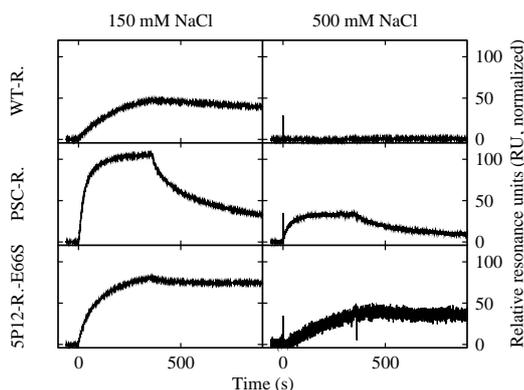
Figure 6: Effect of salt on binding of RANTES variants to CCR5 in DDM/CHAPS/CHS. Interaction of the different variants was probed with 500 mM NaCl, after which a control injection was performed at 150 mM NaCl. RANTES variants were injected at 36 nM. The binding profiles in absence of both 2D7 and 5P12-RANTES-E66S are shown as references on the left.

RANTES(2-68)) which could anchor it to CCR5, can still bind with a similar affinity, although to a slightly lower amplitude, in the presence of 500 mM NaCl (see Figure 6).

With 500 mM NaCl in the running buffer, we could not detect the low-amplitude signal from Maraviroc. However, when including 1 μM Maraviroc in the high salt buffer, the interaction with 5P12-RANTES-E66S, 5P12-RANTES-biotin, and PSC-RANTES was affected in a similar manner as in the low salt (150 mM) buffer (data not shown). This indicates that, although not directly detected, binding of Maraviroc in the presence of 500 mM NaCl is possible. This is similar to binding of 5P12-RANTES-E66S and PSC-RANTES, and consistent with Maraviroc interaction with CCR5 being mainly driven by hydrophobic interactions (except for the interaction with Glu-283) through contacts with the aromatic rings and aliphatic chains of residues Trp-86, Tyr-108, Tyr-251, Phe-109, and Ile-198 in the transmembrane helical groove of CCR5 [45, 47].

Mechanism of interaction by WT-RANTES

As discussed above, different competition experiments were performed with either Maraviroc, 5P12-RANTES-E66S, or 2D7 as the blocking agent. These assays proved the specificity of interaction for most ligands, except for WT-RANTES. Indeed, WT-RANTES could bind CCR5 in both DDM/CHAPS/CHS and FC-12, as well as β1AR-m23 in DDM/CHAPS/CHS. In addition, its binding was only slightly affected by the presence of other ligands such as Maraviroc, 5P12-RANTES-E66S, or 2D7. Finally, its binding site could not be saturated. These data, taken together with the salt sensitivity of the interaction, indicate the possibility for binding of WT-RANTES to either a different site on CCR5, *e.g.* the highly charged intracellular part, or to the protein/detergent mixed micelles.

In order to probe the mechanism by which WT-RANTES interacts in a non-saturable manner with both CCR5 and β1AR-m23, the behavior of additional RANTES variants was tested. The variants used for this purpose varied in their C-terminus, but not in their core and N-terminus, the parts assumed to be involved in binding to CCR5 [54–56]. As observed in Figure 7, the binding profile of WT-RANTES, WT-RANTES-biotin, and RANTES-E66S varied considerably. Indeed, the dissociation rate was faster for WT-RANTES-biotin compared to WT-RANTES. It was even faster for RANTES-E66S. The apparent faster association phase for these two variants, as seen on Figure 7, is a consequence of faster dissociation as the effective association phase (k_{obs}) is governed both by the association and dissociation rates: $k_{obs} = (k_{on} \times \text{concentration}) + k_{off}$. These results, together with the results from the saturation assay (see Figure 5), indicate that binding of WT-RANTES to CCR5 may share some similarity with the linear oligomerization of RANTES, a process involving the charged residue E66 (located in the C-terminus) [80–82]. This hypothesis fits with the dramatic effect of salt on the interaction of WT-RANTES. Indeed, the dimer-dimer interaction involved in the formation of the linear oligomers involves several salt bridges with
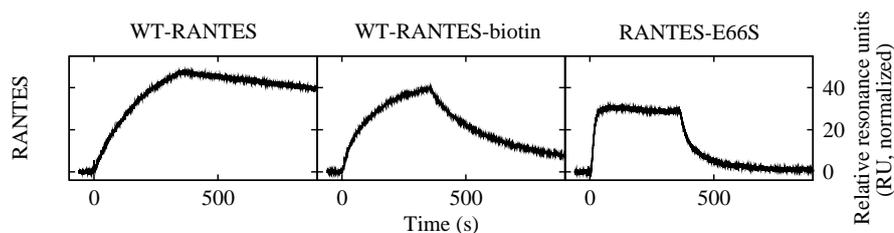
Figure 7: Effect of C-terminal modifications in the binding profile of RANTES. RANTES variants were injected at 36 nM.

K25, E26, R44, and E66 [82]. This hypothesis also reconciles assays where the binding of WT-RANTES was shown not to saturate (see Figure 5). Indeed, a linear oligomerization process through the C-terminus yields linear chains, which means that molecules accumulate with a fixed rate [82], contrary to unspecific aggregation which yields higher rates as the randomly- and multiply-branched aggregate grows in size. Such oligomerization is not observed for 5P12-RANTES-E66S because of its C-terminus (E66S). For PSC-RANTES, in principle, there should be oligomerization by this mechanism. However, due to the faster dissociation rate of PSC-RANTES (precluding accumulation of the chemokine on the chip), we could not clearly observe it.

Conclusions

The kinetics data presented here complement the study by Escola et al. [93] who explained the mechanism by which PSC-RANTES displays its high anti-HIV potency. These data suggest that for 5P12-RANTES (as for Maraviroc) the HIV-1 entry inhibition mechanism relies on tight interaction with CCR5 and long-term blockade of the binding site for gp120, whereas for PSC-RANTES, this activity is based on CCR5 sequestration inside the cell as shown previously [93]. Indeed, PSC-RANTES and 5P12-RANTES display different phenotypes [20, 24, 93] and their anti-HIV activity is modulated differently by mutations in CCR5 [94]. PSC-RANTES (and WT-RANTES) are both able to activate CCR5 and cause its internalization [26]. However, when CCR5 is bound to PSC-RANTES, it is sequestered in the cell and does not recycle to the cell surface [93]. On the contrary, 5P12-RANTES neither activates nor internalizes CCR5 [24]. Here, we explain the very similar anti-HIV potency of 5P12-RANTES and PSC-RANTES (respectively 28 and 25 pM) [24] as a result of higher affinity (mainly because of a slower dissociation rate) in the case of 5P12-RANTES (see Table 1) and CCR5 sequestration in the cell for PSC-RANTES [93]. The K_D for 5P12-RANTES-E66S and 5P12-RANTES-biotin is $\sim$5-20x lower ($\sim$5-20x higher affinity) than for PSC-RANTES (see Table 1). The effect is even more pronounced for the dissociation rate which is $\sim$35-350x slower for 5P12-RANTES variants compared to PSC-RANTES. Thus, association of CCR5 with 5P12-RANTES is longer-lived than with PSC-RANTES. However, PSC-RANTES does not only interact with CCR5 on the cell surface, but induces internalization and sequesters CCR5 in the cell with more potency than WT-RANTES [93]. Once CCR5 is sequestered in the cell, it is not available for interaction with gp120.

In Figure 8, we show a model explaining the phenotypes of Maraviroc and the different RANTES variants. In this model, Maraviroc and 5P12-RANTES-E66S bind to the orthosteric binding site on CCR5, which either partially overlaps with the binding site for Maraviroc or is under control of an allosteric mechanism triggered by the presence of Maraviroc (as observed here for 5P12-RANTES-E66S and PSC-RANTES, and by others for WT-RANTES [42, 45, 95, 96]). Indeed, as proposed by many before, the chemokines interact with both the extracellular loops and transmembrane groove using their core and N-terminus, respectively [54–56]. Overall, our results for 5P12-RANTES-E66S and PSC-RANTES agree with the two-site model [54, 57]. However, WT-RANTES behaves differently in our setup. Indeed, WT-RANTES binds not on the orthosteric site, but on a different location. One possibility is that WT-RANTES binds on either the highly charged intracellular side of the receptor, on the detergent-stabilized transmembrane surface of CCR5 (and β1AR-m23), or on the detergents forming the GPCR/detergent mixed micelle, or using a combination of these mechanisms. This behavior of WT-RANTES, however, might be related to its propensity to form linear oligomers at high
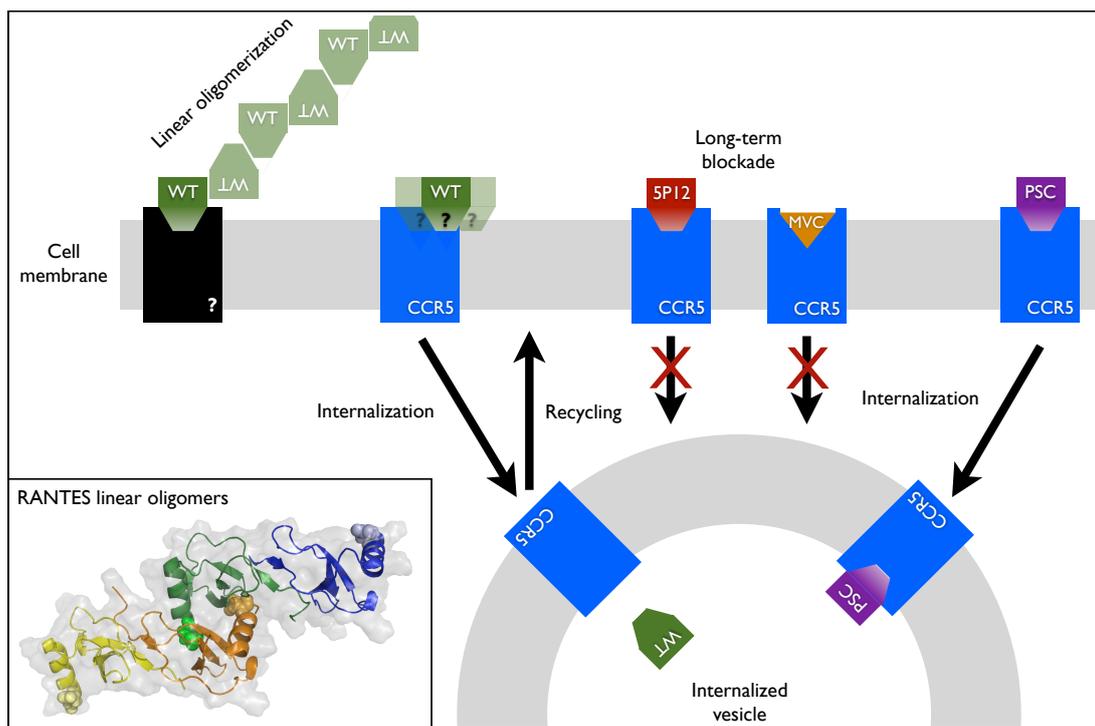
Figure 8: Schematic model for the anti-HIV mechanisms of Maraviroc and different RANTES variants. Although 5P12-RANTES and PSC-RANTES display similar anti-HIV potencies, their dissociation rates from CCR5 are very different. This fits with the fact that, whereas 5P12-RANTES causes neither CCR5 signaling nor internalization, PSC-RANTES internalizes CCR5 and sequesters it in the cell. Thus, the high anti-HIV potency of 5P12-RANTES is obtained, as for Maraviroc, through long-term blockade of CCR5, while PSC-RANTES prevents gp120 from interacting with CCR5 by hiding it in the cell [93]. In addition, in our SPR setup, although the exact binding site for WT-RANTES on CCR5 is undefined, linear oligomerization of WT-RANTES following its initial attachment is clearly observed. The inset shows the arrangement of two dimers (yellow and orange, as well as green and blue pairs) of WT-RANTES in a linear oligomer. Residue E66 is shown as spheres. The figure with PDB 2L9H [82] was prepared using PyMOL (Schrödinger).

concentrations [82]. Indeed, the C-terminus mutants RANTES-E66S and WT-RANTES-biotin have considerably different binding profiles both displaying faster dissociation. This could therefore be related to the capacity of RANTES to bind to and linearly oligomerize on glycosaminoglycans through its C-terminus [80–82], a process important for preconcentration of the chemokines in the vicinity of their receptors [72–74]. As already discussed earlier, this linear oligomerization process is not observed for 5P12-RANTES-E66S as its modified C-terminus (with the E66S mutation) precludes the formation of chains of dimers. For PSC-RANTES, the fast dissociation precludes additive accumulation of the chemokine during following injections, preventing observation of this phenomenon.

We believe the SPR setup discussed here which uses our insect cell-overexpressed CCR5 can be useful as a complement to *in vivo* data, as was recently shown for Visfatin/NAMPT [97]. In the current study, we could complement previously published data and show the different mechanisms by which PSC-RANTES and 5P12-RANTES reach very similar anti-HIV potency. We could also observe linear oligomerization of WT-RANTES.

Acknowledgments

baculoviruses, while Christian Opitz is acknowledged for insect cell overexpression of β1AR-m23.

Supporting information

Interaction with MIP-1β

In addition to observing the interaction of 2D7, several RANTES variants, and Maraviroc, we could observe the interaction of CCR5 with an additional, MIP-1β. The fitted K_D was $\sim$180 nM (see Figure 9). The affinity was lower compared to the K_D in COS-7 cells ($\sim$2 nM) [88] and HEK-293 cells ($\sim$0.2 nM) [90] or the IC_{50} measured in COS-7 cells ($\sim$7 nM) [88] and CHO-K1 cells ($\sim$10 nM) [98]. High concentration of MIP-1β (1 μM) was necessary for observation of a clear binding signal.
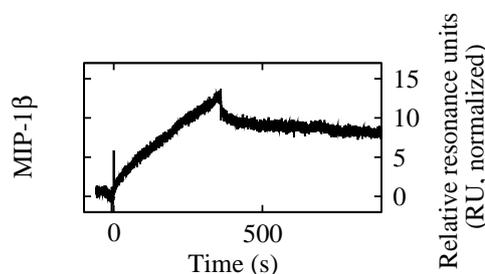

Figure 9: Binding profile of MIP-1β in DDM/CHAPS/CHS. MIP-1β was injected at 1 μM.

Comparison with previous studies

Although the K_D for WT-RANTES is very similar to the value previously published by Navratilova et al. [62] (*i.e.* 2.6 nM vs 3.9 nM), both the association and dissociation rates are very different, with the k_{on} and k_{off} values from Navratilova et al. [62] being both two orders of magnitude faster. There is no obvious reason for this, except maybe the source of CCR5 (insect cells vs Cf2Th mammalian cells) or the lipids used as additives in the detergent mix (50 nM DOPC vs 35 nM DOPC + 15 nM DOPS for Navratilova et al. [62]), although the latter does not affect 2D7 binding as shown by Navratilova et al. [59]. Nevertheless, it cannot be excluded that specific binding of DOPS to CCR5 (with nM affinity) could have a noticeable impact on its RANTES binding properties. One additional factor which could affect the binding of RANTES is the source of CCR5. While Navratilova et al. [62] used CCR5 overexpressed at low yield in Cf2Th canine thymocyte cells, our CCR5 was overexpressed in the baculovirus/insect cell system. It is well known that glycosylation is different in these two systems [99].

Finally, the flow rate could cause the observed differences. Indeed, whereas our experiments were performed with a flow rate of 50 μL/min, Navratilova et al. [62] used a faster flow rate of 100 μL/min. With a too slow flow rate, artifacts can arise. For example, mass transport (also called mass transfer) effects can slow down the effective association rate, thereby increasing the apparent K_D (resulting in an apparent lower affinity) [78]. On the other hand, if the flow rate is too slow, rebinding can occur during the dissociation phase. In this case, as the molecule rebinds to the surface before exiting the flow cell, the apparent dissociation rate is slowed down, thereby reducing the apparent K_D (resulting in an apparent higher affinity) [100]. We tested this possibility by running our samples at 100 μL/min. Figure 10 shows a comparison of binding profiles for RANTES variants using different flow rates. As shown in Figure 10, data for both PSC-RANTES and 5P12-RANTES-E66S are neither affected by mass transport effects nor by rebinding of the ligands during the dissociation phase. Indeed, both the k_{on} and k_{off} rates

recorded with a flow rate of 100 μL/min are very similar to those measured with a flow rate of 50 μL/min (with both association and dissociation phases being almost exactly superposable). However, for WT-RANTES, the situation is different. Indeed, both the association and dissociation rates are increased by a factor of $\sim$10 with a clearly visible change in the binding profile (see Figure 10). The K_D, however, is not affected as both changes are compensated. These accelerated rates for WT-RANTES, however, are more consistent with data from Navratilova et al. [62] with which they nevertheless still differ by one order of magnitude.
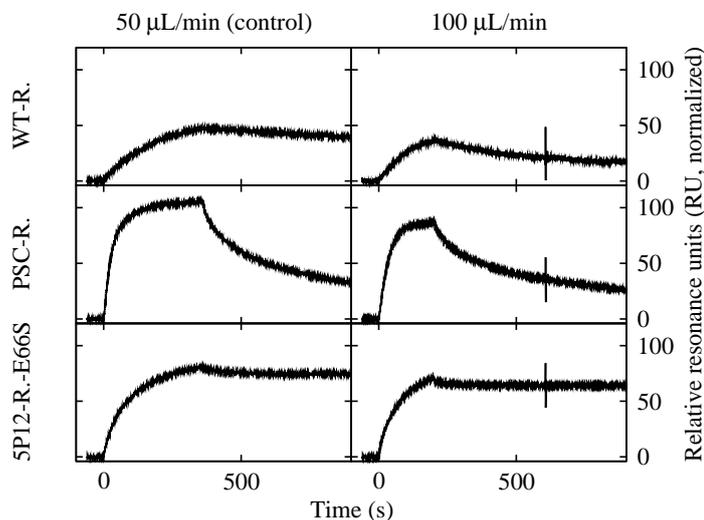
Figure 10: Effect of the flow rate on the binding profiles for RANTES variants. RANTES variants were injected at 36 nM for 360 s at 50 μL/min (left) and for 210 s at 100 μL/min (right).

Different 5P12-RANTES variants

To probe whether the E66S mutation affected the interaction of 5P12-RANTES-E66S with CCR5, we used 5P12-RANTES without the E66S mutation (5P12-RANTES-biotin, a 5P12-RANTES variant C-terminally coupled to biotin). Figure 11 shows that the E66S mutation in 5P12-RANTES-E66S does not significantly affect the binding profile. Except for the faster dissociation rate observed for 5P12-RANTES-biotin, other fitted parameters are similar for both 5P12-RANTES variants (see Table 1 in the main document).
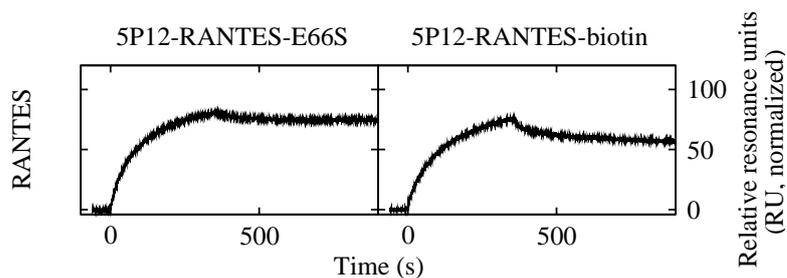
Figure 11: Comparison of binding profiles for 5P12-RANTES-E66S and 5P12-RANTES C-terminally coupled to biotin. Both RANTES variants were injected at 36 nM.

118

References

[1] Lederman, M. M., A. Penn-Nicholson, M. Cho, and D. Mosier, 2006. Biology of CCR5 and its role in HIV infection and treatment. *JAMA* 296:815–826.

[2] Lusso, P., 2006. HIV and the chemokine system: 10 years later. *EMBO J.* 25:447–456.

[3] Schuitemaker, H., A. B. van t Wout, and P. Lusso, 2011. Clinical significance of HIV-1 coreceptor usage. *J. Trans. Med.* 9:S5.

[4] Singer, I. I., S. Scott, D. W. Kawka, J. Chin, B. L. Daugherty, J. A. DeMartino, J. DiSalvo, S. L. Gould, J. E. Lineberger, L. Malkowitz, M. D. Miller, L. Mitnaul, S. J. Siciliano, M. J. Staruch, H. R. Williams, H. J. Zweerink, and M. S. Springer, 2001. CCR5, CXCR4, and CD4 are clustered and closely apposed on microvilli of human macrophages and T cells. *J. Virol.* 75:3779–3790.

[5] Cocchi, F., A. DeVico, D. Garzino, S. Arya, R. Gallo, and P. Lusso, 1995. Identification of RANTES, MIP-1α, and MIP-1β as the major HIV-suppressive factors produced by CD8+ T cells. *Science* 270:1811–1815.

[6] Lederman, M. M., R. S. Veazey, R. Offord, D. E. Mosier, J. Dufour, M. Mefford, M. J. Piatak, J. D. Lifson, J. R. Salkowitz, B. Rodriguez, A. Blauvelt, and O. Hartley, 2004. Prevention of vaginal SHIV transmission in Rhesus macaques through inhibition of CCR5. *Science* 306:485–487.

[7] Liu, R., W. A. Paxton, S. Choe, D. Ceradini, S. R. Martin, R. Horuk, M. E. MacDonald, H. Stuhlmann, R. A. Koup, and N. R. Landau, 1996. Homozygous defect in HIV-1 coreceptor accounts for resistance of some multiply-exposed individuals to HIV-1 infection. *Cell* 86:367–377.

[8] Samson, M., F. Libert, B. J. Doranz, J. Rucker, C. Liesnard, C.-M. Farber, S. Saragosti, C. Lapouméroulie, J. Cognaux, C. Forceille, G. Muyldermans, C. Verhofstede, G. Burtonboy, M. Georgesstar, T. Imai, S. Rana, Y. Yi, R. J. Smyth, R. G. Collman, R. W. Doms, G. Vassart, and P. Marc, 1996. Resistance to HIV-1 infection in Caucasian individuals bearing mutant alleles of the CCR-5 chemokine receptor gene. *Nature* 382:722–725.

[9] Benkirane, M., D. Y. Jin, R. F. Chun, R. A. Koup, and K. T. Jeang, 1997. Mechanism of transdominant inhibition of CCR5-mediated HIV-1 infection by ccr5Δ32. *J. Biol. Chem.* 272:30603–30606.

[10] Arenzana-Seisdedos, F., J.-L. Virelizier, D. Rousset, I. Clark-Lewis, P. Loetscher, B. Moser, and M. Baggiolini, 1996. HIV blocked by chemokine antagonist. *Nature* 383:400.

[11] Oravecz, T., M. Pall, G. Roderiquez, M. D. Gorrell, M. Ditto, N. Y. Nguyen, R. Boykins, E. Unsworth, and M. A. Norcross, 1997. Regulation of the receptor specificity and function of the chemokine RANTES (Regulated on Activation, Normal T Cell Expressed and Secreted) by dipeptidyl peptidase IV (CD26)-mediated cleavage. *J. Exp. Med.* 186:1865–1872.

[12] Ylisastigui, L., J. Vizzavona, E. Drakopoulou, P. Paindavoine, C. Calvo, M. Parmentier, J. C. Gluckman, C. Vita, and A. Benjouad, 1998. Synthetic full-length and truncated RANTES inhibit HIV-1 infection of primary macrophages. *AIDS* 12:977–984.

[13] Struyf, S., I. De Meester, S. Scharpé, J.-P. Lenaerts, P. Menten, J. M. Wang, P. Proost, and J. Van Damme, 1998. Natural truncation of RANTES abolishes signaling through the CC chemokine receptors CCR1 and CCR3, impairs its chemotactic potency and generates a CC chemokine inhibitor. *Eur. J. Immunol.* 28:1262–1271.

[14] Proost, P., I. De Meester, D. Schols, S. Struyf, A.-M. Lambeir, A. Wuyts, G. Opdenakker, E. De Clercq, S. Scharpé, and J. Van Damme, 1998. Amino-terminal truncation of chemokines by CD26/dipeptidyl-peptidase IV. *J. Biol. Chem.* 273:7222–7227.

[15] Schols, D., P. Proost, S. Struyf, A. Wuyts, I. D. Meester, S. Scharpé, J. V. Damme, and E. D. Clercq, 1998. CD26-processed RANTES(3-68), but not intact RANTES, has potent anti-HIV-1 activity. *Antivir. Res.* 39:175–187.

[16] Lim, J. K., W. Lu, O. Hartley, and A. L. DeVico, 2006. N-terminal proteolytic processing by cathepsin G converts RANTES/CCL5 and related analogs into a truncated 4-68 variant. *J. Leukoc. Biol.* 80:1395–1404.

[17] Simmons, G., P. R. Clapham, L. Picard, R. E. Offord, M. M. Rosenkilde, T. W. Schwartz, R. Buser, T. N. C. Wells, and A. E. I. Proudfoot, 1997. Potent inhibition of HIV-1 infectivity in macrophages and lymphocytes by a novel CCR5 antagonist. *Science* 276:276–279.

[18] Mack, M., B. Luckow, P. J. Nelson, J. Cihak, G. Simmons, P. R. Clapham, N. Signoret, M. Marsh, M. Stangassinger, F. Borlat, T. N. Wells, D. Schlöndorff, and A. E. Proudfoot, 1998. Aminooxypentane-RANTES induces CCR5 internalization but inhibits recycling: A novel inhibitory mechanism of HIV infectivity. *J. Exp. Med.* 187:1215–1224.

[19] Mosier, D. E., G. R. Picchio, R. J. Gulizia, R. Sabbe, P. Poignard, L. Picard, R. E. Offord, D. A. Thompson, and J. Wilken, 1999. Highly potent RANTES analogues either prevent CCR5-using human immunodeficiency virus type 1 infection in vivo or rapidly select for CXCR4-using variants. *J. Virol.* 73:3544–3550.

[20] Hartley, O., H. Gaertner, J. Wilken, D. Thompson, R. Fish, A. Ramos, C. Pastore, B. Dufour, F. Cerini, A. Melotti, N. Heveker, L. Picard, M. Alizon, D. Mosier, S. Kent, and R. Offord, 2004. Medicinal chemistry applied to a synthetic protein: Development of highly potent HIV entry inhibitors. *Proc. Nat. Acad. Sci.* 101:16460–16465.

[21] Proudfoot, A. E. I., C. A. Power, A. J. Hoogewerf, M.-O. Montjovent, F. Borlat, R. E. Offord, and T. N. C. Wells, 1996. Extension of recombinant human RANTES by the retention of the initiating methionine produces a potent antagonist. *J. Biol. Chem.* 271:2599–2603.

[22] Polo, S., V. Nardese, C. Santis, C. Arcelloni, R. Paroni, F. Sironi, A. Verani, M. Rizzi, M. Bolognesi, and P. Lusso, 2000. Enhancement of the HIV-1 inhibitory activity of RANTES by modification of the N-terminal region: Dissociation from CCR5 activation. *Eur. J. Immunol.* 30:3190–3198.

[23] Hartley, O., K. Dorgham, D. Perez-Bercoff, F. Cerini, A. Heimann, H. Gaertner, R. E. Offord, G. Pancino, P. Debré, and G. Gorochov, 2003. Human immunodeficiency virus type 1 entry inhibitors selected on living cells from a library of phage chemokines. *J. Virol.* 77:6637–6644.

[24] Gaertner, H., F. Cerini, J.-M. Escola, G. Kuenzi, A. Melotti, R. Offord, I. Rossitto-Borlat, R. Nedellec, J. Salkowitz, G. Gorochov, D. Mosier, and O. Hartley, 2008. Highly potent, fully recombinant anti-HIV chemokines: Reengineering a low-cost microbicide. *Proc. Nat. Acad. Sci.* 105:17706–17711.

[25] Mack, M., J. Pfirstinger, J. Haas, P. J. Nelson, P. Kufer, G. Riethmüller, and D. Schlöndorff, 2005. Preferential targeting of CD4-CCR5 complexes with bifunctional inhibitors: A novel approach to block HIV-1 infection. *J. Immunol.* 175:7586–7593.

[26] Gaertner, H., O. Lebeau, I. Borlat, F. Cerini, B. Dufour, G. Kuenzi, A. Melotti, R. J. Fish, R. Offord, J. Y. Springael, M. Parmentier, and O. Hartley, 2008. Highly potent HIV inhibition: Engineering a key anti-HIV structure from PSC-RANTES into MIP-1β/CCL4. *Prot. Eng. Des. Sel.* 21:65–72.

[27] Wells, T., F. Guyecoulin, and K. Bacon, 1995. Peptides from the amino terminus of RANTES cause chemotaxis of human T-lymphocytes. *Biochem. Biophys. Res. Com.* 211:100–105.

[28] Nishiyama, Y., T. Murakami, S. Shikama, K. Kurita, and N. Yamamoto, 2002. Anti-HIV-1 peptides derived from partial amino acid sequences of CC-Chemokine RANTES. *Bioorgan. Med. Chem.* 10:4113–4117.

[29] Ramnarine, E. J., A. L. DeVico, and S. C. Vigil-Cruz, 2006. Analogues of N-terminal truncated synthetic peptide fragments derived from RANTES inhibit HIV-1 infectivity. *Bioorgan. Med. Chem. Lett.* 16:93–95.

[30] Nardese, V., R. Longhi, S. Polo, F. Sironi, C. Arcelloni, R. Paroni, C. DeSantis, P. Sarmientos, M. Rizzi, M. Bolognesi, V. Pav one, and P. Lusso, 2001. Structural determinants of CCR5 recognition and HIV-1 blockade in RANTES. *Nat. Struc. Biol.* 8:611–615.

[31] Vangelista, L., R. Longhi, F. Sironi, V. Pavone, and P. Lusso, 2006. Critical role of the N-loop and β-strand hydrophobic clusters of RANTES-derived peptides in anti-HIV activity. *Biochem. Biophys. Res. Com.* 351:664–668.

[32] Lusso, P., L. Vangelista, R. Cimbro, M. Secchi, F. Sironi, R. Longhi, M. Faiella, O. Maglio, and V. Pavone, 2011. Molecular engineering of RANTES peptide mimetics with potent anti-HIV-1 activity. *FASEB J.* 25:1230–1243.

[33] Veazey, R. S., B. Ling, L. C. Green, E. P. Ribka, J. D. Lifson, M. Piatak, M. M. Lederman, D. Mosier, R. Offord, and O. Hartley, 2009. Topically applied recombinant chemokine analogues fully protect macaques from vaginal simian-human immunodeficiency virus challenge. *J. Infect. Dis.* 199:1525–1527.

[34] Cerini, F., A. Landay, C. Gichinga, M. M. Lederman, R. Flyckt, D. Starks, R. E. Offord, F. Le Gal, and O. Hartley, 2008. Chemokine analogues show suitable stability for development as microbicides. *J. AIDS* 49:472–476.

[35] Chelius, D., K. Jing, A. Lueras, D. S. Rehder, T. M. Dillon, A. Vizel, R. S. Rajan, T. Li, M. J. Treuheit, and P. V. Bondarenko, 2006. Formation of pyroglutamic acid from N-terminal glutamic acid in immunoglobulin gamma antibodies. *Anal. Chem.* 78:2370–2376.

[36] Skelton, N. J., F. Aspiras, J. Ogez, and T. J. Schall, 1995. Proton NMR assignments and solution conformation of RANTES, a chemokine of the C-C type. *Biochemistry* 34:5329–5342.

[37] Baba, M., O. Nishimura, N. Kanzaki, M. Okamoto, H. Sawada, Y. Iizawa, M. Shiraishi, Y. Aramaki, K. Okonogi, Y. Ogawa, K. Meguro, and M. Fujino, 1999. A small-molecule, nonpeptide CCR5 antagonist with highly potent and selective anti-HIV-1 activity. *Proc. Nat. Acad. Sci.* 96:5698–5703.

[38] Strizki, J. M., S. Xu, N. E. Wagner, L. Wojcik, J. Liu, Y. Hou, M. Endres, A. Palani, S. Shapiro, J. W. Clader, W. J. Greenlee, J. R. Tagat, S. McCombie, K. Cox, A. B. Fawzi, C. C. Chou, C. Pugliese-Sivo, L. Davies, M. E. Moreno, D. D. Ho, A. Trkola, C. A. Stoddart, J. P. Moore, G. R. Reyes, and B. M. Baroudy, 2001. SCH-C (SCH 351125), an orally bioavailable, small molecule antagonist of the chemokine receptor CCR5, is a potent inhibitor of HIV-1 infection in vitro and in vivo. *Proc. Nat. Acad. Sci.* 98:12718–12723.

[39] Maeda, K., H. Nakata, Y. Koh, T. Miyakawa, H. Ogata, Y. Takaoka, S. Shibayama, K. Sagawa, D. Fukushima, J. Moravek, Y. Koyanagi, and H. Mitsuya, 2004. Spirodiketopiperazine-based CCR5 inhibitor which preserves CC-chemokine/CCR5 interactions and exerts potent activity against R5 human immunodeficiency virus type 1 in vitro. *J. Virol.* 78:8654–8662.

[40] Tagat, J. R., S. W. McCombie, D. Nazareno, M. A. Labroli, Y. Xiao, R. W. Steensma, J. M. Strizki, B. M. Baroudy, K. Cox, J. Lachowicz, G. Varty, and R. Watkins, 2004. Piperazine-based CCR5 antagonists as HIV-1 inhibitors. IV. Discovery of 1-[(4,6-Dimethyl-5-pyrimidinyl)carbonyl]-4-[4-2-methoxy-1(R)-4-(trifluoromethyl)phenylethyl-3(S)-methyl-1-piperazinyl]-4-methylpiperidine (Sch-417690/Sch-D), a potent, highly selective, and orally bioavailable CCR5 antagonist. *J. Med. Chem.* 47:2405–2408.

[41] Takashima, K., H. Miyake, N. Kanzaki, Y. Tagawa, X. Wang, Y. Sugihara, Y. Iizawa, and M. Baba, 2005. Highly potent inhibition of human immunodeficiency virus type 1 replication by TAK-220, an orally bioavailable small-molecule CCR5 antagonist. *Antimicrob. Agents Chemother.* 49:3481–3489.

[42] Dorr, P., M. Westby, S. Dobbs, P. Griffin, B. Irvine, M. Macartney, J. Mori, G. Rickett, C. Smith-Burchnell, C. Napier, R. Webster, D. Armour, D. Price, B. Stammen, A. Wood, and M. Perros, 2005. Maraviroc (UK-427,857), a potent, orally bioavailable, and selective small-molecule inhibitor of chemokine receptor CCR5 with broad-spectrum anti-human immunodeficiency virus type 1 activity. *Antimicrob. Agents Chemother.* 49:4721–4732.

[43] Dragic, T., A. Trkola, D. A. Thompson, E. G. Cormier, F. A. Kajumo, E. Maxwell, S. W. Lin, W. Ying, S. O. Smith, T. P. Sakmar, and J. P. Moore, 2000. A binding pocket for a small molecule inhibitor of HIV-1 entry within the transmembrane helices of CCR5. *Proc. Nat. Acad. Sci.* 97:5639–5644.

[44] Maeda, K., D. Das, H. Ogata-Aoki, H. Nakata, T. Miyakawa, Y. Tojo, R. Norman, Y. Takaoka, J. Ding, G. F. Arnold, E. Arnold, and H. Mitsuya, 2006. Structural and molecular interactions of CCR5 inhibitors with CCR5. *J. Biol. Chem.* 281:12688–12698.

[45] Kondru, R., J. Zhang, C. Ji, T. Mirzadegan, D. Rotstein, S. Sankuratri, and M. Dioszegi, 2008. Molecular interactions of CCR5 with major classes of small-molecule anti-HIV CCR5 antagonists. *Mol. Pharmacol.* 73:789–800.

[46] Garcia-Perez, J., P. Rueda, I. Staropoli, E. Kellenberger, J. Alcami, F. Arenzana-Seisdedos, and B. Lagane, 2011. New insights into the mechanisms whereby low molecular weight CCR5 ligands inhibit HIV-1 infection. *J. Biol. Chem.* 286:4978–4990.

[47] Grunbeck, A., T. Huber, R. Abrol, B. Trzaskowski, W. A. Goddard, and T. P. Sakmar, 2012. Genetically encoded photo-cross-linkers map the binding site of an allosteric drug on a G protein-coupled receptor. *ACS Chem. Biol.* 7:967–972.

[48] Kang, Y., Z. Wu, T. C. K. Lau, X. Lu, L. Liu, A. K. L. Cheung, Z. Tan, J. Ng, J. Liang, H. Wang, S. Li, B. Zheng, B. Li, L. Chen, and Z. Chen, 2012. CCR5 antagonist TD-0680 uses a novel mechanism for enhanced potency against HIV-1 entry, cell-mediated infection, and a resistant variant. *J. Biol. Chem.* 287:16499–16509.

[49] Ogert, R. A., L. Ba, Y. Hou, C. Buontempo, P. Qiu, J. Duca, N. Murgolo, P. Buontempo, R. Ralston, and J. A. Howe, 2009. Structure-function analysis of human immunodeficiency virus type 1 gp120 amino acid mutations associated with resistance to the CCR5 coreceptor antagonist Vicriviroc. *J. Virol.* 83:12151–12163.

[50] Tilton, J. C., C. B. Wilen, C. A. Didigu, R. Sinha, J. E. Harrison, C. Agrawal-Gamse, E. A. Henning, F. D. Bushman, J. N. Martin, S. G. Deeks, and R. W. Doms, 2010. A Maraviroc-resistant HIV-1 with narrow cross-resistance to other CCR5 antagonists depends on both N-terminal and extracellular loop domains of drug-bound CCR5. *J Virol.* 84:10863–10876.

[51] Nedellec, R., M. Coetzer, M. M. Lederman, R. E. Offord, O. Hartley, and D. E. Mosier, 2011. Resistance to the CCR5 inhibitor 5P12-RANTES requires a difficult evolution from CCR5 to CXCR4 coreceptor use. *PLoS ONE* 6:e22020.

[52] Roche, M., M. R. Jakobsen, J. Sterjovski, A. Ellett, F. Posta, B. Lee, B. Jubb, M. Westby, S. R. Lewin, P. A. Ramsland, M. J. Churchill, and P. R. Gorry, 2011. HIV-1 escape from the CCR5 antagonist maraviroc associated with an altered and less-efficient mechanism of gp120-CCR5 engagement that attenuates macrophage tropism. *J. Virol.* 85:4330–4342.

[53] Safarian, D., X. Carnec, F. Tsamis, F. Kajumo, and T. Dragic, 2006. An anti-CCR5 monoclonal antibody and small molecule CCR5 antagonists synergize by inhibiting different stages of human immunodeficiency virus type 1 entry. *Virology* 352:477–484.

[54] Blanpain, C., B. J. Doranz, A. Bondue, C. Govaerts, A. de Leener, G. Vassart, R. W. Doms, A. Proudfoot, and M. Parmentier, 2003. The core domain of chemokines binds CCR5 extracellular domains while their amino terminus interacts with the transmembrane helix bundle. *J. Biol. Chem.* 278:5179–5187.

[55] Duma, L., D. Häussinger, M. Rogowski, P. Lusso, and S. Grzesiek, 2007. Recognition of RANTES by extracellular parts of the CCR5 receptor. *J. Mol. Biol.* 365:1063–1075.

[56] Yoshiura, C., Y. Kofuku, T. Ueda, Y. Mase, M. Yokogawa, M. Osawa, Y. Terashima, K. Matsushima, and I. Shimada, 2010. NMR analyses of the interaction between CCR5 and its ligand using functional reconstitution of CCR5 in lipid bilayers. *J. Am. Chem. Soc.* 132:6768–6777.

[57] Siciliano, S. J., T. E. Rollins, J. DeMartino, Z. Konteatis, L. Malkowitz, G. Van Riper, S. Bondy, H. Rosen, and M. S. Springer, 1994. Two-site binding of C5a by its receptor: an alternative binding paradigm for G protein-coupled receptors. *Proc. Nat. Acad. Sci.* 91:1214–1218.

[58] Maeda, K., D. Das, P. D. Yin, K. Tsuchiya, H. Ogata-Aoki, H. Nakata, R. B. Norman, L. A. Hackney, Y. Takaoka, and H. Mitsuya, 2008. Involvement of the second extracellular loop and transmembrane residues of CCR5 in inhibitor binding and HIV-1 fusion: Insights into the mechanism of allosteric inhibition. *J. Mol. Biol.* 381:956–974.

[59] Navratilova, I., J. Sodroski, and D. G. Myszka, 2005. Solubilization, stabilization, and purification of chemokine receptors using biosensor technology. *Anal. Biochem.* 339:271–281.

[60] Wu, L., G. LaRosa, N. Kassam, C. J. Gordon, H. Heath, N. Ruffing, H. Chen, J. Humblias, M. Samson, M. Parmentier, J. P. Moore, and C. R. Mackay, 1997. Interaction of chemokine receptor CCR5 with its ligands: multiple domains for HIV-1 gp120 binding and a single domain for chemokine binding. *J. Exp. Med.* 186:1373–1381.

[61] Nguyen, D., and D. Taub, 2002. Cholesterol is essential for macrophage inflammatory protein 1β binding and conformational integrity of CC chemokine receptor 5. *Blood* 99:4298–4306.

[62] Navratilova, I., M. Dioszegi, and D. G. Myszka, 2006. Analyzing ligand and small molecule binding activity of solubilized GPCRs using biosensor technology. *Anal. Biochem.* 355:132–139.

[63] Navratilova, I., M. Pancera, R. Wyatt, and D. G. Myszka, 2006. A biosensor-based approach toward purification and crystallization of G protein-coupled receptors. *Anal. Biochem.* 353:278–283.

[64] Rich, R. L., A. R. Miles, B. K. Gale, and D. G. Myszka, 2009. Detergent screening of a G-protein-coupled receptor using serial and array biosensor technologies. *Anal. Biochem.* 386:98–104.

[65] Navratilova, I., J. Besnard, and A. L. Hopkins, 2011. Screening for GPCR ligands using surface plasmon resonance. *ACS Med. Chem. Lett.* 2:549–554.

[66] Silin, V., E. Karlik, K. Ridge, and D. Vanderah, 2006. Development of surface-based assays for transmembrane proteins: Selective immobilization of functional CCR5, a G protein-coupled receptor. *Anal. Biochem.* 349:247–253.

[67] Nisius, L., M. Rogowski, L. Vangelista, and S. Grzesiek, 2008. Large-scale expression and purification of the major HIV-1 coreceptor CCR5 and characterization of its interaction with RANTES. *Prot. Expr. Purif.* 61:155–162.

[68] Mirzabekov, T., N. Bannert, M. Farzan, W. Hofmann, P. Kolchinsky, L. Wu, R. Wyatt, and J. Sodroski, 1999. Enhanced expression, native purification, and characterization of CCR5, a principal HIV-1 coreceptor. *J. Biol. Chem.* 274:28745–28750.

[69] Ren, H., D. Yu, B. Ge, B. Cook, Z. Xu, and S. Zhang, 2009. High-level production, solubilization and purification of synthetic human GPCR chemokine receptors CCR5, CCR3, CXCR4 and CX3CR1. *PLoS ONE* 4:e4509.

[70] Jarvis, D., 1997. The baculoviruses, New York, Plenum Press, chapter Baculovirus expression vectors., 389–431.

[71] Zaitseva, M., K. Peden, and H. Golding, 2003. HIV coreceptors: Role of structure, posttranslational modifications, and internalization in viral-cell fusion and as targets for entry inhibitors. *Biochim. Biophys. Acta Biomembr.* 1614:51–61.

[72] Johnson, Z., M. H. Kosco-Vilbois, S. Herren, R. Cirillo, V. Muzio, P. Zaratin, M. Carbonatto, M. Mack, A. Smailbegovic, M. Rose, R. Lever, C. Page, T. N. C. Wells, and A. E. I. Proudfoot, 2004. Interference with heparin binding and oligomerization creates a novel anti-inflammatory strategy targeting the chemokine system. *J. Immunol.* 173:5776–5785.

[73] Proudfoot, A. E. I., T. M. Handel, Z. Johnson, E. K. Lau, P. LiWang, I. Clark-Lewis, F. Borlat, T. N. C. Wells, and M. H. Kosco-Vilbois, 2003. Glycosaminoglycan binding and oligomerization are essential for the in vivo activity of certain chemokines. *Proc. Nat. Acad. Sci.* 100:1885–1890.

[74] Murooka, T. T., M. M. Wong, R. Rahbar, B. Majchrzak-Kita, A. E. I. Proudfoot, and E. N. Fish, 2006. CCL5-CCR5-mediated apoptosis in T cells. *J. Biol. Chem.* 281:25184–25194.

[75] Wilken, J., D. Hoover, D. A. Thompson, P. N. Barlow, H. McSparron, L. Picard, A. Wlodawer, J. Lubkowski, and S. B. Kent, 1999. Total chemical synthesis and high-resolution crystal structure of the potent anti-HIV protein AOP-RANTES. *Chem. Biol.* 6:43–51.

[76] Serrano-Vega, M. J., F. Magnani, Y. Shibata, and C. G. Tate, 2008. Conformational thermostabilization of the $\beta 1$-adrenergic receptor in a detergent-resistant form. *Proc. Nat. Acad. Sci.* 105:877–882.

[77] Ober, R. J., and E. Ward, 1999. The choice of reference cell in the analysis of kinetic data using BIAcore. *Anal. Biochem.* 271:70–80.

[78] Karlsson, R., and A. Fält, 1997. Experimental design for kinetic analysis of protein-protein interactions with surface plasmon resonance biosensors. *J. Immunol. Meth.* 200:121–133.

[79] Myszka, D. G., 1999. Improving biosensor analysis. *J. Mol. Recogn.* 12:279–284.

[80] Appay, V., A. Brown, S. Cribbes, E. Randle, and L. G. Czaplewski, 1999. Aggregation of RANTES is responsible for its inflammatory properties. Characterization of nonaggregating, noninflammatory RANTES mutants. *J. Biol. Chem.* 274:27505–27512.

[81] Czaplewski, L. G., J. McKeating, C. J. Craven, L. D. Higgins, V. Appay, A. Brown, T. Dudgeon, L. A. Howard, T. Meyers, J. Owen, S. R. Palan, P. Tan, G. Wilson, N. R. Woods, C. M. Heyworth, B. I. Lord, D. Brotherton, R. Christison, S. Craig, S. Cribbes, R. M. Edwards, S. J. Evans, R. Gilbert, P. Morgan, E. Randle, N. Schofield, P. G. Varley, J. F. Fisher, J. P. Waltho, and M. G. Hunter, 1999. Identification of amino acid residues critical for aggregation of human CC chemokines macrophage inflammatory protein MIP-1α, MIP-1β, and RANTES. Characterization of active disaggregated chemokine variants. *J. Biol. Chem.* 274:16077–16084.

[82] Wang, X., C. Watson, J. Sharp, T. Handel, and J. Prestegard, 2011. Oligomeric structure of the chemokine CCL5/RANTES from NMR, MS, and SAXS data. *Structure* 19:1138–1148.

[83] Cooper, M. A., 2003. Label-free screening of bio-molecular interactions. *Anal. Bioanal. Chem.* 377:834–842.

[84] Langelaan, D. N., P. Ngweniform, and J. K. Rainey, 2011. Biophysical characterization of G-protein coupled receptor–peptide ligand binding. *Biochem. Cell Biol.* 89:98–105.

[85] Lee, B., M. Sharron, C. Blanpain, B. J. Doranz, J. Vakili, P. Setoh, E. Berg, G. Liu, H. R. Guy, S. R. Durell, M. Parmentier, C. N. Chang, K. Price, M. Tsang, and R. W. Doms, 1999. Epitope mapping of CCR5 reveals multiple conformational states and distinct but overlapping structures involved in chemokine and coreceptor function. *J. Biol. Chem.* 274:9617–9626.

[86] O'Malley, M. A., M. E. Helgeson, N. J. Wagner, and A. S. Robinson, 2011. Toward rational design of protein detergent complexes: Determinants of mixed micelles that are critical for the in-vitro stabilization of a G-protein coupled receptor. *Biophys. J.* 101:1938–1948.

[87] Thompson, A. A., J. J. Liu, E. Chun, D. Wacker, H. Wu, V. Cherezov, and R. C. Stevens, 2011. GPCR stabilization using the bicelle-like architecture of mixed sterol-detergent micelles. *Methods* 55:310–317.

[88] Raport, C. J., J. Gosling, V. L. Schweickart, P. W. Gray, and I. F. Charo, 1996. Molecular cloning and functional characterization of a novel human CC chemokine receptor (CCR5) for RANTES, MIP-1β, and MIP-1α. *J. Biol. Chem.* 271:17161–17166.

[89] Blanpain, C., I. Migeotte, B. Lee, J. Vakili, B. J. Doranz, C. Govaerts, G. Vassart, R. W. Doms, and M. Parmentier, 1999. CCR5 binds multiple CC-chemokines: MCP-3 acts as a natural antagonist. *Blood* 94:1899–1905.

[90] Napier, C., H. Sale, M. Mosley, G. Rickett, P. Dorr, R. Mansfield, and M. Holbrook, 2005. Molecular cloning and radioligand binding characterization of the chemokine receptor CCR5 from rhesus macaque and human. *Biochem. Pharmacol.* 71:163–172.

[91] Navenot, J. M., Z. X. Wang, J. O. Trent, J. L. Murray, Q. X. Hu, L. DeLeeuw, P. S. Moore, Y. Chang, and S. C. Peiper, 2001. Molecular anatomy of CCR5 engagement by physiologic and viral chemokines and HIV-1 envelope glycoproteins: differences in primary structural requirements for RANTES, MIP-1α, and vMIP-II Binding. *J. Mol. Biol.* 313:1181–1193.

[92] Samson, M., G. LaRosa, F. Libert, P. Paindavoine, M. Detheux, G. Vassart, and M. Parmentier, 1997. The second extracellular loop of CCR5 is the major determinant of ligand specificity. *J. Biol. Chem.* 272:24934–24941.

[93] Escola, J. M., G. Kuenzi, H. Gaertner, M. Foti, and O. Hartley, 2010. CC chemokine receptor 5 (CCR5) desensitization: Cycling receptors accumulate in the trans-golgi network. *J. Biol. Chem.* 285:41772–41780.

[94] Choi, W.-T., R. Nedellec, M. Coetzer, P. Colin, B. Lagane, R. E. Offord, O. Hartley, and D. E. Mosier, 2012. CCR5 mutations distinguish N-terminal modifications of RANTES (CCL5) with agonist versus antagonist activity. *J. Virol.* .

[95] Garcia-Perez, J., P. Rueda, J. Alcami, D. Rognan, F. Arenzana-Seisdedos, B. Lagane, and E. Kellenberger, 2011. Allosteric model of maraviroc binding to CC chemokine receptor 5 (CCR5). *J. Biol. Chem.* 286:33409–33421.

[96] Thiele, S., A. Steen, P. C. Jensen, J. Mokrosinski, T. M. Frimurer, and M. M. Rosenkilde, 2011. Allosteric and orthosteric sites in CC chemokine receptor (CCR5), a chimeric receptor approach. *J. Biol. Chem.* 286:37543–37554.

[97] van den Bergh, R., S. Morin, H.-J. Sass, S. Grzesiek, M. Vekemans, E. Florence, H. Thanh Thi Tran, R. G. Imiru, L. Heyndrickx, G. Vanham, P. de Baetselier, and G. Raes, 2012. Monocytes contribute to differential immune pressure on R5 versus X4 HIV through the adipocytokine Visfatin/NAMPT. *PLoS ONE* 7:e35074.

[98] Bondue, A., S.-C. Jao, C. Blanpain, M. Parmentier, and P. J. LiWang, 2002. Characterization of the role of the N-Loop of MIP-1β in CCR5 binding. *Biochemistry* 41:13548–13555.

[99] Lopez, M., D. Tetaert, S. Juliant, M. Gazon, M. Cerutti, A. Verbert, and P. Delannoy, 1999. O-glycosylation potential of lepidopteran insect cell lines. *Biochim. Biophys. Acta* 1427:49–61.

[100] Nieba, L., S. E. Nieba-Axmann, A. Persson, M. Hämäläinen, F. Edebratt, A. Hansson, J. Lidholm, K. Magnusson, A. F. Karlsson, and A. Plückthun, 1997. BIACORE analysis of histidine-tagged proteins using a chelating NTA sensor chip. *Anal. Biochem.* 252:217–228.

7   High pressure NMR reveals close similarity between cold and alcohol protein denaturation due to a reduction of the hydrophobic effect

Original Manuscript

Vajpai, N., Nisius, L., Wiktor, M., Grzesiek, S.

High pressure NMR reveals close similarity between cold and alcohol protein denaturation due to a reduction of the hydrophobic effect

Navratna Vajpai[1,2], Lydia Nisius[1], Maciej Wiktor[1] and Stephan Grzesiek[1]

[1]Biozentrum, University of Basel, Klingelbergstrasse 50/70, 4056 Basel, Switzerland

[2]Current Address: Discovery Sciences, AstraZeneca, Mereside, Alderley Park, Macclesfield, Cheshire, SK104TG, UK

To whom correspondence should be addressed (stephan.grzesiek@unibas.ch)

file: 20120903 PhD thesis with figures.docx
last saved: 13-12-04 17:07
word count: 42555
char count: 232710
page count: 19

Abstract

Proteins denature not only at high, but also at low temperature as well as high pressure. These denatured states are not easily accessible for experiment, since usually heat denaturation causes aggregation, whereas cold or pressure denaturation occur at temperatures well below the freezing point of water or pressures above 5 kbar, respectively. Here we have obtained atomic details of the pressure-assisted, cold-denatured state of ubiquitin at 2500 bar and 258 K by high-resolution NMR techniques. Under these conditions, a folded, native-like and a disordered state exist in slow exchange. Secondary chemical shifts show that the disordered state has structural propensities for a native-like N-terminal b-hairpin and a-helix and a non-native C-terminal a-helix. These propensities are very similar to the previously described alcohol-denatured (A-) state. Similar to the A-state, ^{15}N relaxation data indicate that the secondary structure elements move as independent segments. The close similarity of pressure-assisted, cold-denatured and alcohol-denatured state with native- and non-native secondary elements supports a hierarchical mechanism of folding and indicates that similar to alcohol, pressure and cold reduce the hydrophobic effect. Indeed, at non-denaturing concentrations of methanol, a complete transition from the native to the A-state can be achieved at ambient temperature by varying the pressure from 1 to 2500 bar. The methanol-assisted pressure transition is completely reversible and can also be induced in protein G. This method should allow detailed studies of the hydrophobic contribution to protein stability by tuning the strength of the hydrophobic effect in a continuous and completely reversible manner.

\body

Introduction

It has long been known that proteins unfold not only at high temperatures, but also at high pressures (1) as well as low temperatures (2). The so-called heat, pressure and cold denaturations can be described in a unified way by Hawley's theory (1, 3). This theory assumes a simplified two-state model of protein unfolding, where the free energy difference between folded and unfolded states is a general parabolic function of temperature and pressure:

$$\Delta G = \frac{\Delta \beta}{2}(p - p_0)^2 + \Delta \alpha (p - p_0)(T - T_0) - \frac{\Delta C_p}{2T_0}(T - T_0)^2 +$$
$$\Delta V_0 (p - p_0) - \Delta S_0 (T - T_0) + \Delta G_0$$

(1)

In Eq. (1) D indicates the difference of the respective value between denatured and native state, b is the compressibility factor $(\partial V / \partial p)_T$, a the thermal expansivity factor $(\partial V / \partial T)_p$, C_p the heat capacity $T(\partial S / \partial T)_p$ and p_0, T_0 an arbitrarily chosen reference point. Since usually D$b < 0$ and D$C_p > 0$, DG has a maximum, but tends to $-\infty$ for very large and very small values of both T and p. The phase boundary between denatured and native states is then given by the condition D$G = 0$, which corresponds to a tilted ellipse within the pT plane.

The two-state model is clearly an oversimplification, since both folded and unfolded states can be heterogeneous and due to the paucity of data it is also unclear whether the heat-, cold- or pressure-denatured states are identical. Nevertheless the model presents a very valuable general framework to pinpoint the main contributing thermodynamic entities, which are intimately linked to protein hydration and the hydrophobic effect (4, 5). Thus DC_p is positive and proportional to the number of hydrophobic residues (6, 7), which may be attributed to the increase of water order around exposed hydrophobic groups. Similarly, the negative sign of Db can be explained from the fact that water in the vicinity of exposed hydrophobic groups such as those of an unfolded protein has a much higher compressibility than that of hydrophilic surface water, bulk water or the protein interior (8, 9). Therefore, at high pressures the exposure of the hydrophobic core leads to a decrease in the volume of the system and unfolding is favored, i.e. the hydrophobic effect is reduced (10-12).

The cold-denatured state of proteins is usually not easily accessible since cold denaturation temperatures are almost always below the freezing point of water. An exception

129

has been reported for the protein L9, where the reduction of hydrophobic interactions by a destabilizing leucine to alanine point mutation lead to a heterogeneous cold-denatured state above 273 K with native and non-native structural elements (13). Supercooled solutions of native proteins have been investigated by NMR by Szyperski and colleagues in small capillaries that prevent water freezing (14). However, only in the case of the cold shock protein of *Bacillus caldolyticus*, cold denaturation could be observed, but no structural data were presented (15). For ubiquitin, cold denaturation under normal pressure has not been observed down to temperatures of 238 K (16). A reverse micelle system has been proposed to overcome the limitation from water freezing (17). In this system, the progressive heterogeneous disappearance of native state ubiquitin NMR resonances at temperatures below 253 K and the lack of appearance of new resonances was interpreted as evidence for a heterogeneous cold-denatured state and the presence of a more stable core around ubiquitin's a-helix in the remaining native state (17).

The freezing point of water is lowered by high pressure, since liquid water has the unusual property of higher density than ice. Thus water can be kept liquid down to 251 K at a pressure of 2.07 kbar (3). This fact together with the pressure-induced destabilization of proteins makes cold denaturation at higher pressures more easily observable than at ambient pressure. Pressure-assisted cold denaturation has been followed for ubiquitin (18-20) using high-pressure quartz NMR tubes. The analysis of chemical shift data, resonance intensities and ^{15}N relaxation (18-20) showed that the pressure-assisted cold unfolding of ubiquitin is not a simple two-state process, but that several intermediates exist at 3 kbar and pH 4.6. At 273 K one intermediate is locally unfolded in the segments of residues 33-42 and 70–76. At a pressure of 2 kbar and temperatures below 273 K (21), a further set of resonances is observed that was identified with a floppy unfolded state. However, due to the small sample volume of about 15 ml of the conventional pressure cells used, sensitivity was severely limited and no structural information on the pressure-assisted cold-denatured state was derived.

Here, we have characterized the pressure-assisted cold denaturation of ubiquitin using a newly developed high-pressure NMR cell (*Daedalus Innovations LLC, PA, USA*) with a significantly larger sample volume of ~120 ml. The obtained high sensitivity provided sequence-specific backbone and side chain ^{13}C$^{\beta}$ assignments at pressures from 1 to 2500 bar. The sequence-specific information on chemical shifts and ^{15}N relaxation data indicates that the cold-denatured state is an unfolded ensemble with a high propensity for a first b-hairpin and a-helix that are similar to the native state. In contrast, the C-terminal has high propensity

for a non-native second a-helix. These structural propensies are very similar to the conformational ensemble of ubiquitin's A-state (22, 23), which is induced by 60 % methanol at pH 2 (24) at ambient temperature, as well as of ubiquitin's urea-denatured state (25, 26). The close similarity between pressure-assisted cold-denatured state and A-state is further proven by the fact that the transition from a native- to an A-state-like NMR spectrum can be induced at pH 4.5 and 45 % methanol at 308 K by the application of pressure. All the described forms of destabilization of ubiquitin's native state seem to lead to a similar unfolded state ensemble suggesting a robust folding pathway via ubiquitin's first b-hairpin and a-helix.

The high similarity of methanol- and pressure-destabilized states further suggests that the main mechanism of pressure unfolding is the reduction of the hydrophobic effect. A similar transition from the native to a partially unfolded state can be induced for protein G in the presence of methanol at a pressure of 2500 bar and ambient temperatures.

Results and Discussion

Resonance assignments

When ubiquitin is cooled from ambient to low temperatures at 2500 bar (pH 6.5), the onset of cold denaturation becomes visible in ^{15}N-HSQC spectra at about 278 K by the appearance of a new set of resonances in a narrow spectral region typical for the expected disordered polypeptide of the cold-denatured state. At 258 K both native and cold-denatured state show a maximum number of cross peaks at about equal intensities (Fig. 1). The spectral changes induced by pressure and cold temperature are completely reversible. Apparently at 258 K and 2500 bar cold-denatured and native state coexist in an approximate 1:1 equilibrium in slow exchange on the chemical shift scale. No cross peaks could be detected in an EXSY experiment (not shown) with a mixing time of 3.2 s, which sets a lower limit to the exchange time of about 20 s.

Assignments of the folded state at 258 K and 2500 bar were obtained by following the ^{15}N-HSQC spectra from ambient conditions through a combined pressure and temperature path (298 K/1 bar → 298 K/2500 bar → 258 K/2500 bar). As the temperature is decreased, the folded state cross peaks broaden to some extent in a heterogeneous way with disappearance of a few resonances, indicating varied disorder of these residues. In total 61 backbone resonances could be assigned (Fig. 1). Differential broadening of the folded state by pressure has been observed before at room temperature (pH 4.6, 3000 bar) using ^{15}N

transverse relaxation measurements (20). At ambient and at low temperature, the affected residues are located mainly in the region D21-I44, indicating the destabilization of ubiquitin's a-helix and of the irregular region connecting to strand b3 by high pressure.

Resonances of the cold-denatured state were assigned from a combination of triple resonance 3D experiments. The quality of these spectra at 258 K and 2500 bar is very good and allowed the unambiguous backbone resonance assignment for 57 residues in the cold-denatured state and also confirmed the assignment of the folded state. These data cover 80 % of all non-proline residues. Unassigned residues in the denatured state include the N-terminal methionine and several residues in the C-terminal tail (Fig. 1).

Secondary structure information from 13Ca, 13C', and 15N chemical shifts

The deviations of observed chemical shifts for backbone nuclei from their random coil values, known as secondary chemical shifts ($\Delta\delta = \delta_{obs} - \delta_{rc}$), can be used as a fast and accurate measure of polypeptide secondary structure (27, 28). Not surprisingly, the secondary shifts $\Delta\delta C^a$, $\Delta\delta C'$ and $\Delta\delta N$ for the folded state at 258 K, 2500 bar and at 298 K, 1 bar are almost identical (Fig. 2) indicating that the native state backbone conformation is almost completely preserved even at the low temperature and high pressure. It is noted that referencing of the chemical shifts was achieved indirectly via the resonance frequency of water (29), which was calibrated to TSP in a separate experiment yielding a temperature and pressure dependence of the form $\delta_{H2O}(p, T)/ppm = 7.866 - 1.612 \cdot 10^{-4}$ bar$^{-1} \cdot p - 1.025 \cdot 10^{-2}$ K$^{-1} \cdot T$ $+ 5.945 \cdot 10^{-7}$ bar^{-1}K$^{-1} \cdot p \cdot T$ (SI Appendix Fig. S1). The good agreement of the native state secondary shifts under both conditions indicates that this method is also adequate for obtaining secondary structure information at 258 K and 2500 bar.

Fig. 3 shows the secondary shifts $\Delta\delta C^a$, $\Delta\delta C'$ and $\Delta\delta N$ for the pressure-assisted cold-denatured state at 258 K, 2500 bar. The negative secondary shifts for $^{13}C^a$ and $^{13}C'$ in the region of residues 1 to 18 indicate a propensity for an extended b-type structure reminiscent of the native first b-hairpin. This is also supported by the ^{15}N secondary shifts, which are positive in this region and show a dip for residues 9 to 11, indicative of a b-turn. It is revealing to compare these secondary shifts to respective secondary shifts of the A-state (22, 23) and the urea-denatured state (25) (Fig. 3). Both A-state and urea-denatured state have a very similar pattern as the cold-denatured state in this part of the sequence, albeit the size of $\Delta\delta C^a$ and $\Delta\delta C'$ values of the cold-denatured state and the urea-denatured state is about 25-50% of the A-state values. Since A-state and native state secondary shifts are of very similar

size in this region, it may be concluded that the first b-hairpin is populated to about 25-50 % in the cold-denatured state.

Compared to the A-state and the urea-denatured state, ^{15}N secondary shifts of the cold-denatured state show a distinct positive offset (Fig. 3), which was not noticed for the folded state at 258 K (Fig. 2, see above). To characterize this effect we have also determined the chemical shifts of a ^{15}N-labeled nonapeptide as a function of pressure in the range from 1 to 2500 bar and temperature from 258 to 298 K (SI Appendix Fig. S2). The ^{15}N chemical shifts have an approximate linear dependence on pressure and temperature, which on average corresponds to coefficients of $(2.93 +/- 0.53) \cdot 10^{-4}$ ppm/bar and $(-17.0 +/- 9.3) \cdot 10^{-3}$ ppm/K. This indicates that the ^{15}N chemical shift of an exposed amide is much more influenced by pressure and temperature than that of a buried amide or the chemical shift of ^{13}C^a and ^{13}C' nuclei. Presumably, the compression of the hydrogen bonds between the exposed amide and water is responsible for this behavior. To correct for this effect relative to ambient conditions (298 K, 1 bar), the ^{15}N secondary shift of the cold-denatured state at 258 K, 2500 bar was adjusted by -1.41 ppm (Fig. 3, red bars), which brings the secondary shift pattern in closer agreement to A-state and urea-denatured states.

The similarity between cold-denatured and A-state continues beyond the first b-hairpin. Residues 23 to 32 show similar positive $\Delta\delta C^a$ and $\Delta\delta C'$ shifts for cold-denatured and A-state, indicative of an a-helix, which is located at the same position as the native a-helix. Their absolute size is about 20 % (cold-denatured) or 50 % (A-state) of the native secondary shifts, which indicates that both states contain respective fractional populations of native state in this region. Also the $\Delta\delta N$ shifts of cold-denatured and A-state have a similar sequence pattern. However, the rather small $\Delta\delta N$ values of the cold-denatured state may be affected by an overall offset resulting from inaccurate compensation of the non-specific pressure effect on ^{15}N shifts of exposed amides (see above). It is also noted that the urea-denatured state has close to zero or even negative $\Delta\delta C^a$ and $\Delta\delta C'$ shifts in the region of residues 23 to 32, which are not indicative of an a-helical conformation. In contrast, a-helical C^a-C^a contacts on the order of 10-20 % of the native state have been found in structural ensembles calculated from extensive RDC, PRE and SAXS data (26). This may not necessarily be a contradiction since binding of urea apparently leads to backbone conformations, which are more extended than the typical random coil (30). This in turn would bias the observed chemical shift, which is averaged over the small fraction of a-helical and the large fraction of unfolded conformations, towards the extended values, i.e. to negative $\Delta\delta C^a$ and $\Delta\delta C'$ shifts.

A high similarity between cold-denatured and A-state is also found in the second half of the protein for residues 38 to 76. In native state ubiquitin, this part largely consists of the anti-parallel b-sheet b4/b3/b5 that closes the structure by its connection to strand b1. However, in the A-state, this part is switched to the long a-helix a' (22, 23) (Fig. 4). The pattern of positive $\Delta\delta C^a$ and $\Delta\delta C'$ as well as mixed positive/negative $\Delta\delta N$ secondary shifts of the cold-denatured state is highly similar to the A-state (Fig. 3). It is noted that the center part of helix a' has somewhat reduced secondary shifts both in the cold-denatured and A-state, indicative of a weakening of helix propensity - a feature which had been overlooked previously (22, 23). Again the absolute size of the secondary shifts is about 50 % of the A-state values in this region. Thus along the entire sequence the cold-denatured state has deviations from 'pure random coil' behavior which correspond to approximately 50 % of the secondary structure propensities of the A-state.

Backbone dynamics

The backbone dynamics of the two states at 258 K and 2500 bar has been characterized by ^{15}N T_1, T_2 and {^{1}H}-^{15}N NOE relaxation experiments. With the exception of the flexible C-terminus beyond residue V70, rather uniform T_1, T_2, and {^{1}H}-^{15}N NOE values are observed for the folded state resonances (Fig. 5A), indicative of a mostly homogeneous, well folded structure. Excluding residues with obvious exchange contributions to T_2 (31) or fast backbone motions (NOE < 0.6), the average T_2/T_1 ratio (0.035) corresponds to a rotational correlation time τ_c of 16.9 ns. Thus τ_c is increased 4.1 fold compared to folded ubiquitin at 300 K and 1 bar (4.1 ns) (31). This is in good agreement with a ratio of 3.64 for the water self-diffusion coefficients ($D_{300K/1bar}$ = 2.41 10^{-5} cm^2/s, $D_{258K/2500bar}$ = 6.60 10^{-6} cm^2/s) (32). Apparently the Stokes-Einstein relation is approximately fulfilled, albeit at 258 K, 2500 bar τ_c is about 11 % larger than expected from the value at 300 K. This increase may be caused by an increase in the hydration shell of ubiquitin at low temperature and high pressure or by genuine differences in the pressure and temperature dependence of water rotational and translation diffusion (32). As noted before, a number of folded state residues in the region D21-I44 showed signs of pressure-induced exchange broadening consistent with ^{15}N T_2 data at room temperature (20). These were excluded from the estimate of τ_c. Due to the low intensity of the resonances at 258 K no quantitative analysis of the exchange was attempted.

In contrast to the folded state, the ^{15}N backbone resonances of the denatured state at 258 K, 2500 bar show strong variations in their relaxation behavior (Fig. 5B). Thus the {^{1}H}-^{15}N NOE values are reduced from an average of 0.74 to 0.4 indicative of larger amplitude local

backbone motions on the subnanosecond time scale. The NOE values are rather uniform and very similar to data (average 0.4) for the A-state at 300 K (22). Furthermore, T_1 increases and T_2 decreases along the sequence from residue Q2 to about Q40 indicating slower overall motions in the C-terminal part. An identical behavior is found for the A-state.

In the absence of exchange broadening, the ^{15}N T_2/T_1 ratio is to good approximation independent of rapid internal motions and of the magnitude of the chemical shift anisotropy and depends only on the overall rotational diffusion tensor (31). Brutscher et al. have used this property to estimate effective tumbling times along the sequence of the A-state (22). Fig. 6 shows the ^{15}N T_2/T_1 ratio for the denatured and folded state at 258 K, 2500 bar in comparison to the A-state at 300 K. In addition, also the expected T_2/T_1 ratio of an isotropic rotator is given as a function of the isotropic τ_c. For the cold-denatured state, the T_2/T_1 ratio decreases from about 0.4 at residue Q2 to about 0.06 in the region between residues Q40 to V70, corresponding to an increase in the effective rotational correlation time from about 4 ns to 13 ns. This profile is very similar to the A-state, albeit the A-state ratios are shifted to higher values due to the faster tumbling at 300 K. It has been noted previously (22) that the A-state T_2/T_1 ratios form plateaus with different values along the sequence, which roughly correspond to the first b-hairpin as well as helices a and a'. It was thus concluded that these secondary structure elements move independently from each other. Similar plateaus are observed for the cold-denatured state, although the difference between helix a and a' is not as pronounced, which may also be expected from the decreased slope of the T_2/T_1 curve at larger rotational correlation times. For both conditions, a similar increase in T_2/T_1 is observed around residue I35, which indicates increased mobility of the linker between helix a and a'. It is also evident that the N-terminal residues Q2 to F4 of the cold-denatured state are more flexible than the rest of the b-hairpin, whereas no such N-terminal fraying is observed in the A-state. With the exception of this minor difference, the overall ^{15}N relaxation behavior of both cold-denatured and A-state is very similar. It may thus be concluded that also the cold-denatured state consists of the three independently moving secondary structure elements b-hairpin, helix a and helix a'.

Pressure-induced unfolding in methanol

Both cold and pressure denaturation are linked to a reduction in the energetic cost of exposing hydrophobic groups to water in the cold or under pressure, i.e. to a reduction of the hydrophobic effect. Since methanol also reduces the strength of the hydrophobic effect, it seems not surprising that the A-state at 60 % methanol and pH 2 has strong similarities to the

pressure-assisted cold-denatured state. This observation prompted us to test whether a combination of methanol and pressure would also induce an A-state like structural ensemble of ubiquitin.

This is indeed the case. At pH 4.6, 45 % methanol and 308 K, predominantly native state resonances are observed in the ^{1}H-^{15}N HSQC at 1 bar (Fig. 7A). However, also a second set of very weak resonances is visible, which according to their intensities corresponds to about 14 % population. When pressure is increased gradually towards 2500 bar, the native state resonances become weaker at the expense of the second set of resonances. The transition is almost complete at 2500 bar (Fig. 7A), where the second state has a population of about 93 %. An assignment of the backbone resonances shows that the ^{13}C^a, ^{13}C' and ^{15}N secondary shifts of this pressure-induced state (Fig. 7C) are almost identical to the A-state at 298 K (Fig. 3). These results clearly show that pressure has a very similar effect on the conformation of ubiquitin as methanol.

A few general conclusions follow from a closer look at the behavior of individual resonances during the pressure variation from 1 to 2500 bar (Fig. 7B): (i) since distinct sets of resonances are observed for native and A-state, the exchange time between both states is significantly longer than the inverse of their chemical shift separation, i.e. tens of milliseconds. (ii) From the intensity-derived population ratios it follows that the free energy of the native state is about 4.5 kJ/mol lower than that of the A-state at 1 bar, whereas at 2500 bar, it is about 6.7 kJ/mol higher. (iii) The chemical shift change of resonances for both states during the pressure variation shows that their conformations vary to some extent with pressure. Thus pressure not only changes the depth of the free energy wells for both states, but also their shape.

The pressure-induced transition is completely reversible and will allow a detailed analysis of the transition from ubiquitin's native to its A-state. Such an analysis is currently in progress. The methanol/pressure transition can also be induced in other proteins. SI Appendix Fig. S3 shows the continuous pressure-induced unfolding for protein G at 60 % methanol and 303 K, pH 2.5. Again a second distinct set of resonances becomes visible at high pressure, which is populated to about 45 % at 2500 bar. Such an A-state of protein G has not been observed before under normal pressure conditions. The backbone assignment (SI Appendix Fig. S4) and analysis of secondary shifts (Fig. 8A) reveals that the A-state of protein G mainly consists of one central helix that is in a similar position as the native state helix (Fig. 8B). However, its N-terminal end is extended by about one helical turn to residue

17 and its population is reduced to about 50 % as indicated by a respective reduction in the size of secondary shifts. In addition small propensities for b-conformations are observed in the A-state at the positions of the native state N-terminal and C-terminal b-strands 1-4.

Conclusion

Here we have presented a detailed structural characterization of ubiquitin under pressure-assisted cold denaturing conditions, which is based on extensive assignments of the backbone resonances at 258 K and 2500 bar and the analysis of secondary chemical shifts and ^{15}N relaxation data. Under these conditions, ubiquitin exists in slow exchange equilibrium between a folded and a disordered state. The folded state closely resembles the native state structure of ubiquitin as determined in crystal or in solution, although as shown previously for high pressure at room temperature (20) enhanced mobility of many residues, in particular in the C-terminal part, is evident from the ^{15}N relaxation data.

The disordered state is not purely random coil, but has propensities for a native-like N-terminal b-hairpin and a-helix as well as a non-native C-terminal a-helix that are very similar to those described previously for the A-state (22). These structural propensities are on the order of 20 % of fully formed secondary structure elements. Similar to the A-state, ^{15}N relaxation data indicate an independent segmental motion of these three secondary structure elements with limited mobility of the backbone N-H vectors on the subnanosecond time scale. It is noted that the propensities for residual structure do not contradict earlier findings of high solvent exchange rates under cold denaturing conditions (33), since the residual structural populations are in fast exchange with other conformations on the chemical shift scale of milliseconds. A certain similarity also exists to ubiquitin's urea-denatured state where propensities for a native-like N-terminal b-hairpin and a-helix have been reported (25, 26). However, the latter state is considerably more flexible on the nanosecond time scale as evident from its strongly reduced $\{^{1}H\}$-^{15}N NOE values (34).

The residual native-like structure in the cold-denatured state of ubiquitin is consistent with a hierarchical order of protein folding where larger entities of native structure form from smaller native-like pieces (35). Evidence for hierarchical folding has been given in certain cases, e.g. for cytochrome c from the heterogeneity of hydrogen exchange rates under mild unfolding conditions (36) and for a destabilized mutant of L9 that allowed observation of a cold-denatured state containing native and non-native structural elements at ambient temperatures (13). For ubiquitin, intermediates in folding have been identified in kinetic

experiments (37) and have previously been postulated from heterogeneous line broadening of the cold-denatured state in a reverse micelle system (17). Our analysis reveals the following complex folding landscape: the structural propensies in the N-terminal part of the cold-denatured state are native-like, but they are non-native in the C-terminal part. Thus the formation of the C-terminal a-helix is off-pathway. This off-pathway structure first needs to unfold before the native C-terminal b-sheet can form and close the structure via the parallel connection from the C-terminal strand b5 to the N-terminal strand b1. The latter connection has the largest sequence separation, i.e. contact order in ubiquitin. Its formation is thus the most entropically disfavored of all. Since average contact order and folding speed of single domain proteins are inversely correlated (38), it is expected that the formation of the antiparallel sheet b1/b5 is the rate-limiting final step in the folding of ubiquitin. The concomitant presence of the on-pathway N-terminal b-hairpin and a-helix and the off-pathway C-terminal a-helix in the cold-denatured state is consistent with such an order of folding events. Furthermore also the inverse process of unfolding has been shown to start by breaking sheet b1/b5 in the case of thermal (39) and pressure (40) denaturation. We conclude therefore that an A-state-like conformational ensemble is the major thermodynamic and presumably also kinetic intermediate nearest to the native state in the ubiquitin folding pathway.

The observation of cold or pressure denaturation is severely limited by the low temperatures and high pressures required. The cold denaturation temperature of ubiquitin at ambient pressure is below 238 K (16), whereas at room temperature pressure denaturation occurs at 5.4 kbar (41). Similar cold denaturation temperatures at ambient pressure and unfolding pressures at ambient temperature are required for many other proteins (3). The simultaneous application of low temperature and pressure allowed us to observe about 50 % of denatured ubiquitin at 258 K and the current maximal pressure of 2500 bar suitable for high-sensitivity NMR experiments. The close similarity of the pressure-assisted cold-denatured state and the methanol-denatured state is consistent with the notion that in both cases the destabilization results from the weakening of the hydrophobic effect. We could show here that the combination with methanol shifts the unfolding transition further into the easily observable pressure and temperature range. Indeed a complete transition from native state to unfolded ensemble occurs at 308 K, 45 % methanol in the pressure range from 1 to 2500 bar. The unfolded ensemble under these conditions is highly similar to both the pressure-assisted cold and the methanol-denatured state of ubiquitin. A similar transition is

observable for protein G. The methanol-assisted pressure transitions are completely reversible. This opens the way to follow the unfolding of proteins via a tunable weakening of the hydrophobic effect in a continuous manner by atomic-resolution NMR experiments.

Experimental procedures

Sample preparation

$^{15}N/^{13}C$-labeled human ubiquitin was prepared as described (42). NMR samples for the pressure-assisted cold-denatured state contained 1.0 mM $^{15}N/^{13}C$-labeled protein in 10 mM potassium phosphate buffer, 0.02 % NaN_3, 90/10% H_2O/D_2O, pH 6.5. For measurements under methanol-destabilizing conditions, a further ubiquitin sample contained 0.6 mM $^{15}N/^{13}C$-labeled protein 30 mM sodium acetate, 45 % methanol, 45 % H_2O, 10 % D_2O, pH 4.6.

$^{15}N/^{13}C$-labeled protein G was prepared as described (43). For measurements under methanol-destabilizing conditions, the sample contained 0.25 mM $^{15}N/^{13}C$-labeled protein G, 25 mM potassium phosphate, 50 % methanol, 40 % H_2O, 10 % D_2O, pH 2.5.

High-pressure measurements

All experiments were carried out using a commercial high-pressure NMR cell (*Daedalus Innovations LLC, PA, USA*) with an inner diameter of 3 mm and an active volume of 120 mL. The tube was rated to 2500 bar and used in an aluminum alloy static pressure cell connected to a high pressure generator (High Pressure Equipment Company) via a pressure line. Both line and pressure generator were filled with extra-low viscosity paraffin wax (Sigma-Aldrich id 95369).

NMR experiments

All NMR spectra were recorded on Bruker Avance DRX800 or DRX600 spectrometers equipped with a triple resonance pulsed field gradient TXI probes. Backbone assignments were achieved using standard three-dimensional CBCA(CO)NH, HNCA, HNCO and ^{15}N-edited ^{1}H-^{1}H nuclear Overhauser effect spectroscopy (NOESY) experiments. ^{15}N relaxation measurements (T_1, T_2, {^{1}H}-^{15}N NOE) for the cold-denatured state of ubiquitin were recorded at 600 MHz. All spectra were processed with NMRPipe (44) and evaluated with NMRView (45) or PIPP (46).

Analysis of relaxation data

Resonance intensities of NMR relaxation spectra were extracted using the program nlinLS contained in NMRPipe (44). T_1 and T_2 decay curves were then fitted to the intensities

by an in-house written routine implemented in Matlab (MathWorks, Inc.) using Monte Carlo estimation of errors.

Determination of secondary shifts

Chemical shifts for native state ubiquitin (293 K, 1 bar, pH 6.6) are from BMRB entry 6457 and for urea-denatured ubiquitin (8 M urea, 10 mM glycine 90 %/10 % H_2O/D_2O, pH 2.5, 298 K) from BMRB entry 16626. For the latter, an offset of 0.2 ppm was added to account for an uncorrected shift of the water line used for indirect referencing in the presence of urea. Chemical shifts of the ubiquitin's A-state (60 % methanol, 30 % H_2O, 10 % D_2O, pH 2, 298 K) were obtained as described (23).

Secondary chemical shifts were obtained by subtracting random coil shifts generated by the University of Kopenhagen web server http://www1.bio.ku.dk/english/research/pv/sbin_lab/staff/MAK/randomcoil/script/), which uses protein sequence, pH and temperature corrections (47-49).

Acknowledgements

References

1. Hawley, S. A. (1971) Reversible pressure--temperature denaturation of chymotrypsinogen. *Biochemistry* 10**:** 2436-2442.
2. Privalov, P. L., Griko, Y. V., Venyaminov, S. Y. & Kutyshenko, V. P. (1986) Cold denaturation of myoglobin. *J Mol Biol* 190**:** 487-498.
3. Smeller, L. (2002) Pressure-temperature phase diagrams of biomolecules. *Biochim Biophys Acta* 1595**:** 11-29.
4. Kauzmann, W. (1959) Some factors in the interpretation of protein denaturation. *Adv Protein Chem* 14**:** 1-63.
5. Tanford, C. (1962) Contribution of Hydrophobic Interactions to the Stability of the Globular Conformation of Proteins. *J Am Chem Soc* 84**:** 4240-4247.
6. Privalov, P. L. (1979) Stability of proteins: small globular proteins. *Adv Protein Chem* 33**:** 167-241.
7. Baldwin, R. L. (1986) Temperature dependence of the hydrophobic interaction in protein folding. *Proc Natl Acad Sci USA* 83**:** 8069-8072.
8. Sarupria, S. & Garde, S. (2009) Quantifying water density fluctuations and compressibility of hydration shells of hydrophobic solutes and proteins. *Phys Rev Lett* 103**:** 037803.
9. Smolin, N. & Winter, R. (2006) A molecular dynamics simulation of SNase and its hydration shell at high temperature and high pressure. *Biochim Biophys Acta* 1764**:** 522-534.
10. Kauzmann, W. (1987) Protein stabilization - thermodynamics of unfolding. *Nature* 325**:** 763-764.
11. Hummer, G., Garde, S., García, A. E., Paulaitis, M. E. & Pratt, L. R. (1998) The pressure dependence of hydrophobic interactions is consistent with the observed pressure denaturation of proteins. *Proc Natl Acad Sci USA* 95**:** 1552-1555.
12. Grigera, J. R. & McCarthy, A. N. (2010) The behavior of the hydrophobic effect under pressure and protein denaturation. *Biophys J* 98**:** 1626-1631.
13. Shan, B., McClendon, S., Rospigliosi, C., Eliezer, D. & Raleigh, D. P. (2010) The Cold Denatured State of the C-terminal Domain of Protein L9 Is Compact and Contains Both Native and Non-native Structure. *J Am Chem Soc* 132**:** 4669-4677.
14. Szyperski, T. & Mills, J. L. (2011) NMR-based structural biology of proteins in supercooled water. *J Struct Funct Genomics* 12**:** 1-7.
15. Szyperski, T., Mills, J. L., Perl, D. & Balbach, J. (2006) Combined NMR-observation of cold denaturation in supercooled water and heat denaturation enables accurate measurement of deltaC(p) of protein unfolding. *Eur Biophys J* 35**:** 363-366.
16. Skalicky, J., Sukumaran, D., Mills, J. & Szyperski, T. (2000) Toward structural biology in supercooled water. *J Am Chem Soc* 122**:** 3230-3231.
17. Babu, C. R., Hilser, V. J. & Wand, A. J. (2004) Direct access to the cooperative substructure of proteins and the protein ensemble via cold denaturation. *Nat Struct Mol Biol* 11**:** 352-357.
18. Kitahara, R., Yamada, H., Akasaka, K. & Wright, P. E. (2002) High pressure NMR reveals that apomyoglobin is an equilibrium mixture from the native to the unfolded. *J Mol Biol* 320**:** 311-319.
19. Kitahara, R. & Akasaka, K. (2003) Close identity of a pressure-stabilized intermediate with a kinetic intermediate in protein folding. *Proc Natl Acad Sci USA* 100**:** 3167-3172.
20. Kitahara, R., Yokoyama, S. & Akasaka, K. (2005) NMR snapshots of a fluctuating protein structure: ubiquitin at 30 bar-3 kbar. *J Mol Biol* 347**:** 277-285.

21. Kitahara, R., Okuno, A., Kato, M., Taniguchi, Y., Yokoyama, S. & Akasaka, K. (2006) Cold denaturation of ubiquitin at high pressure. *Magn Reson Chem* 44 Spec No**:** S108-13.

22. Brutscher, B., Brüschweiler, R. & Ernst, R. R. (1997) Backbone Dynamics and Structural Characterization of the Partially Folded A State of Ubiquitin by 1H, 13C, and 15N Nuclear Magnetic Resonance Spectroscopy †. *Biochemistry* 36**:** 13043-13053.

23. Cordier, F. & Grzesiek, S. (2004) Quantitative comparison of the hydrogen bond network of A-state and native ubiquitin by hydrogen bond scalar couplings. *Biochemistry* 43**:** 11295-11301.

24. Wilkinson, K. D. & Mayer, A. N. (1986) Alcohol-induced conformational changes of ubiquitin. *Arch Biochem Biophys* 250**:** 390-399.

25. Meier, S., Strohmeier, M., Blackledge, M. & Grzesiek, S. (2007) Direct Observation of Dipolar Couplings and Hydrogen Bonds across a β-Hairpin in 8 M Urea. *J Am Chem Soc* 129**:** 754-755.

26. Huang, J.-R. & Grzesiek, S. (2010) Ensemble calculations of unstructured proteins constrained by RDC and PRE data: a case study of urea-denatured ubiquitin. *J Am Chem Soc* 132**:** 694-705.

27. Spera, S. & Bax, A. (1991) Empirical correlation between protein backbone conformation and C.alpha. and C.beta. 13C nuclear magnetic resonance chemical shifts. *J Am Chem Soc* 113**:** 5490–5492.

28. Wishart, D. S., Sykes, B. D. & Richards, F. M. (1991) Relationship between nuclear magnetic resonance chemical shift and protein secondary structure. *J Mol Biol* 222**:** 311-333.

29. Markley, J. L., Bax, A., Arata, Y., Hilbers, C. W., Kaptein, R., Sykes, B. D., Wright, P. E. & Wüthrich, K. (1998) in *J Biomol NMR*, Vol. 12, pp. 1-23.

30. Huang, J.-R., Gabel, F., Jensen, M. R., Grzesiek, S. & Blackledge, M. (2012) Sequence-Specific Mapping of the Interaction between Urea and Unfolded Ubiquitin from Ensemble Analysis of NMR and Small Angle Scattering Data. *J Am Chem Soc* 134**:** 4429-4436.

31. Tjandra, N., Feller, S. E., Pastor, R. W. & Bax, A. (1995) Rotational diffusion anisotropy of human ubiquitin from 15N NMR relaxation. *J Am Chem Soc* 117**:** 12562-12566.

32. Prielmeier, F., Lang, E., Speedy, R. & Lüdemann, H. (1987) Diffusion in supercooled water to 300 MPa. *Phys Rev Lett*.

33. Nash, D. P. & Jonas, J. (1997) Structure of the pressure-assisted cold denatured state of ubiquitin. *Biochem Bioph Res Co* 238**:** 289-291.

34. Wirmer, J., Peti, W. & Schwalbe, H. (2006) Motional properties of unfolded ubiquitin: a model for a random coil protein. *J Biomol NMR* 35**:** 175-186.

35. Fitzkee, N. C., Fleming, P. J., Gong, H., Panasik, N., Street, T. O. & Rose, G. D. (2005) Are proteins made from a limited parts list? *Trends Biochem Sci* 30**:** 73-80.

36. Bai, Y., Sosnick, T. R., Mayne, L. & Englander, S. W. (1995) Protein folding intermediates: native-state hydrogen exchange. *Science* 269**:** 192-197.

37. Khorasanizadeh, S., Peters, I. D. & Roder, H. (1996) Evidence for a three-state model of protein folding from kinetic analysis of ubiquitin variants with altered core residues. *Nat Struct Biol* 3**:** 193-205.

38. Plaxco, K. W., Simons, K. T. & Baker, D. (1998) Contact order, transition state placement and the refolding rates of single domain proteins. *J Mol Biol* 277**:** 985-994.

39. Cordier, F. & Grzesiek, S. (2002) Temperature-dependence of protein hydrogen bond properties as studied by high-resolution NMR. *J Mol Biol* 317**:** 739-752.

40. Nisius, L. & Grzesiek, S. (2012) Key stabilizing elements of protein structure identified through pressure and temperature perturbation of its hydrogen bond network. *Nat Chem***:** in press, DOI:10.1038/nchem.1396.

41. Herberhold, H. & Winter, R. (2002) Temperature- and Pressure-Induced Unfolding and Refolding of Ubiquitin: A Static and Kinetic Fourier Transform Infrared Spectroscopy Study †. *Biochemistry* 41**:** 2396-2401.

42. Sass, J., Cordier, F., Hoffmann, A., Cousin, A., Omichinski, J., Lowen, H. & Grzesiek, S. (1999) Purple membrane induced alignment of biological macromolecules in the magnetic field. *J Am Chem Soc* 121**:** 2047-2055.

43. Vajpai, N., Gentner, M., Huang, J.-R., Blackledge, M. & Grzesiek, S. (2010) Side-chain chi(1) conformations in urea-denatured ubiquitin and protein G from (3)J coupling constants and residual dipolar couplings. *J Am Chem Soc* 132**:** 3196-3203.

44. Delaglio, F., Grzesiek, S., Vuister, G., Zhu, G., Pfeifer, J. & Bax, A. (1995) Nmrpipe - a Multidimensional Spectral Processing System Based on Unix Pipes. *J Biomol NMR* 6**:** 277-293.

45. Johnson, B. & Blevins, R. (1994) NMR VIEW - A COMPUTER-PROGRAM FOR THE VISUALIZATION AND ANALYSIS OF NMR DATA. *J Biomol NMR* 4**:** 603-614.

46. Garrett, D., Powers, R., Gronenborn, A. & Clore, G. (1991) A common sense approach to peak picking in two-, three-, and four dimensional spectra using automatic computer analysis of contour diagrams. *J Magn Reson* 95**:** 214-220.

47. Kjaergaard, M., Brander, S. & Poulsen, F. M. (2011) Random coil chemical shift for intrinsically disordered proteins: effects of temperature and pH. *J Biomol NMR* 49**:** 139-149.

48. Kjaergaard, M. & Poulsen, F. M. (2011) Sequence correction of random coil chemical shifts: correlation between neighbor correction factors and changes in the Ramachandran distribution. *J Biomol NMR* 50**:** 157-165.

49. Schwarzinger, S., Kroon, G., Foss, T., Chung, J., Wright, P. & Dyson, H. (2001) Sequence-dependent correction of random coil NMR chemical shifts. *J Am Chem Soc* 123**:** 2970-2978.

Figure Legends

<u>Fig. 1:</u> (A) ^{1}H-^{15}N HSQC spectrum of uniformly ^{15}N,^{13}C-labeled ubiquitin at 258 K and 2500 bar (pH 6.5). Peaks are labeled with assignment information for the folded state (green) and the cold-denatured state (blue). Negative contour lines are shown in red. The amino acid sequence of ubiquitin is indicated at the top with assigned residues underlined for both states. The spectrum was acquired for 1.5 hrs at a sample concentration of 1 mM on an 800 MHz spectrometer. (B) enlarged region of the box shown in A.

<u>Fig. 2:</u> Secondary chemical shifts analysis (^{13}C^α, ^{13}C', ^{15}N) of the native state of ubiquitin at low temperature and high pressure (258 K, 2500 bar) and at ambient conditions (293 K, 1 bar, pH 6.6). Secondary structure elements of the native state are drawn at the top.

<u>Fig. 3:</u> Secondary chemical shift analysis (^{13}C^α, ^{13}C', ^{15}N) of the cold-denatured state (258 K, 2500 bar), the urea-denatured state (298 K, 1 bar), and (C) the A-state (298 K, 1 bar) of ubiquitin. Secondary structure elements of the A-state are drawn at the top. The red bars for the ^{15}N secondary shift of the cold-denatured state (D_{258K}) are shifted relative to standard referencing (black bars) by -1.41 ppm to account for the uniform pressure effect on solvent exposed amide groups (see text).

<u>Fig. 4:</u> Structural switch from native state (left) to A-state (right). Corresponding structural elements are coded by identical colors: N-terminal b-hairpin (orange), central a-helix (magenta), C-terminal half (green). The C-terminal half switches from a b-sheet structure in the native state to the long a-helix a' in the A-state. The structural scheme of the A-state is adapted from Brutscher et al. (22).

<u>Fig. 5:</u> ^{15}N relaxation data of ubiquitin at 258 K and 2500 bar recorded at 600 MHz. T_1 (top), T_2 (middle), and {^{1}H}-^{15}N NOE (bottom) values for the folded (A) and the denatured (B) state are shown along the primary sequence. Secondary structure elements of the folded state (left) and the A-state (right) are drawn at the top of each panel.

<u>Fig. 6:</u> T_2/T_1 ratios calculated from 600 MHz ^{15}N relaxation data for ubiquitin. Black curve: folded state (258 K, 2500 bar) T_2/T_1 ratios as a function of residue number (bottom horizontal

axis). Blue curve: cold-denatured state (258 K, 2500 bar). Red curve: A-state (300 K, 1 bar) replotted from Brutscher et al. (22). The dashed green curve shows the T_2/T_1 ratio for an isotropic rotator at 600 MHz as a function of t_c (top horizontal axis). Secondary structure elements of the A-state are drawn at the bottom.

Fig. 7: Pressure-induced unfolding of ubiquitin in 45 % methanol at 308 K (A) ^{1}H-^{15}N HSQC recorded on a 600 MHz spectrometer at pressures of 1 (dark blue), 500 (blue), 1000 (green), 1500 (magenta), 2000 (orange), and 2500 bar (red), respectively. (B) expanded region of (A) showing the transition in the glycine region. Resonances are labeled with assignment information corresponding to the native state (dark blue) or the pressure-induced A-state (red). (C) Secondary chemical shift analysis (^{13}C$^\alpha$, ^{13}C', ^{15}N) of the pressure-induced unfolded state of ubiquitin in 45 % methanol (308 K, 2500 bar). The secondary shifts are almost identical to the A-state (see Fig. 3). Secondary structure elements of the A-state are drawn at the top.

Fig. 8: Secondary chemical shift analysis (^{13}C$^\alpha$, ^{13}C', ^{15}N) of the two observable states of protein G in 50 % methanol, pH 2.5, 303 K, 2500 bar. See SI Appendix Fig. S3 and S4 for respective ^{1}H-^{15}N HSQC spectra. (A) Secondary shifts of the unfolded A-state. (B) Secondary shifts of the folded, native state. Respective secondary structure elements are drawn at the top of each panel.
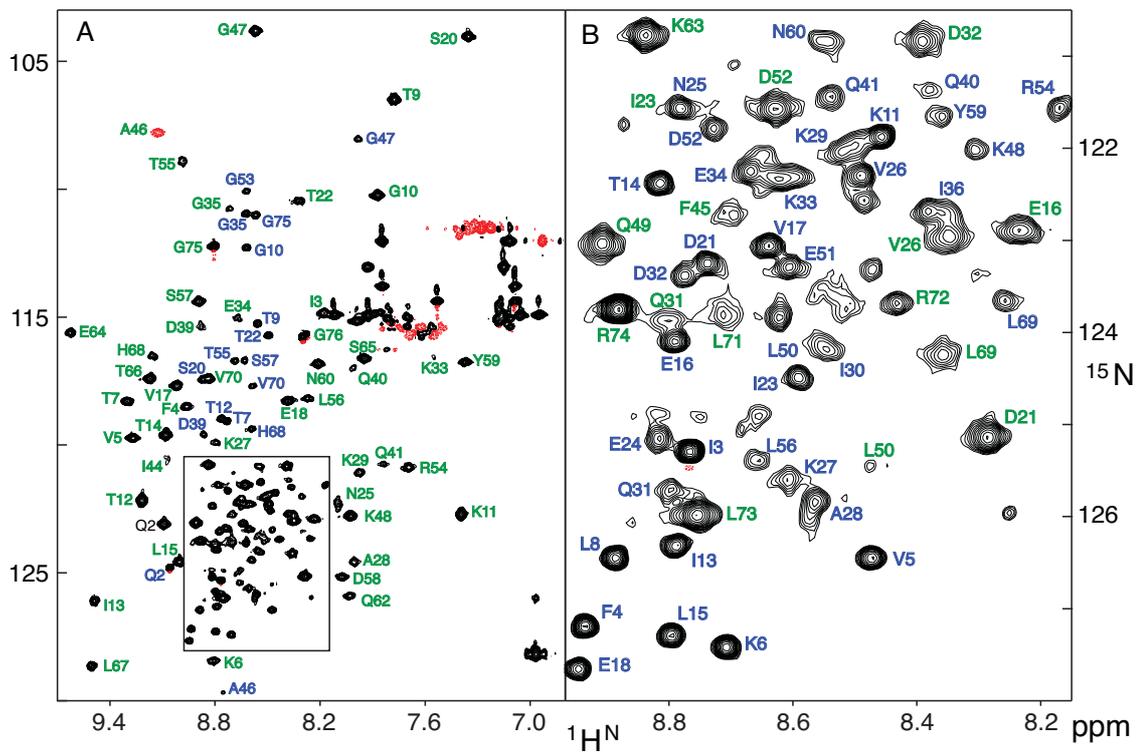
Figure 1: Vajpai et al.

Figure 2: Vajpai et al.

147

Figure 3 Vajpai et al.

148

native state

N
17
23
34
39
72
C

C
72
A-state
34
39
23
17
N
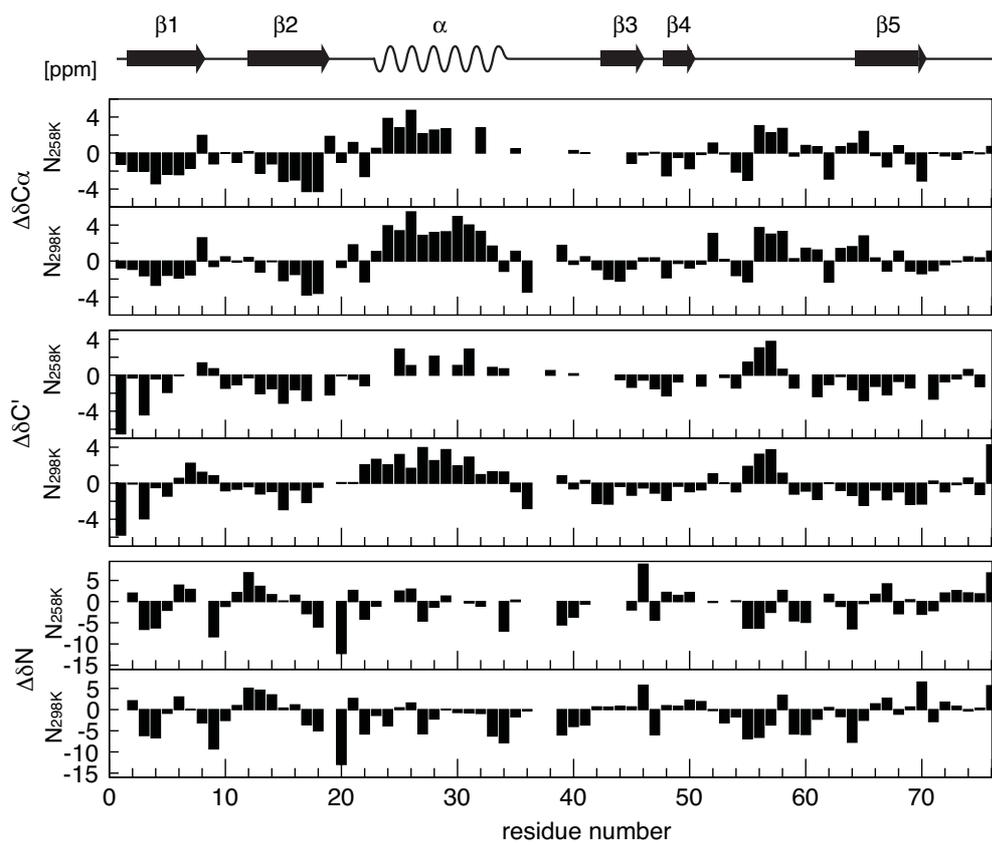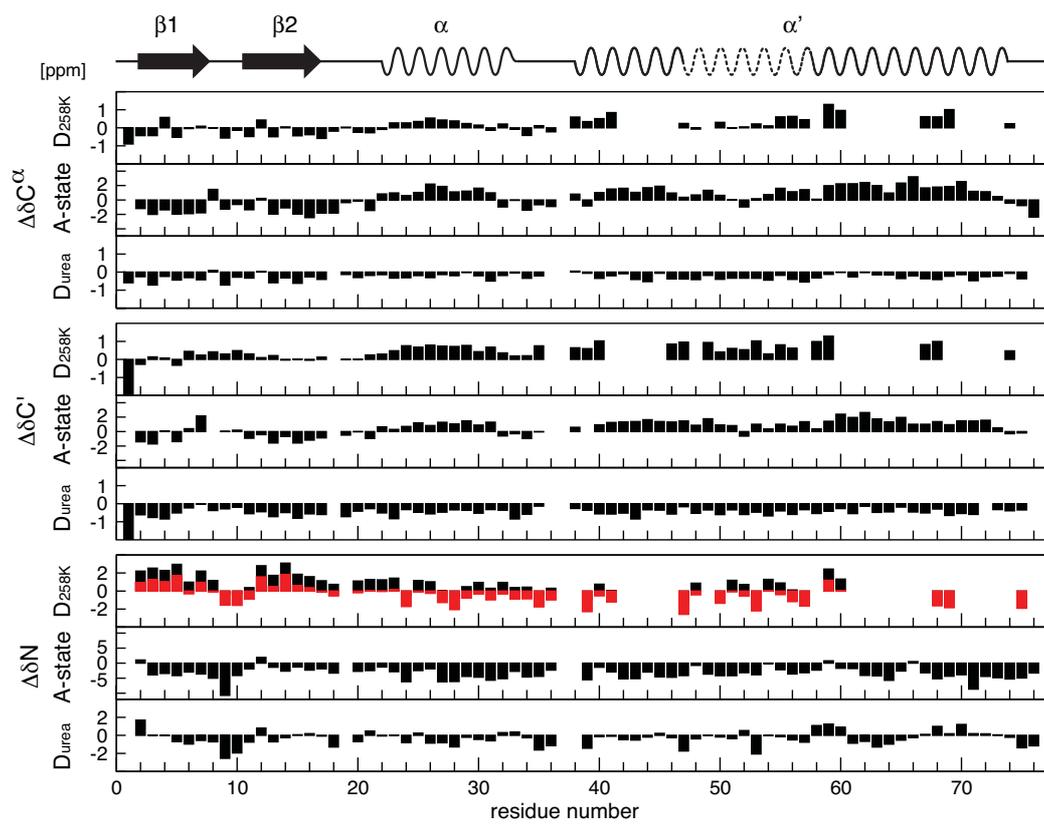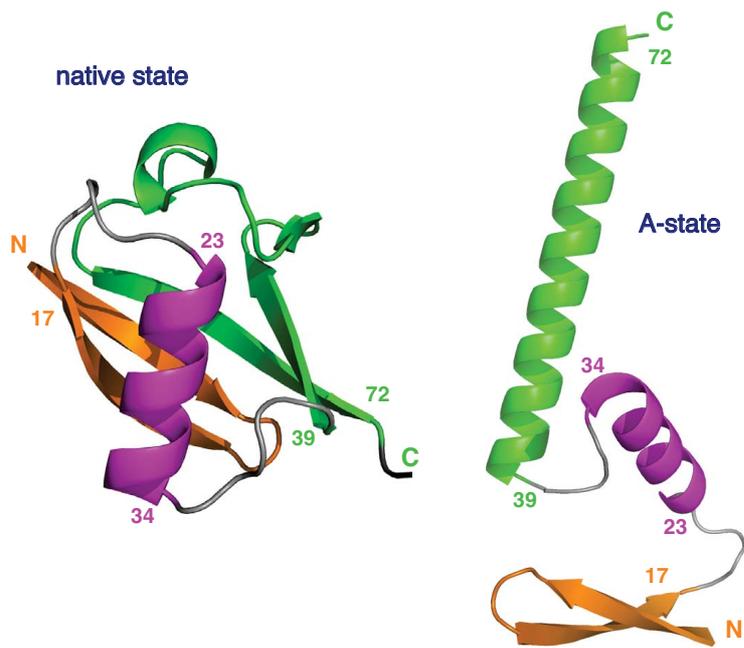
Figure 4 Vajpai et al.
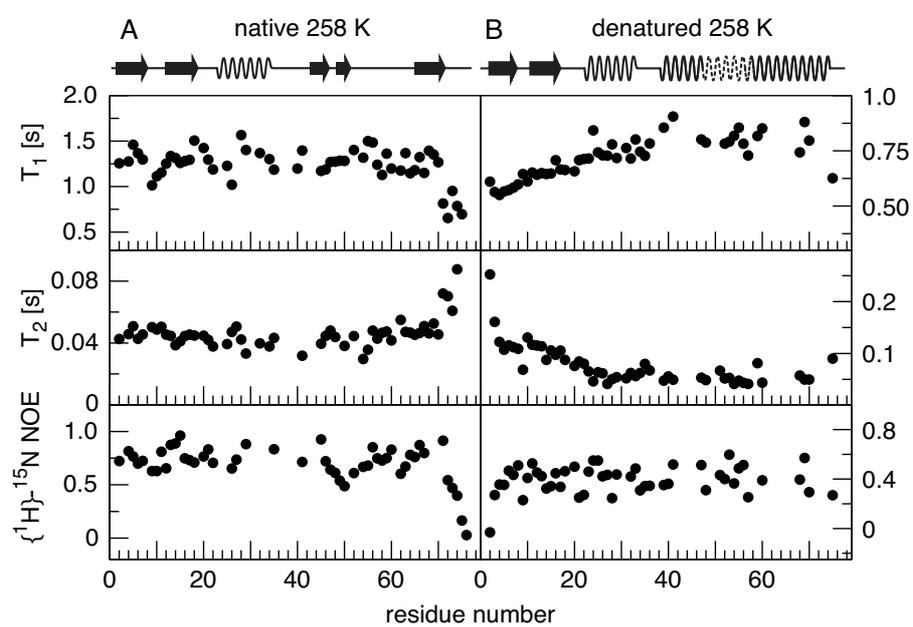
Figure 5 Vajpai et al.
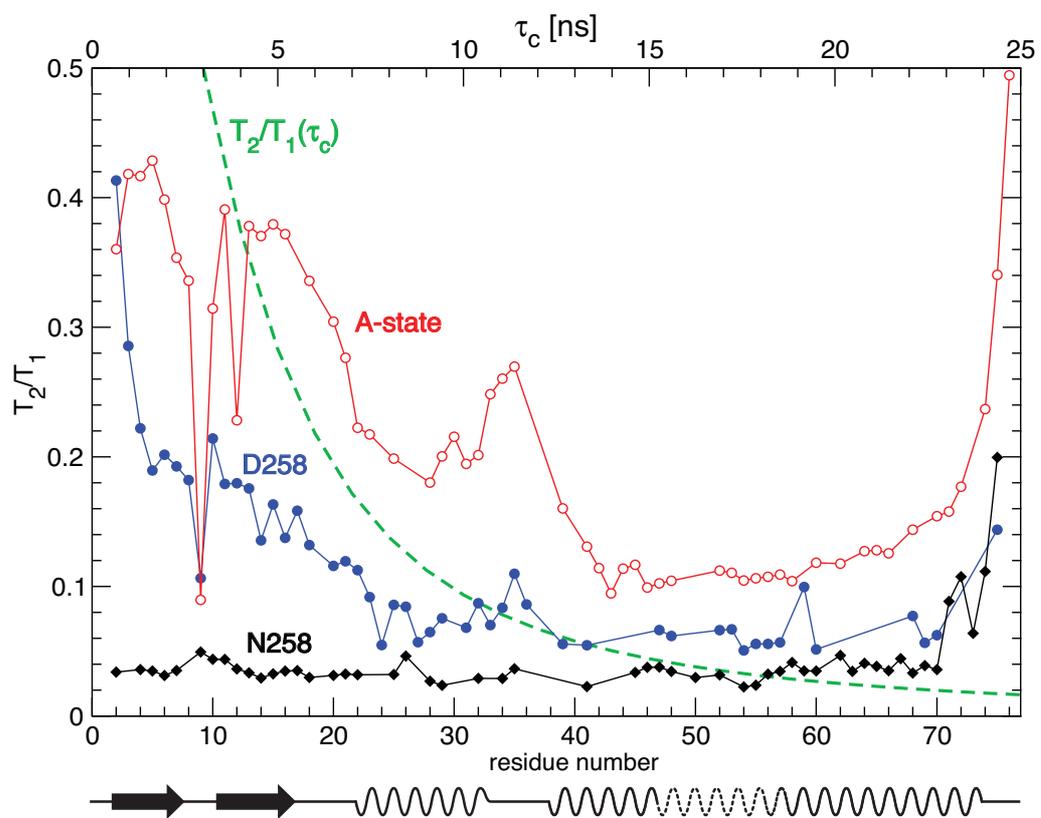
Figure 6 Vajpai et al.

151
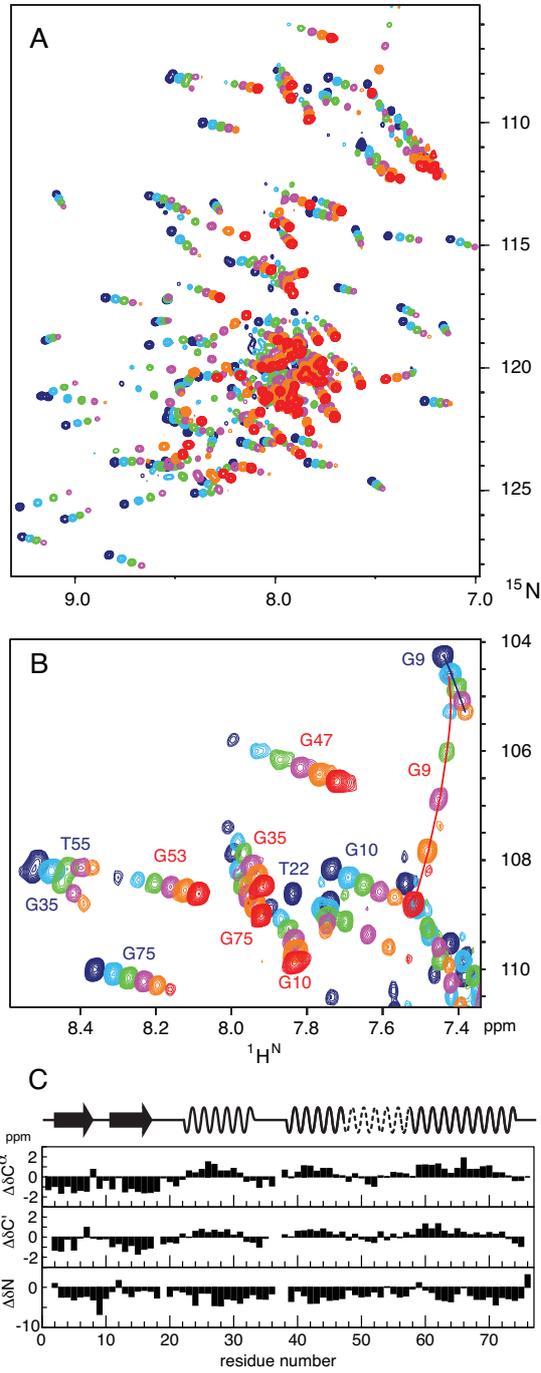
Figure 7 Vajpai et al.
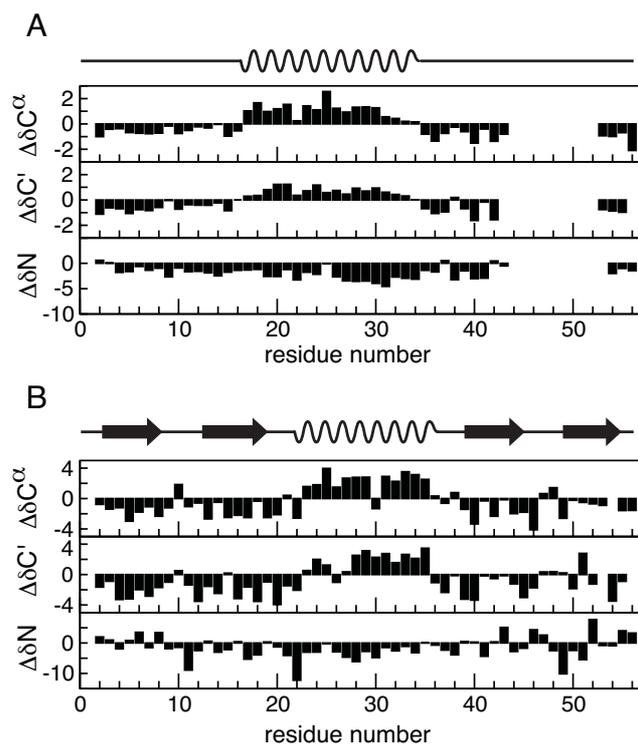
Figure 8 Vajpai et al.

High pressure NMR reveals close similarity between cold and alcohol protein denaturation due to a reduction of the hydrophobic effect

Supporting Information

Navratna Vajpai[1,2], Lydia Nisius[1], Maciej Wiktor[1] and Stephan Grzesiek[1]

[1]Biozentrum, University of Basel, Klingelbergstrasse 50/70, 4056 Basel, Switzerland
[2]Current Address: Discovery Sciences, AstraZeneca, Mereside, Alderley Park, Macclesfield, Cheshire, SK104TG, UK

*Address correspondence to:

Stephan Grzesiek

Focal Area Structural Biology and Biophysics, Biozentrum

University of Basel, CH-4056 Basel, Switzerland

Phone: ++41 61 267 2100

FAX: ++41 61 267 2109
Email: Stephan.Grzesiek@unibas.ch

Table S1: Pressure and temperature dependence of water chemical shift relative to TSP. The chemical shift of the water ^{1}H resonance relative to TSP was determined on a sample of 5 mM TSP, 95% H_2O/5 % D_2O, 10 mM phosphate, pH 6.5 on a Bruker Avance DRX600 spectrometer using the Daedalus 3 mm pressure cell rated to 2500 bar. Reproducibility of the chemical shift was better than 3 ppb as estimated from duplicate measurements.

T [K]	p [bar]	1H [ppm]	T [K]	p [bar]	1H [ppm]
255	2500	5.233	313	1	4.653
258	2500	5.205	313	625	4.669
261	2500	5.177	313	1250	4.685
264	2500	5.149	313	1875	4.702
267	2500	5.122	313	2500	4.719
270	2500	5.095	323	1	4.551
273	1	5.081	323	625	4.572
273	625	5.069	323	1250	4.592
273	1250	5.065	323	1875	4.612
273	1875	5.068	323	2500	4.631
273	2500	5.071	333	1	4.454
283	1	4.968	333	625	4.479
283	625	4.966	333	1250	4.502
283	1250	4.969	333	1875	4.524
283	1875	4.974	333	2500	4.547
283	2500	4.982	343	1	4.349
293	1	4.862	343	625	4.380
293	625	4.867	343	1250	4.406
293	1250	4.873	343	1875	4.430
293	1875	4.883	343	2500	4.455
293	2500	4.894	313	1	4.653
303	1	4.756	313	625	4.669
303	625	4.766	313	1250	4.685
303	1250	4.778	313	1875	4.702
303	1875	4.791	313	2500	4.719
303	2500	4.805			

Figure S1: Pressure and temperature dependence of water chemical shift relative to TSP
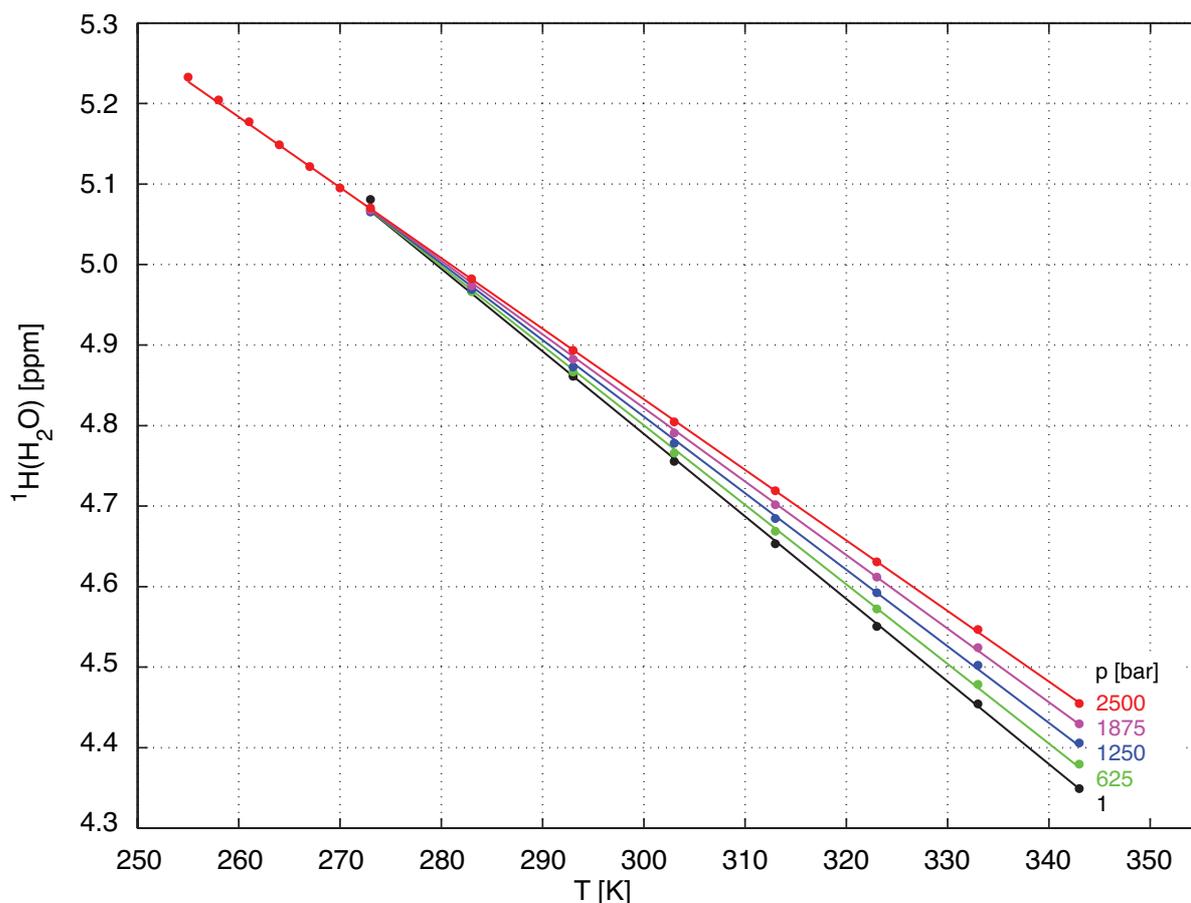
The pressure and temperature dependence of the water chemical shift according to Table S1 is shown. The solid lines present a global fit against p and T according to

$$\delta_{H2O}(p, T) = (a_0 + a_1 \cdot p + a_2 \cdot T + a_3 \cdot p*T)$$

with

	a_0 [ppm]	a_1 [ppm/bar]	a_2 [ppm/K]	a_3 [ppm/(bar*K)]
a_i	7.866E+00	−1.612E−04	−1.025E−02	5.945E−07
$Da_i{}^*$	7.137E−03	3.751E−06	2.316E−05	1.240E−08

*error in the parameters a_i derived from the linear fit using an experimental error of 2 ppb for the chemical shift of water. The mean deviation of the measured points from the fit is 3.6 ppb.

It is noted that the final functional form

$$\delta_{H2O}(p, T)/ppm = 7.866 - 1.612 \cdot 10^{-4}\ bar^{-1} \cdot p - 1.025 \cdot 10^{-2}\ K^{-1} \cdot T + 5.945 \cdot 10^{-7}\ bar^{-1} K^{-1} \cdot p \cdot T$$

is in very good agreement with literature values (1) for the temperature dependence of the water chemical shift at ambient pressure

$$\delta_{H2O}(1\ bar, T)/ppm = 5.051 - 0.0111\ K^{-1}\ (T+273.15\ K).$$

Figure S2: Temperature and pressure dependence of amide 15N chemical shift of the nonapeptide EGAAWAASS
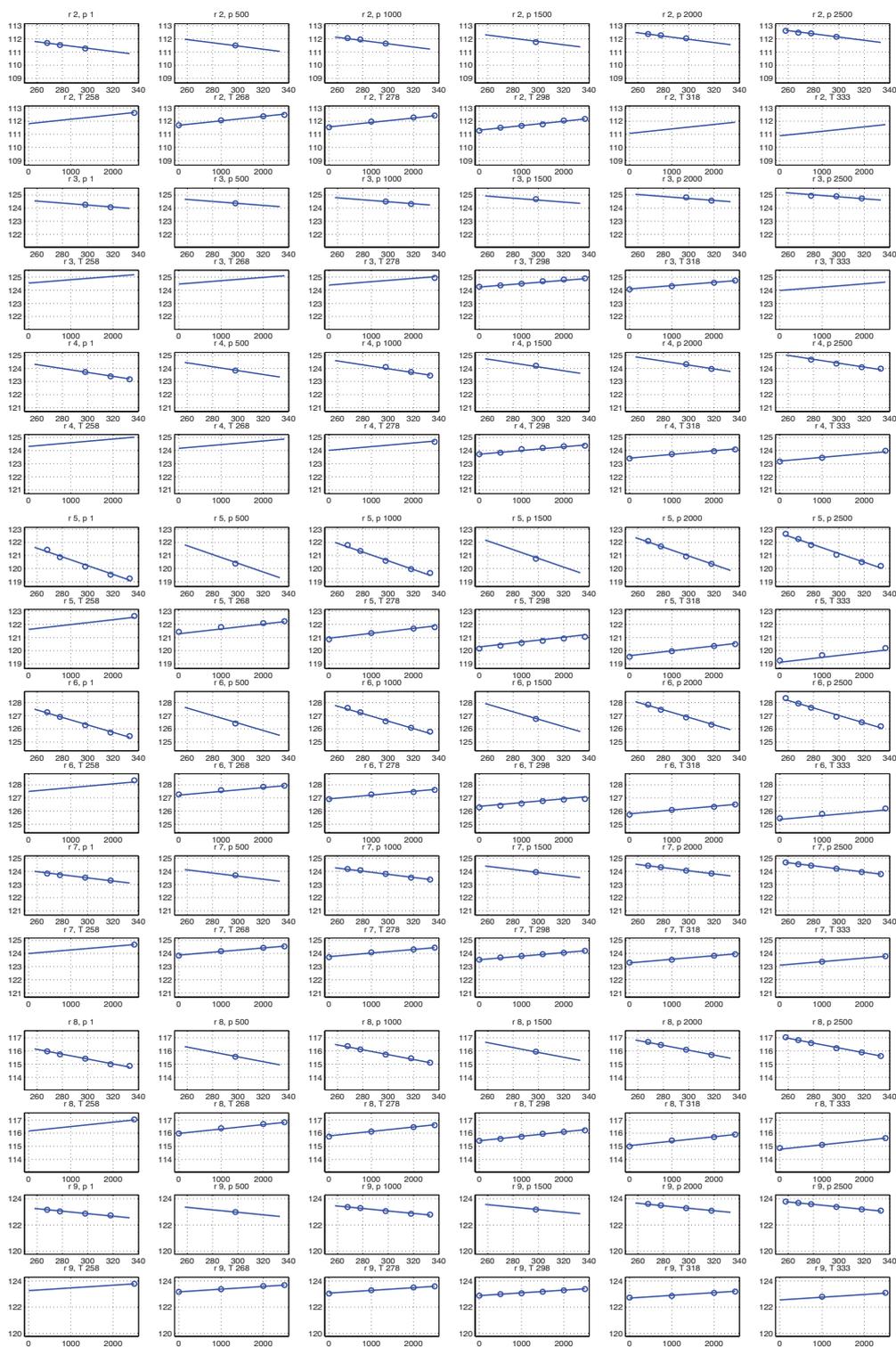
^{15}N chemical shifts [ppm] are shown as a function of residue number r, temperature T [K] and pressure p [bar]. Uniformly ^{15}N-labeled peptide (~1 mM) was dissolved in 10 mM sodium acetate-d5, pH 4.5, 95/5% H_2O/D_2O. Chemical shift referencing was achieved by indirect referencing to water, whose chemical shift had been temperature- and pressure-adjusted

according to Figure S1. The ^{15}N chemical shifts are fitted (straight line) to a linear function of the form $\delta_{15N}(p, T)/ppm = a_0 + a_1 \cdot p + a_2 \cdot T$ using the following parameters:

Residue Nr	a_1 [10^{-4} ppm/bar]	a_2 [10^{-3} ppm/K]
2	3.40	−12.3
3	2.52	−7.5
4	2.81	−14.8
5	3.70	−33.3
6	2.88	−28.4
7	2.72	−11.9
8	3.37	−18.5
9	2.07	−9.4
Average	2.93	−17.0
Std	0.53	9.3

Figure S3: Pressure-induced unfolding of protein G in 50 % methanol at 303 K, pH 2.5
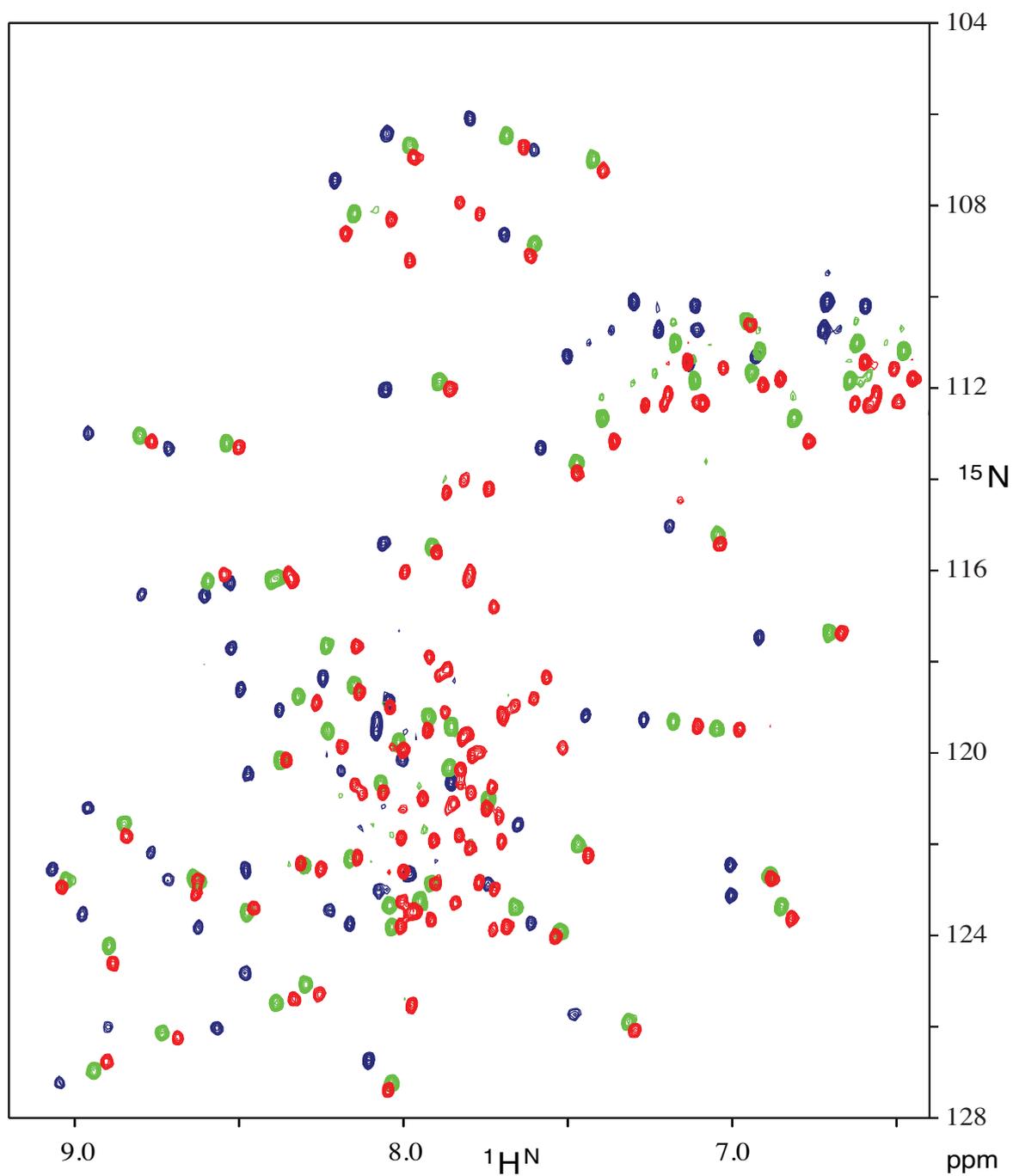
^{1}H-^{15}N HSQC recorded on a 800 MHz spectrometer at pressures of 1 (dark blue), 1500 (green), and 2500 bar (red), respectively.

Figure S4: Assignment of native and unfolded state of protein G in 50 % methanol at 303 K, 2500 bar, pH 2.5
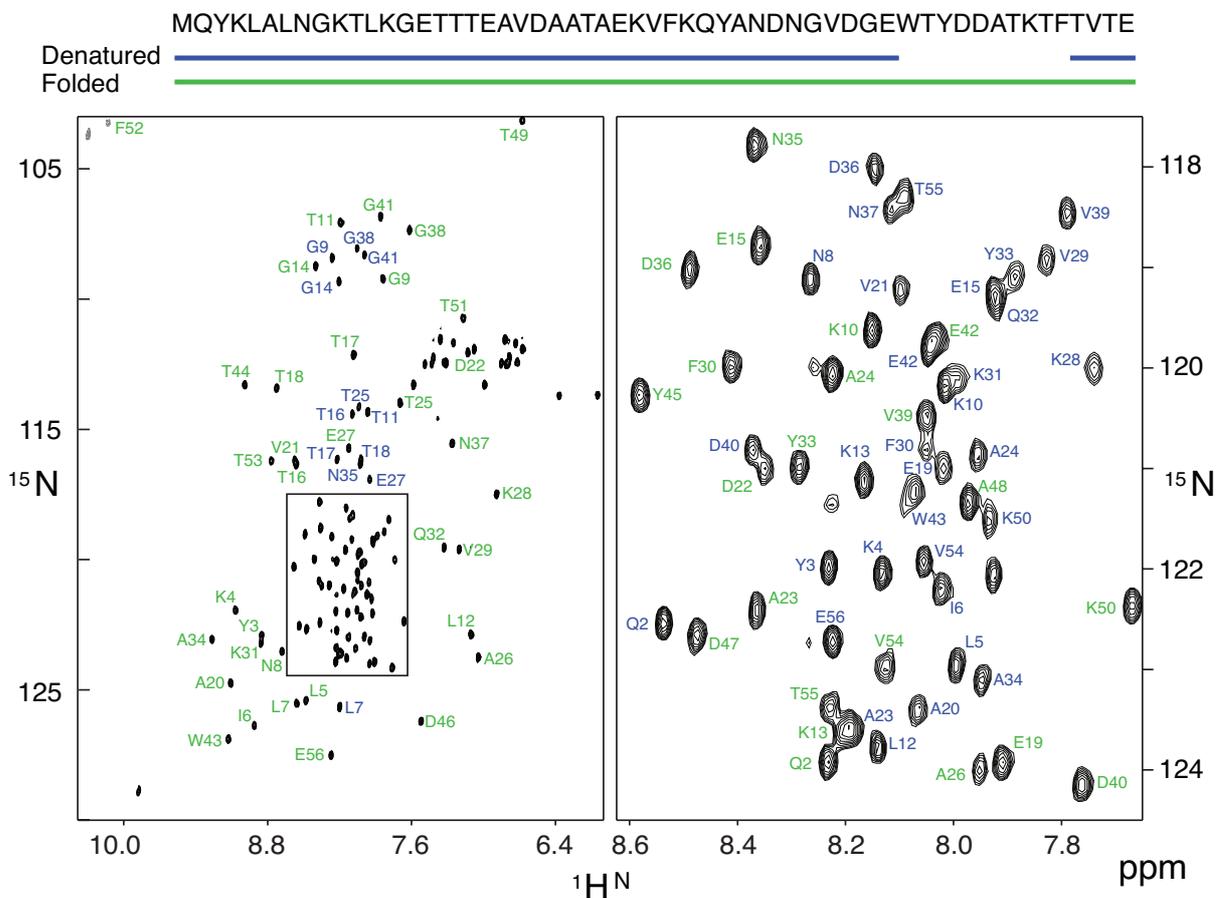
^{1}H-^{15}N HSQC spectrum of protein G. Peaks are labeled with assignment information for the folded state (green) and the pressure/methanol-denatured state (blue). The amino acid sequence of protein G is indicated at the top with assigned residues underlined for both states.

References

1.   Gottlieb, H. E., Kotlyar, V. & Nudelman, A. (1997) *J. Org. Chem.* **62,** 7512-7515.

8 Conclusions and perspectives

In this thesis we sought to study CCR5 and its interaction with RANTES by NMR. We started with the CCR5 expressed in insect cells, however, to obtain an access to a cost-efficient uniform isotope labeling a CCR5-tailored E. coli expression system was additionally established. The receptor produced in both systems was analyzed in detail with regards to the secondary structure contents, oligomeric state, particle size, stability and functionality.

Carefully performed immunoprecipitation assay revealed that in the presence of Fos-Choline-12, a detergent used for high-yield purification, CCR5 is not recognized by the conformation dependent antibody 2D7. This finding corrected the previous observations made in the group and at the same time lead to a better SPR setup, where CCR5 interactions with numerous ligands could be studied.

Large-scale detergent screening revealed that CCR5 is readily solubilized by ionic and zwitterionic detergents but not by the milder maltosides. This fact is consistent for the receptor produced in both insect cells and in E. coli but comes as a surprise, since the maltosides are indisputably the most successful detergent family in GPCR structure determination. This observation, together with the high aggregation tendency and very low thermal stability, again observed for the receptor from both sources, may be an indication that CCR5 is intrinsically very unstable. Hence, some kind of significant stabilization e.g. thermostabilizing mutations yielding a better-behaved receptor may be an important step towards CCR5 structure determination.

The established E. coli expression system enables to obtain milligram quantities of 15N,13C,2H-labeled CCR5. Using this material a set of 3D experiments was recorded and we have currently attempted the assignment. Unfortunately, the quality of the spectrum suffers from overlap and line broadening and needs further improvements. The fact that the majority of the resonances remain invisible is most likely either a consequence of a nonoptimal detergent system or, again, a symptom of the receptor intrinsic instability.

Using SPR we studied CCR5 interactions with 2D7, MIP-1β and various RANTES variants. It was shown that wild type RANTES aggregates on the surface of the receptor micelle via a mechanism compatible with a linear oligomerization, which

161

can be abolished by a E66S mutation, the same one that renders RANTES unable to form tetramers. The higher CCR5 binding affinity of 5P12-RANTES, explains why 5P12-RANTES, which does not cause CCR5 internalization is similarly potent anti-HIV microbicide as PSC-RANTES, which upon binding causes CCR5 endocytosis.

It was shown by NMR that 5P12-RANTES-E66S even at high concentration is purely monomeric and with the exception of the flexible N-terminus its structure is similar to the structure of the wild type RANTES. Using the example of RANTES-E66S perturbation by Fos-Choline-12 it was demonstrated that the selection of detergent is crucial not only for the receptor (which is usually the only criterion) but also for the ligand.

By applying high-pressure NMR techniques cold denaturation of ubiquitin was studied. The secondary shift analysis revealed that the cold-denatured state closely resembles the alcohol-denatured state. This indicates a common mechanism of pressure, cold and alcohol denaturation via a reduction of the hydrophobic effect. The presented method should be a useful tool to study the hydrophobic component of the protein stability.

9 Bibliography

1. Takeda, S., Kadowaki, S., Haga, T., Takaesu, H. and Mitaku, S. (2002) Identification of G protein-coupled receptor genes from the human genome sequence. FEBS Lett 520, 97-101.

2. Fredriksson, R., Lagerstrom, M. C., Lundin, L. G. and Schioth, H. B. (2003) The G-protein-coupled receptors in the human genome form five main families. Phylogenetic analysis, paralogon groups, and fingerprints. Mol Pharmacol 63, 1256-1272.

3. Overington, J. P., Al-Lazikani, B. and Hopkins, A. L. (2006) How many drug targets are there? Nat Rev Drug Discov 5, 993-996.

4. Bockaert, J. and Pin, J. P. (1999) Molecular tinkering of G protein-coupled receptors: an evolutionary success. EMBO J 18, 1723-1729.

5. Filmore, D. (2004) It's a GPCR world. Modern Drug Discovery 7, 24-28.

6. de Abreu, R. A., van Baal, J. M., Bakkeren, J. A., de Brugn, C. H. and Schretlen, E. D. (1982) High-performance liquid chromatographic assay for identification and quantitation of nucleotides in lymphocytes and malignant lymphoblasts. J Chromatogr 227, 45-52.

7. Strader, C. D., Fong, T. M., Tota, M. R., Underwood, D. and Dixon, R. A. (1994) Structure and function of G protein-coupled receptors. Annu Rev Biochem 63, 101-132.

8. Pierce, K. L., Premont, R. T. and Lefkowitz, R. J. (2002) Seven-transmembrane receptors. Nat Rev Mol Cell Biol 3, 639-650.

9. Goodman, O. B., Jr., Krupnick, J. G., Santini, F., Gurevich, V. V., Penn, R. B., Gagnon, A. W., Keen, J. H. and Benovic, J. L. (1996) Beta-arrestin acts as a clathrin adaptor in endocytosis of the beta2-adrenergic receptor. Nature 383, 447-450.

10. Wolfe, B. L. and Trejo, J. (2007) Clathrin-dependent mechanisms of G protein-coupled receptor endocytosis. Traffic 8, 462-470.

11. Marchese, A., Paing, M. M., Temple, B. R. and Trejo, J. (2008) G protein-coupled receptor sorting to endosomes and lysosomes. Annu Rev Pharmacol Toxicol 48, 601-629.

12. Scarselli, M. and Donaldson, J. G. (2009) Constitutive internalization of G protein-coupled receptors and G proteins via clathrin-independent endocytosis. J Biol Chem 284, 3577-3585.

13. Nisius, L. (2010) Expression, Purification and Characterization of the HIV-1 coreceptor CCR5 and its ligand RANTES and High-pressure NMR investigations of hydrogen bonds in biomolecules. PhD Thesis, University of Basel, Faculty of Science, doi: 10.5451/unibas-005398107.

14. Bernstein, F. C., Koetzle, T. F., Williams, G. J., Meyer, E. F., Jr., Brice, M. D., Rodgers, J. R., Kennard, O., Shimanouchi, T. and Tasumi, M. (1977) The Protein

Data Bank: a computer-based archival file for macromolecular structures. J Mol Biol 112, 535-542.

15. White, S. H. (2004) The progress of membrane protein structure determination. Protein Sci 13, 1948-1949.

16. Palczewski, K., Kumasaka, T., Hori, T., Behnke, C. A., Motoshima, H., Fox, B. A., Le Trong, I., Teller, D. C., Okada, T., Stenkamp, R. E., Yamamoto, M. and Miyano, M. (2000) Crystal structure of rhodopsin: A G protein-coupled receptor. Science 289, 739-745.

17. Rasmussen, S. G., Choi, H. J., Rosenbaum, D. M., Kobilka, T. S., Thian, F. S., Edwards, P. C., Burghammer, M., Ratnala, V. R., Sanishvili, R., Fischetti, R. F., Schertler, G. F., Weis, W. I. and Kobilka, B. K. (2007) Crystal structure of the human beta2 adrenergic G-protein-coupled receptor. Nature 450, 383-387.

18. Cherezov, V., Rosenbaum, D. M., Hanson, M. A., Rasmussen, S. G., Thian, F. S., Kobilka, T. S., Choi, H. J., Kuhn, P., Weis, W. I., Kobilka, B. K. and Stevens, R. C. (2007) High-resolution crystal structure of an engineered human beta2-adrenergic G protein-coupled receptor. Science 318, 1258-1265.

19. Warne, T., Serrano-Vega, M. J., Baker, J. G., Moukhametzianov, R., Edwards, P. C., Henderson, R., Leslie, A. G., Tate, C. G. and Schertler, G. F. (2008) Structure of a beta1-adrenergic G-protein-coupled receptor. Nature 454, 486-491.

20. Jaakola, V. P., Griffith, M. T., Hanson, M. A., Cherezov, V., Chien, E. Y., Lane, J. R., Ijzerman, A. P. and Stevens, R. C. (2008) The 2.6 angstrom crystal structure of a human A2A adenosine receptor bound to an antagonist. Science 322, 1211-1217.

21. Lebon, G., Warne, T., Edwards, P. C., Bennett, K., Langmead, C. J., Leslie, A. G. and Tate, C. G. (2011) Agonist-bound adenosine A2A receptor structures reveal common features of GPCR activation. Nature 474, 521-525.

22. Chien, E. Y., Liu, W., Zhao, Q., Katritch, V., Han, G. W., Hanson, M. A., Shi, L., Newman, A. H., Javitch, J. A., Cherezov, V. and Stevens, R. C. (2010) Structure of the human dopamine D3 receptor in complex with a D2/D3 selective antagonist. Science 330, 1091-1095.

23. Wu, B., Chien, E. Y., Mol, C. D., Fenalti, G., Liu, W., Katritch, V., Abagyan, R., Brooun, A., Wells, P., Bi, F. C., Hamel, D. J., Kuhn, P., Handel, T. M., Cherezov, V. and Stevens, R. C. (2010) Structures of the CXCR4 chemokine GPCR with small-molecule and cyclic peptide antagonists. Science 330, 1066-1071.

24. Shimamura, T., Shiroishi, M., Weyand, S., Tsujimoto, H., Winter, G., Katritch, V., Abagyan, R., Cherezov, V., Liu, W., Han, G. W., Kobayashi, T., Stevens, R. C. and Iwata, S. (2011) Structure of the human histamine H1 receptor complex with doxepin. Nature 475, 65-70.

25. Haga, K., Kruse, A. C., Asada, H., Yurugi-Kobayashi, T., Shiroishi, M., Zhang, C., Weis, W. I., Okada, T., Kobilka, B. K., Haga, T. and Kobayashi, T. (2012) Structure of the human M2 muscarinic acetylcholine receptor bound to an antagonist. Nature 482, 547-551.

26. Kruse, A. C., Hu, J., Pan, A. C., Arlow, D. H., Rosenbaum, D. M., Rosemond, E., Green, H. F., Liu, T., Chae, P. S., Dror, R. O., Shaw, D. E., Weis, W. I., Wess, J. and Kobilka, B. K. (2012) Structure and dynamics of the M3 muscarinic acetylcholine receptor. Nature 482, 552-556.

27. Hanson, M. A., Roth, C. B., Jo, E., Griffith, M. T., Scott, F. L., Reinhart, G., Desale, H., Clemons, B., Cahalan, S. M., Schuerer, S. C., Sanna, M. G., Han, G. W., Kuhn, P., Rosen, H. and Stevens, R. C. (2012) Crystal structure of a lipid G protein-coupled receptor. Science 335, 851-855.

28. Manglik, A., Kruse, A. C., Kobilka, T. S., Thian, F. S., Mathiesen, J. M., Sunahara, R. K., Pardo, L., Weis, W. I., Kobilka, B. K. and Granier, S. (2012) Crystal structure of the micro-opioid receptor bound to a morphinan antagonist. Nature 485, 321-326.

29. Wu, H., Wacker, D., Mileni, M., Katritch, V., Han, G. W., Vardy, E., Liu, W., Thompson, A. A., Huang, X. P., Carroll, F. I., Mascarella, S. W., Westkaemper, R. B., Mosier, P. D., Roth, B. L., Cherezov, V. and Stevens, R. C. (2012) Structure of the human kappa-opioid receptor in complex with JDTic. Nature 485, 327-332.

30. Granier, S., Manglik, A., Kruse, A. C., Kobilka, T. S., Thian, F. S., Weis, W. I. and Kobilka, B. K. (2012) Structure of the delta-opioid receptor bound to naltrindole. Nature 485, 400-404.

31. Gautier, A., Kirkpatrick, J. P. and Nietlispach, D. (2008) Solution-state NMR spectroscopy of a seven-helix transmembrane protein receptor: backbone assignment, secondary structure, and dynamics. Angew Chem Int Ed Engl 47, 7297-7300.

32. Reckel, S., Gottstein, D., Stehle, J., Lohr, F., Verhoefen, M. K., Takeda, M., Silvers, R., Kainosho, M., Glaubitz, C., Wachtveitl, J., Bernhard, F., Schwalbe, H., Guntert, P. and Dotsch, V. (2011) Solution NMR structure of proteorhodopsin. Angew Chem Int Ed Engl 50, 11942-11946.

33. Balistreri, C. R., Caruso, C., Grimaldi, M. P., Listi, F., Vasto, S., Orlando, V., Campagna, A. M., Lio, D. and Candore, G. (2007) CCR5 receptor: biologic and genetic implications in age-related diseases. Ann N Y Acad Sci 1100, 162-172.

34. Choe, H., Martin, K. A., Farzan, M., Sodroski, J., Gerard, N. P. and Gerard, C. (1998) Structural interactions between chemokine receptors, gp120 Env and CD4. Semin Immunol 10, 249-257.

35. Liu, R., Paxton, W. A., Choe, S., Ceradini, D., Martin, S. R., Horuk, R., MacDonald, M. E., Stuhlmann, H., Koup, R. A. and Landau, N. R. (1996) Homozygous defect in HIV-1 coreceptor accounts for resistance of some multiply-exposed individuals to HIV-1 infection. Cell 86, 367-377.

36. Samson, M., Libert, F., Doranz, B. J., Rucker, J., Liesnard, C., Farber, C. M., Saragosti, S., Lapoumeroulie, C., Cognaux, J., Forceille, C., Muyldermans, G., Verhofstede, C., Burtonboy, G., Georges, M., Imai, T., Rana, S., Yi, Y., Smyth, R. J., Collman, R. G., Doms, R. W., Vassart, G. and Parmentier, M. (1996) Resistance to HIV-1 infection in caucasian individuals bearing mutant alleles of the CCR-5 chemokine receptor gene. Nature 382, 722-725.

37. Stephens, J. C., Reich, D. E., Goldstein, D. B., Shin, H. D., Smith, M. W., Carrington, M., Winkler, C., Huttley, G. A., Allikmets, R., Schriml, L., Gerrard, B., Malasky, M., Ramos, M. D., Morlot, S., Tzetis, M., Oddoux, C., di Giovine, F. S., Nasioulas, G., Chandler, D., Aseev, M., Hanson, M., Kalaydjieva, L., Glavac, D., Gasparini, P., Kanavakis, E., Claustres, M., Kambouris, M., Ostrer, H., Duff, G., Baranov, V., Sibul, H., Metspalu, A., Goldman, D., Martin, N., Duffy, D., Schmidtke, J., Estivill, X., O'Brien, S. J. and Dean, M. (1998) Dating the origin of

the CCR5-Delta32 AIDS-resistance allele by the coalescence of haplotypes. Am J Hum Genet 62, 1507-1515.

38. Duncan, S. R., Scott, S. and Duncan, C. J. (2005) Reappraisal of the historical selective pressures for the CCR5-Delta32 mutation. J Med Genet 42, 205-208.

39. Kondru, R., Zhang, J., Ji, C., Mirzadegan, T., Rotstein, D., Sankuratri, S. and Dioszegi, M. (2008) Molecular interactions of CCR5 with major classes of small-molecule anti-HIV CCR5 antagonists. Mol Pharmacol 73, 789-800.

40. Gaertner, H., Cerini, F., Escola, J. M., Kuenzi, G., Melotti, A., Offord, R., Rossitto-Borlat, I., Nedellec, R., Salkowitz, J., Gorochov, G., Mosier, D. and Hartley, O. (2008) Highly potent, fully recombinant anti-HIV chemokines: reengineering a low-cost microbicide. Proc Natl Acad Sci USA 105, 17706-17711.

41. Lederman, M. M., Veazey, R. S., Offord, R., Mosier, D. E., Dufour, J., Mefford, M., Piatak, M., Jr., Lifson, J. D., Salkowitz, J. R., Rodriguez, B., Blauvelt, A. and Hartley, O. (2004) Prevention of vaginal SHIV transmission in rhesus macaques through inhibition of CCR5. Science 306, 485-487.

42. Lusso, P., Vangelista, L., Cimbro, R., Secchi, M., Sironi, F., Longhi, R., Faiella, M., Maglio, O. and Pavone, V. (2011) Molecular engineering of RANTES peptide mimetics with potent anti-HIV-1 activity. FASEB J 25, 1230-1243.

43. Nardese, V., Longhi, R., Polo, S., Sironi, F., Arcelloni, C., Paroni, R., DeSantis, C., Sarmientos, P., Rizzi, M., Bolognesi, M., Pavone, V. and Lusso, P. (2001) Structural determinants of CCR5 recognition and HIV-1 blockade in RANTES. Nat Struct Biol 8, 611-615.

44. Doms, R. W. and Peiper, S. C. (1997) Unwelcomed guests with master keys: how HIV uses chemokine receptors for cellular entry. Virology 235, 179-190.

45. Baggiolini, M., Dewald, B. and Moser, B. (1997) Human chemokines: an update. Annu Rev Immunol 15, 675-705.

46. Blanpain, C., Lee, B., Vakili, J., Doranz, B. J., Govaerts, C., Migeotte, I., Sharron, M., Dupriez, V., Vassart, G., Doms, R. W. and Parmentier, M. (1999) Extracellular cysteines of CCR5 are required for chemokine binding, but dispensable for HIV-1 coreceptor activity. J Biol Chem 274, 18902-18908.

47. Blanpain, C., Wittamer, V., Vanderwinden, J. M., Boom, A., Renneboog, B., Lee, B., Le Poul, E., El Asmar, L., Govaerts, C., Vassart, G., Doms, R. W. and Parmentier, M. (2001) Palmitoylation of CCR5 is critical for receptor trafficking and efficient activation of intracellular signaling pathways. J Biol Chem 276, 23795-23804.

48. Kraft, K., Olbrich, H., Majoul, I., Mack, M., Proudfoot, A. and Oppermann, M. (2001) Characterization of sequence determinants within the carboxyl-terminal domain of chemokine receptor CCR5 that regulate signaling and receptor internalization. J Biol Chem 276, 34408-34418.

49. Percherancier, Y., Planchenault, T., Valenzuela-Fernandez, A., Virelizier, J. L., Arenzana-Seisdedos, F. and Bachelerie, F. (2001) Palmitoylation-dependent control of degradation, life span, and membrane expression of the CCR5 receptor. J Biol Chem 276, 31936-31944.

50. Farzan, M., Mirzabekov, T., Kolchinsky, P., Wyatt, R., Cayabyab, M., Gerard, N. P., Gerard, C., Sodroski, J. and Choe, H. (1999) Tyrosine sulfation of the amino terminus of CCR5 facilitates HIV-1 entry. Cell 96, 667-676.

51. Mondor, I., Ugolini, S. and Sattentau, Q. J. (1998) Human immunodeficiency virus type 1 attachment to HeLa CD4 cells is CD4 independent and gp120 dependent and requires cell surface heparans. J Virol 72, 3623-3634.

52. Roderiquez, G., Oravecz, T., Yanagishita, M., Bou-Habib, D. C., Mostowski, H. and Norcross, M. A. (1995) Mediation of human immunodeficiency virus type 1 binding by interaction of cell surface heparan sulfate proteoglycans with the V3 region of envelope gp120-gp41. J Virol 69, 2233-2239.

53. Tanaka, Y., Adams, D. H., Hubscher, S., Hirano, H., Siebenlist, U. and Shaw, S. (1993) T-cell adhesion induced by proteoglycan-immobilized cytokine MIP-1 beta. Nature 361, 79-82.

54. Webb, L. M., Ehrengruber, M. U., Clark-Lewis, I., Baggiolini, M. and Rot, A. (1993) Binding to heparan sulfate or heparin enhances neutrophil responses to interleukin 8. Proc Natl Acad Sci USA 90, 7158-7162.

55. Luster, A. D., Greenberg, S. M. and Leder, P. (1995) The IP-10 chemokine binds to a specific cell surface heparan sulfate site shared with platelet factor 4 and inhibits endothelial cell proliferation. J Exp Med 182, 219-231.

56. Farzan, M., Chung, S., Li, W., Vasilieva, N., Wright, P. L., Schnitzler, C. E., Marchione, R. J., Gerard, C., Gerard, N. P., Sodroski, J. and Choe, H. (2002) Tyrosine-sulfated peptides functionally reconstitute a CCR5 variant lacking a critical amino-terminal region. J Biol Chem 277, 40397-40402.

57. Cormier, E. G., Persuh, M., Thompson, D. A., Lin, S. W., Sakmar, T. P., Olson, W. C. and Dragic, T. (2000) Specific interaction of CCR5 amino-terminal domain peptides containing sulfotyrosines with HIV-1 envelope glycoprotein gp120. Proc Natl Acad Sci USA 97, 5762-5767.

58. Bannert, N., Craig, S., Farzan, M., Sogah, D., Santo, N. V., Choe, H. and Sodroski, J. (2001) Sialylated O-glycans and sulfated tyrosines in the NH2-terminal domain of CC chemokine receptor 5 contribute to high affinity binding of chemokines. J Exp Med 194, 1661-1673.

59. Rucker, J., Samson, M., Doranz, B. J., Libert, F., Berson, J. F., Yi, Y., Smyth, R. J., Collman, R. G., Broder, C. C., Vassart, G., Doms, R. W. and Parmentier, M. (1996) Regions in beta-chemokine receptors CCR5 and CCR2b that determine HIV-1 cofactor specificity. Cell 87, 437-446.

60. Oppermann, M., Mack, M., Proudfoot, A. E. and Olbrich, H. (1999) Differential effects of CC chemokines on CC chemokine receptor 5 (CCR5) phosphorylation and identification of phosphorylation sites on the CCR5 carboxyl terminus. J Biol Chem 274, 8875-8885.

61. Berger, E. A., Murphy, P. M. and Farber, J. M. (1999) Chemokine receptors as HIV-1 coreceptors: roles in viral entry, tropism, and disease. Annu Rev Immunol 17, 657-700.

62. Murphy, P. M. (1994) The molecular biology of leukocyte chemoattractant receptors. Annu Rev Immunol 12, 593-633.

63. Cocchi, F., DeVico, A. L., Garzino-Demo, A., Arya, S. K., Gallo, R. C. and Lusso, P. (1995) Identification of RANTES, MIP-1 alpha, and MIP-1 beta as the major HIV-suppressive factors produced by CD8+ T cells. Science 270, 1811-1815.

64. Feng, Y., Broder, C. C., Kennedy, P. E. and Berger, E. A. (1996) HIV-1 entry cofactor: functional cDNA cloning of a seven-transmembrane, G protein-coupled receptor. Science 272, 872-877.

65. Gordon, C. J., Muesing, M. A., Proudfoot, A. E., Power, C. A., Moore, J. P. and Trkola, A. (1999) Enhancement of human immunodeficiency virus type 1 infection by the CC-chemokine RANTES is independent of the mechanism of virus-cell fusion. J Virol 73, 684-694.

66. Czaplewski, L. G., McKeating, J., Craven, C. J., Higgins, L. D., Appay, V., Brown, A., Dudgeon, T., Howard, L. A., Meyers, T., Owen, J., Palan, S. R., Tan, P., Wilson, G., Woods, N. R., Heyworth, C. M., Lord, B. I., Brotherton, D., Christison, R., Craig, S., Cribbes, S., Edwards, R. M., Evans, S. J., Gilbert, R., Morgan, P., Randle, E., Schofield, N., Varley, P. G., Fisher, J., Waltho, J. P. and Hunter, M. G. (1999) Identification of amino acid residues critical for aggregation of human CC chemokines macrophage inflammatory protein (MIP)-1alpha, MIP-1beta, and RANTES. Characterization of active disaggregated chemokine variants. J Biol Chem 274, 16077-16084.

67. Bacon, K. B., Premack, B. A., Gardner, P. and Schall, T. J. (1995) Activation of dual T cell signaling pathways by the chemokine RANTES. Science 269, 1727-1730.

68. Bacon, K. B., Szabo, M. C., Yssel, H., Bolen, J. B. and Schall, T. J. (1996) RANTES induces tyrosine kinase activity of stably complexed p125FAK and ZAP-70 in human T cells. J Exp Med 184, 873-882.

69. Szabo, M. C., Butcher, E. C., McIntyre, B. W., Schall, T. J. and Bacon, K. B. (1997) RANTES stimulation of T lymphocyte adhesion and activation: role for LFA-1 and ICAM-3. Eur J Immunol 27, 1061-1068.

70. Wang, X., Watson, C., Sharp, J. S., Handel, T. M. and Prestegard, J. H. (2011) Oligomeric structure of the chemokine CCL5/RANTES from NMR, MS, and SAXS data. Structure 19, 1138-1148.

71. Appay, V., Brown, A., Cribbes, S., Randle, E. and Czaplewski, L. G. (1999) Aggregation of RANTES is responsible for its inflammatory properties. Characterization of nonaggregating, noninflammatory RANTES mutants. J Biol Chem 274, 27505-27512.

72. Crump, M. P., Gong, J. H., Loetscher, P., Rajarathnam, K., Amara, A., Arenzana-Seisdedos, F., Virelizier, J. L., Baggiolini, M., Sykes, B. D. and Clark-Lewis, I. (1997) Solution structure and basis for functional activity of stromal cell-derived factor-1; dissociation of CXCR4 activation from binding and inhibition of HIV-1. EMBO J 16, 6996-7007.

73. Dealwis, C., Fernandez, E. J., Thompson, D. A., Simon, R. J., Siani, M. A. and Lolis, E. (1998) Crystal structure of chemically synthesized [N33A] stromal cell-derived factor 1alpha, a potent ligand for the HIV-1 "fusin" coreceptor. Proc Natl Acad Sci USA 95, 6941-6946.

74. Fernandez, E. J., Wilken, J., Thompson, D. A., Peiper, S. C. and Lolis, E. (2000) Comparison of the structure of vMIP-II with eotaxin-1, RANTES, and MCP-3 suggests a unique mechanism for CCR3 activation. Biochemistry 39, 12837-12844.

75. Liwang, A. C., Wang, Z. X., Sun, Y., Peiper, S. C. and Liwang, P. J. (1999) The solution structure of the anti-HIV chemokine vMIP-II. Protein Sci 8, 2270-2280.

76. Lodi, P. J., Garrett, D. S., Kuszewski, J., Tsang, M. L., Weatherbee, J. A., Leonard, W. J., Gronenborn, A. M. and Clore, G. M. (1994) High-resolution solution structure of the beta chemokine hMIP-1 beta by multidimensional NMR. Science 263, 1762-1767.

77. Chung, C. W., Cooke, R. M., Proudfoot, A. E. and Wells, T. N. (1995) The three-dimensional solution structure of RANTES. Biochemistry 34, 9307-9314.

78. Proudfoot, A. E. (2002) Chemokine receptors: multifaceted therapeutic targets. Nat Rev Immunol 2, 106-115.

79. Fernandez, E. J. and Lolis, E. (2002) Structure, function, and inhibition of chemokines. Annu Rev Pharmacol Toxicol 42, 469-499.

80. Duma, L., Haussinger, D., Rogowski, M., Lusso, P. and Grzesiek, S. (2007) Recognition of RANTES by extracellular parts of the CCR5 receptor. J Mol Biol 365, 1063-1075.

81. Hoover, D. M., Shaw, J., Gryczynski, Z., Proudfoot, A. E. I. and Wells, T. (2000) The Crystal Structure of Met-Rantes: Comparison with Native Rantes and Aop-Rantes. Protein Pept Letters 7, 73-82.

82. Nisius, L., Rogowski, M., Vangelista, L. and Grzesiek, S. (2008) Large-scale expression and purification of the major HIV-1 coreceptor CCR5 and characterization of its interaction with RANTES. Protein Expr Purif 61, 155-162.

83. Abramoff, M. D., Magalhaes, P. J. and Ram, S. J. (2004) Image Processing with ImageJ. Biophotonics International 11, 36-42.

84. Morrow, J. A., Segall, M. L., Lund-Katz, S., Phillips, M. C., Knapp, M., Rupp, B. and Weisgraber, K. H. (2000) Differences in stability among the human apolipoprotein E isoforms determined by the amino-terminal domain. Biochemistry 39, 11657-11666.

85. Vaughn, J. L., Goodwin, R. H., Tompkins, G. J. and McCawley, P. (1977) The establishment of two cell lines from the insect Spodoptera frugiperda (Lepidoptera; Noctuidae). In Vitro 13, 213-217.

86. Mirzabekov, T., Bannert, N., Farzan, M., Hofmann, W., Kolchinsky, P., Wu, L., Wyatt, R. and Sodroski, J. (1999) Enhanced expression, native purification, and characterization of CCR5, a principal HIV-1 coreceptor. J Biol Chem 274, 28745-28750.

87. Rich, R. L., Miles, A. R., Gale, B. K. and Myszka, D. G. (2009) Detergent screening of a G-protein-coupled receptor using serial and array biosensor technologies. Anal Biochem 386, 98-104.

88. Oppermann, M. (2004) Chemokine receptor CCR5: insights into structure, function, and regulation. Cell Signal 16, 1201-1210.

89. Navratilova, I., Besnard, J. and Hopkins, A. L. (2011) Screening for GPCR Ligands Using Surface Plasmon Resonance. ACS Med Chem Lett 2, 549-554.

90. Navratilova, I., Pancera, M., Wyatt, R. T. and Myszka, D. G. (2006) A biosensor-based approach toward purification and crystallization of G protein-coupled receptors. Anal Biochem 353, 278-283.

91. Navratilova, I., Sodroski, J. and Myszka, D. G. (2005) Solubilization, stabilization, and purification of chemokine receptors using biosensor technology. Anal Biochem 339, 271-281.

92. Baneres, J. L., Martin, A., Hullot, P., Girard, J. P., Rossi, J. C. and Parello, J. (2003) Structure-based analysis of GPCR function: conformational adaptation of both agonist and receptor upon leukotriene B4 binding to recombinant BLT1. J Mol Biol 329, 801-814.

93. Baneres, J. L., Mesnier, D., Martin, A., Joubert, L., Dumuis, A. and Bockaert, J. (2005) Molecular characterization of a purified 5-HT4 receptor: a structural basis for drug efficacy. J Biol Chem 280, 20253-20260.

94. Delaglio, F., Grzesiek, S., Vuister, G. W., Zhu, G., Pfeifer, J. and Bax, A. (1995) NMRPipe: a multidimensional spectral processing system based on UNIX pipes. J Biomol NMR 6, 277-293.

95. Goddard, T. D. and Kneller, D. G. (SPARKY 3, University of California, San Francisco.

96. Markley, J. L., Bax, A., Arata, Y., Hilbers, C. W., Kaptein, R., Sykes, B. D., Wright, P. E. and Wuthrich, K. (1998) Recommendations for the presentation of NMR structures of proteins and nucleic acids--IUPAC-IUBMB-IUPAB Inter-Union Task Group on the standardization of data bases of protein and nucleic acid structures determined by NMR spectroscopy. Eur J Biochem 256, 1-15.

97. Kjaergaard, M., Brander, S. and Poulsen, F. M. (2011) Random coil chemical shift for intrinsically disordered proteins: effects of temperature and pH. J Biomol NMR 49, 139-149.

98. Kjaergaard, M. and Poulsen, F. M. (2011) Sequence correction of random coil chemical shifts: correlation between neighbor correction factors and changes in the Ramachandran distribution. J Biomol NMR 50, 157-165.

99. Schwarzinger, S., Kroon, G. J., Foss, T. R., Chung, J., Wright, P. E. and Dyson, H. J. (2001) Sequence-dependent correction of random coil NMR chemical shifts. J Am Chem Soc 123, 2970-2978.

100. Shen, Y., Lange, O., Delaglio, F., Rossi, P., Aramini, J. M., Liu, G., Eletsky, A., Wu, Y., Singarapu, K. K., Lemak, A., Ignatchenko, A., Arrowsmith, C. H., Szyperski, T., Montelione, G. T., Baker, D. and Bax, A. (2008) Consistent blind protein structure generation from NMR chemical shift data. Proc Natl Acad Sci USA 105, 4685-4690.

101. Shen, Y., Vernon, R., Baker, D. and Bax, A. (2009) De novo protein structure generation from incomplete chemical shift assignments. J Biomol NMR 43, 63-78.

102. Wishart, D. S., Bigam, C. G., Holm, A., Hodges, R. S. and Sykes, B. D. (1995) 1H, 13C and 15N random coil NMR chemical shifts of the common amino acids. I. Investigations of nearest-neighbor effects. J Biomol NMR 5, 67-81.

103. Navratilova, I., Dioszegi, M. and Myszka, D. G. (2006) Analyzing ligand and small molecule binding activity of solubilized GPCRs using biosensor technology. Anal Biochem 355, 132-139.

<center>CURRICULUM VITAE</center>

MACIEJ WIKTOR

PERSONAL INFORMATION

Name:	Maciej WIKTOR
Address:	Welschmattstrasse 23, 4055 Basel, Switzerland
Telephone	(0041) 61 267 2097
E-mail:	maciej.wiktor@unibas.ch
Nationality:	Polish
Date of birth:	January 12th 1985
Gender:	Male
Marital status:	Bachelor
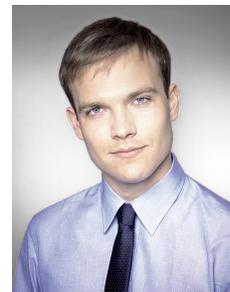
EDUCATION

09/2008 – present   PhD in Biophysics: "Towards NMR analysis of the HIV-1 coreceptor CCR5 and its interaction with RANTES and high pressure NMR investigation of ubiquitin cold and alcohol denaturation"
Department of Structural Biology, Biozentrum, University of Basel, Switzerland, Supervisor: Prof. Stephan Grzesiek

10/2006 – 06/2008   MSc in Biotechnology of Peptides and Proteins: "Structural studies of synaptobrevin-2 and its complex with SNAP-25 and syntaxin-1A", grade very good (5.0/5.0)
Department of Molecular Physiology & Biological Physics, University of Virginia, Charlottesville, USA, Supervisor: Prof. Lukas Tamm (2nd year)
Laboratory of Protein Engineering, Faculty of Biotechnology, University of Wrocław, Poland, Supervisor: Prof. Jacek Otlewski (1st year)

10/2006 – 06/2007   Management and Engineering of Production, Wrocław University of Economics, Wrocław, Poland

10/2003 – 06/2006   BSc in Biotechnology: "Methods of identification of proteins with a potential pharmaceutical importance", grade good plus (4.5/5.0)
Institute of Biochemistry and Molecular Biology, Faculty of Natural Sciences, University of Wrocław, Poland, Supervisor: Prof. Jacek Otlewski

RESEARCH EXPERIENCE

08/2008 – 10/2012   Department of Structural Biology, Biozentrum, University of Basel, Switzerland, Laboratory of Prof. Stephan Grzesiek

07/2007 – 06/2008   Department of Molecular Physiology & Biological Physics, University of Virginia, Charlottesville, USA, Laboratory of Prof. Lukas Tamm

03/2007 – 06/2007   Department of Crystallography, Faculty of Chemistry, University of Wrocław, Poland, Laboratory of Prof. Tadeusz Lis

10/2004 – 06/2007   Laboratory of Protein Engineering, Faculty of Biotechnology, University of Wrocław, Poland, Laboratory of Prof. Jacek Otlewski

PUBLICATIONS

Wiktor M, Morin S, Sass H-J, Kebbel F, Grzesiek S (2012) Biophysical and structural investigation of bacterially expressed and engineered CCR5, a G protein-coupled receptor. J Biomol NMR (in revision).

Morin S, Wiktor M, Sass H-J, Hartley O, Grzesiek S (2012) Modulation of RANTES binding to CCR5 by modifications in the N-terminus and C-terminus (in preparation).

Vajpai N, Nisius L, Wiktor M, Grzesiek S (2012) High pressure NMR reveals close similarity between cold and alcohol protein denaturation due to a reduction of the hydrophobic effect. Proc Natl Acad Sci USA (in revision).

Makowski M, Lisowski M, Maciag A, Wiktor M, Szlachcic A, Lis T. (2010) Two pentadehydropeptides with different configurations of the ΔPhe residues. Acta Crystallogr C Organic Compounds C66:o119-o123.

Ellena JF, Liang B, Wiktor M, Stein A, Cafiso DS, Jahn R, Tamm LK (2009) Dynamic structure of lipid-bound synaptobrevin suggests a nucleation-propagation mechanism for trans-SNARE complex formation. Proc Natl Acad Sci USA 106:20306-20311.

ADDITIONAL TRAINING

17–22/02/2012	Keystone Symposia meeting "G Protein-Coupled Receptors: Molecular Mechanisms and Novel Functional Insights", Banff, Canada
21–25/08/2011	EUROMAR 2011, Frankfurt am Main, Germany
23–25/01/2011	Interdisciplinary workshop "From biological machines to molecular devices of the future" organized by Swiss Academy of Sciences, Rigi-Kulm, Switzerland
23–24/06/2009	Course "Writing and publishing a journal paper" organized by Heather Silyn-Roberts from the University of Auckland, Basel, Switzerland
23–24/06/2009	Course "Making an effective seminar or conference presentation" organized by Heather Silyn-Roberts from the University of Auckland, Basel, Switzerland
20–24/10/2008	7th NCCR Practical Course and EMBN Summer School on Membrane Protein 2D Crystallization and Observation, Basel, Switzerland

SCHOLARSHIPS AND AWARDS

07/2007 – 06/2008	Scholarship of the University of Virginia for a Visiting Graduate Student
10/2007 – 06/2008	Scholarship of the Polish Minister of Science and Higher Education for the scientific achievements
10/2007 – 06/2008	Scholarship of the President of the City of Wrocław
10/2004 – 06/2007	Scholarships of the University of Wrocław awarded annually to the students with the highest grade average (received continuously for 3 years)
02/10/2003	Honorary immatrikulation of the best student of each major by the President of the University of Wrocław

ADDITIONAL ACTIVITIES

10/2010 – 10/2012	PhD Students Representative of Biozentrum, University of Basel, Switzerland (directly involved in the organization of the PhD Retreat 2011, monthly career seminars and German course for PhD students)
10/2006 – 06/2008	Member of Student Scientific Association of Biotechnology "Przybysz" at Faculty of Biotechnology, University of Wrocław, Poland
10/2006 – 06/2007	Member of Student Government of Faculty of Biotechnology, University of Wrocław, Poland
09/2008 – 10/2012	Teaching experience at Biozentrum, University of Basel (practical classes in NMR, theoretical exercises in structural biology)

COMPUTER SKILLS

Word, Excel, Power Point, Illustrator, Photoshop, Linux (basic), Pymol, VMD, NMRPipe, Sparky

LANGUAGES

Polish (mother tongue), English (fluent, certificates: FCE, TOEFL, GRE), German (intermediate)

STRENGTHS

Creativity, initiative, critical thinking, devotion to details, team-work, strong motivation, self-dependence, responsibility

HOBBIES

Skiing, mountain hiking, ballroom dancing, voyages, gardening, aquaristics

REFERENCES

PhD thesis supervisor:

Professor Stephan Grzesiek
Department of Structural Biology
Biozentrum, University of Basel
Klingelbergstrasse 50/70, Rm. 386,
CH-4056 Basel, Switzerland
Phone: +41 61 267 21 00
Fax: +41 61 267 21 09
e-mail: stephan.grzesiek@unibas.ch

MSc thesis supervisor:

Professor Lukas Tamm
Department of Molecular Physiology
& Biological Physics
University of Virginia School of Medicine
480 Ray C. Hunt Dr., Snyder Bldg., Rm. 350,
Charlottesville, VA 22908, USA
Phone: +1 434 924 5108
Fax: +1 434-243-8271
e-mail: lkt2e@virginia.edu

Basel, September 3rd 2012